THE UNIVERSITY *of* EDINBURGH

Buckling of Circular Steel Cylindrical Shells under Different Loading Conditions

Thesis submitted in fulfilment of the requirements for the degree of Doctor of Philosophy
By

Lei Chen

Supervisors: Professor J. Michael Rotter

Dr Jian-Fei Chen

The University of Edinburgh
February 2011

Declaration

This thesis, entitled “Buckling Analysis of Circular Cylindrical Shells under Different Loading Conditions”, is submitted to the Institute for Infrastructure & Environment, The School of Engineering, The University of Edinburgh, Scotland, UK, for the Degree of Doctor of Philosophy.

The research, on which this thesis is based, was carried out between October 2007 and July 2010 under the supervision of Professor J.M. Rotter. It is solely the work of the author except where otherwise acknowledged in the text. It has not formed the basis of a submission for any other degree.

The publications based on this thesis are as follows:

Chen, L., Doerich, C. and Rotter, J.M. (2008) “A Study of Cylindrical Shells under Bending in the Elastic-Plastic Range”, 5th European Conference on Steel and Composite Stuctures, Graz, Austria.

Chen, L., Doerich, C. and Rotter, J.M. (2008) “A Study of Cylindrical Shells under Global Bending in the Elastic-Plastic Range”, Steel Construction—Design and Research, 1 (2008), 59-65.

Abstract

Cylindrical shells are widely used in civil engineering. Examples include cooling towers, pipelines, nuclear containment vessels, steel silos and tanks for storage of bulk solids and liquids, and pressure vessels. The loading condition for these shells is quite varied depending on the function of the shell. Axial compression, global bending, external or internal pressure and wind loading are some of the most common loading forms for realistic structures.

The failure of these cylindrical shell structures is often controlled by elastic or elastic-plastic buckling failure. Yield failure may occur in thick cylinders in some situations. A cylindrical shell under different loading conditions may display quite different buckling behaviour. The objective of this thesis is to investigate the characteristics of different buckling behaviours of cylindrical shell structures under axial compression, global bending, uniform external pressure and wind pressure. Some challenging practical problems in the design of these shell structures are explored.

This thesis is expected to have some far-reaching impacts in defining how to design cylindrical shell structures to give them adequate strength to resist extreme events. Many aspects will be based on the latest Eurocode (EN 1993-1-6, 2007) and Recommendations (ECCS EDR5, 2008). The results show both some strength and some weaknesses in the Eurocode in design of shell structures. New methods are proposed for some practical problems. Some new conclusions and suggestions are derived and are expected to provide some useful knowledge for the improvement of the Eurocode in cylindrical shell design in general.

Acknowledgement

I am deeply grateful to my supervisor, Professor J.M. Rotter, for his encouragement, generous support and enlightening guidance in carrying out this research and in producing this thesis.

I would like to thank Dr Jian-fei Chen and Dr Cornelia Doerich for their invaluable suggestions and constructive comments during my study. I would like to thank Dr Martin Gillie for his advice on my thesis writing. I would also like thank the friends and colleagues in the University of Edinburgh for their help and support.

I would like to express my special thanks to my parents, my sister and my girlfriend for their love, care and support during the last three years. I am much indebted to them.

Finally, financial support from the China Scholarships Council and the University of Edinburgh is greatly acknowledged.

Table of Contents

Nomenclature

The definition of the symbols in the thesis unless otherwise stated

σ_{cl}	Classical elastic buckling stress for perfect cylindrical shells under uniform axial compression
E	Young's modulus
r	Radius of the cylindrical shells
t	Thickness of the cylindrical shell walls
ν	Poisson ratio
P_{cr}	Linear critical load under axial compression
I	Second moment of area
L	Length of a column or a cylinder
ℓ	Axial half-wavelength of the buckle
w	Radial displacement of the cylindrical shells
P	Applied axial compressive load
α	Elastic imperfection reduction factor
λ	Relative slenderness
R_{cr}	Classical elastic critical resistance
R_{pl}	Plastic reference resistance
R_k (R_{GMNIA})	Critical load determined by experiment or from GMNIA analyses
β	Plastic range factor
λ_o	Squash limit relative slenderness
λ_p	Plastic limit slenderness
χ	Characteristic strength
η	Interaction exponent
η_o	Plastic limit interaction exponent
δ_0	Imperfection amplitude
θ	Circumferential coordinate in cylinder middle surface
D	Flexural stiffness of cylindrical shells with $D = \frac{Et^3}{12\left(1-\upsilon^2\right)}$
σ_x	Meridional stress of cylindrical shells

σ_θ	Circumferential stress of cylindrical shell
ρ	Local radius of the cross-section of the cylindrical shell
Ω	Dimensionless length parameter with $\Omega = (L/r)(t/r)^{1/2}$
ω	Dimensionless length parameter with $\omega = L/\sqrt{rt}$
σ_{cr}	Critical buckling stress for imperfect cylindrical shells
ϕ	Mean curvature of the shell in bending
M_{cr}	Classical elastic critical moment for cylinders in bending
M_{Braz}	Brazier moment for cylinders in bending
ϕ_{cr}	Curvature of the shell in bending according to the linear bending theory
ξ	Ovalization parameter
M_{LBA}	Critical bending moment derived from linear bifurcation analysis
M_{MNA}	Critical bending moment derived from materially nonlinear analysis
M_{GNA}	Critical bending moment derived from geometrically nonlinear analysis
σ_y	Yield stress
M_y	Initial first yield moment for cylinders in bending
M_p	Full plastic moment for cylinders in bending
M_{GMNIA} (M_k)	Critical bending moment derived from geometrically and materially nonlinear analysis of imperfect cylinders
ϕ_y	Curvature of the shell in bending at the linear first yield
E_T	Tangent modulus
σ_p	Critical axial compressive stress for cylinders in pure uniform axial compression with consideration of plasticity
$\sigma_{\theta cr}$	Critical circumferential buckling stress
C_θ ($C_{\theta s}$)	External pressure buckling factor ($C_{\theta s}$ for short cylinders)
m	Buckling wave number
m_{cr}	Critical buckling wave number
$\sigma_{x,m}$	Meridional membrane stress
$\sigma_{\theta,m}$	Circumferential membrane stress
p	Applied external pressure
$\sigma_{\theta cr,D}$	Elastic critical circumferential stress derived from classical linear

	Donnell-type shell buckling theory
$\sigma_{b\theta cr}$	Elastic critical circumferential stress with considering the pre-buckling bending deformation
$\sigma_{m\theta cr}$	Buckling stress based on the pre-buckling membrane stress assumption
C_P	The wind pressure coefficient around the circumference of the shell
$q_{cr,LBA}$	Linear critical buckling pressure for cylinders under external pressure
$q_{w,LBA}$	Linear critical stagnation pressure for cylinders under wind pressure
$q_{u,LBA}$	Linear critical pressure for cylinders under uniform external pressure
$q_{w,GNA}$	Nonlinear critical buckling stagnation pressure for cylinders under wind pressure
$q_{w,GMNA}$	Critical buckling stagnation pressure for cylinders under wind pressure (derived from GMNA)
$\Delta w_{0\theta}$	The equivalent amplitude of the dimple
$\ell_{g\theta}$	The gauge of length in circumferential direction
$q_{w,GNIA}$	Critical buckling stagnation pressure for cylinders under wind pressure (derived from GNIA)
ℓ_{eff}	The effective length of the stepped wall cylinder
C	Membrane stiffness of the cylinder with $C=\frac{Et}{1-\nu^2}$
ε_0	The circumferential strain before buckling
ε_z	Meridional strain after buckling
ε_θ	Circumferential strain after buckling
t_{eq}	Equivalent uniform thickness
$p_{cr,D}$	Linear buckling pressure derived from Donnell's linear shell theory
$p_{cr,S}$	Buckling pressure obtained from the weighted smeared wall method
$p_{cr,FE}$	Buckling pressure obtained from the finite element predictions
$k_{\min}$	The minimum bending stiffness coefficient
$I_{r,\min}$	Minimum second moment of area of the cross-section of the ring stiffener

Chapter 1 Introduction

1.1 Background to the problem

Cylindrical shells are widely used in civil engineering. Examples include cooling towers, pipelines, nuclear containment vessels, metal silos and tanks for storage of bulk solids and liquids, and pressure vessels. The loading conditions for these shells are quite varied depending on the specific function of the shell. Axial compression, global bending, external or internal pressure and wind loading are some of the most common loading forms in practical structures. A common application of cylindrical shells is design of silos and tanks (Fig. 1-1).

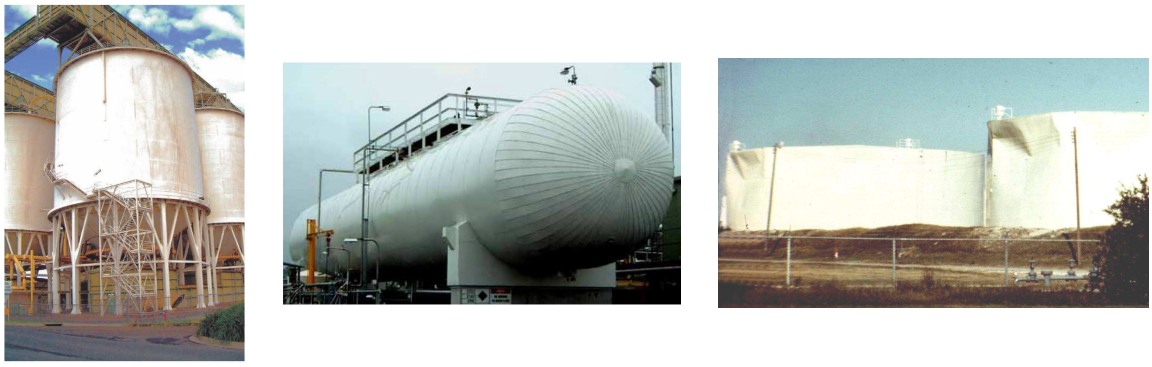

(a) Silo (b) Saddle-supported tank (c) Tank under wind loading

Figure 1-1: Cylindrical shell structures in engineering (photographs courtesy by J.M. Rotter)

Cylindrical shells used in engineering are generally very thin, and the mechanical behaviour is more complex than that of other structures like beams, columns and plates. The strength of a shell structure is often controlled by the buckling failure (Fig. 1-1c). A cylindrical shell under different loading conditions may display quite different buckling behaviour. So it is essential to understand the buckling behaviour of shell structures in different conditions comprehensively and establish suitable design methods.

1.2 Buckling problems in shell structure design

Shell structures are widely used in many fields. The buckling and stability analysis of cylindrical shells is an active research area in recent years. The collapse

of shell structures is a common phenomenon in the real world. Failure is believed to be caused by either local buckling or global buckling of the shell. By contrast, failure controlled by loss of material strength is not very common in practical shell structures. Exploration of buckling behaviour of cylindrical shells involves many different aspects. This thesis focuses on the buckling behaviour of cylindrical shells under uniform axial compression, global bending, uniform external pressure and wind loading.

A cylindrical shell under uniform axial compression is one of the most common applications. Axial compression in a cylinder arises from many different causes. For heavy structures like towers and chimneys, self-weight provides uniform axial compression. For a silo (Fig. 1-1a), the frictional force between the solids and shell wall imposes substantial axial compression. For a shell with a closed roof, axial compression is caused by the weight of the roof. In addition, many shells under other loading conditions can also induce or include either symmetrical or unsymmetrical axial compression.

The first theoretical shell buckling problem to be solved was the cylindrical shell under axial compression (Lorenz, 1908; Timoshenko, 1910; Southwell, 1914). This analysis determined the linear bifurcation stress of a perfect cylinder under ideal conditions of medium length, with pre-buckling stresses unaffected by boundary conditions but inducing the constraint of circumferential displacement during buckling. This buckling stress is known as the “classical elastic buckling stress”:

$$\sigma_{cl} = \frac{E}{\sqrt{3(1-\nu^2)}}\frac{t}{r} \cong 0.605\frac{Et}{r} \tag{1.1}$$

The buckling strength of a thin cylindrical shell under axial compression is more sensitive to imperfections than shells under other loading conditions. The buckling behaviour changes greatly with changing pattern of geometry, loading and boundary conditions, and the form and amplitude of the imperfections. For these reasons, the axially compressed cylinders are more extensively studied. However, this buckling problem is not the main topic in this thesis. Knowledge of this buckling problem can be found in many shell buckling published papers and books.

Cylindrical shell structures under global bending are common that can be found in civil engineering. In a saddle-supported tank (Fig. 1-1b) that is supported at both ends, the shell acts as a beam in bending, leading to axial compression at top but axial tension at bottom of the shell. This axial compression or tension varies around the circumference and along the length. When the tank is filled with water or other liquids, the tank is subject to combined bending and internal pressure. The thickness of many of these cylinders is generally much thinner than that of a pipeline or a tubular structural member, but it is often much thicker than that of a highly imperfection sensitive thin shell used in tanks and squatter silos. Desired thickness lies in an uncomfortable range which is extremely thin for the structural tube community and very thick for the shell buckling community. The buckling strength of these structures is dominated by extensive plasticity, but the fully plastic state is usually far from being attained. Yielding and buckling can occur simultaneously and the two may interact with each other, depending on the specific geometries and other conditions. The mechanical behaviour of these cylinders is more difficult to understand.

Cylindrical shells under uniform external pressure have been studied by many researchers. The buckling behaviour of these cylinders is quite different from that of cylinders under uniform axial compression. The effects of cylinder length, of restraining conditions at the boundaries and of the length of the pressurised zone all have great influences on the critical buckling load, especially for short cylinders. So it is necessary to clearly understand the effect of these factors on the critical buckling load. In EN 1993-1-6 (2007), for short cylinders, the meridional end rotation is not considered separately in defining the external pressure factor and all equations are based on the classical pre-buckling membrane stress condition. However, this may cause inaccurate results for short, and especially for extremely short, cylinders. This buckling problem will be discussed in this thesis.

Cylindrical storage tanks or silos are susceptible to buckling due to wind loading when they are empty or partially filled. Figure 1-1(c) shows an example of the buckling phenomenon of a stocky cylindrical shell caused by wind loading. Wind loading is a complex asymmetrical loading form. Buckling behaviour of cylinders

under wind loading is quite different from that under uniform external pressure. Due to the complexity of its mechanical behaviour, buckling analysis of cylinders under wind loading is currently usually investigated by either experiment or computational analysis. In this thesis, this problem is explored using nonlinear finite element analysis.

Cylindrical shells of stepwise varying wall thickness are typically found in cylindrical containment structures of moderate length, like vertical-axis tanks and silos. The thickness changes because the stress resultants are much larger at lower levels. Increase of internal pressure and axial compression in the shell is addressed by increasing the wall thickness. A buckle caused by external pressure or wind usually extends to several of the top thinner parts of a shell. In the European Standard for Shells EN 1993-1-6 (2007) and the European Recommendations on Shell Buckling ECCS EDR5 (2008), a complex design method based on the research of Resinger & Greiner (1974; 1976) and Greiner (1981) was introduced. The process is awkward in practical design of silos and tanks. A much simpler method called "weighted smeared wall method" is proposed in this thesis to deal with this buckling problem.

The imperfection-sensitivity analysis of cylindrical shells is one of the most significant problems in shell design. Imperfections are unavoidable during the process of shell construction. The large discrepancy between classical buckling stress predictions and experimental buckling strength was first shown to be predominantly caused by geometric imperfections in the shell surface by Koiter (1945). The buckling strength of a cylindrical shell depends much on the form and amplitude of the imperfection. So a key problem in design process is to identify and characterise appropriate "worst" and practically-relevant geometric imperfections, including both their shapes and amplitudes (Rotter, 1985; Teng and Rotter, 2004). Imperfection sensitivity is almost always seen in shell buckling problems, where imperfections have a significant influence on the buckling strength.

1.3 Design Rules

The latest Eurocode (EN 1993-1-6, 2007)-“Strength and Stability of Shell Structures” is the first generic standard to deal with both strength and stability of shells and the first to attempt to accommodate all forms of static structural analysis within the framework of the same design philosophy. The latest 5th edition of the ECCS European Recommendations for the Buckling of Steel Shells (edited by Rotter, 2008) provides an extensive commentary on existing rules relating to the buckling in the Eurocode, but extends far beyond it in giving recommendations, expansions, advice, warnings, explanations and examples. Other related codes include the DIN standard on silo loads (1987), ACI standard on silo loads (1991), Australian standard on silo loads (1996), Eurocode 1: Actions in silos and tanks (EN 1991-4, 2006), Eurocode 3: Design of steel structures: Part 4.1: Silos (2007) and Eurocode 3: Design of steel structures: Part 4.2: Steel tanks (2007).

1.4 Research approach

The study of shell structures involves a lot of areas covering small or large deformations, elastic, elastic-plastic, hardening, bifurcation, snap-through, imperfection-sensitivity, stability, and collapse analyses. The mechanical properties of cylindrical shells determine that theoretical analysis is quite complex and difficult, sometimes causing unexpected mistakes. The strength of cylindrical shells measured in laboratory tests also falls far below the ideal strength. The reason for this great difference and the loss of strength is mainly caused by geometric imperfections in the shell surface. How to define practically relevant geometric imperfections properly is a major challenge for researchers. Factors such as different fabricating methods, simpler loading cases as well as their boundary conditions all make it difficult to ensure that the experimental model is completely consistent with practical structures. In addition, it is not easy to obtain accurate buckling strength of imperfect cylindrical shells through costly experiments. However, many experimental results are already documented in the literature. For example, a lot of experimental data is available for axial compressive buckling from many earlier or later authors: Lee (1962), Batterman (1965), Bardi and Kyriakides (2006) along with the experimental data for

cylinders in bending derived by Suer et al. (1958), Dow and Peterson (1960), Elchalakani et al. (2002), Jullien and Limam (2002), Mathon and Limam (2006), Limam (2010), etc. Considering the difficulty to conduct experiments and the existence of many existing test data, it is not necessary to conduct experiments for present study.

The development of the computer makes it possible to perform nonlinear finite element analyses to derive accurate and reliable results. Computational skills can now allow the finite element model to approximate practical structures quite well. The latest Eurocode (EN 1993-1-6, 2007) represents a major advance in defining the use and interpretation of computational calculations of all kinds in design of shells, and permits each kind of calculation to be entered into some part of the hand calculation process (Rotter, 1998, 2002). This thesis will use the finite element software ABAQUS to simulate the shell buckling analysis. The arc-length method is used to capture the buckling strength accurately.

1.5 Research objective

This study deals with some challenging practical problems in the design of cylindrical shells, some of which have not been fully understood yet in the current literature. This project is expected to have some far-reaching impacts in defining how to design cylindrical shell structures to give them adequate strength to resist extreme events. Many aspects will be based on the latest Eurocode (EN 1993-1-6, 2007) and the ECCS Recommendations (ECCS EDR5, 2008). The results show both some strengths and weaknesses in the Eurocode in the design of shell structures.

1.6 Review of thesis contents

Based on linear or non-linear finite element analysis, this thesis focuses on the buckling behaviour of thin cylindrical shells under both uniform and non-uniform loading conditions. Both perfect and imperfect cylinders are investigated. Cylinders of either uniform thickness or stepwise variable wall thickness are included. The contents are described below.

Chapter 2 presents a general overview of shell buckling. Various bifurcation buckling types are introduced for different kinds of structures, columns and plates. The historical and current developments for shell buckling research are generalized. The imperfection-sensitivity study of cylindrical shells, elastic-plastic analyses for thicker shells, and related aspects of shell buckling in EN 1993-1-6 (2007) and ECCS EDR5 (2008), are introduced. Cylinders under axial compression are discussed and outlined in this chapter. The buckling analysis of an elastic cylindrical shell under axial compression is conducted using the finite element software ABAQUS. Imperfections in terms of either the perfect shell buckling eigenmode or a weld Type A depression (Rotter and Teng, 1989) are adopted, respectively. The aim is to verify the sensitivity of the elastic buckling strength of a thin-walled cylindrical shell to initial imperfections.

In Chapter 3, nonlinear stability analysis of cylindrical shells under global bending in the elastic range is studied. Different buckling behaviours of short, medium-length and long cylinders are investigated. Effects of geometric nonlinearity and the ovalization of the cross-section on the buckling behaviour are discussed. Finally, the effect of the geometric imperfections on the buckling strength of a long cylinder is explored.

In Chapter 4, an imperfection-sensitivity study of cylindrical shells of moderate length in global bending in the elastic-plastic range is studied. Effects of geometric and material nonlinearity on the buckling strength are explored. A weld depression imperfection with different amplitudes is adopted to explore the imperfection sensitivity of buckling strength. Cylinders with different radius to thickness ratios are involved. Then two different material hardening models are studied to investigate the influence of material hardening on the buckling strength. Results have been mapped onto the shell buckling capacity curve of EN 1993-1-6 (2007) and show how the capacity curve of the European shell buckling standard can be exploited to capture very complicated phenomena accurately. Finally, the buckling behaviour of cylindrical shells under combined global bending and axial compression in the elastic-plastic range is presented.

Chapter 5 presents a study of cylindrical shells under uniform external pressure. The elastic buckling behaviour for short, medium-length and long cylinders is re-examined. It focuses on the influence of meridional rotation and pre-buckling bending deformation on the buckling strength of short cylinders, especially extremely short cylinders, while in EN 1993-1-6 (2007), these two effects are not considered separately for short cylinders. Different fitted equations for the external pressure factor are proposed, depending on different boundary conditions.

Chapter 6 presents a comprehensive study of thin cylindrical shells of uniform thickness under wind pressure. Analyses focus on practical geometries of silos and tanks. Linear bifurcation analysis (LBA) and geometrically nonlinear analysis (GNA) are performed to investigate the buckling behaviour of shells with different geometries. The results indicate that the linear buckling behaviour and the nonlinear buckling behaviour may be quite different, depending on the specific geometries. Geometrically and materially nonlinear analysis (GMNA) is performed to explore the influence of plasticity on the buckling behaviour. Finally, geometrically nonlinear imperfection sensitivity study (GNIA) is conducted to explore the buckling behaviour of imperfect cylinders under wind pressure. The most detrimental form of an imperfection depends on the nonlinear buckling mode of specific aspect ratio cylinders.

Chapter 7 presents a study of the buckling behaviour of cylinders of stepwise varying wall thickness under either uniform external pressure or wind pressure. A new method is introduced, referred to here as “weighted smeared wall method” based on Trahair’s idea for stepped wall cylinders (Trahair, 1983). The buckling strength prediction derived from this method is close to accurate finite element predictions. It provides a much simpler way to deal with stepped wall cylinders than the method in EN 1993-1-6 (2007) or ECCS EDR5 (2008).

Chapter 8 presents an investigation of the requirements of minimum bending stiffness of ring stiffeners for cylindrical shells under wind pressure. Cylindrical shells with different aspect ratios are studied. The influence of bending stiffness of the ring stiffener on the buckling behaviour is discussed. Linear bifurcation analysis

(LBA) and geometrically nonlinear analysis (GNA) are presented separately. A new criterion is proposed to determine the minimum stiffness coefficient.

Chapter 9 summarizes the conclusions drawn from previous chapters. The problems encountered in the present study are reviewed. The areas for the future research are highlighted.

Chapter 2 A general outline of buckling in shells

2.1 An overview of shell buckling

2.1.1 Various types of buckling mode

Buckling may evoke an image of failure of a structure with very large deformation. However, from a scientific and engineering point of view, buckling phenomena generally occur before the deformations are very large, and the structure may appear to be not deformed or only slightly deformed (Bushnell, 1985). Buckling of structures is an important phenomenon in structural mechanics, because buckling often (but not always) leads to failure of structures. It is particularly important in shell structures because it often occurs without any obvious warning, and can have catastrophic effects (Calladine, 1983).

Earlier buckling analysis began with Euler's (1757) analysis of the bifurcation buckling of a column. Euler developed a theory to calculate the complete post-buckling behaviour of a straight pin-ended column under axial compression and obtained the critical load P_{cr} known as the Euler load (Eq. 2.1).

$$P_{cr} = \frac{\pi^2 EI}{\ell^2} \tag{2.1}$$

Post-buckling paths for perfect and imperfect columns under axial load are shown in Fig. 2-1a. For an imperfect column, the relationship between the deflection w at the middle of the column and the axial load P is given with sufficient accuracy by the equation (Timoshenko and Gere, 1961):

$$w = \frac{a_1}{P_{cr}/P - 1} \tag{2.2}$$

in which a_1 is the initial deflection at the middle of the column.

When the load is approaching the critical load P_{cr} , the deflection rises progressively but the critical load can not be exceeded, based on the assumption of small displacement theory.

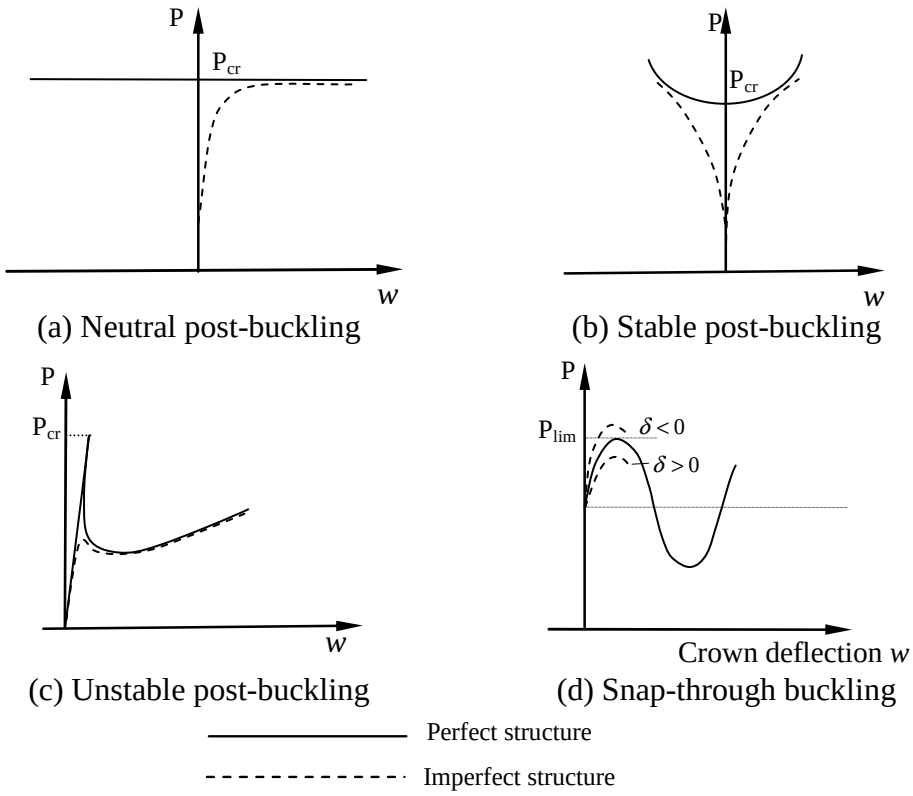

Figure 2-1: Load-deflection curves for various types of buckling mode (originally by Bushnell, 1985)

Different structures may display different post-buckling behaviour. An axially compressed isotropic flat plate displays a symmetric stable post-buckling behaviour as shown in Fig. 2-1b. The failure load is higher than the predicted classical critical load due to the stable post-buckling load-displacement path. A cylindrical shell under axial compression displays an unstable post-buckling behaviour as shown in Fig. 2-1c. The structure can collapse suddenly without any further obvious deformation after the bifurcation load P_{cr} is reached. This buckling is commonly termed bifurcation buckling, which is a significant buckling pattern in shell buckling analysis. An arch bridge can display a snap-through buckling mode as shown in Fig. 2-1d. The structure is stable under increasing load until a local maximum point is reached. After this point, the equilibrium path becomes unstable and the structure

buckles dramatically. The structure jumps to a shape that resembles the original structure in an inverted form. When this type of buckling occurs, the maximum load is referred to as a limit load $P_{\lim}$. In shell buckling analysis, snap-through buckling may also be found under certain conditions (e.g. spherical domes).

The load-displacement paths for various types of loading for imperfect structures may be different (Fig. 2-1). For structures with a snap-through buckling mode (Fig. 2-1d), the response of an imperfect structure is similar to that of a perfect structure and the limit load varies with the imperfection amplitude δ. For structures with neutral or stable post-buckling path (Fig. 2-1a and b), the effect of geometric imperfections is less significant. A faster growth of deflections is observed as the bifurcation load of a perfect system is approached, but the equilibrium path remains stable and continuously rising (ECCS EDR5, 2008). For structures with a bifurcation buckling mode and unstable post-buckling path (Fig. 2-1c), the situation becomes quite different. The imperfection plays an important role in affecting both the structural response and the instability load. The critical load may have a considerably lower value than the bifurcation load for the perfect structure.

2.1.2 Shell buckling

Classical analysis of elastic buckling of a simple column leads to the development of the 'classical' theory of elastic buckling of many structures, like two-dimensional flat plates and three-dimensional curved shells. In the field of shell buckling research, a moderately long perfect elastic cylindrical shell under uniform axial compression was first to be investigated and the classical buckling strength σ_{cl} (Eq. 1.1) is commonly used as a reference value for all the analyses. It is restricted to the perfect cylinders with simply supported boundary conditions, a uniform membrane pre-buckling stress state and in elastic material.

Why does buckling occur in a cylindrical shell? For thin-walled cylindrical shells, in general, the membrane stiffness is several orders of magnitude greater than the bending stiffness (Bushnell, 1985). Before buckling, the structure deforms slightly as the shell can absorb a great deal of membrane strain energy without deforming too much. While at the buckling load, the shell fails rather dramatically as it exchange its

membrane energy for bending energy, which requires the shell to deform a lot to absorb all the energy from bending strains (Bushnell, 1985).

Two different types of shell buckling exist, namely nonlinear collapse and bifurcation buckling (Fig. 2-2). Nonlinear collapse is predicted by a nonlinear stress analysis. At the collapse load, the slope of the load-deflection curve, also called the tangent stiffness of the structure, is equal to zero. After the collapse load, the load decreases with increasing displacement to satisfy mechanical equilibrium. Failure of a structure will occur if the load is maintained or increased. This type of instability is often called snap-through buckling.

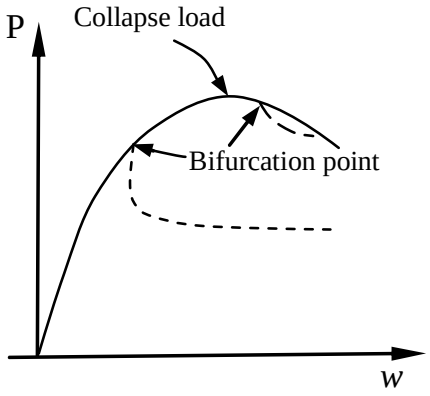

Figure 2-2: Load-deflection curve for two different types of shell buckling

Bifurcation buckling refers to a different kind of failure mode that is often predicted by a linear eigenvalue analysis or a nonlinear analysis that may involve either geometric nonlinearity or material nonlinearity or both of them. At the buckling load, the deformation begins to grow in a new pattern, which is quite different from the pre-buckling pattern. The nonlinear load-deflection path may be followed using the arc length method (Riks, 1979). Each iterative step must be checked to determine if negative eigenvalues have appeared. The appearance of negative eigenvalues indicates that a bifurcation point on the load-deflection curve has been passed. When this situation occurs, a subsequent nonlinear analysis should be performed, beginning at the last step before the first negative eigenvalue appears, using a smaller increment to trace the accurate bifurcation load. Sometimes the same process must be checked repeatedly to obtain an accurate result.

Buckling failure may be of either the collapse or bifurcation type, depending on the specific conditions. If the bifurcation point appears after the collapse point in the load-displacement path (Fig. 2-2), the collapse load should be regarded as the critical buckling load of the structure. Snap-through buckling is then dominant and controls the failure of the structure. The entire load-deflection path corresponds to a pre-buckling deformation mode.

When the bifurcation point appears before the collapse point in the load-displacement path (Fig. 2-2), the pre-buckling path before the bifurcation point follows a pre-buckling deformation mode. After the bifurcation point, the load-deflection path corresponds to a different post-buckling deformation mode. In this situation, the bifurcation load should be regarded as the critical buckling load to control the failure of the structure.

2.1.3 Nonlinear elastic theories for buckling in cylindrical shells

Several nonlinear elastic theories for circular cylindrical shells, including Donnell theory, Timoshenko shell theory, Modified Flügge theory and Sanders' theory, and Rotter and Jumikis's theory are introduced briefly next. These theories give the theoretical basis for most of the research in the stability analysis of cylindrical shells.

- **Donnell theory**

Donnell's nonlinear theory was developed by Donnell (1933) for circular cylindrical shells, in connection with the analysis of torsional buckling of thin-walled tubes. It assumes the shell is sufficiently thin, the strain is sufficiently small, and Hooke's law is still applicable. The theory complies with the Kirchhoff-Love hypotheses and assumes the deformation is dominated by the normal radial displacement and the in-plane displacements are negligible. The bending curvature is assumed to be related to the normal radial displacement only. Due to its approximations, Donnell's theory has limitations in its scope and applicability, but it is still widely used in many buckling and post-buckling problems due to its simplicity.

- **Timoshenko shell theory**

In the 1940s, Timoshenko developed and extended Donnell's theory on shells. His theory considered the influence of the axial and circumferential displacements on the bending curvature changes, which were neglected by Donnell. Thus, Timoshenko's shell theory has a wider application than Donnell's theory.

- **Modified Flügge theory**

The so called shallow shell approximations in Donnell's shell theory are not applicable for a cylindrical shell, under the condition that in-plane displacements are no longer neglected. A typical example relates to an intermediate aspect ratio cylinder under asymmetric wind pressure. Flügge's modified theory makes up this deficiency and takes in-plane displacements into consideration to derive expressions for the stress and strain components.

On the other hand, Flügge derived basic equations for the buckling of circular cylindrical shells under typical loading conditions (Flügge, 1932), without resort to the shallow shell approximation. However, Flügge's modified theory is not sufficiently accurate in some cases, since the pre-buckling state is assumed to be a membrane stress state. This neglects the effect of the bending deformations near boundary conditions or under unsymmetrical bending.

- **Sanders theory**

Sanders theory (1963) was first developed for finite deformations of thin shells, which was focussed on circular cylindrical shells. It takes the finite deformations of non-shallow shells with small strains and moderately small rotations into account. The Sanders equations are much more complex than those of the Donnell theory but somewhat simpler than those of the Modified Flügge theory. Since its generality makes it directly applicable to non-shallow shells with any geometric configuration, Sanders' theory has been favoured in structural analysis, especially using the finite element method (Yamaki, 1984).

- **Complete expressions for nonlinear elastic theory**

All the above theories used simplifications to try to make the nonlinear equations simple enough to produce useful algebraic analyses. However, in the new era of

powerful computer formulations, there is no special merit in simplifying the expressions and the complete nonlinear strain-displacement relationships may be adopted, as derived for example by Combescure (1986) and Rotter and Jumikis (1988) and exploited in their analyses (Teng and Rotter, 1989; Combescure, 1998).

2.2 Imperfection-sensitivity analysis of cylindrical shells

2.2.1 Buckling strength of imperfect cylindrical shells

The imperfection-sensitivity analysis of cylindrical shells has remained an active area of research. The large discrepancy between the classical buckling stress prediction and experimental buckling strength was first shown to be predominantly caused by geometric imperfections in the shell surface by Koiter (1945). Koiter was the first to develop the asymptotic theory for the initial post-buckling behaviour of perfect and imperfect structures. The ultimate aim of all imperfection sensitivity analyses is to determine the maximum load-carrying capacity of the imperfect structures.

Koiter (1945) showed that the buckling strength of axially compressed cylindrical shells is very sensitive to the initial geometric imperfections and the imperfection in the form of a perfect shell buckling eigen-mode would be very deleterious. This concept was later widely accepted for a long time. A minor imperfection could have a disproportionate effect on the buckling strength (Almroth, 1963, 1966).

The effect of an imperfection on the buckling strength can be expressed by a "knock-down factor" α, which is the ratio of the critical buckling stress σ_{cr} for the imperfect structures achieved under elastic conditions to the classical elastic critical stress σ_{cl} for perfect structures.

2.2.2 "Worst" and "practically-relevant" geometric imperfections

Following Koiter's work, imperfection in the form of the perfect shell buckling eigenmode has long been regarded as the worst imperfection form and this type of imperfection appears to cause the most serious reduction to the buckling strength. Many pieces of research have reviewed and developed Koiter's theory and many

applications of the theory could be found in shell buckling analysis (Koiter, 1963; Hutchinson and Koiter, 1970; Tvergaard, 1976; Singer, 1982; Calladine, 1983; Yamaki, 1984; etc).

It has been widely accepted that the buckling strength of a cylindrical shell is dependent on imperfections, so a key problem in design process is to identify and characterise the appropriate "worst" and practically-relevant geometric imperfections, including both their shapes and amplitudes (Teng and Rotter, 2004). However, because of the huge range of potential imperfection shapes (Yamaki, 1984), and the poor relationship of simple forms to measured imperfections (Ding et al, 1996; Teng et al., 2005), there has long been a debate concerning the "worst" form of imperfection and the "practically relevant" form (Rotter, 2004).

One of the simplest solutions to this controversy is the adoption of a circumferential weld depression imperfection (Fig. 2-3) (Hutchinson 1965; Rotter and Teng, 1989; Teng and Rotter, 1992), which is seen in practical civil engineering constructions and is often either the worst or close to the worst (Rotter and Zhang, 1990; Song et al., 2004) when measured using accepted stick measurements (EN 1993-1-6, 2007).

This type of imperfection is the most practically relevant since it relates to the construction process of circular silos and tanks which are commonly built from rolled steel plates. The weld depression is formed during the rolling process and subsequent welding during construction (Rotter and Teng, 1989). This type of imperfection has been adopted as a realistic form by a wide range of studies (Teng and Rotter, 1992; Rotter, 1996, 1997b; Holst, 2000; Schmidt and Winterstetter, 2001; Pircher et al, 2001; etc.).

One major advantage of the circumferential weld depression is that it is easily defined (Rotter and Teng, 1989), local, continuous with the remainder of the shell, and can be used in studies of a wide range of different problems for comparison. This arises because its effects on the elastic buckling strength of cylinders have been accurately and thoroughly documented in the past.

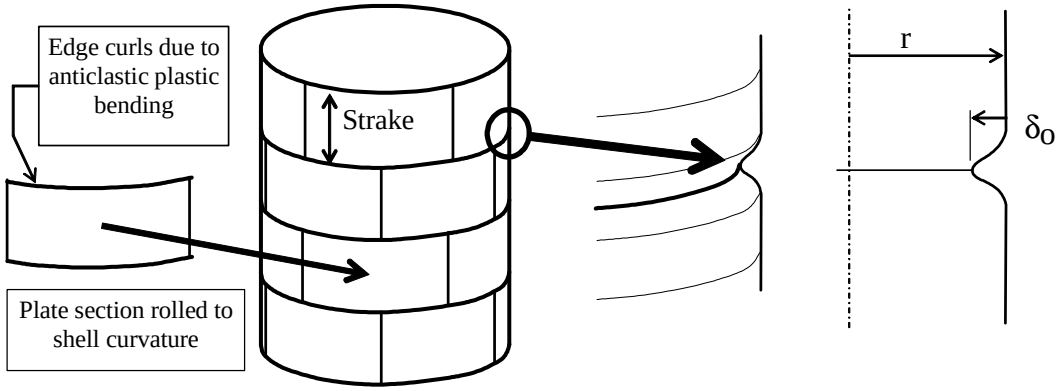

Figure 2-3: Development of circumferential weld depression imperfections (Rotter, 2002)

Though the weld depression imperfection has been proved to be more realistic and "worst" than any other imperfection, the real structure may have many different forms of imperfection, which have naturally a somewhat random distribution due to other fabrication processes. So in addition to the eigenmode imperfection and the weld depression imperfection mentioned above, other researches may adopt many different types of imperfection for different studies, such as the local imperfection in the form of the rectangular shape or ring shape (Greiner, 1995), the imperfection in the form of the pre- or post-buckling mode for perfect cylinders (Esslinger and Geier, 1972; Cai, 2003; Song et al., 2004; Guggenberger et al., 2004; Doerich, 2007). Due to the complexity and uncertainty of the imperfection form, it is usually difficult to determine the most detrimental and practical imperfection form under a specific condition. Different factors, such as loading conditions, boundary conditions and buckling behaviour of the specific structure, all should be considered to determine an appropriate imperfection form.

The residual stresses resulting from the process of welding are another form of imperfection though they have not received much attention. However, the residual stresses are found to have usually a beneficial effect towards the failure load (Rotter, 1996; Holst et al., 2000; Pircher and Bridge, 2001).

So the initial imperfections contribute to the majority loss of the buckling strength comparing with the classical buckling strength and play a significant role in the thin cylindrical shell buckling analyses. More details about how to choose appropriate

imperfection forms and imperfection amplitudes for design can be found in EN 1993-1-6 (2007).

2.3 Elastic-plastic analyses for thicker shells

For thin cylinders ($r/t > 500$), yield occurs in the post buckling range, especially in regions of local bending, and bifurcation buckling occurs before the beginning of yield. In this situation, elastic buckling strength is dominant in the design process and plasticity of the material plays no role in shell buckling analyses. The buckling behaviour is entirely elastic and the outcome of GMNIA and GNIA analyses are identical (Chapter 8, ECCS EDR5, 2008). However, under some especially complex loading conditions, it is difficult to define the boundary between thin shells and thick shells, and is thus difficult to determine whether plasticity affects the buckling behaviour. In this situation, caution should be taken at all times to observe the outcomes of GMNIA and GNIA.

For quite short thick shells, yield occurs in regions of local bending before elastic bifurcation buckling occurs. When the yield stress is reached, the deformation of the structure develops quickly until the plastic limit load is reached, which represents the state of material rupture or unacceptable large plastic deformation, when stability phenomena do not intervene. Its simplest and clearest expression is in the classical plastic limit load, which is derived from a small displacement theory analysis and is important in defining slenderness.

Inclusion of geometric nonlinearity in an evaluation of the plastic limit state requires caution for both geometrically hardening and softening structures (Rotter, 2005b). For softening structures, the distinction between the plastic limit and buckling is lost and the peak load is the same as that for plastic buckling, unless bifurcation occurs. In hardening structures, plastic limit depends on the maximum permitted deformation (Rotter, 2002).

For some moderate thickness cylinders, they are generally much thinner than pipelines and tubular structural members, but are often much thicker than cylinders subject to the highly imperfection sensitive very thin shells used in tanks and squatter

silos. Their thickness lies in an uncomfortable range which is extremely thin for the structural tube community and very thick for the shell buckling community. The buckling strength of these structures is dominated by extensive plasticity, but the fully plastic state is usually far from being attained. Buckling and yielding may interact with each other for these structures, depending on the specific geometry of the cylinders. The geometrically and materially nonlinear analysis of an imperfect structure must be performed to determine the elastic-plastic limit load.

The plastic limit load is commonly assessed as the ideal value of the plastic reference resistance. This resistance is a significant reference value in the elastic-plastic buckling analysis of cylindrical shells. This resistance can be simply evaluated based on the membrane theory calculations or linear elastic shell bending theory calculations. The Ilyushin yield criterion is the simplest plasticity criterion for a shell and always provides a safe estimation. This criterion is only applied to the stress state at a single point and does not allow for the development of a complete plastic mechanism that is necessary for a true plastic collapse to occur (Rotter, 2008a). In the elastic-plastic stability analysis of cylindrical shells, the plastic reference resistance is required as a formal part of the elastic-plastic buckling strength assessment and should always be evaluated using a small-displacement theory rigid-plastic or elastic-plastic analysis (MNA) (Chapter 7, ECCS EDR5, 2008).

2.4 The European Standard EN 1993-1-6 (2007) and European Recommendations ECCS EDR5 (2008) for steel shell buckling analysis

The most relevant standard in steel shell buckling analysis is the European standard EN 1993-1-6 (2007). It is the first standard to take numerical solutions into account, including computational treatments for shells. It extends its application to a wider range of shell structures under all types of loading and stress conditions. It also includes a hand calculation assessment. The European Recommendations ECCS EDR5 (2008) provides an extensive commentary on the rules in EN 1993-1-6 (2007) relating all aspects of shell buckling, but extends far beyond it in giving

recommendations, expansions, advice and warnings, explanations and examples, all of which should give users considerably more insight and confidence in applying the rules of EN 1993-1-6 (2007) (Rotter, 2008).

2.4.1 Types of shell buckling analysis in EN 1993-1-6 (2007)

The purpose of any shell buckling analysis is to determine the final buckling strength of a shell structure under specific conditions (loading conditions, boundary conditions and material properties, etc). Several methods are described in EN 1993-1-6(2007) for shell buckling analysis. The challenge for designers and researchers is to choose the simplest and most effective method to obtain accurate and reasonable results. So a summary of different methods is described below.

- **Linear analysis (LA)**

The simplest treatment of shell buckling analysis is linear elastic stress analysis termed LA, which is based on the assumption of small displacement theory and elastic material for perfect structures. It can be used to evaluate the plastic reference resistance R_{pl} (Fig. 2-4). The evaluated membrane stress resultants should be used to estimate R_{pl}. This method of estimating R_{pl} is conservative, but it may be very conservative where local loads or geometric features lead to high, locally elevated stresses (Schmidt and Rotter, 2008).

- **Linear bifurcation analysis (LBA)**

Linear bifurcation analysis (LBA) is a small displacement stability analysis that assumes a perfect geometry, linear elastic material behaviour and no change in geometry (small displacement theory) before the infinitesimal displacements of the secondary path (Rotter, 2005a). It is based on LA stresses, and is classed as part of the LA analysis. It accurately determines the elastic critical load R_{cr} (Fig. 2-4), which is an important reference load for all analyses, since it is required in the definition of relative slenderness of cylindrical shells. Linear bending and stretching shell theory is adopted. LBA analysis can not capture the snap-through buckling, so caution should be made where the snap-through buckling may occur.

- **Geometrically nonlinear analysis (GNA)**

When geometrical nonlinearity may affect the buckling behaviour and can not be neglected, geometrically nonlinear analysis (GNA) should be adopted. It is an elastic buckling analysis of perfect shells and the pre-buckling deformations are taken into account using large displacement theory (Fig. 2-4). The elastic snap-though buckling can be detected using this analysis. For most thin shells, failure is controlled by elastic buckling and plasticity does affect the buckling behaviour, so GNA analysis can often capture an accurate strength assessment of a perfect shell.

- **Materially nonlinear analysis (MNA)**

An accurate estimation of the plastic reference resistance R_{pl} of a perfect shell is termed MNA, with the assumption of a small deflection theory and nonlinear material model (Fig. 2-4). The plastic reference resistance R_{pl} is needed for the definition of relative slenderness together with the elastic critical load R_{cr} .

- **Geometrically and materially nonlinear analysis (GMNA)**

Geometrically and materially nonlinear analysis (GMNA) considers the effect of both geometric and material nonlinearity on the buckling behaviour of a perfect shell (Fig. 2-5). It identifies the elastic-plastic buckling resistance of the perfect structure. If the structure is not sensitive to imperfections or if the imperfection does not need to be considered in some situations, this analysis can be adopted.

- **Geometrically nonlinear analysis with imperfections (GNIA)**

When an imperfection of the shell is introduced into the geometrically nonlinear analysis (GNA), the analysis is termed GNIA. Now, it is well known that the buckling strength of a cylindrical shell is very sensitive to imperfections, and for most thin cylinders like tanks and silos, the failure is controlled by elastic buckling rather than yield failure, so GNIA is a common type of analysis that can be applicable to many buckling problems for cylindrical shells.

- **Geometrically and materially nonlinear analysis with imperfections (GMNIA)**

When an imperfection of the shell is introduced into the geometrically and materially nonlinear analysis (GMNA), the analysis is termed as GMNIA analysis (Fig. 2-5). GMNIA analysis is the most comprehensive analysis for shell buckling analysis. It identifies the elastic-plastic buckling resistance for imperfect structures. GNIA and GMNIA emphasize the influence of imperfections. The difficulty in these two analyses is to choose an appropriate type of imperfection, depending on the specific buckling problem.

Different types of computational shell buckling analysis are summarized in Table 2-1, which gives a full description of the characteristic of each analysis in EN 1993-1-6 (2007).

Table 2-1: Computational shell buckling analysis (after EN 1993-1-6, 2007 and ECCS EDR5, 2008)

Type of analysis	Terminology	Shell theory	Material law	Shell geometry
Linear elastic shell analysis	LA	Linear	Linear	Perfect
Linear bifurcation analysis	LBA	Linear	Linear	Perfect
Geometrically nonlinear elastic analysis	GNA	Non-linear	Linear	Perfect
Materially nonlinear analysis	MNA	Linear	Non-linear	Perfect
Geometrically and materially nonlinear analysis	GMNA	Non-linear	Non-linear	Perfect
Geometrically nonlinear elastic analysis with imperfections	GNIA	Non-linear	Linear	Imperfect
Geometrically and materially nonlinear analysis with imperfections	GMNIA	Non-linear	Non-linear	Imperfect

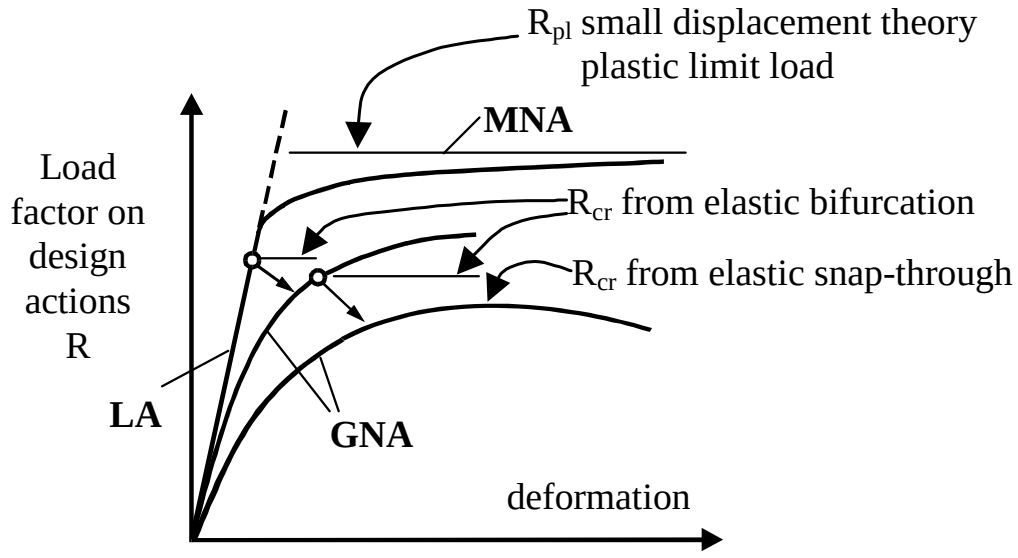

Figure 2-4: Calculated load-displacement relationship curves for LA, LBA, MNA and GNA analyses (Rotter, 2002)

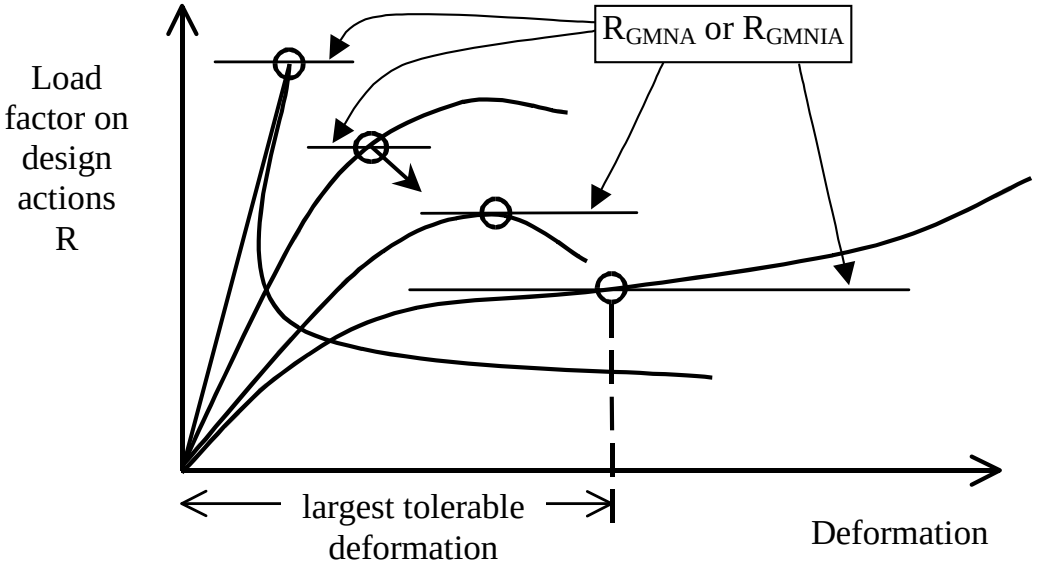

Figure 2-5: Criteria of failure for GMNA and GMNIA analyses (Rotter, 2002)

2.4.2 The capacity curves for shell buckling in EN 1993-1-6 (2007)

The capacity curves (Fig. 2-6) for a structure describe the relationship between the buckling strength and the relative slenderness λ. The relative slenderness is defined in terms of the plastic limit reference resistance R_{pl} (small displacement theory with

ideal elastic-plastic analysis (MNA), producing $R_{MNA} = R_{pl}$), and the linear elastic critical resistance R_{cr} (linear bifurcation analysis (LBA), producing $R_{LBA} = R_{cr}$).

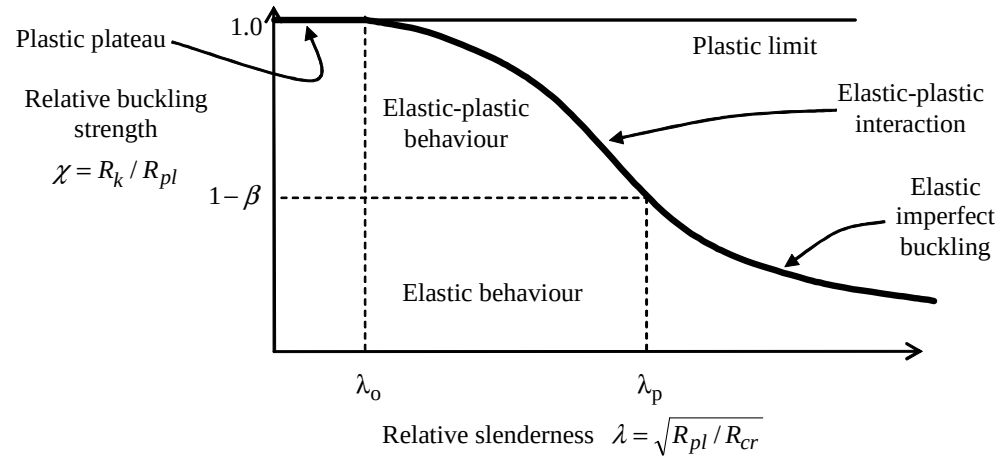

(a) Traditional strength vs slenderness curve

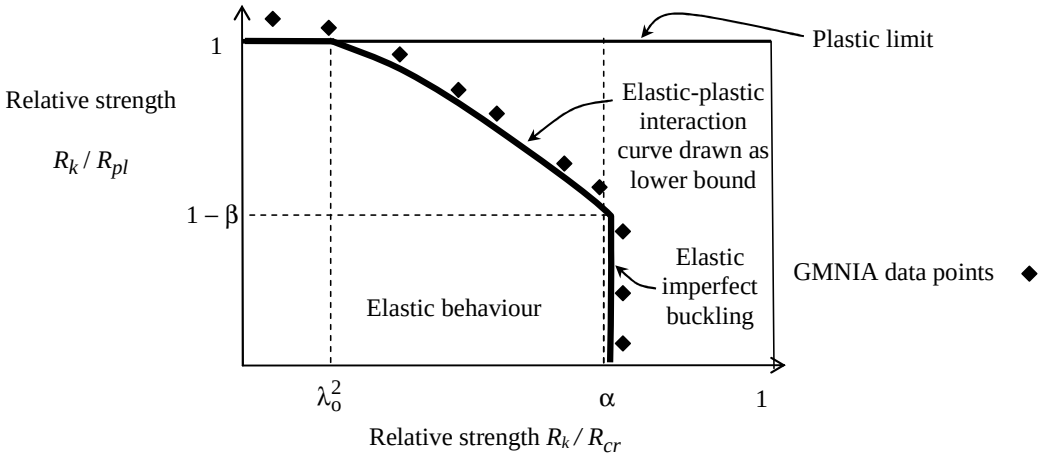

(b) Transformed relative strengths (Rotter, 2002, 2007)

Figure 2-6: Capacity curve of EN 1993-1-6 (2007)

The relative slenderness λ is defined as

$$\lambda = \sqrt{R_{pl} / R_{cr}} \tag{2.3}$$

and the dimensionless strength parameter χ is defined as

$$\chi = R_k / R_{pl} \tag{2.4}$$

where the characteristic resistance R_k is determined by experiment or from a geometrically and materially nonlinear analysis of the imperfect structure (termed GMNIA, producing $R_{GMNIA} = R_k$).

The shape of the EN 1993-1-6 (2007) capacity curve, shown in Fig. 2-6(a), was devised by Rotter (1999) and is given by

$$\chi = 1 \qquad \text{when} \qquad \lambda \le \lambda_0 \tag{2.5}$$

$$\chi = 1 - \beta\left(\frac{\lambda - \lambda_0}{\lambda_p - \lambda_0}\right)^{\eta} \qquad \text{when} \qquad \lambda_0 < \lambda < \lambda_p \tag{2.6}$$

$$\chi = \alpha / \lambda^2 \qquad \text{when} \qquad \lambda_p < \lambda \tag{2.7}$$

with $\lambda_p = \sqrt{\alpha/(1-\beta)}$

This relationship between resistance and slenderness is controlled by the parameters α, β, λ_0 and η, each of which describes a separate feature of the behaviour (Rotter, 2005a and b). Under elastic conditions, the elastic imperfection reduction factor α describes the loss of strength due to geometric nonlinearity and imperfection sensitivity. The load level at which yielding first impacts on the buckling strength is captured by the plastic range factor β. The slenderness at which the plastic reference resistance is exceeded as a result of strain hardening is captured by the squash limit relative slenderness λ_0, and the shape of the elastic-plastic curve by the interaction exponent η.

It is difficult to extract the key parameters α, β, λ_0, and η from plotted results in the form of Fig. 2-6(a), so Rotter (2002, 2007) devised a transformation as Fig. 2-6(b) which permits these parameters for any structural system to be accurately obtained with relative ease.

2.4.3 Geometrical imperfections in EN 1993-1-6 (2007)

The principal tolerances and imperfections concerned in EN 1993-1-6 (2007) include three forms of deviations normal to the nominal surface. They are out-of-roundness, eccentricities and local dimples. The related imperfections adopted in this thesis, like eigenmode imperfections and weld depression imperfections, are related to the dimple tolerances. The amplitude of the imperfection related to the dimple tolerances is based on gauge measurements and should be measured in both the meridional and circumferential directions. The gauges are devised related to the size of buckles that are expected to form under each of the different basic load cases (ECCS EDR5, 2008).

The depth Δw_0 (Fig. 2-7) should be measured and adopted according to the following rules in EN 1993-1-6 (2007):

> *The depth of initial dimple* Δw_0 *should be assessed in terms of dimple parameters* $U_{0x}, U_{0\theta}, U_{0w}$ *given by:*
>
> $$U_{0x} = \Delta w_{0x} / \ell_{gx} \qquad U_{0\theta} = \Delta w_{0\theta} / \ell_{g\theta} \tag{2.8}$$
>
> $\ell_{gx}, \ell_{g\theta}$ *and* ℓ_{gw} *are gauge of lengths given by:*
>
> $$\ell_{gx} = 4\sqrt{rt} \tag{2.9}$$
>
> $$\ell_{g\theta} = 2.3(\ell/r)^{1/2}(t/r)^{1/4} r \ , \quad but \ \ell_{g\theta} \le r \tag{2.10}$$
>
> *Where* ℓ *is the meridional length of the shell segment.*
>
> $$\ell_{gw} = 25t \qquad or \qquad \ell_{gw} = 25t_{\min} \tag{2.11}$$
>
> *but with* $\ell_{gw} \le 500mm$. $t_{\min}$ *is the thickness of the thinnest plate at the weld.*
>
> *The value of the dimple parameters* $U_{0x}, U_{0\theta}, U_{0w}$ *should satisfy the conditions:*
>
> $$U_{0x} \le U_{0,\max} \qquad U_{0\theta} \le U_{0,\max}$$
> $$U_{0w} \le U_{0,\max} \tag{2.12}$$
>
> *where* $U_{0,\max}$ *is the dimple tolerance parameter for the relevant fabrication tolerance quality class and can be adopted according to 1993-1-6 (2007).*

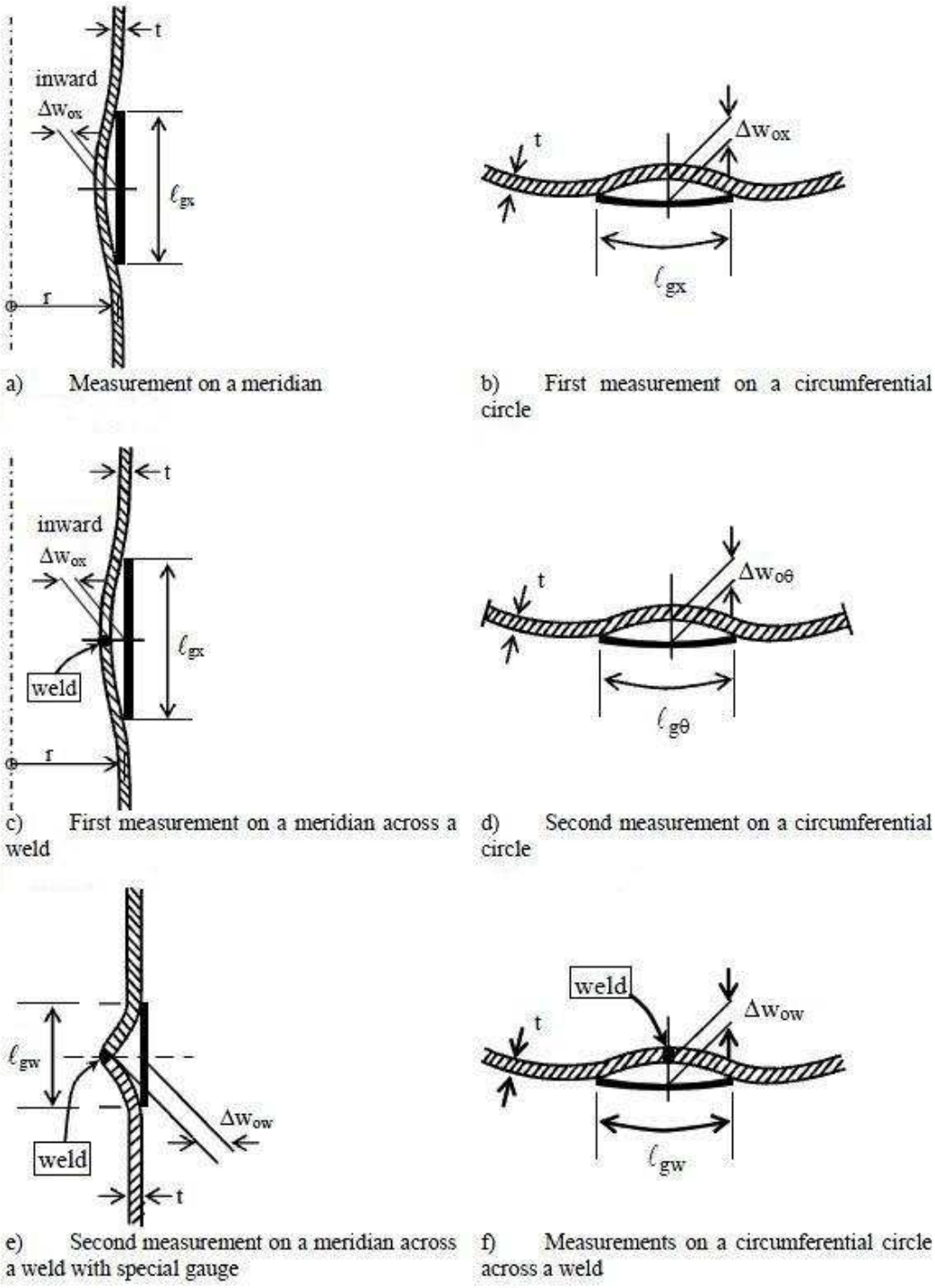

Figure 2-7: Measurement of the depth Δw_0 of initial dimples (picture taken from ECCS EDR5, 2008)

2.4.4 General rules of EN 1993-1-6 (2007) on boundary conditions

The practical cylindrical shells are restrained by ring stiffener, roof, or be anchored at their ends against displacement. The boundary conditions for a cylindrical shell with different functions may take different forms. The effect of boundary conditions for the buckling strength of some cylindrical shells is extremely important. In EN 1993-1-6 (2007), the categories of boundary condition are shown in Table 2-2.

Table 2-2: Boundary conditions for shells (EN 1993-1-6, 2007)

Boundary condition code	Simple term	Description	Normal displace-ments	Meridional displacements	Meridional rotation
BC1r	Clamped	radially restrained meridionally restrained rotation restrained	$w = 0$	$u = 0$	$\beta_\phi = 0$
BC1f		radially restrained meridionally restrained rotation free	$w = 0$	$u = 0$	$\beta_\phi \neq 0$
BC2r		radially restrained meridionally free rotation restrained	$w = 0$	$u \neq 0$	$\beta_\phi = 0$
BC2f	pinned	radially restrained meridionally free rotation free	$w = 0$	$u \neq 0$	$\beta_\phi \neq 0$
BC3	Free edge	radially free meridionally free rotation free	$w \neq 0$	$u \neq 0$	$\beta_\phi \neq 0$
Note: the circumferential displacement v is very closely linked to the displacement w normal to the surface so separate boundary conditions are not identified for these two parameters, but the values in column 4 should be adopted for displacement v.					

For the buckling limit state, special attention should be paid to the boundary conditions which are relevant to the incremental displacements of buckling (as opposed to pre-buckling displacements). Examples of relevant boundary

conditions are shown in Fig. 2-8, in which the codes of Table 2-2 are used.

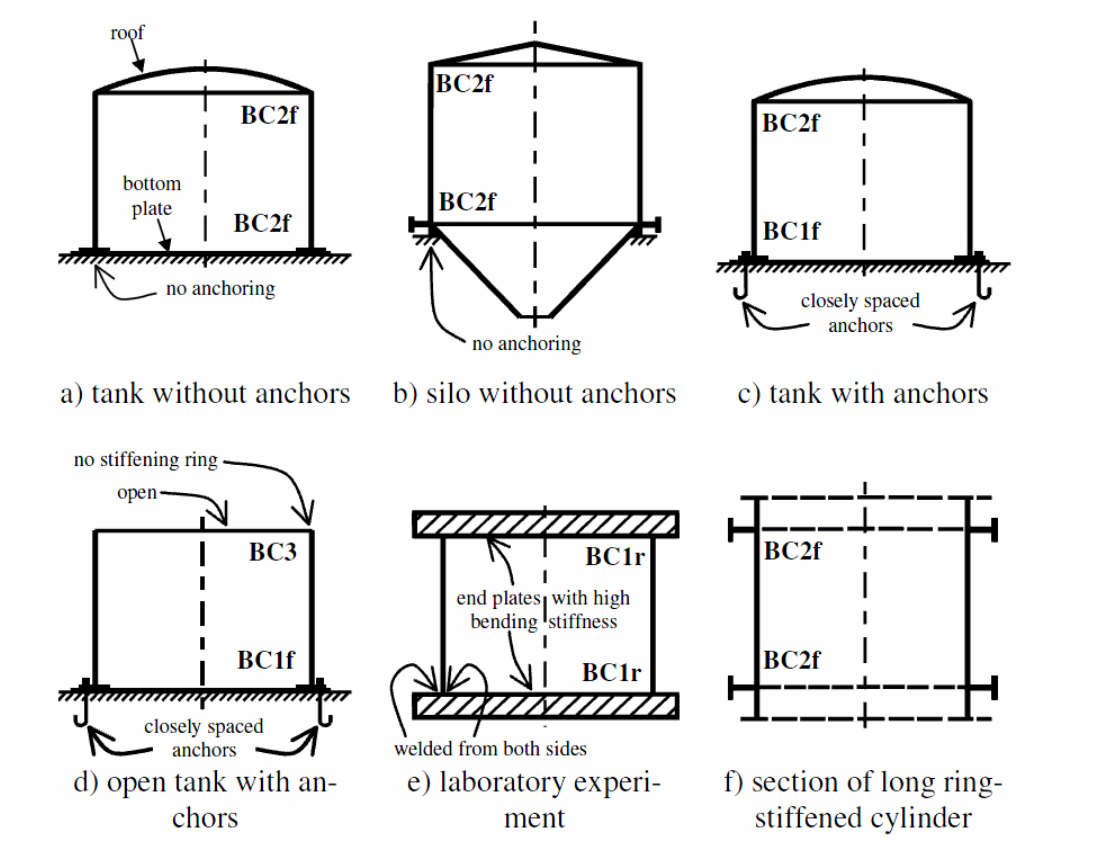

Figure 2-8: Schematic examples of boundary conditions for the buckling limit state (EN 1993-1-6, 2007)

2.5 Finite element analysis package ABAQUS

2.5.1 Brief introduction to finite element method and finite element package ABAQUS

Due to the complex mechanical behaviour of shell structures, it is quite difficult to obtain analytical solutions for many practical buckling problems. Fortunately, the computational ability of the computer develops quickly nowadays. Many complex problems that could not be solved theoretically could be solved based on computational analysis. The finite element method (FEM) was first proposed by Courant (1943) and then developed by many researchers (Clough 1960; Zienkiewicz and Taylor, 1971; Martin and Carey, 1975; Bathe, 1976; Hughes, 1987; etc).

The FEM is a method utilizing certain numerical techniques, such as a directional integration method, Rayleigh-Ritz method or Galerkin method, to find approximate solutions of partial differential equations (PDE) as well as of integral equations. The finite element software ABAQUS (HKS, 2006) is a powerful tool to perform numerical predictions for many different types of analysis in civil engineering applications. The theoretical formulation of ABAQUS is based on the finite element stiffness method. It is a comprehensive, commercial general-purpose finite element analysis product. However, before using ABAQUS to design a computational approach, both engineers and researchers should understand the mechanical behaviour of the structure well for their problems, so the important aspects of the finite element analysis, such as the mesh, the elements, the boundary conditions and the analysis method are well understood and correctly applied to obtain accurate and reliable results for engineering design.

2.5.1 Type of element and method used for shell buckling analyses in this thesis

In this thesis, some challenging practical shell buckling problems in the design of cylindrical shells were studied using ABAQUS. Different types of analysis discussed in 2.4.1 (LA, LBA, GNA, GNIA, and GMNIA) could all be conducted using ABAQUS. The powerful geometrically nonlinear formulation in ABAQUS gives assurance that the results will be accurate and reliable. In most cases, general S4 element, which is a fully integrated, general-purpose, finite-membrane-strain element, was used. Accurate results could be obtained by using this element when the dominate deformation of the shell is in-plane bending. When the shell may be subjected to out-plane bending, the four-node rectangular shell element with reduced integration S4R could be used. Compared with the full integration shell element S4, S4R shell element could eliminate the effect of shear locking. The element S4R was used for cylinders in global bending in this thesis. However, the results using the two types of element are proved to be very close in most situations.

For linear bifurcation analysis, the eigenvalue extraction method was used to extract the lowest eigenvalue as the linear elastic buckling load. In non-linear problems, the modified Riks method (Riks, 1979) was used. The process of the

analysis was controlled by automatic control of the step increment, which was provided for all relevant analysis procedures. The ABAQUS/Standard automatically selected the convergence tolerances and the increments required for the step. The convergence of the solution was achieved by using an “arc length method” (Wempner, 1971, Riks, 1979, Ramm, 1981 and Crisfield, 1983). ABAQUS Standard uses the “the arc length along the static equilibrium path in load displacement space” (HKS, 2003). The load-factor at each iteration is modified so that the solution follows some specified path until convergence is achieved. Using this method, the bifurcation buckling point and the equilibrium point with a negative stiffness matrix in the load-displacement path could be detected. The critical load for the shells under this loading condition could thus be determined. This method is the best known methods to describe the nonlinear buckling behaviour of shells.

2.6 Cylindrical shells under axial compression

2.6.1 Introduction

The buckling of a thin cylindrical shell under axial compression has received more attention than any other buckling problem due to its economic importance and extraordinary discrepancy between test and theory caused by its high sensitivity to geometric imperfections (Rotter, 2004). This buckling problem have been extensively studied in recent decades (Timoshenko, 1961; Fischer, 1962, 1963; Almroth, 1966; Hoff, 1966; Flügge, 1973; Brush and Almroth, 1976; Singer, 1982, 1983; Calladine, 1983, Yamaki, 1984; Bushnell, 1985; Teng, 1996, 2000; Blachut, 1998; Rotter, 1998, 2003; Limam, 2011). These studies mainly focused on nonlinear pre-buckling behaviour and its effects on bifurcation buckling, the post-buckling behaviour of a perfect cylindrical shell, and most importantly, the effect of initial geometric imperfections on buckling strength.

The buckling strength of an axially compressed thin cylindrical shell depends on many factors, such as the geometric parameters (radius r, thickness t and length L) of the cylinder, elastic modulus E, yield stress σ_y, the amplitude and form of a minor imperfection in its geometry, the end boundary conditions and the patterns of loading condition, etc.

2.6.2 Nonlinear post-buckling behaviors of perfect elastic cylinders

The classical elastic buckling analysis for perfect thin cylinders under uniform axial compression assumes that the state of stress before buckling is perfectly uniform and consists of membrane stress alone. The typical load-axial shortening curve is shown in Fig. 2-9 (Rotter, 2004). The dotted line corresponds to a load-axial shortening path of linear bifurcation analysis. The well-known classical elastic critical stress is expressed by Eq. 1.1.

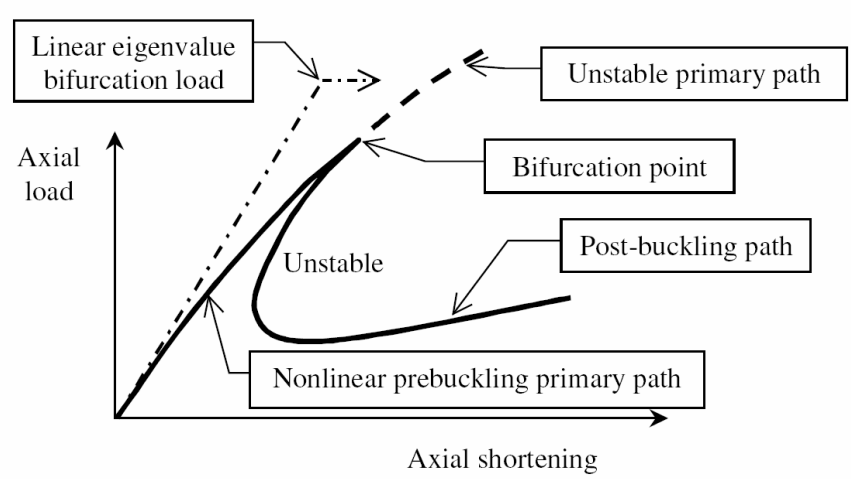

Figure 2-9: Typical load-end shortening relationship for an axially compressed cylinder (Rotter, 2004)

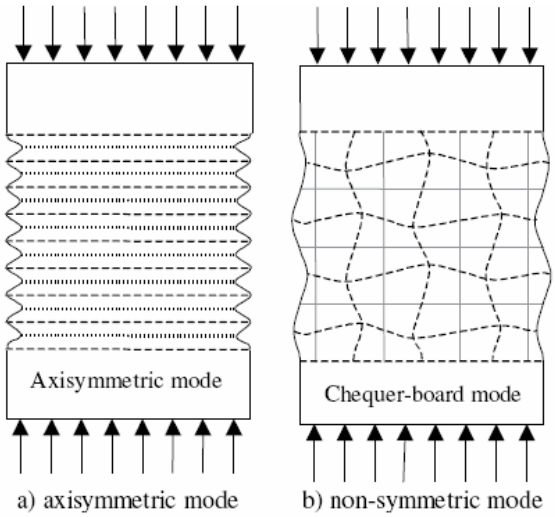

Figure 2-10: Typical buckling modes for axially compressed cylinders (Rotter, 2004)

Through geometrically nonlinear analysis, the load-axial shortening curve shows that the nonlinear pre-buckling primary path displays a very linear path before the bifurcation point. This corresponds to an axisymmetrical mode of deformation. While after the bifurcation point, the cylindrical shell suddenly bifurcates into a non-axisymmetrical mode of deformation, with several full waves of buckling mode around the circumference (Rotter, 2004). This usually includes several waves up the column height (Fig. 2-10b), which corresponds to an unstable post-buckling path in Fig. 2-9. At buckling, the load decreases quickly and the length of the cylinder actually increases. As the load falls, bifurcation after bifurcation occurs as the mode of deformation switches from one circumferential wave number to another in dynamic jumps (Rotter, 2004).

The number of the waves around the circumference and the wavelength of the buckles in both axial and circumferential directions may vary without altering the buckling load much. So a number of modes can be critical simultaneously. The linear axial half-wavelength for an axisymmetric mode (Fig. 2-10a) is given by (Rotter, 2004):

$$\lambda_{cl} = \frac{\pi}{\left[12(1-\upsilon^2)\right]^{1/4}}\sqrt{rt} \cong 1.728\sqrt{rt} \tag{2.13}$$

The critical buckling mode for Fig. 2-10b can be described in terms of the number of full waves around the circumference in this mode, given by (Rotter, 2004):

$$n_{cl} = \sqrt[4]{(3/4)(1-\nu^2)}\sqrt{r/t} \cong 0.909\sqrt{r/t} \tag{2.14}$$

For quite thin shells, the value of n_{cl} is large, and the buckling may occur locally, since the buckle can form in a zone about the size of a single wavelength.

A rather comprehensive research of the effects of end boundary conditions on buckling strength was given by Hoff (1966). The ends of the cylindrical shell had three translational degrees of freedom and one rotational degree of freedom. The restraint of any freedom could affect the displacement and membrane stress during the buckling process. The local bending of the pre-buckling displacement near the ends could lead to a small loss of bifurcation buckling strength.

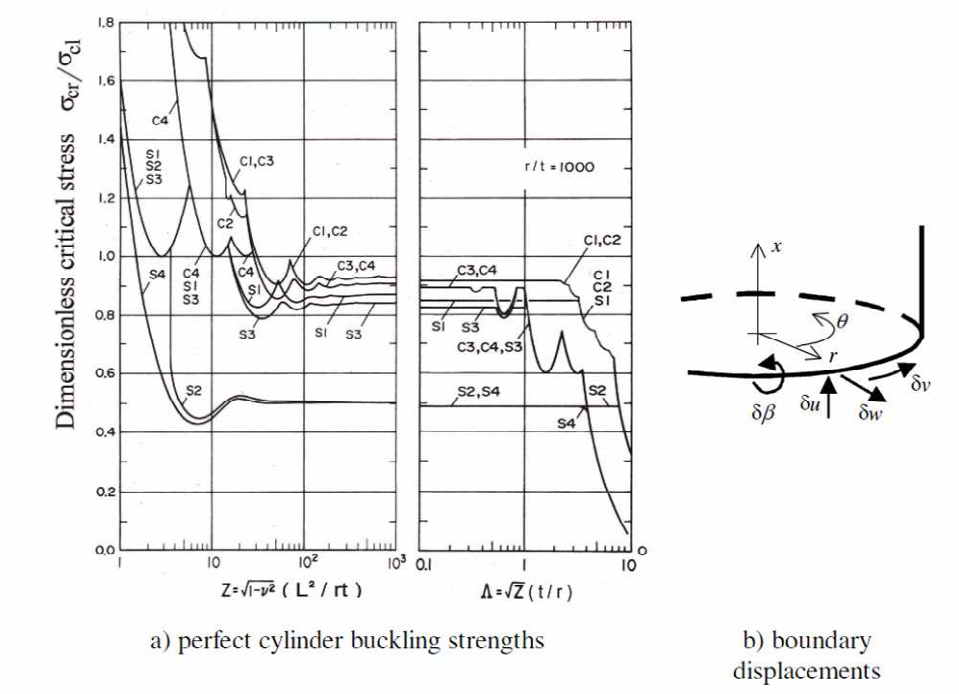

Figure 2-11: Effect of boundary conditions and shell length on perfect shell buckling load (Yamaki, 1984)

More extensive and detailed discussions of the classification of boundary conditions and the influence of different boundary conditions on buckling strength could be found in Yamaki (1984). It was discovered that if the cylinders were free to displace in the circumferential direction, then the perfect shell buckling strength was affected most, falling to about half the classical value. However, the changes of other boundary conditions had a much smaller effect (Yamaki, 1984). The effect of boundary conditions and shell length on perfect shell buckling load derived by Yamaki is shown in Fig. 2-11.

2.6.3 Imperfection sensitivity analysis for elastic cylinders

The imperfection sensitivity analysis for elastic cylindrical shells under axial compression has been widely studied. Koiter (1945) was the first to identify that the imperfection in the form of the perfect shell buckling mode is very deleterious to the buckling strength. He formulated a perturbation analysis theory for axially compressed cylindrical shells which reveals an extreme sensitivity of buckling loads to initial geometrical imperfections. He presented an asymptotic formula for the

bifurcation buckling stress of cylinders under axial compression with small amplitude sinusoidal imperfections in form of axisymmetric buckling mode (Fig.2-10a) as (Koiter, 1963):

$$\sigma_{cr} = \sigma_{cl}\left\{1-\psi\left|\frac{\delta_0}{t}\right|\left[\left(1+\frac{2t}{\psi\delta_0}\right)^{1/2}-1\right]\right\} \tag{2.15}$$

where δ_0 is the amplitude of the imperfection and $\psi = 0.75\sqrt{3\left(1-\upsilon^2\right)} \cong 1.239$.

Rotter and Teng (1989) used a more "practically relevant" weld depression imperfection to study the buckling strength of a cylindrical shell under axial compression. The relationship between the buckling stress ratio σ_{cr}/σ_{cl} and dimensionless imperfection amplitude δ_0/t is shown in Fig. 2-12. The two different types of imperfection including the eigenmode imperfection and Type A weld depression imperfection were considered. The Type A imperfection is defined by (Rotter and Teng, 1989):

$$w_0 = w_0 e^{-(\pi x/\lambda)}\left(\cos\frac{\pi x}{\lambda} + k\sin\frac{\pi x}{\lambda}\right) \tag{2.16}$$

in which x is the axial distance form the weld centre, λ is linear bending half wavelength defined by

$$\lambda = \frac{\pi}{\left[3(1-\upsilon^2)\right]^{1/4}}\sqrt{rt} \cong 2.44\sqrt{rt} \tag{2.17}$$

It is obvious that a minor imperfection has a disproportionate effect on the buckling strength and the buckling strength is affected by both the shape and amplitude of the imperfection.

In Fig. 2-12, it seems the eigenmode imperfection has a more significant effect on the buckling strength than weld depression imperfection, which is not correct. Imperfection amplitudes for different types of imperfection are described in different ways. The eigenmode imperfection is axisymmetric about the axis of perfect geometry, so the maximum inward and outward radial deviations normal to the

surface are equal. By contrast, the weld depression just has inward deviations at the weld depression centre. The imperfection amplitude is the maximum deviation of the imperfection to the axis of perfect geometry. So if the same values of amplitudes are given for these two imperfections, the inward deviations of the two imperfections are equal. But the eigenmode imperfection also has outward deviations, leading to more reduction in the buckling strength.

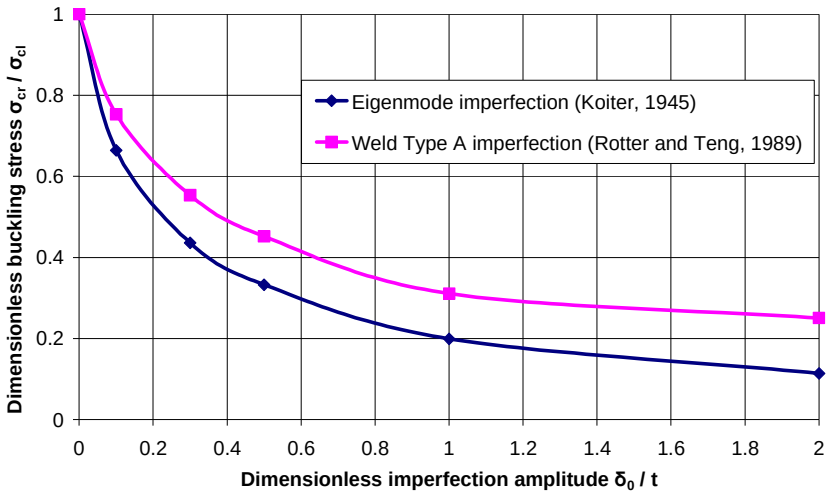

Figure 2-12: Imperfection Sensitivity curves for cylindrical shells under uniform axial compression ($r/t = 500, L/r = 3$)

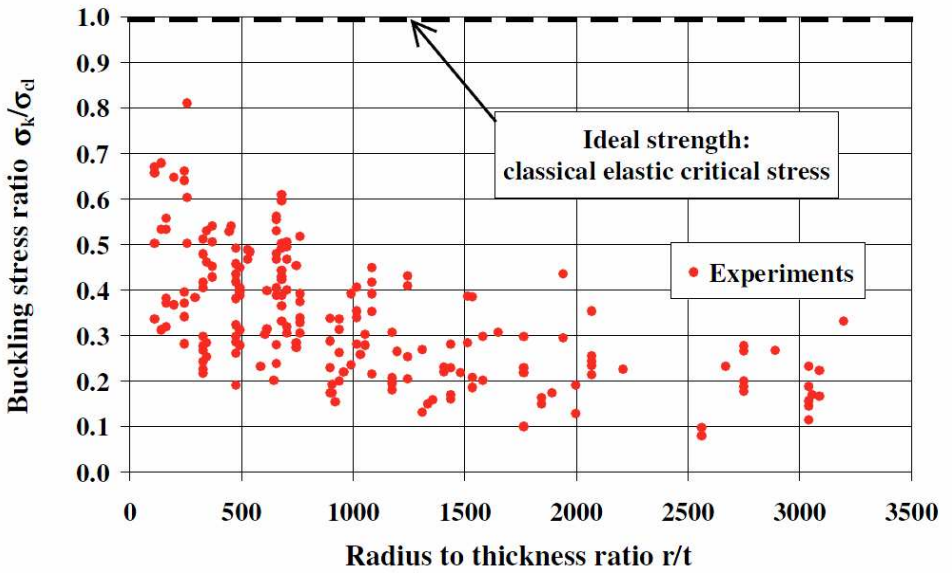

Figure 2-13: Experimental strengths of isotropic axially compressed cylinders (Harris et al., 1957)

The sensitivity of the buckling strength to imperfections explains the low strengths investigated in experiments. The experimental buckling strengths of axially compressed cylinders (Fig. 2-13) are scatted far below the ideal buckling strength for perfect cylinders, which is caused by the indeterminate imperfections during shell fabrication (Harris et al. 1957).

The contributions of imperfections to the discrepancy of the buckling strength between experiment and theory for axially compressed cylinders have led to an enormous amount of research. Yamaki's (1984) study showed that the buckling strength was less sensitive to asymmetric imperfection than that with symmetric imperfection. As a result, most of the research on the imperfection sensitivity study of axially compressed cylinders focused on the effect of the axisymmetric imperfection forms. Some notable research includes Karman and Tsien (1941), Donnell and Wan (1950), Hutchinson (1965), Amazigo (1969), Cohen (1971), Hutchinson *et al*. (1971), Singer (1982), Teng and Rotter (1992), Rotter and Zhang (1990), Rotter (1996, 1997b), Limam et al. (2011).

However, the most "worst" and "practically relevant" imperfection should be determined considering many factors, such as loading conditions, shell geometry or boundary conditions, and most importantly the linear or nonlinear buckling mode of a shell. One imperfection that is most damaging for one particular condition is not necessarily the most damaging one for another (Song et al., 2004). For example, the weld depression imperfection is the most deleterious type for a cylinder under uniform axial compression. However, for an intermediate aspect ratio cylindrical shell under asymmetric wind pressure, the nonlinear buckling mode is a local axial compressive buckling mode at the upper part of the cylinder. In this situation, if the weld depression is occasionally in the buckling area or near the buckling area, then this imperfection can cause a considerable reduction in the buckling strength. By contrast, if the weld depression is far away from the buckling area, its effect decreases (Pircher, 2004). For cylindrical shells under wind pressure, the "worst" and "practically relevant" imperfection is more difficult to be determined than other buckling problems. The buckling analysis of cylindrical shells under wind pressure is discussed in Chapters 6 and 7.

2.6.4 Elastic-plastic imperfection sensitivity analysis

Most literatures on imperfection sensitivity analysis of cylindrical shells under axial compression focused on elastic buckling strength. But for thicker cylinders, yielding and buckling may occur simultaneously and may both affect the failure load. For thin cylinders, elastic bifurcation buckling occurs before the yield stress is reached and the deformation mode changes from an axisymmetric pre-buckling mode to a non-axisymmetric post-buckling mode, called the “diamond” mode (Fig. 2-10b) which displays both axial and circumferential waves throughout the structure (Tvergaard, 1983a, b).

However, for thick shells, yield stress is reached near the ends of the cylinder before elastic bifurcation buckling occurs. Then the local deformation develops at both ends in the form of the outward axial half-waves. The maximum load occurs simultaneously as the axisymmetric deformed shape is localized at both ends. The axisymmetric failure occurs if the bifurcation point is near the limit load, or a non-axisymmetric “elephant foot” failure will occur if the bifurcation point appears at the decreasing primary bifurcated branch. Tvergaard (1983a, b) also showed that the circumferential order of the solution decreases as the radius-to-thickness ratio decreases and that a weak hardening makes either an axisymmetric failure or an “elephant foot” failure easier to occur.

The analysis of the transition between the axisymmetric mode and the “diamond” mode for a perfect cylinder was studied by Goto and Zhang (1999). They found that the boundary conditions are a deciding factor for obtaining various types of buckling modes. They also found two successive bifurcation points for a moderately thick cylinder with built-in ends. The first one of these was on the fundamental branch, near the limit load leading to an axisymmetric mode, while the second one, on the decreasing primary bifurcated branch, led to a localized non-axisymmetric secondary mode, named ‘‘elephant foot’’. The thinner the shell was, the earlier the secondary mode occurred. Thus, if the shell was thin enough, the second bifurcation point superseded the first one, preventing any localization and giving rise to a ‘‘diamond’’ mode. Conversely, if the shell was thick enough, the second bifurcation point disappeared—at least in the computed range—and the failure was very likely

axisymmetric (Goto and Zhang, 1999). The circumferential wave number decreased with thickness. In the case of simply supported ends, the wave was very near the ends, so that, if it existed, the localization never led to a second bifurcation.

Grognec and Van (2008) examined the numerical computations of critical loads, bifurcation modes and the advanced post-buckling behaviour of compressed shells in the elastic-plastic range. They first made comparisons between the numerical results and the available analytical solutions in the case of axisymmetric modes with a linear isotropic hardening or a non-linear isotropic hardening. Then they described the post-buckling behaviour of cylinders and obtained the both axisymmetric and non-axisymmetric deformed shapes. These included the "diamond" modes or the "elephant foot" modes mentioned above. The also explored how the geometric, material parameters and the boundary conditions affect the buckling mode types. They concluded that in the case of sufficiently thick shells and for some combinations of r/t and stress-strain properties, the axisymmetric mode switches into a non-axisymmetric post-buckling mode after the limit load and the second bifurcation mode, or so-called "elephant foot" mode, occurred. While for thin shells, the non-axisymmetric buckling mode, or so-called "diamond" mode, occurred before the limiting load. Bifurcation modes and post-bifurcation behaviour of a cylinder under axial compression are indicated in detail at Table 2-2.

Table 2-3: Bifurcation modes and post-bifurcation behaviours of a cylinder under axial compression (Grognec and Van, 2008)

Cylinders	Simply supported edges	Built-in edges	Free edges
Thick	Sinusoidal axisymmetric mode Post-bif: localization at the ends	Sinusoidal axisymmetric mode Post-bif: localization somewhat far from the ends	Damped sinusoidal axisymmetric mode
Moderately Thick	(Results between those for thick and thin cylinders)	Axisymmetric mode (+localization) "Elephant foot" secondary mode	(Results between those for thick and thin cylinders)
Thin	"Diamond" mode	"Diamond" mode	Damped Sinusoidal non- axisymmetric mode

Rotter (2008b) studied the elastic-plastic imperfection sensitivity of axial compressed cylinders. The cylindrical shells were treated as medium length (EN 1993-1-6, 2007), so the imperfection is far from the ends and the boundary conditions were not important in determining the buckling strength. The perfect elastic-plastic material was used with a yield stress $\sigma_y = 250MPa$. A single axisymmetric Type A weld depression imperfection (Rotter and Teng, 1989) at the centre of the cylinders was adopted. The cylinders with radius to thickness ratios in the range $20 < r/t < 2000$ and with geometric imperfections with amplitudes in the range $0 < \delta_0 / t < 2$ were studied. The buckling strengths for different conditions were explored using the program NEPAS. The results were used to calibrate the parameters of the European standard on Shell Buckling EN 1993-1-6 (2007) to deliver accurate representations of the calculated buckling strengths.

This study tries to investigate the relationship between different failure modes including elastic buckling mode, plastic buckling mode and plastic collapse mode with change of slenderness. The buckling resistance strengths are shown in Fig. 2-14 (Rotter, 2008). The boundaries between the three modes depend almost uniquely on the slenderness. The cylinders with very small geometric imperfections suffer very little from plasticity before reaching full yield because the stress field of uniform compression permits high stresses without yielding.

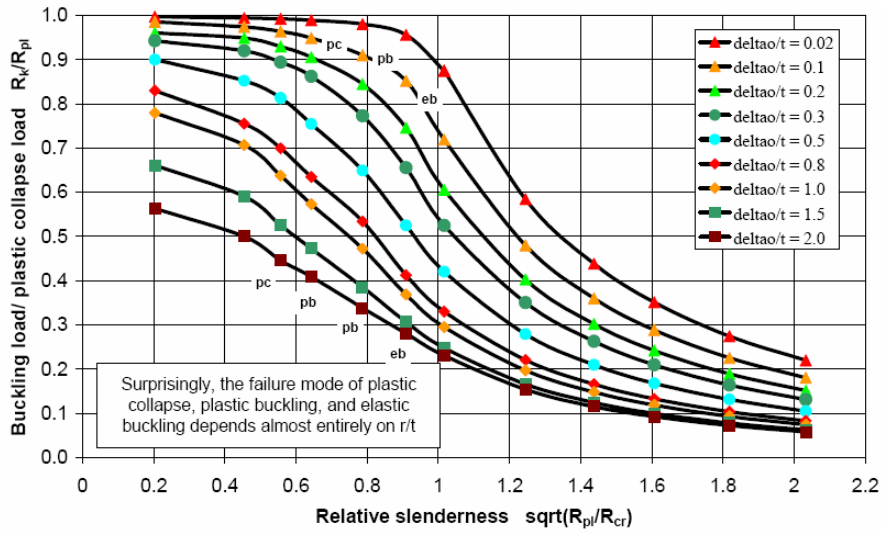

Figure 2-14: Elastic-plastic buckling and collapse strengths of imperfect cylinders (Rotter, 2008)

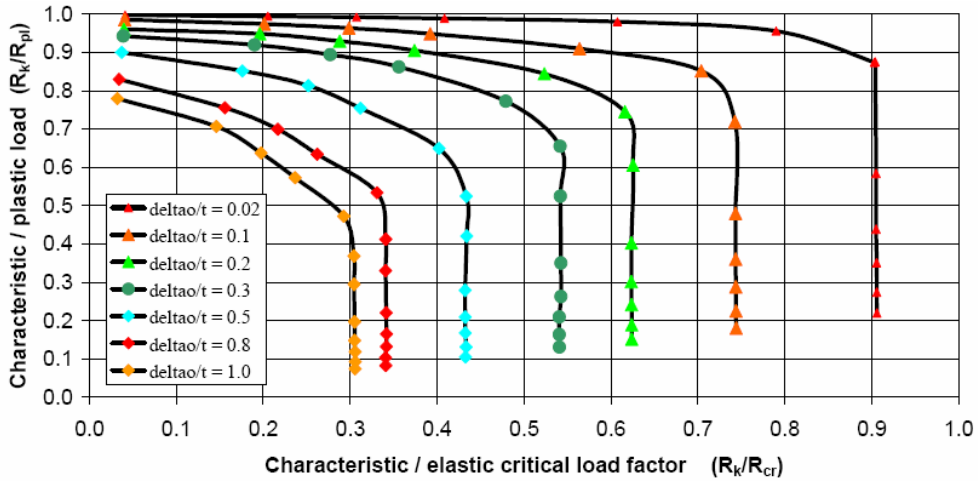

Figure 2-15: Alternative capacity curves for parameter extraction (Rotter, 2008)

The alternative capacity curve is shown in Fig. 2-15 (Rotter, 2008). The elastic imperfection reduction factor can be seen as vertical lines at fixed values of imperfection sensitivity α. These are followed by a sharp change of direction when yielding begins to affect the buckling resistance, which is related to the plastic range factor β. Above this point, the curve shape can be expressed by an interaction exponent η. These parameters can be closely represented by (Rotter, 2008)

$$\alpha = \frac{1}{1 + 2.2(\delta_0 / t)^{0.8}} \tag{2.18}$$

$$\beta = 0.54\sqrt{\delta_0 / t} \tag{2.19}$$

$$\eta = \frac{5.4}{1 + 4.6(\delta_0 / t)} \tag{2.20}$$

The procedure is undertaken not only to capture these strengths with simple relationships, but to illustrate to researchers working on other elastic-plastic buckling problems how they may exploit the EN 1993-1-6 (2007) formulation to their own advantage (Rottter, 2008).

Buckling of circular cylindrical shells under combined axial compression and pressure has also studied by many researchers. Through these studies, it has been repeatedly shown that, when an axially compressed cylinder is internally pressurized,

the tensile circumferential membrane stress reduces the deleterious effects of imperfections and the buckling axial load increases. At very low internal pressures, the cylindrical shell fails near an imperfection by elastic buckling in a mode similar to that for un-pressurized cylinders (Rotter and Teng, 1989). At high internal pressures, the buckling mode becomes axi-symmetric (Fung and Sechler, 1957; Harris et al, 1957; Weingarten et al, 1965; Rotter and Teng, 1989). The changing buckling mode reflects the declining imperfection-sensitivity of the buckling load.

In thin steel cylinders ($r/t > 250$), the buckling collapse stress for axial compression is usually low compared with yield stress, so elastic investigations are directly relevant. However, once the internal pressure becomes significant, high bending as well as membrane stresses arise near the base of the cylinder and local yielding may then occur. This failure mode is commonly known as the 'elephant's foot' buckling (Rotter, 2006). Yielding in a thin cylinder occurs in the zone of local bending adjacent to a boundary support, a change in wall thickness, stiffener, or other local disturbance. The strength appears to be less sensitive to random imperfections.

2.7 Conclusions

In this chapter, some fundamental aspects of shell buckling analysis were introduced. For thin-wall cylindrical shells, the discrepancy between membrane stiffness and bending stiffness is generally of several orders. The big stiffness difference has shown that a steel shell structure would be susceptible to buckling, especially for thin-walled shells (Bushnell, 1985). Due to their low mass and high membrane stiffness, cylindrical shells might have several buckling modes without changing the buckling load significantly. The big difference of in-plane and out-plane stiffness, together with the high buckling modes, would lead to a high sensitivity of buckling strength to imperfections.

The mechanical behaviour of cylindrical shells is quite complex, especially when the cylinder is subjected to asymmetric loading conditions. It is more complicated when geometric and material nonlinearities are considered. As a result, only some fundamental problems in the area of shell buckling analysis can be accurately solved

theoretically. In most situations, computational methods, commonly including the finite element methods which are based on the basic nonlinear shell theory, have to be adopted to obtain accurate numerical results. Engineers and researchers should have a good understanding of the buckling behaviour of the shells and pay attention to every possible factor that may affect the buckling behaviour, such as the mesh, the elements, the boundary conditions and the analysis method, etc. Any possible checks with other reliable analytical or experimental results are necessary.

Cylindrical shell under axial compression is one of the most common problems in shell buckling analyses. Previous researches were summarised and an imperfection sensitivity analysis was performed to give a general understanding of the shell buckling behaviour. However, this thesis focuses on the buckling behaviour of cylindrical shells under other common loading conditions, such as global bending, uniform external pressure and asymmetric wind pressure. Many practical buckling problems are discussed next.

Chapter 3 Nonlinear Stability Analysis of Elastic Cylinders under Global Bending

3.1 Introduction and literature review

Many cylindrical shells are used in structural applications in which the dominant loading condition is global bending. Key examples are chimneys, wind generation towers, tubular piles and tall silos. The failure of these thin-walled structures in bending is an active research area in recent decades. The theoretical maximum bending stress that will cause buckling of a cylindrical shell was commonly accepted as being equal to 1.3 times the classic elastic critical stress for uniform compression (Flugge, 1932; Timoshenko, 1932). However, Seide and Weingarten (1961) later investigated the stability of circular cylindrical shells under pure bending by means of Batdorf's modified Donnell's equation and the Galerkin method. Their results showed that the maximum critical bending stress is for all practical purposes equal to the critical compressive stress, when the ratio of bending and compressive stresses is minimized with respect to the wave length. Seide and Weingarten's results (1961) described the local buckling in a good manner for short cylinders with relatively little ovalization as the bending moment increases.

For long elastic thin-walled cylinders subjected to pure bending, the cross-section tends to take on an oval shape as the bending moment increases. This results in a loss of bending stiffness and a limit point instability, called snap-through buckling. This phenomenon is also termed the Brazier effect, after the original research of Brazier (1927).

Brazier's work used a simplified theory, but was later verified by Reissner (1959 and 1961) and Fabian (1977), who used the "large deflection" nonlinear shell theory to derive an accurate nonlinear solution. Brazier's solution agreed quite well with the accurate nonlinear solution. Axelrad (1962) investigated the instability behaviour of cylindrical shells in bending according to a nonlinear flexible shell theory. Calladine (1983) used a "two stage" energy method to discuss the Brazier effect in a circular tube and his results were exactly the same as those found by Brazier. Other major

research on the ovalization instability of cylindrical shells in bending can be found in Kyriakides and Shaw (1982), Axelrad and Emmerling (1984), Tang (1984), Corona and Kyriakides (1988) and Karamanos and Tassoulas (1991).

The critical bending moment obtained by Seide and Weingarten for short cylinders with little ovalization is almost double Brazier's maximum bending moment for an infinitely long cylindrical shell with Brazier ovalization of the cross-section (Calladine, 1983). However, in terms of intermediate long cylinders, the response of the structure involves a coupling of ovalization instability and bifurcation instability. With increasing length, the amount of ovalization of the cross-section increases, but the Brazier critical ovalization is not achieved, and the elastic critical bending moment falls steadily towards the value corresponding to an infinitely long cylinder.

For cylindrical shells in bending, much research has been presented on the relationship between the ovalization instability and bifurcation instability. Akselrad (1965) first considered the interaction of the above two forms of instability and introduced the effect of ovalization as a pre-buckling deformation on the local buckling. Local buckling was assumed to occur when the maximum compressive stress at most compressed fibre reached the critical value for uniform compressed cylinders, with radius equal to the local radius of the ovalized shell at the "critical" point.

Calladine (1983) extended Brazier's original calculations by adding the "local buckling" condition, and examined the effect of internal or external pressure in combination with bending moment. Tatting et al. (1995) concluded that local buckling almost always occurs before the limit moment is reached for finite length shells.

Li (2002) investigated the nonlinear bending response and buckling of ring-stiffened cylindrical shells under pure bending, using a modified Brazier approach based on the minimum potential energy principle and Seide-Weingarten's approximation.

Karamanos (2002) examined instability in long thin elastic tubes in bending. The relationship between the curvature and the development of ovalization was analyzed in detail. Houliara and Karamanos (2006) studied a long elastic tubular shell in bending using nonlinear finite element techniques. They concluded that in elastic cylinders, bifurcation into a non-symmetric buckling mode also occurs shortly before the snap-though buckling condition, but the moment at the bifurcation point and at the snap-though instability point are so close as to be almost indistinguishable. Other major studies include Brush and Almroth (1975), Stephens et al. (1975), Chen and Kempner (1976), Libai and Bert (1994).

Limam et al. (2006, 2010) studied the buckling behaviour of both thick and thin cylindrical shells under combined bending and internal pressure using an experimental method. It concludes that internal pressure can significantly stabilize the structure by delaying localization and collapse. It may lead to a collapse load higher than the buckling stress for cylinders in moderate length.

Based on current research, for elastic cylindrical shells under global bending, except extremely short cylinders, the failure strength is mainly dominated by local bifurcation buckling caused by axial compressive stress at the most compressed fibre, with a consideration of the effect of a pre-buckling ovalization of the cross-section. The aim of this chapter is to explore this nonlinear instability behaviour in elastic cylinders in pure bending. Cylinders with different length to radius ratios and radius to thickness ratios are studied to investigate this instability behaviour comprehensively. The effect of ovalization of the cross-section on the buckling behaviour of cylinders with different geometries is discussed. The effect of a geometric imperfection on the buckling strength of a long cylinder with $r/t = 80$ is also investigated.

3.2 Theoretical solutions for elastic cylindrical shells subjected to global bending

When a thin cylindrical shell is subjected to global bending, one side experiences relatively uniform axial compressive stresses while the other experiences relatively

uniform axial tensile stresses. The deformation pattern of a cylinder in bending is shown as Fig. 3-1.

The size of typical buckles under axial compressive stress regimes is rather small and extends over a very small zone, with the axial compressive stress reaching the critical value. The critical value must extend over a zone large enough to form an axial compressive buckle. So the first estimate of the elastic buckling strength in bending is the condition in which the most compressed fibre reaches the buckling stress for uniform axial compression.

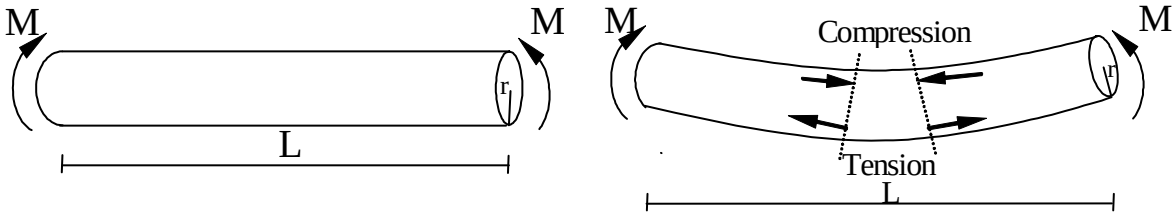

(a) Un-deformed form (b) Deformed form

Figure 3-1: Deformation of cylinders in bending

For a perfect short cylinder, the buckling load of a circular cylinder in bending was determined by Seide and Weingarten (1961) using Batdorf's modification of Donnell's equation which is expressed as:

$$Q(w) = D\nabla^4 w + \frac{Et}{r^2}\nabla^{-4}\frac{\partial^4 w}{\partial x^4} - t\left(\sigma_x \frac{\partial^2 w}{\partial x^2} + \sigma_\theta \frac{1}{r^2}\frac{\partial^2 w}{\partial \theta^2} + 2\tau_{x\theta}\frac{1}{r}\frac{\partial^2 w}{\partial x \partial \theta}\right) = 0 \qquad (3.1)$$

where $\nabla^4 = operator\left(\frac{\partial^4}{\partial x^4} + \frac{2}{r^2}\frac{\partial^4}{\partial x^2 \partial \theta^2} + \frac{1}{r^4}\frac{\partial^4}{\partial \theta^4}\right)$; ∇^{-4} is inverse operator by $\nabla^{-4}\left(\nabla^4 f\right) = f$.

The Galerkin method was then used to derive the stability criterion, by assuming a radial deflection w given in terms of an infinite series as

$$\omega = \sin\frac{m\pi x}{L}\sum_{n=0}^{\infty} a_n \cos n\theta \qquad (3.2)$$

Seide and Weingarten's method (1961) assumed a linear undeformed pre-buckling state and did not consider the effect of the ovalization of the cross-section.

So it is applicable to short cylinders without ovalization before bifurcation buckling occurs. Their results verified that the bending stress for the critical moment is equal to the buckling stress for uniform compression. Based on their solution, the critical buckling moment and the corresponding bending stress could be estimated directly according to Eqs 3.3 and 3.4. They were based on the linear Euler bending theory for beams and the "classical buckling stress" expression for cylinders under uniform axial compression, respectively. The moment and stress values were given by:

$$M_{cr} = \pi r^2 t \sigma_{cl} = \pi \left[\frac{E}{\sqrt{3(1-\nu^2)}} \left(\frac{t}{r} \right) \right] r^2 t = 1.814 \left(\frac{E}{\sqrt{1-\nu^2}} \right) t^2 r \cong 1.90 E t^2 r \tag{3.3}$$

$$\sigma_{cl} = \frac{E}{\sqrt{3\left(1-\nu^2\right)}} \left(\frac{t}{r} \right) \cong 0.605 \frac{Et}{r} \tag{3.4}$$

For an infinitely long cylinder in bending, a limit point occurs as a result of ovalization. The critical bending moment, called the Brazier moment (Brazier, 1927), was obtained from the minimum strain energy principle, and can be expressed as:

$$M_{Braz} = 0.987 \left(\frac{E}{\sqrt{1-\nu^2}} \right) t^2 r \cong 1.035 E t^2 r \tag{3.5}$$

However, the increased axial stress on the compression side, which is concentrated locally due to ovalization will cause bifurcation instability at a lower moment than that given by Eq. 3.5. The results of Hutchinson (1968), Reddy and Calladine (1978), Tatting et al. (1995) and Karamanos (2002) have all verified that the bifurcation buckling caused by axial compressive stress after some ovalization occurs before the Brazier moment is reached in long cylinders. However, the values of the critical moment at the bifurcation point and at the Brazier maximum moment are very close.

For intermediate long cylinders, bifurcation buckling occurs with less ovalization of the cross-section as the ovalization is partly restrained by the end boundaries. At the bifurcation point, the axial compressive stress on the most compressed fiber (Fig. 3-1b) should be equal to the buckling stress for a uniformly compressed cylinder

with a radius equal to the local radius of the cross-section with ovalization, at the point where the compressive stress is greatest. The critical bending stress should be calculated by replacing the radius r in Eq. 3.4 by the local radius ρ as

$$\sigma_{cr} \cong 0.605\frac{Et}{\rho} \tag{3.6}$$

Calladine (1983) assumed a "two stage" deformation process based on the energy method to derive the critical bending moment for finite length cylinders in bending. The relationship between the dimensionless moment $M_{\lim} / M_{cr}$ and the dimensionless length parameter Ω is shown in Fig. 3-2, where $M_{\lim}$ is the maximum bending moment that varies with the length and M_{cr} is expressed by Eq. 3.3 and Ω is given by

$$\Omega = (L / r)(t / r)^{1/2} \tag{3.7}$$

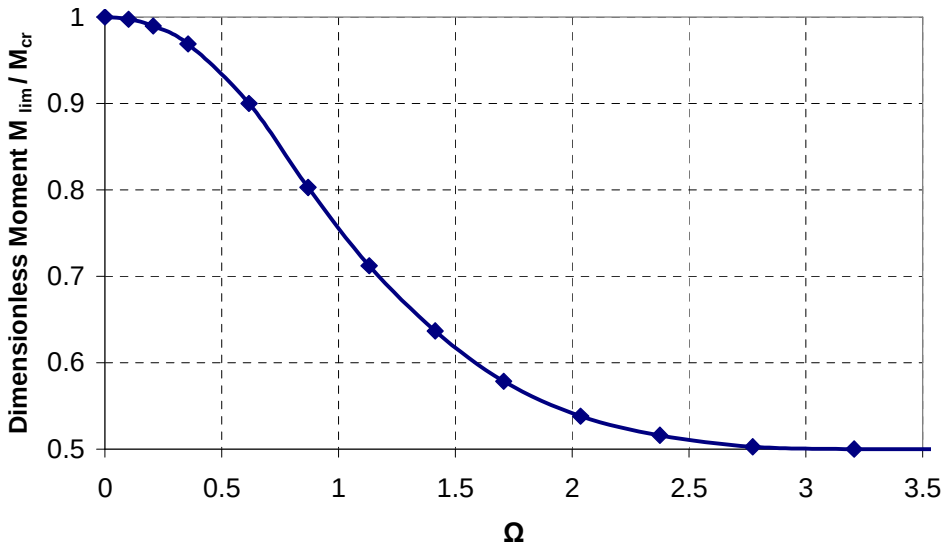

Figure 3-2: Relationship between the dimensionless moment $M_{\lim} / M_{cr}$ and the dimensionless parameter Ω (after Calladine, 1983)

Calladine's solutions (1983) were based on cylinders in the range $L / r > 3$, so that only the circumferential bending strain energy and longitudinal stretching strain energy were considered. So Calladine's results are not accurate enough for very short cylinders when the shear strain energy cannot be neglected.

Li (2002) investigated the nonlinear bending response of finite length cylindrical shells with stiffening rings based on a modified Brazier approach and the Rayleigh-Ritz method. The deformation of the shell was assumed to be quite small compared with the radius of the cylinder, so the strain-displacement relationships could be expressed in a comparatively simple way.

However, for long cylinders, the cross-section experiences considerable ovalization before buckling, so more complex nonlinear strain-displacement relationships have to be considered to obtain accurate results. This makes theoretical calculations more complex and difficult. Fortunately, powerful nonlinear finite element analysis software makes many complex problems in shell buckling analysis much easier to solve and it can usually be used to obtain accurate results with careful modelling. Thus the complex theoretical derivation process can be avoided.

Through this chapter, a cylinder of finite length L is subjected to rotations at both ends of θ, leading to uniform bending moments throughout the length. If the deformation is completely uniform along the length, all sections are subject to the same curvature, but the local changes of deformation near the boundaries, variations in the ovalization along the length, the appearance of bifurcation buckles, and local deformations associated with an imperfection, all lead to non-uniformity of the curvatures. To make the interpretation simple, uniform and clear, all the deformations are expressed in terms of the mean curvature

$$\phi = \frac{2\theta}{L} \tag{3.8}$$

3.3 Scope of the calculations

Nonlinear stability analyses of cylinders in bending were undertaken with radius to thickness ratios in the range $10 \le r/t \le 500$. The length to radius ratio was varied from a very small value to a very large value to investigate the different buckling behaviours at different lengths. The dimensions were all expressed in terms of the wall thickness *t*. The material was elastic mild steel with $E = 2.0 \times 10^5 MPa$ and $\nu = 0.3$. The end boundaries were subjected to a global moment and were kept

circular using rigid rings. To realize such boundaries in ABAQUS, one reference point was first established at the centre of both top and bottom cross-sections respectively, then “COUPLING” command was used to impose a kinematic coupling constraint between the reference node and the corresponding group of nodes located on top and bottom surfaces. It must be used in conjunction with the “KINEMATIC” option. All the displacements were restricted, the rotation in the direction of applied moment was free, and the other rotations were restricted. Finally, a displacement boundary condition by giving a value of rotation was imposed to realize the required loading conditions.

For the imperfection sensitivity analysis, Rotter and Teng's (1989) axi-symmetric Type A weld depression imperfection was adopted and was assumed to be a single local feature, not interacting with any other imperfections. Due to the symmetry, a 180° half cylinder model is adequate to model the problem accurately (Fig. 3-3). A very fine finite element mesh with element sizes equal to $0.25\sqrt{rt}$ was used to accurately capture the local buckling behaviour.

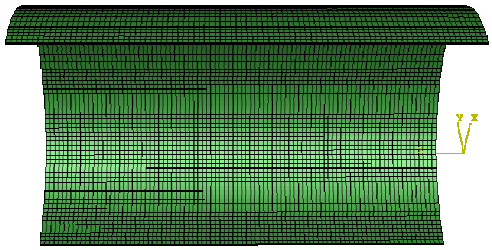

Figure 3-3: Finite element model for cylinders in bending

3.4 Numerical results

3.4.1 Dimensionless moment-curvature curves

Cylinders with a fixed radius to thickness ratio but of different lengths were studied first. The changing form of the calculated moment-curvature curves for cylinders with radius to thickness ratio $r/t = 10$ is shown in Fig 3-4, because this plot shows moment against curvature, all curves begin with the same slope EI. The value of the applied moment is normalized by the critical elastic bending moment

M_{cr} (Eq. 3.3) as $m = M/M_{cr}$. The curvature is normalized as $\kappa = \phi/\phi_{cr}$, where ϕ is the mean curvature throughout the cylinder and ϕ_{cr} is calculated according to the linear bending theory as

$$\phi_{cr} = \frac{t}{r^2\sqrt{3(1-\nu^2)}} \tag{3.9}$$

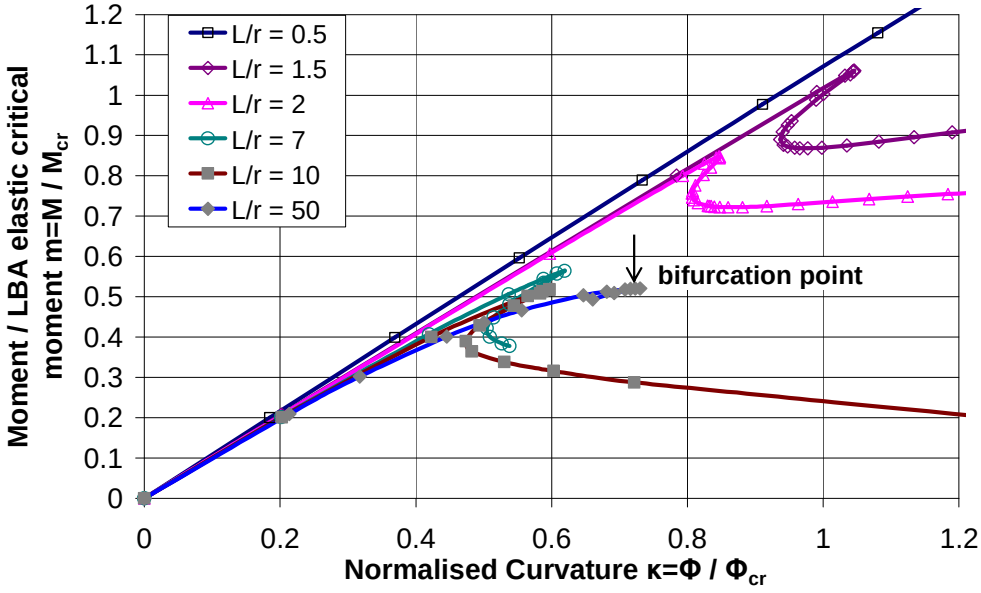

Figure 3-4: Dimensionless moment-curvature curves for cylinders in bending (*r / t=10*)

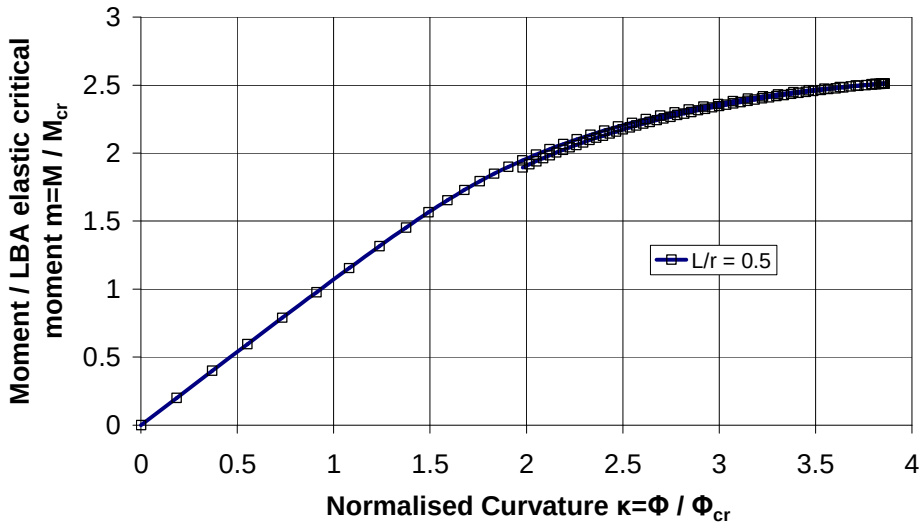

Figure 3-5: Moment-curvature curves for cylinders with *L / r=0.5* and *r / t=10*

For extremely short cylinders (e.g. $L/r = 0.5$), the half wavelength of the buckle is long, so that the buckle is restrained by the boundary conditions, and the critical bending moment may exceed the elastic critical moment M_{cr} and the dimensionless moment parameter m can reach a large value at the limit point. This occurs for $L/r = 0.5$ with $m = 2.51$, as shown in Fig. 3-5. The reason for this high moment is the constraint on the buckle size caused by the two very close boundary conditions. Local buckling occurs near the two ends of the cylinder and two buckles are clearly detected (Fig. 3-6a). The post-buckling path is particularly sharp. After the bifurcation point, the curve traces the original pre-buckling path with decreasing load, and pre-buckling and post-buckling path have similarities of deformation.

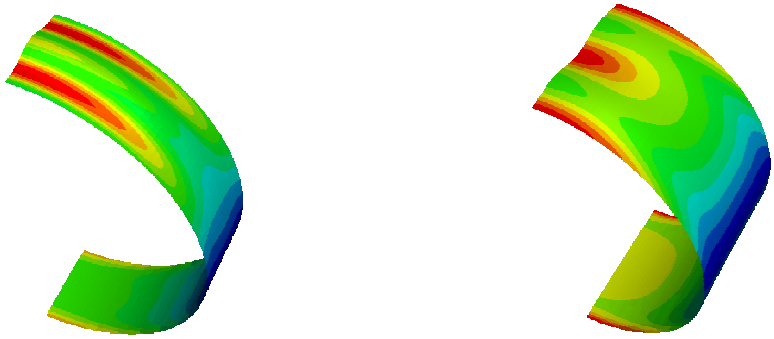

(a) $L/r = 0.5$ (b) $L/r = 1$

Figure 3-6: Buckling modes for very short cylinders

With a small increase in L/r, the bending effect near the ends quickly decays (Fig. 3-6b for $L/r = 1$). The most compressed fibre is located at the centre of the shell causing local bifurcation buckling which dominates the buckling behaviour. But, to some extent, the half wavelength of the axial buckle is still long and bifurcation buckling is still restrained by the boundaries. The buckling stress required to form an axial compressive buckle is somewhat larger than the classical value for medium-length cylinders under axial compression, which is independent of the boundary conditions. Bifurcation buckling for $L/r = 1$ occurs at the centre of the shell and the critical bending moment is about 1.35 times M_{cr}.

With increasingly larger values of L/r (e.g. $L/r = 1.5$), bifurcation buckling occurs when the moment is $1.06\,M_{cr}$. The strength is limited by bifurcation buckling with a steep post-buckling fall, quickly followed by a recovery (Fig. 3-4). The value

of the limit moment is close to M_{cr} indicating that the critical bending stress is close to the critical stress for a cylinder under axial compression. Also, the local deformations near the boundary condition almost have no effect on the buckling strength. The curvature at the critical load is close to that according to linear bending theory. For a cylinder with a typical geometry, boundary conditions affect the buckling strength insignificantly and the ovalization of the cross-section before bifurcation buckling is negligible. The critical bending moment can be estimated approximately according to Seide and Weingarten's (1961) analysis.

With a further increase of L/r ($L/r = 2$ in Fig. 3-4), bifurcation buckling occurs when the dimensionless moment parameter m reaches 0.85. The critical bending moment is less than the elastic critical moment M_{cr}, which indicates that the cross-section becomes oval to some extent when bifurcation buckling occurs. The local radius of curvature of the shell increases due to the oval distortion and thus leads to a reduction in the axial compressive resistance and the critical bending moment.

With a further increase in L/r, the effect of ovalization of the cross-section on the buckling strength becomes more noticeable. The buckling behaviour is a coupling between the flattening of the cross-section and the formation of short wavelength bifurcation buckles. Bifurcation buckling has a more precipitous post-buckling fall for larger values of L/r. As the length increases, progressively more ovalization occurs, producing an increased local radius of curvature near the potential buckling area and the effect of geometric nonlinearity leads to a steady decrease in the axial compressive resistance and the critical bending moment. For a long enough cylinder, the critical bending moment occurs when the ovalization approaches the Brazier critical value, so the critical bending moment has no obvious change with further increase in L/r. The critical bending moment is very close to the value corresponding to an infinitely long tube. For long cylinders, the bifurcation buckling point appears just before the snap-through buckling point. Buckling occurs quite locally and the half wavelength of the buckle is quite small, making the post-buckling path difficult to follow.

The same moment-curvature curves can alternatively be shown as in Fig 3-7. Here the value of the moment is normalized by the Brazier moment as $m' = M / M_{Braz}$. The curvature is normalized as $\kappa' = \phi / \phi_{Braz}$, where ϕ_{Braz} is the curvature when Brazier moment is reached and is calculated according to the linear bending theory as

$$\phi_{Braz} = 0.314 \frac{t}{r^2 \sqrt{1-\nu^2}} \tag{3.10}$$

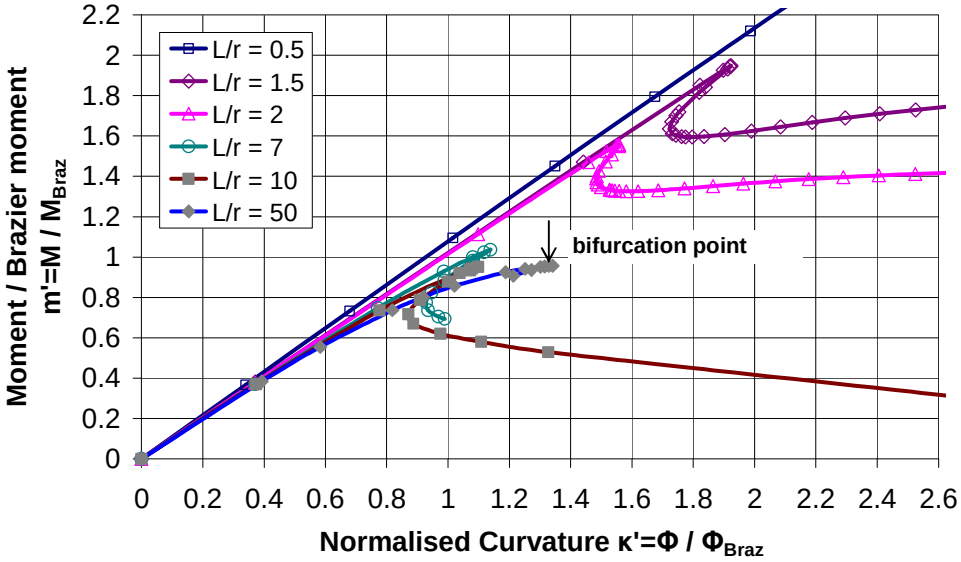

Figure 3-7: Dimensionless moment-curvature curves for cylinders in bending (*r / t=10*)

The characteristics of the curves are the same as Fig. 3-4, but the values of the coordinates have different meanings. When m' is close to 1, it means that the critical moment approaches the Brazier moment and bifurcation buckling occurs with Brazier critical ovalization of the cross-section. When $m' > 1$, it means the critical moment is larger than the Brazier moment due to the restraint of ovalization by the boundary conditions. It can also be noted that for long cylinders with Brazier critical ovalization, the dimensionless curvature κ' at critical load is larger than 1, which is due to the reduced tangential modulus during deformation caused by geometric nonlinearity, but ϕ_{Braz} is calculated based on linear bending theory.

Load-displacement curves for cylinders with $r/t = 50$ are shown in Figs 3-8 and 3-9. These two figures are almost identical because M_{cr} and M_{Braz} are closely

related. The relationship between the dimensionless critical bending moment and the corresponding curvature parameter has similar characteristics as for $r/t=10$.

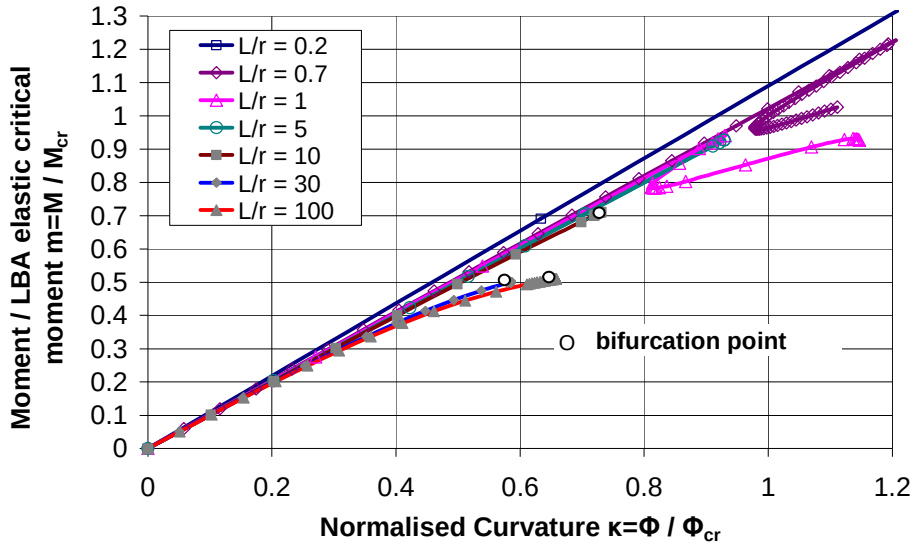

Figure 3-8: Dimensionless moment-curvature curves for cylinders in bending (*r / t=50*)

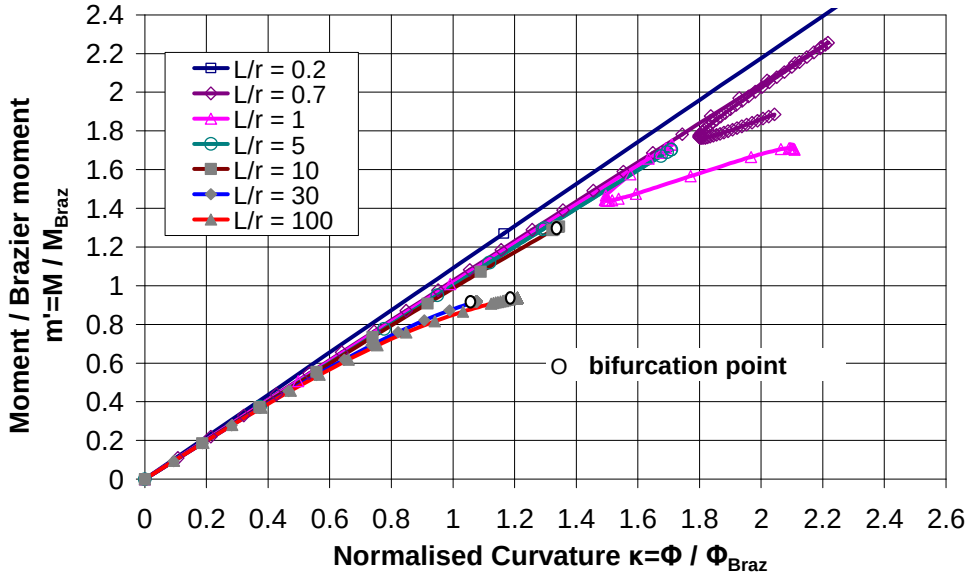

Figure 3-9: Dimensionless moment-curvature curves for cylinders in bending (*r / t=50*)

3.4.2 Maximum critical bending moment prediction for cylinders with different geometries

Taking the maximum moment from each of the moment-curvature curves, the relationship between the dimensionless moment $m_{\lim}=M_{GNA}/M_{cr}$ and the length

parameter ω is shown in Fig. 3-10. In this figure, M_{GNA} is the critical bending moment derived from elastic geometrically nonlinear analysis (GNA), and ω is the dimensionless length parameter, expressed as

$$\omega = \frac{L}{\sqrt{rt}} \tag{3.11}$$

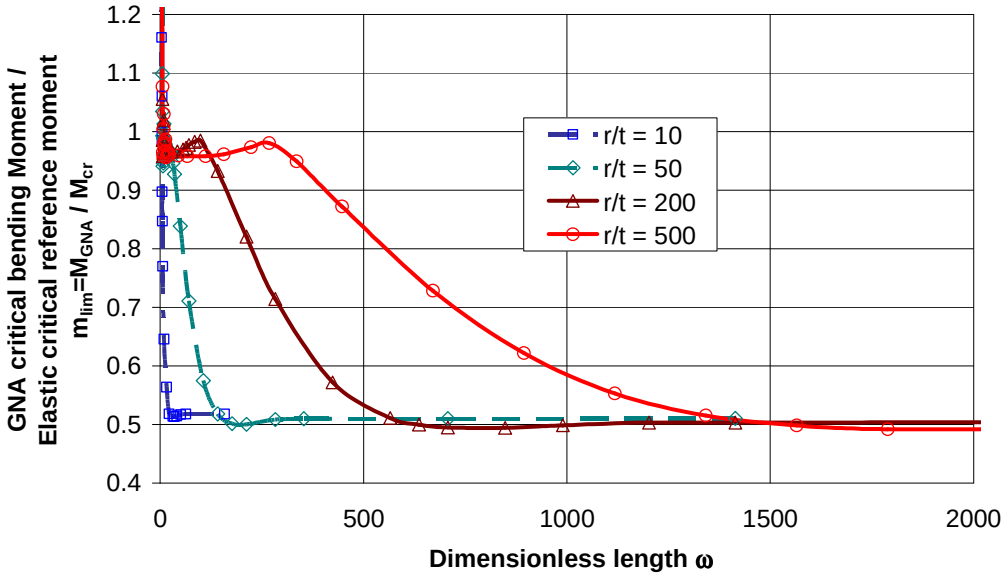

Figure 3-10: Relationship between the dimensionless moment $m_{\lim}$ and the length parameter ω

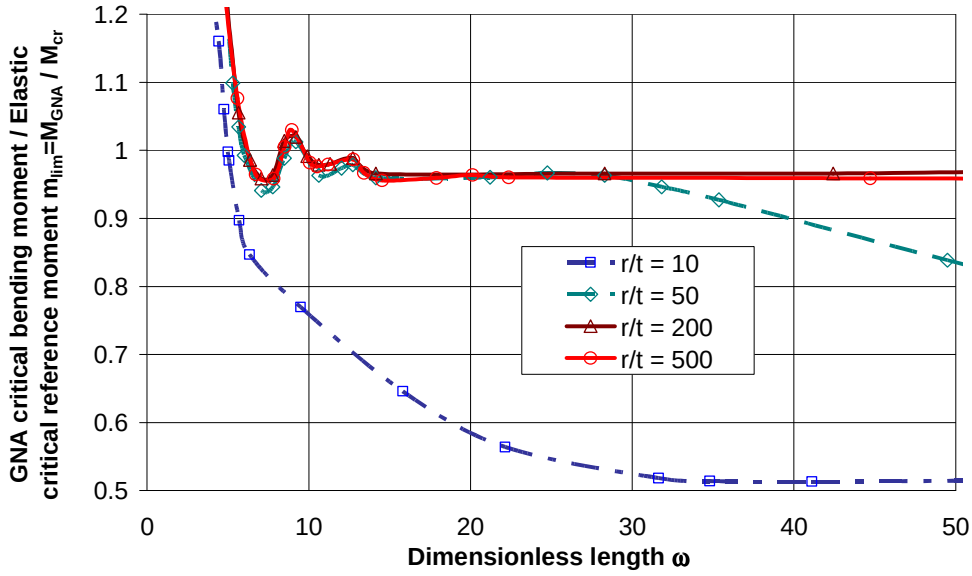

Figure 3-11: Relationship between the dimensionless moment $m_{\lim}$ and the length parameter ω for short cylinders (Detail of Fig. 3-10)

The detail of Fig. 3-10 for short cylinders is shown in Fig. 3-11. The critical moment-length relationship curves for short cylinders with different values of r/t are seen to be identical if the length is expressed in terms of the dimensionless length parameter ω (Fig. 3-11). The only exception to this is the extremely thick cylinder with $r/t=10$, which is discussed further below. For extremely short cylinders, the values of $m_{\lim}$ increase quickly with decreasing length. This is because the boundaries restrain the development of the buckle greatly for these cylinders and thus increase the critical bending moment significantly.

When the cylinder length is not extremely short and lies in an intermediate range, the value of $m_{\lim}$ is close to 1, which indicates that the critical elastic bending moment (GNA) is close to the reference elastic critical moment M_{cr} . This corresponds to the analysis of Seide and Weingarten (1961). They analysed cylinders with radius to thickness ratios in the range $100<r/t<1000$ and drew the conclusion that for relatively short cylinders, the critical bending stress is not more than 10% greater than that for pure compression.

The exception in Fig. 3-11 is for thick cylinders with $r/t=10$, for which the critical bending moment has a more rapid reduction with increasing ω. This indicates that the critical moment in thicker cylinders is more prone to the influence of ovalization of the cross-section at short lengths. But for very thick and short cylinders, due to the high stress concentration on the most compressed fibre, plasticity should be involved in the buckling behaviour. So it is not important that the curve for $r/t=10$ is not consistent with other curves in Fig. 3-11.

It is interesting to note that the curves in Fig. 3-11 have several waves, as described in detail by Seide & Weingarten (1961). This phenomenon is associated with the changing relationship between the cylinder length and the buckle wave length.

For short cylinders with $r/t\geq 50$ in the range $7<\omega<30$, most values of $m_{\lim}$ are slightly less than 1 (Fig. 3-11). This drop is due to the slight effect of geometric nonlinearity caused by bending on the buckling strength M_{GNA}, since M_{cr} is

calculated using the linear bending theory of shells without consideration of any influence of geometric nonlinearity.

With a further increase in L/r, the value of ω at which the ovalization of the cross-section begins to affect the buckling behaviour is different for each value of r/t. For thick cylinders with $r/t = 10$, the oval distortion starts to affect the buckling strength from a very small value of ω. By contrast, for thinner cylinders with $r/t = 500$, this effect intervenes at a very large value of ω. For cylinders under global bending, the value of ω at which the oval distortion starts to affect the buckling behaviour is here defined as the boundary between short and medium-length cylinders.

Table 3-1: The length boundary ω between short and medium-length cylinders under global bending

r/t	L/r	ω (Global bending)	$\omega = 0.5r/t$
10	1.58	5	5
50	3.5	28	25
200	7	99	100
500	12	268	250

The value of ω at which the ovalization begins to affect the buckling behaviour for different values of r/t is shown in Table 3-1. The definition of the boundary between medium-length and long cylinders under uniform axial compression in EN 1993-1-6 (2007) is $\omega = 0.5r/t$ (Table 3-1).

It is clear that that the values of ω that define the boundary between short and medium-length cylinders under global bending, are close to the values of $\omega = 0.5r/t$, which is used to define the boundary between medium-length and long cylinders under uniform axial compression, so $\omega = 0.5r/t$ can also be used to define the boundary between short and medium-length cylinders under global bending. According to this definition, the critical strength of medium-length cylinders under global bending is influenced by the pre-buckling ovalization deformation while the critical strength of medium-length cylinders under uniform axial compression is quite naturally not affected by any comparable pre-buckling geometric nonlinearity.

When the value of ω exceeds $0.5r/t$, the dimensionless moment m_{lim} begins to decrease steadily with further increase of ω due to the effect of ovalization of the cross-section. It is clear that this effect starts at different values of ω for different r/t and that the moment-length curves cannot be brought together using the length parameter ω, as is shown in Figs 3-10 and 3-11. The length parameter Ω (Eq. 3.7) is then adopted to find a unifying relationship between the critical moment and the length that is valid for all values of r/t.

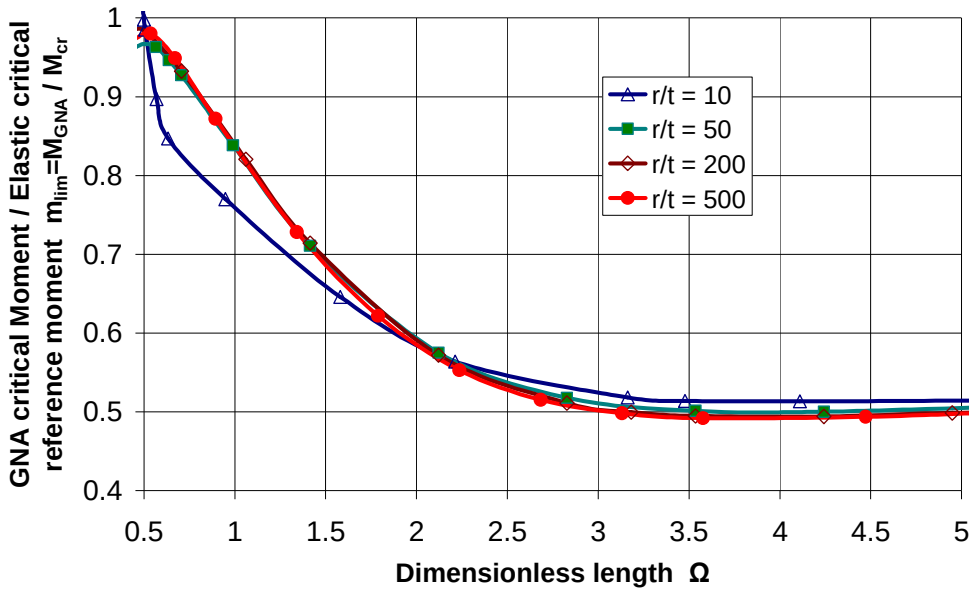

Figure 3-12: Relationship between the dimensionless moment m_{lim} and the length parameter Ω for medium-length and long cylinders

The relationship between the dimensionless critical moment m_{lim} and length parameter Ω for medium-length and long cylinders is shown in Fig. 3-12. In the range $0.5 \le \Omega \le 3$, a combination of ovalization instability and bifurcation instability occurs. The elastic critical moment falls steadily with increasing Ω, as does the amount of ovalization of the cross-section in the local buckling zone. With increasing Ω, the critical moment falls steadily towards a constant corresponding to an infinitely long tube.

The boundary between medium-length cylinders with partial ovalization of the cross-section and long cylinders with Brazier critical ovalization of the cross-section

at the critical bending moment can be defined approximately at $\Omega = 3$. Details of the curves in the range $2 < \Omega < 9$ are shown in Fig. 3-13, where the dimensionless moment parameter $m_{\lim}$ is replaced by $m'_{\lim} = M_{GNA} / M_{Braz}$. The value of $m'_{\lim}$ is smaller than 1 for long cylinders with Brazier critical ovalization, indicating that the elastic critical moment for long cylinders is slightly smaller than the Brazier moment. When $r/t \geq 200$, the dimensionless moment $m'_{\lim}$ with Brazier critical ovalization stabilises on 0.92 (slightly smaller for thinner cylinders). For thicker cylinders, the corresponding value is slightly larger than 0.92 (0.936 for $r/t = 50$ and 0.95 for $r/t = 10$). There are two reasons for this. One is that the M_{GNA} calculated here is the critical value at the bifurcation buckling point, which always occurs before the Brazier moment. The other reason is that the value of $m'_{\lim}$ depends slightly on the value of the radius to thickness ratio. This is because the effect of geometric nonlinearity in the pre-buckling phase depends slightly on *r/t*.

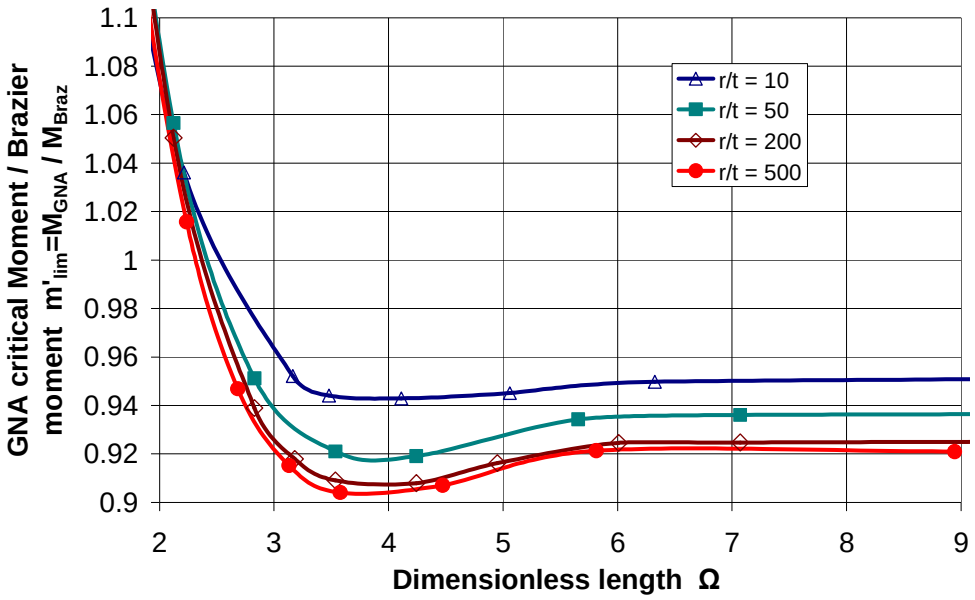

Figure 3-13: Relationship between the dimensionless moment $m'_{\lim}$ and the length parameter Ω for long cylinders

3.5 Imperfection-sensitivity analysis for long cylinders

For cylinders under uniform axial compression, the buckling strength is quite sensitive to geometric imperfections. Both the shape and amplitude of the

imperfection play major roles in shell buckling analysis. As mentioned in Chapter 2, there has long been a debate concerning the "worst" and most "practically relevant" form (Rotter, 2004). One of the simplest solutions to this controversy is adoption of a circumferential weld depression imperfection. This is common in practical civil engineering construction and is often either the worst or close to the worst case (Song et al., 2004) when measured using accepted stick measurements (EN 1993-1-6, 2007). Furthermore, the weld depression imperfection has been verified as being one of the worst imperfections and causes most reduction in buckling strength for cylinders under uniform axial compression. Considering the close relationship of the buckling behaviour under global bending and axial compression, it is natural to study the imperfection sensitivity of cylinders under global bending by referring to the imperfection used for uniform axial compression.

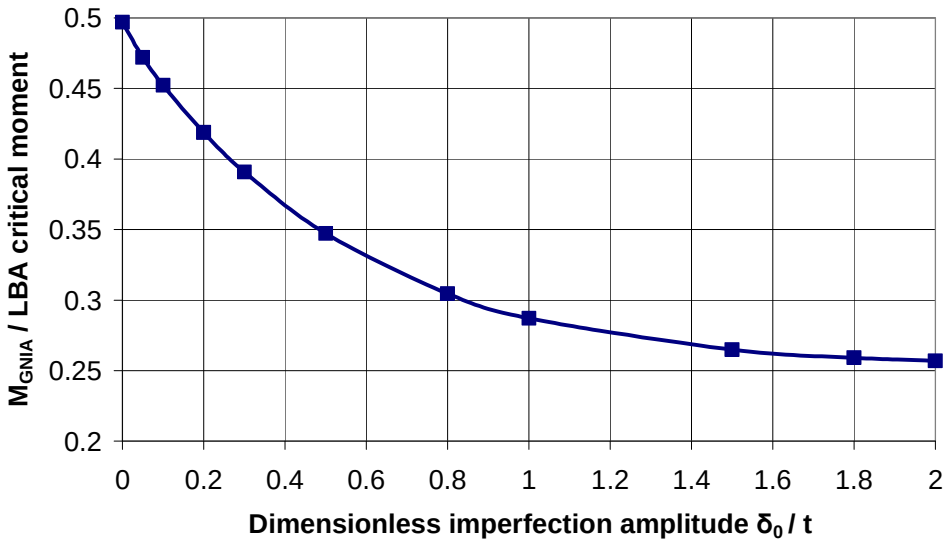

Figure 3-14: Imperfection sensitivity curve for a long cylinder with $r/t = 80$ and $L/r = 50$ under global bending

A single Type A weld depression imperfection was applied at the centre of the cylinder, which was the location where the local bifurcation buckling occurred. The purpose was to study the imperfection sensitivity of the critical bending moment for a long cylinder under global bending. Nonlinear stability analysis for cylinders with a radius to thickness ratio of $r/t = 80$ was conducted with geometric imperfection amplitudes in the range $0 \le \delta_0 / t \le 2$. The dimensions were all expressed in terms of

the wall thickness t, and the length to radius ratio was fixed at $L/r = 50$ for all reported calculations to ensure that Brazier critical ovalisation occurs at the critical bending moment for perfect cylinders. The calculated imperfection sensitivity curve is shown in Fig. 3-14.

The imperfection sensitivity curve indicates that the elastic critical bending moment has a steady reduction with an increase of imperfection amplitude. The value of the critical bending moment for $\delta_0 / t = 2$ is reduced to half the critical moment for a perfect cylinder, which indicates that the buckling strength for a long cylinder under global bending is quite sensitive to weld depression imperfections.

The ovalization of the cross-section under the critical bending moment can be measured through a dimensionless parameter ξ as (Karamanos, 2002)

$$\xi = \frac{D_2 - D_1}{2D} \tag{3.12}$$

where D means the diameter before deformation, D_1 is the diameter normal to the plane of bending at the critical point and D_2 is the diameter on the plane of bending at the critical point. The relationship between the ovalization parameter ξ and dimensionless imperfection amplitude δ_0 / t is shown in Fig. 3-15.

The value of ξ has a steady reduction in the range $0 < \delta_0 / t < 1$, from $\xi = 0.32$ for the perfect geometry to an approximately stable value $\xi = 0.094$ for $\delta_0 / t = 1$. Ovalization of the cross-section at the critical point is alleviated for larger amplitudes, because large imperfection amplitudes cause more reduction in the buckling strength leading to the critical bending moment being reached earlier at a reduced critical moment. When $\delta_0 / t > 1$, ξ increases slightly with increasing values of δ_0 / t. That is because the critical bending moment has little reduction when $\delta_0 / t > 1$, while the original diameter D in the expression for ξ at the centre of cylinder continuously decreases due to the imperfection, leading to a slight increase in ξ.

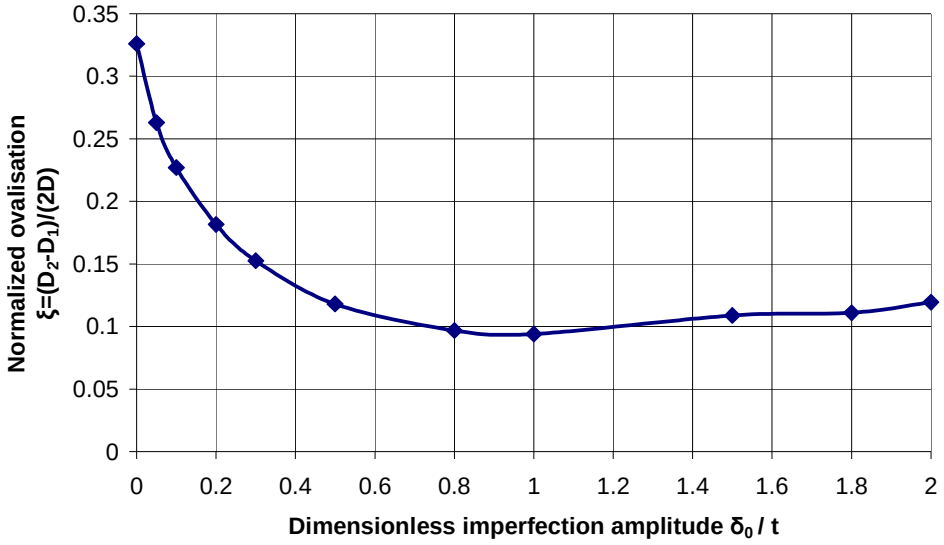

Figure 3-15: Ovalization of the cross-section with change of the imperfection amplitude ($r/t = 80$ and $L/r = 50$)

3.6 Conclusions

Geometrically nonlinear stability analysis of elastic cylinders with different geometries under global bending has been studied. For short cylinders, local bifurcation buckling occurs at the middle on the most compressed side of the shell. There is little ovalization and the critical bending moment by geometrically nonlinear elastic analysis (GNA) is close to the reference elastic critical moment M_{cr}. For extremely short cylinders, local snap-through buckling near the boundaries occurs due to the restraint given by the boundary conditions, so the critical bending moment may rise to several times M_{cr}.

For medium-length cylinders, a combination of ovalization instability and bifurcation instability occurs. The influence of the ovalization of the cross-section should be emphasized because it can lead to a considerable reduction in the elastic buckling stress below the value for uniform axial compression. Longer cylinders have more obvious ovalization in the pre-buckling stage, leading to a more significant reduction in the critical bending moment.

For long cylinders, bifurcation buckling occurs just before snap-through buckling and the two buckling points are almost indistinguishable. The critical moment is

approximately equal to the Brazier moment, with Brazier critical ovalization of the cross-section.

In thick and comparatively short cylinders, plasticity will usually be involved in the buckling behaviour, due to the high local shell bending stress caused by the bending moment. The effect of plasticity on the buckling behaviour of medium-length cylinders under global bending is discussed in Chapter 4.

A geometric imperfection can cause a considerable strength reduction for a long elastic cylinder under global bending. Bifurcation buckling occurs earlier at a reduced critical moment, leading to an alleviation of the ovalization of the cross-section. An imperfection sensitivity analysis for medium-length cylinders with no obvious ovalization of the cross-section is investigated in Chapter 4.

Chapter 4 A study of cylindrical shells under global bending in the elastic-plastic range

4.1 Buckling and plastic collapse of thin cylinders in bending

In Chapter 3, the elastic buckling behaviour of cylindrical shells under global bending was investigated. The characteristics of the buckling behaviour for short, medium-length and long cylinders were investigated, respectively. For a perfect medium-length cylinder without the effects of the boundary conditions and pre-buckling ovalization on the buckling strength, the critical bending stress equals the buckling stress for uniform axial compression and this would give the elastic critical buckling moment as

$$M_{cr} \cong 1.90Et^2r \tag{4.1}$$

This result is very close to that obtained for moderately long cylinders when a linear bifurcation analysis is used (Flugge, 1973; Seide and Weingarten, 1961). In longer cylinders and pipes, the cylinder tends to take on an oval shape under bending, leading to a snap-through buckle, which is termed the Brazier Effect (Brazier, 1927).

Where rings are used to maintain the circularity of the cylinder at moderate intervals, the ovalisation of the cross-section is very greatly constrained, and the elastic nonlinear buckling condition is very close to the linear bifurcation moment defined by Eq. 4.1. This Chapter is concerned only with cylinders that are not very long according to the European Standard EN 1993-1-6 (2007) between boundaries or stiffening rings that are effective in holding the cylinder to a circular form.

For the geometry used in this Chapter ($L/r = 7$), ovalization does not play a significant role. The explanation for this conclusion is deduced from the results in Chapter 3. It was shown in Chapter 3 that for perfect thick cylinders with $r/t = 10$ and $L/r = 7$, the shell has a considerable ovalization when elastic bifurcation buckling occurs. However, the value of the full plastic moment (Eq. 4.3) is less than 5% of the elastic critical bending moment, not to mention the first yield moment. So

yielding of the full cross-section already occurred far before the oval distortion began to develop. The same situation is evident for a cylinder with $r/t = 50$ and $L/r = 7$. For comparatively thin cylinders with $r/t \geq 200$ at $L/r = 7$, the ovalization of the cross-section is negligible even when elastic bifurcation buckling occurs. When plasticity is involved, elastic-plastic buckling may occur at a reduced moment, so that ovalization of the cross-section is far from being developed. So it can be concluded that for all the cylinders with different values of r/t at $L/r = 7$, ovalization does not influence the buckling behaviour.

The above description was concerned only with the strength of perfect cylinders. Since the bifurcating zone of a cylinder in bending is subject to a relatively uniform axial compressive stress and the bifurcation under uniform axial compression occurs with small buckles in limited zones and is known to be extremely imperfection-sensitive, it is natural to suppose that the analyses for perfect cylinders in bending will all produce strengths far in excess of the reliable or experimental strengths of very thin cylinders.

For thick and short cylinders, very high local stresses often develop in shell structures under elastic conditions and these are smoothed away by plasticity long before failure. In some buckling problems, the behaviour of the structure can change drastically as soon as a small region begins to enter the plastic range (Calladine, 1983). This is especially true for an imperfect cylinder in bending, for which the high local bending stress usually develops quite locally nearby the imperfection area. So plasticity would definitely affect the buckling behaviour, depending on the specific geometry.

A second limit to strength occurs in thicker shells (tubes), when the full plastic moment is reached in a cylinder with perfect elastic-plastic properties. First yield occurs when

$$M_Y = \pi r^2 t \sigma_y \tag{4.2}$$

where σ_y is the yield stress, and full plasticity occurs when

$$M_p = 4r^2 t\sigma_y \quad \text{or for thicker tubes} \quad M_p = \frac{4}{3}\sigma_y\left[\left(r+\frac{t}{2}\right)^3 - \left(r-\frac{t}{2}\right)^3\right] \tag{4.3}$$

giving a shape factor of 1.273 for thin shells, or first yield at 79% of the full plastic moment in a perfect shell.

4.2 The EN 1993-1-6 capacity curve for shells in global bending

The capacity curve (Fig. 2-6a) for a structure describes the relationship between the buckling strength and the relative slenderness. For cylinders in global bending, the description may be written as follows. The relative slenderness is defined in terms of the full plastic moment M_p (small displacement theory ideal elastic-plastic analysis, termed MNA, Eq. 4.3), and the linear elastic critical resistance M_{cr} (linear bifurcation analysis, termed LBA, Eq. 4.1).

As an important reference resistance of the elastic-plastic buckling strength assessment, the definition of the plastic reference resistance has sometimes been challenged. It is usually evaluated using a small-displacement theory rigid-plastic or elastic-plastic analysis (MNA) as the plastic limit load under an applied combination of actions (ECCS EDR5, 2008). For the current buckling problem, several MNA analyses were performed for some perfect thick shells in bending. The results agreed well with the predictions using Eq. 4.3. So Eq. 4.3 is adopted to represent the plastic reference resistance throughout this chapter. However, for comparatively thin cylinders, this definition seems to cause some problems due to a complex bending and stretching behaviour of the shell, which will be discussed later.

For another important reference parameter, the linear elastic critical resistance, an accurate definition should be determined from a linear eigenvalue analysis (LBA). In current buckling problems, several LBA analyses for some shells with different radius to thickness ratios were performed using finite element software ABAQUS. The results indicated that the prediction of the linear elastic critical resistance M_{cr} using Eq. 4.1 agreed well with the accurate numerical predictions. The error between the two is usually less than 1%. Even for quite thick cylinders, the error does not

exceed 2%. So Eq. 4.1 is used to describe the elastic critical resistance throughout this chapter.

The relative slenderness λ is defined in the European standard EN 1993-1-6 (2007) as

$$\lambda = \sqrt{M_p / M_{cr}} \tag{4.4}$$

and the dimensionless strength parameter χ is defined as

$$\chi = M_k / M_p \tag{4.5}$$

where the characteristic resistance M_k is determined by experiment or from a geometrically and materially nonlinear analysis of the imperfect structure (termed GMNIA, producing $M_{GMNIA} = M_k$).

4.3 Computations of elastic-plastic buckling strengths

Cylindrical shells in bending were treated as of medium length (EN 1993-1-6, 2007) with a single local weld depression imperfection far from the ends, with end boundaries restrained to remain circular. These boundary conditions effectively prevent ovalization for these shells.

Elastic-plastic imperfect shell buckling calculations (GMNIA) were performed using the program ABAQUS (Hibbit et al, 2003). The lowest resistance determined from GMNIA was deemed to be the best numerical prediction of the elastic-plastic buckling resistance of the imperfect structures. The arc-length method described before in the nonlinear finite element calculation was used to capture the failure load in the load-displacement path.

Due to the close relationship between the buckling behaviour of cylinders under axial compression and global bending, it is natural to use the axisymmetric Type A weld imperfection (Rotter and Teng, 1989) as a “worst” and “most practically” type of imperfection for cylinders in global bending (Rotter, 2004). The imperfection was assumed to be a single local feature, not interacting with other imperfections.

All the calculations reported here used an ideal elastic-plastic stress-strain relation obeying von Mises criterion with the normal flow rule and the flow theory of plasticity in bifurcation calculations, with $E = 2.0 \times 10^5 MPa$ and $\nu = 0.3$. Three different material models including the ideal elastic-plastic material Model A, a first hardening Model B and a second hardening Model C were adopted to explore the effect of strain hardening on the buckling behaviour.

4.4 Buckling strength predictions for cylinders under pure bending with ideal elastic-plastic material

4.4.1 Aspects of finite element analysis

The bifurcation or plastic collapse of shells with radius to thickness ratios in the range $10 \le r/t \le 2000$ was determined with geometric imperfections with amplitudes in the range $0.01 \le \delta_0 / t \le 2$. The dimensions were all expressed in terms of the wall thickness *t*, and the length to radius ratio was kept at $L/r = 7$ for all reported calculations, with selective successful verification at $L/r = 14$ to ensure that ovalization did not alter the outcome. The end boundaries were subjected to a global moment, and were kept circular. A single weld depression imperfection was used at the centre of the cylinder (Fig. 4-1). The ideal elastic-plastic stress-strain relationship was adopted with yield stress $\sigma_y = 250 MPa$. The mesh was verified by accurately reproducing the imperfection sensitivity curve for axial compression (Rotter and Teng, 1989).

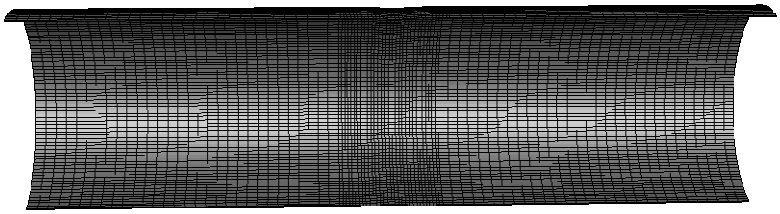

Figure 4-1: Finite element mesh for half cylinder, with careful detail around the central weld

4.4.2 Moment-curvature curves

The changing form of the moment-curvature curve for different radius to thickness ratios is shown in Figs 4-2 and 4-3. In these figures, ϕ is the mean curvature deduced from the change in rotation between the two ends. The geometric imperfection amplitude has here been held constant at δ_o/t = 0.50, though this is a small imperfection in thin shells and a very deep one for thicker shells. The reason for retaining this imperfection at a constant value will be evident later. As the radius to thickness ratio passes from a thick cylinder (r/t=10) to a moderately thin cylinder (r/t=100) to a very thin one (r/t=1000), the moment curvature relationship changes from a smooth relatively ductile response all the way to bifurcation buckling with a precipitous post-buckling fall.

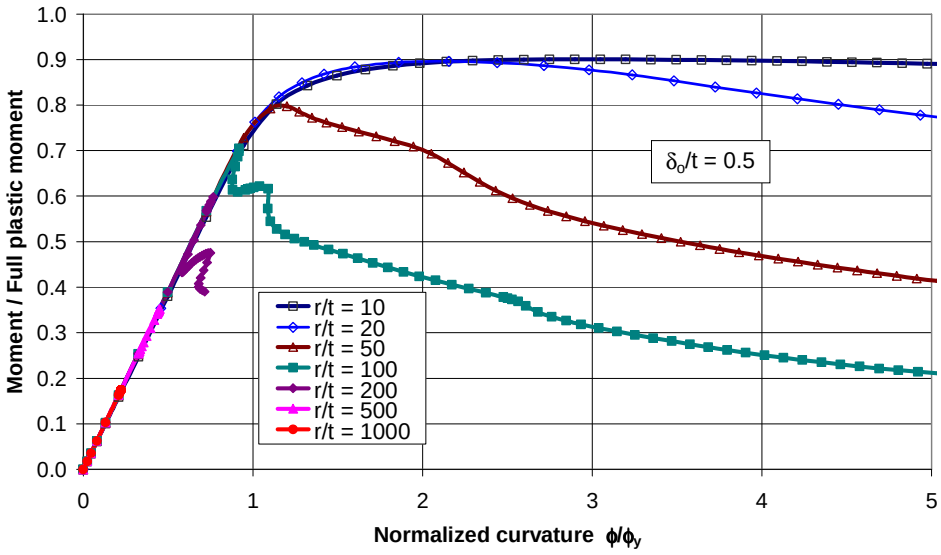

Figure 4-2: Typical moment-curvature curves for cylinders with different radius to thickness ratios (imperfection amplitude δ_o/t = 0.50)

In Fig. 4-2, the bending moments have all been normalised relative to the full plastic moment (Eq. 4.3) and the curvatures of the shell have been normalised relative to the linear bending first yield value ($\phi_y = \frac{\sigma_y}{Er}$). Because the imperfection of δ_o/t = 0.50 is such a major deviation of geometry for r/t=10, it does not achieve the full plastic moment of the perfect geometry, but remains ductile at a plateau near

M/M_p=0.90, which is caused by the complex pattern of bending and stretching yielding at the deep imperfection. In slightly thinner cylinders (r/t=20), the ductility begins to be lost, and soon (r/t=50) the strength is limited by bifurcation with a softening post-buckling response. By r/t=100, the bifurcation has a steep post-buckling fall, quickly followed by recovery and a second bifurcation leading to progressive falls in strength. This pattern is repeated as the shell becomes progressively thinner.

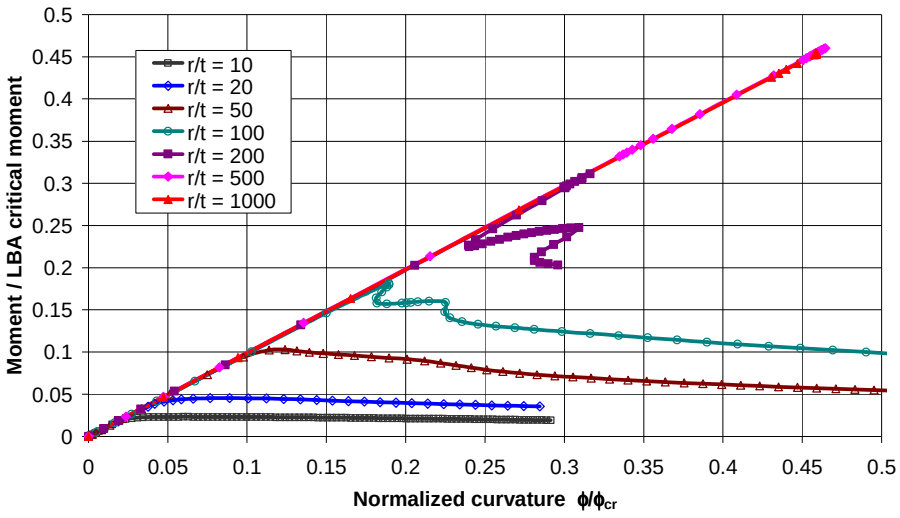

Figure 4-3: Typical moment-curvature curves for cylinders with different radius to thickness ratios (imperfection amplitude $\delta_0/t = 0.50$)

The behaviour of the thinner shells is difficult to see in Fig. 4-2, so the same information is presented in Fig. 4-3 in different form. Here the bending moment has been normalised relative to the linear bifurcation moment (Eq. 4.1) and the curvature relative to the value at which this bifurcation would occur according to linear theory ($\phi_{cr}=M_{cr}/EI$). Since the shell is so short that ovalization is effectively prevented, the pre-buckling path is very close to linear, and shells with $r/t > 300$ all achieve very similar moments at bifurcation, which occurs elastically. The thicker shells bifurcate under plastic conditions and this elastic-plastic buckling occurs over the full range ($50 < r/t < 300$) for this imperfection amplitude.

Similar calculations were performed for a large range of imperfection amplitudes ($0.01 \le \delta_0/t \le 2$) and a large range of radius to thickness ratios ($10 \le r/t \le 2000$) to

explore the full range of behaviour from very thin shells to practical thickness tubes. The peak value of bending moment on each curve was used for the remainder of this study.

The deduced imperfection sensitivity curves for cylinders with different radius to thickness ratios and imperfection amplitudes are shown in Fig. 4-4. For very thin cylinders, the curves represent the single effect of the imperfection amplitude on the elastic buckling strength. While for comparatively thick cylinders the curves represent the effects of both the imperfection amplitude and the plasticity on the buckling strength.

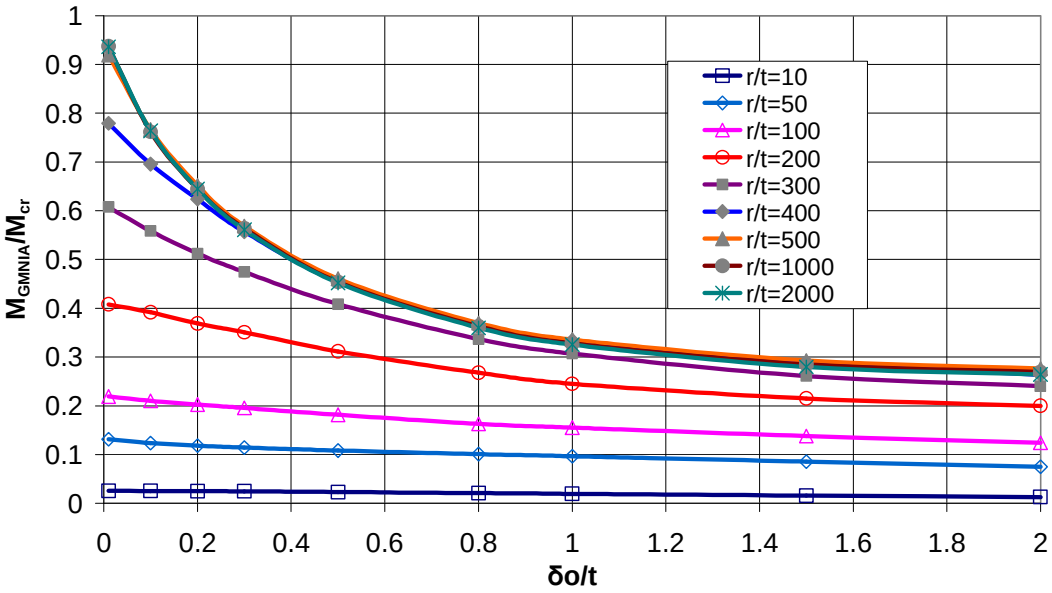

Figure 4-4: Imperfection sensitivity curves for cylinders with different radius to thickness ratios in bending

4.4.3 Buckling strength prediction for cylinders with different geometries

Taking the maximum moment from each curve, complete traditional buckling curves (capacity curves) for cylinders in bending with weld depression geometric imperfections of different amplitudes are shown in Fig. 4-5. These cannot be compared with traditional lower bound curves on experimental data because the amplitude of the imperfection in most experiments remains unknown. However, these predictions can be used to back-figure appropriate imperfection amplitudes to capture the practical experimentally-based relationship between radius to thickness

ratio and imperfection amplitude (e.g. see Rotter, 1997). It may be noted that the strength of thick imperfect cylinders appears to fail to reach the full plastic moment. However, these cylinders have a deep axisymmetric imperfection (δ_o/t = 1 is a large radius reduction when r/t = 20), and this causes the calculated strengths to fall well below the full plastic moment. This effect is not important for any practical shells, since these imperfections are too deep. The practical characteristic imperfection amplitude could be adopted according to Eq. 4-6 (EN 1993-1-6, 2007).

$$\delta_0 = \frac{1}{Q}\sqrt{\frac{r}{t}}t \tag{4.6}$$

where Q is the meridional compression fabrication quality parameter which can be found in EN 1993-1-6 (2007).

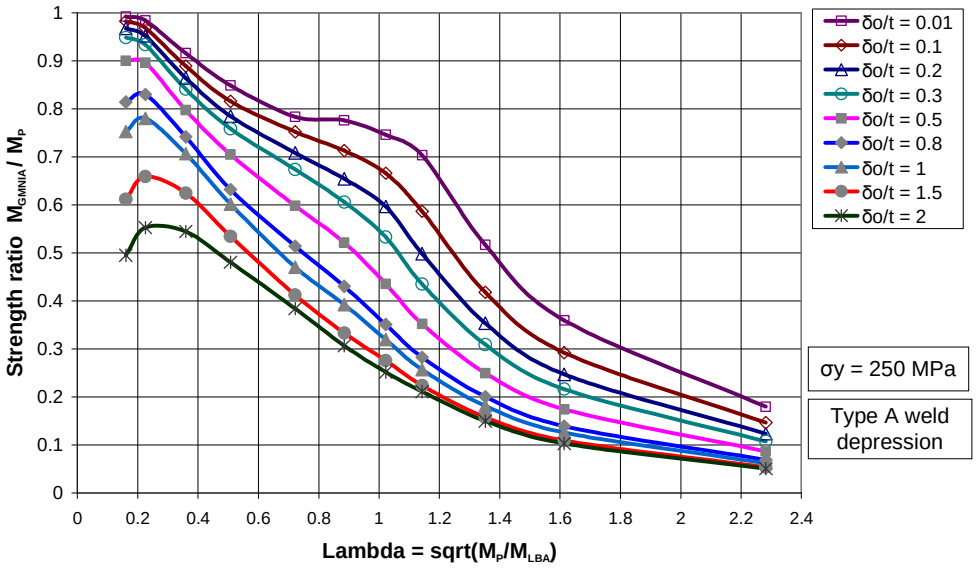

Figure 4-5: Buckling strength (capacity) curves for cylinders in bending with different imperfection amplitudes δ_o/t (constant yield stress σ_y=250MPa and changing r/t)

The same data is shown in Rotter's (2002) alternative form of the capacity curve in Fig. 4-6. The capacity curve parameters may be extracted from this plot, each as a function of the imperfection amplitude δ_o. The very rapid loss of strength after first plasticity can be captured by choosing a value of the exponent η that is less than unity.

In Fig. 4-6, it can be seen that the value of α deduced from these curves is not perfectly stable for a given imperfection amplitude when the radius to thickness ratio is changed along each curve. This is because the effect of geometrically nonlinearity in the pre-buckling phase depends slightly on r/t. Moreover, the curves for small imperfection amplitudes display a remarkable plateau in the range $0.6 < M_k/M_p < 0.8$, which is perhaps the cause of some controversy in the past concerning the appropriate definition of the plastic reference load for cylinders in global bending.

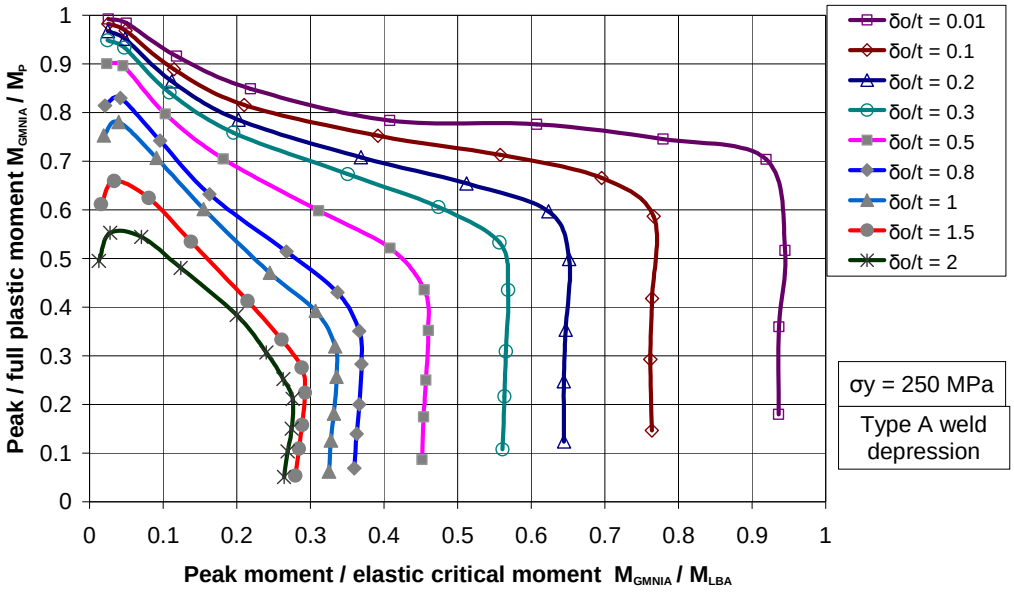

Figure 4-6: Alternative form of capacity curves for cylinders in bending with different imperfection amplitudes δ_o/t (constant yield stress σ_y=250MPa and changing r/t)

To make the information presented in Figs 4-5 and 4-6 accessible to the design process, it is necessary to extract the relevant parameters for the Eurocode buckling curve for each imperfection amplitude using Fig. 4-6.

4.4.4 Extraction of capacity curve parameters

The calculations presented here used an ideal elastic-plastic stress strain curve, and no strain hardening was included. Under this loading condition, the cylinder does not display geometric hardening either (Rotter, 2005). Consequently, it was assumed here, *ab initio*, that the value of the squash limit relative slenderness λ_0 could be taken as zero for all imperfection amplitudes.

The easiest parameter to extract from Fig. 4-6 is the elastic imperfection sensitivity factor α, which is defined (EN 1993-1-6, 2007) as the ratio of the buckling strength found in a geometrically nonlinear elastic analysis that includes imperfections (GNIA) to that found in a linear bifurcation analysis of the perfect structure (LBA). The value of α is found from the vertical straight line (for each imperfection amplitude) that occurs at lower values of the ratio M_k / M_p. This rather precise extraction leads to a classical "imperfection sensitivity curve", which is shown in Fig. 4-7. The lines for different radius to thickness ratios lie perfectly on each other so that they are effectively indistinguishable.

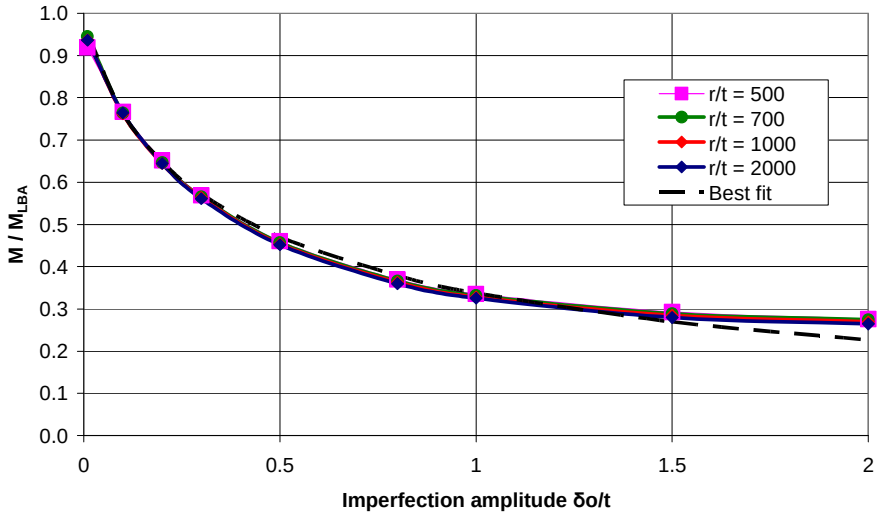

Figure 4-7: Imperfection sensitivity curve giving the value of parameter α (constant yield stress σ_y=250MPa and changing *r/t*)

The plastic range factor β captures (as $1-\beta$) the moment at which yielding first begins to affect the global buckling strength, which is not the same as the first yield moment. It should be noted that the first yield moment defines initial yielding on the surface of the shell at one point, but even after yielding begins the potential buckle is of comparable size to the elastic buckle, and yield must spread over a zone that covers a significant part of one buckle before it impacts significantly on the bending stiffness of the whole area. Thus the value of β must be extracted from Fig. 4-6 by careful examination, and not as a simple numerical deduction as the first yield

moment. Extracted values of β are shown in Fig. 4-8, and plotted as the function $(1-\beta)$ for reasons that will be evident later.

It is immediately evident that the moment at which yield first influences the buckling strength is very sensitive to the amplitude of the geometric imperfection. This aspect of cylinder buckling under bending has not been described very clearly in the past. Thus, the transition from elastic to plastic bifurcation in thin cylindrical shells should be clearly seen as strongly associated with geometric imperfections and tolerance measures that control them.

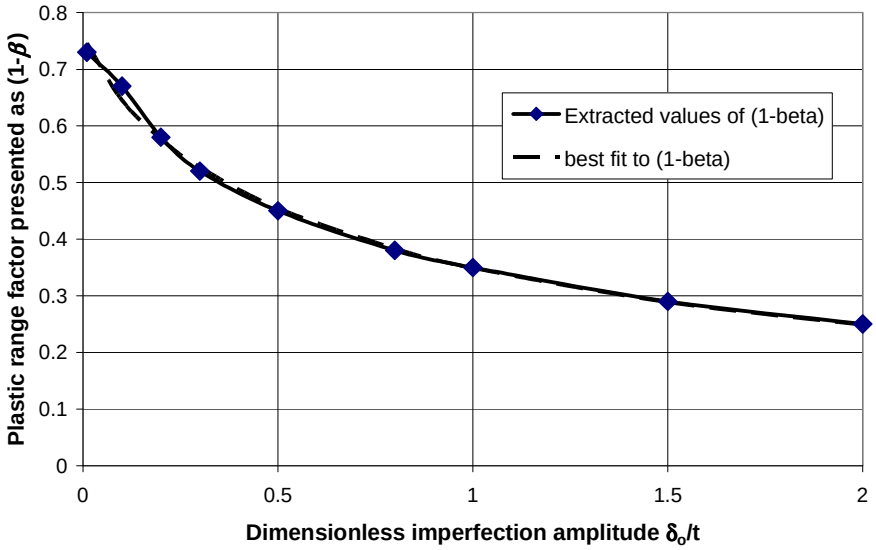

Figure 4-8: Extracted values of the plastic range factor β (constant yield stress σ_y=250MPa and changing *r/t*)

Extraction of the values of the parameter η is less straightforward, and the simplest procedure is to choose a suitable functional form and use a least squares best-fitting procedure to determine the values.

The solid curves shown in Figs 4-7 and 4-8 can be closely approximated by a function of the form

$$\alpha,\ 1-\beta,\ \eta = \frac{a}{1+b\left(\delta_o/t\right)^c} \tag{4.7}$$

The dashed line in Fig. 4-7, which gives a very close approximation to the elastic imperfection reduction factor α is given by

$$\alpha = \frac{1}{1 + 2.00\left(\delta_o / t\right)^{0.8}} \tag{4.8}$$

or a = 1.0, b = 2.00 and c = 0.80.

The plastic range factor β, is accurately modelled by the dashed line in Fig. 4-8, which is given by

$$1 - \beta = \frac{0.77}{1 + 1.2\left(\delta_o / t\right)^{0.8}} \tag{4.9}$$

or a = 0.77, b = 1.20 and c = 0.80.

Finally, least squares minimisation of the calculated values of buckling or maximum moment M_k for all those cases in the elastic-plastic domain leads to a representation of the interaction exponent η represented by

$$\eta = \frac{0.80}{1 + 0.07\left(\delta_o / t\right)^{2}} \tag{4.10}$$

All three of these expressions were derived in a stepwise manner. All three coefficients *a*, *b* and *c* were first permitted free range. A choice was then made of a simple fixed value for the coefficient *c*, since it is desirable to have a simple power in an empirical equation. The second empirical fit then only used *a* and *b*, from which a simple value of the coefficient *b* was chosen. The final fit was made to define the coefficient *a* alone, ensuring that this value was the best choice given the approximations already made in choosing simple values for *b* and *c*.

The results of using Eqs 4.8, 4.9 and 4.10 in Eqs 2.5, 2.6 and 2.7 to represent the complete conventional capacity curves are shown in Fig. 4-9. An extremely good fit to the rather strange forms of these relationships is achieved, which illustrates how powerful is the form of capacity curve represented by Eqs 2.5, 2.6 and 2.7. The greatest deviations occur for very thin cylinders with high amplitude imperfections,

and this conservative error arises because the dashed line in Fig. 4-7 falls below the calculated imperfection sensitivity curve when the imperfection amplitude exceeds δ_o/t = 1.5. Since these are large imperfections, this conservatism seems unimportant.

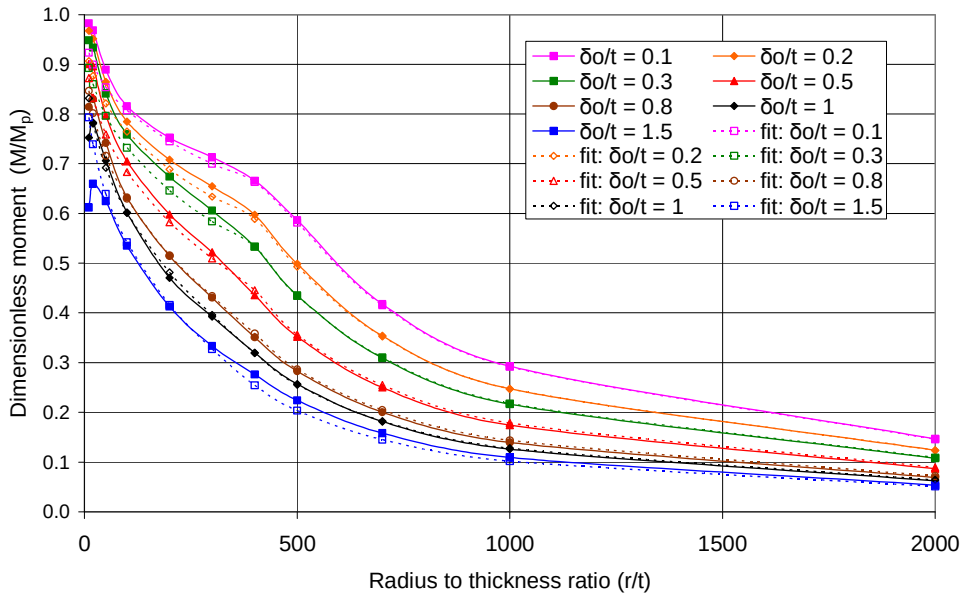

Figure 4-9: Calculated and best fitted capacity curves (constant yield stress σ_y=250MPa and changing *r* / *t*)

Equations 4.8, 4.9 and 4.10 can be implemented directly into the Eurocode EN 1993-1-6 (2007), since the tolerance level and assumed imperfection amplitude associated with a particular Fabrication Quality Class are already defined there. These expressions offer a very considerable enhancement over the simple fixed values of β and η and the empirical lower bound for α currently given in EN 1993-1-6 (2007).

4.5 Buckling strength predictions for cylinders under pure global bending with hardening Model B

4.5.1 The stress-strain relationship for hardening Model B

In this section, the material was given an isotropic hardening modulus $h = 4000MPa$ once the shell reached the first yield stress (Fig. 4-10). The tangent modulus E_T is related to Young's modulus E and h by

$$\frac{1}{E_T} = \frac{1}{E} + \frac{1}{h}$$

The final plateau stress was chosen as 284MPa which gives a 14% rise above the first yield value. The buckling behaviour due to this strain hardening was investigated next.

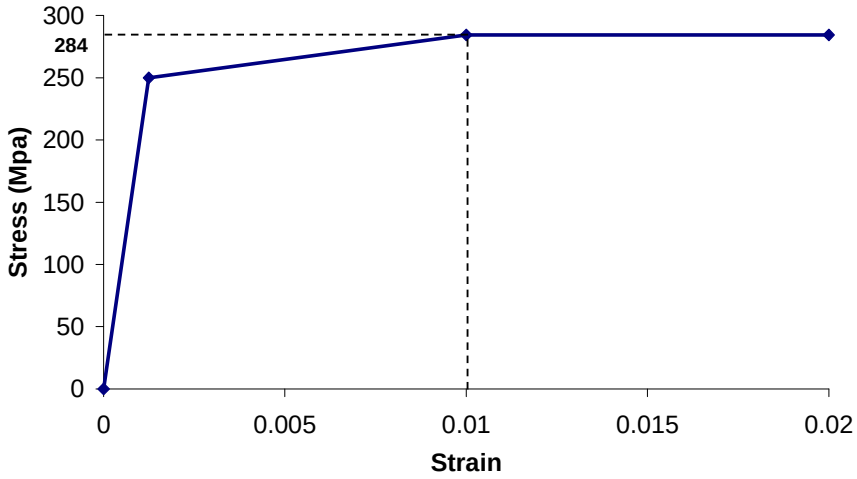

Figure 4-10: The stress- strain relationship for hardening Model B

4.5.2 Buckling strength prediction

The changing form of moment-curvature curves with different radius to thickness ratios for hardening Model B are shown in Figs 4-11 and 4-12. The geometric imperfection amplitude has here been held constant at δ_o/t = 0.50. The behaviour undergoes radical changes from bifurcation with a precipitous post-buckling fall at high radius to thickness ratios to a smooth rounded response due to ductile plasticity in thick cylinders. The moment and curvature are normalized as for the ideal elastic-plastic material model.

Compared with the moment-curvature curves for the ideal elastic-plastic material model (Figs 4-2 and 4-3), in Figs 4-11 and 4-12, for thick shells, because the first yield stress is already reached before the elastic buckling occurs, the moment-curvature curves have a strengthening stage after reaching the first yield stress due to the strain hardening, and thus the buckling strength increased to some extent depending on how much the buckling strength is affected by the plasticity for each

radius to thickness ratio. Thicker cylinders are more influenced by the strain hardening. For thin shells, where elastic buckling occurs without involving the effect of plasticity, the curves are exactly the same as the corresponding curves in Figs 4-2 and 4-3.

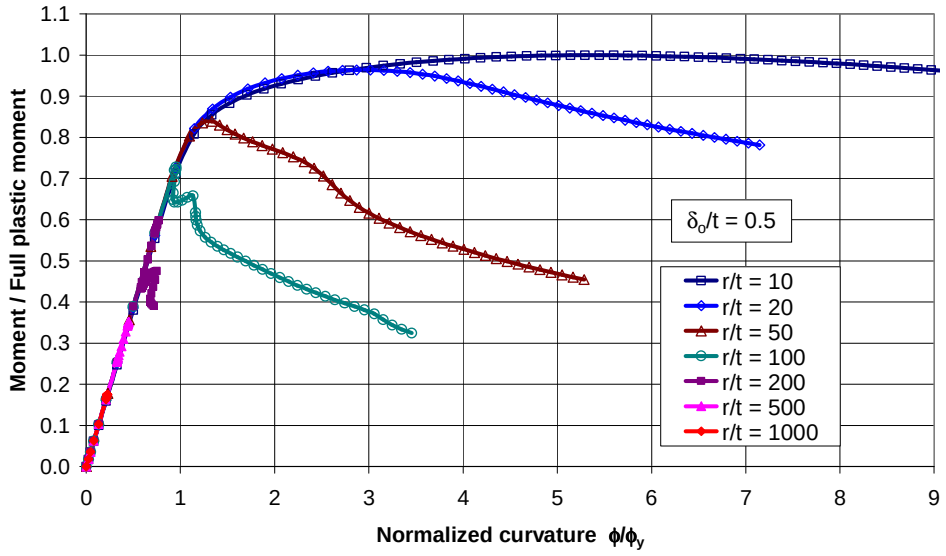

Figure 4-11: Typical moment-curvature curves for cylinders with different radius to thickness ratio (imperfection amplitude δ_o/t = 0.50)

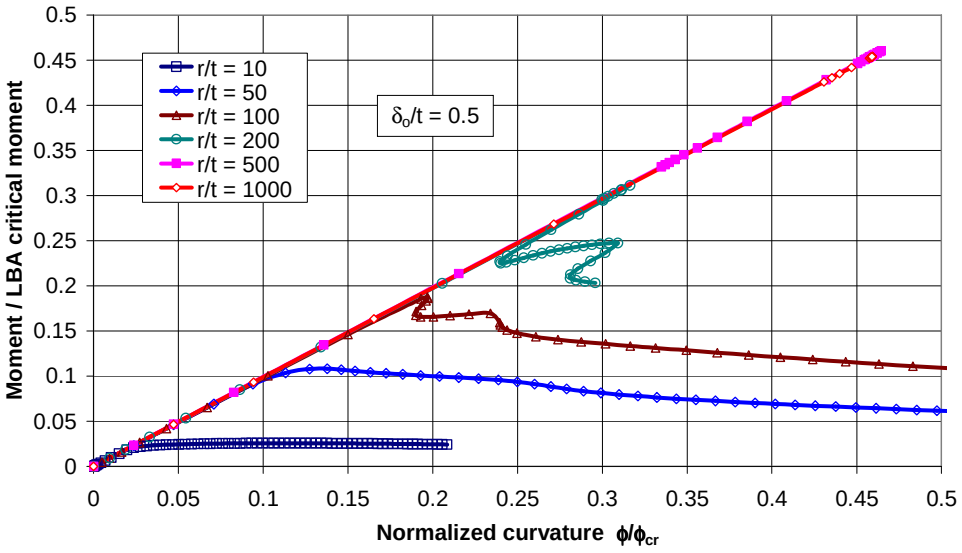

Figure 4-12: Typical moment-curvature curves for cylinders with different radius to thickness ratio (imperfection amplitude $\delta_o/t = 0.50$)

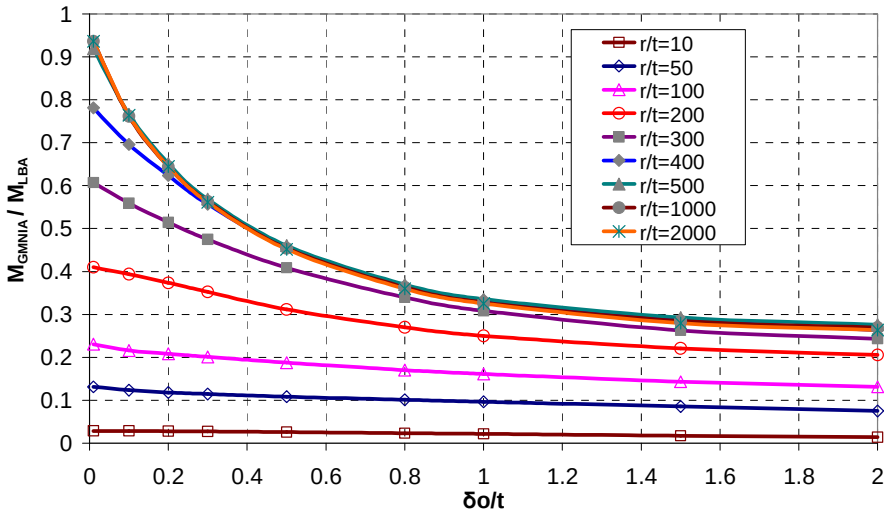

Figure 4-13: Imperfection sensitivity curves for cylinders with different radius to thickness ratios in bending (Model B)

The imperfection sensitivity curves for hardening Model B with different radius to thickness ratios and imperfection amplitudes are shown in Fig. 4-13. Compared with the imperfection sensitivity curves for the ideal the elastic-plastic Model A (Fig. 4-4), the curves for very thin cylinders are precisely the same because plasticity has no effect on the buckling strength. For comparatively thick cylinders, where the curves represent the effects of both imperfection amplitude and plasticity on the buckling strength, the curves for these cylinders for the two material models are different, depending on the specific radius to thickness ratio.

The complete traditional buckling curves (capacity curves) and alternative form of capacity curves for cylinders in bending with weld depression geometric imperfections of different amplitudes are shown in Figs 4-14 and 4-15. Compared with the capacity curves for the ideal elastic-plastic material model (Figs 4-5 and 4-6), the values of M_k / M_p for hardening Model B have an obvious increase for thick shells ($10 \le r/t < 100$).

For very thick shells ($r/t = 10$), after the first yield stress at the most compressed fibre is reached, the plastic strain needs to develop a lot to almost the whole cross-section before the collapse moment is reached. So the whole hardening stage is experienced. After the first yield, the stress value in the plastic zone might increase

to the value of the final yield stress during the development of the yield zone, and the cross-section can thus bear more bending moment due to increased stresses in the plastic range.

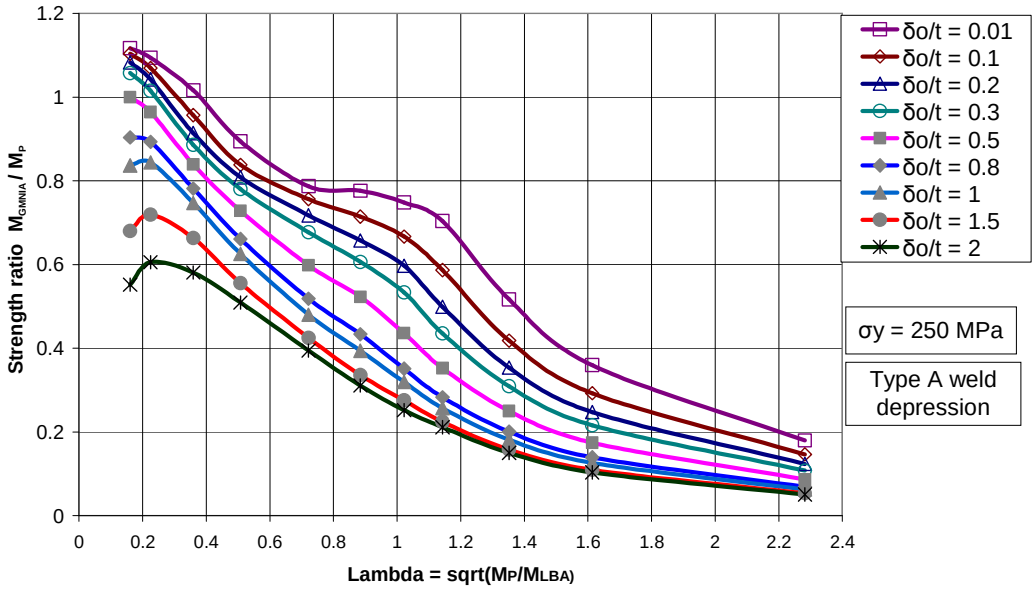

Figure 4-14: Buckling strength (capacity) curves for cylinders in bending with different imperfection amplitudes δ_o/t (Model B and changing r/t)

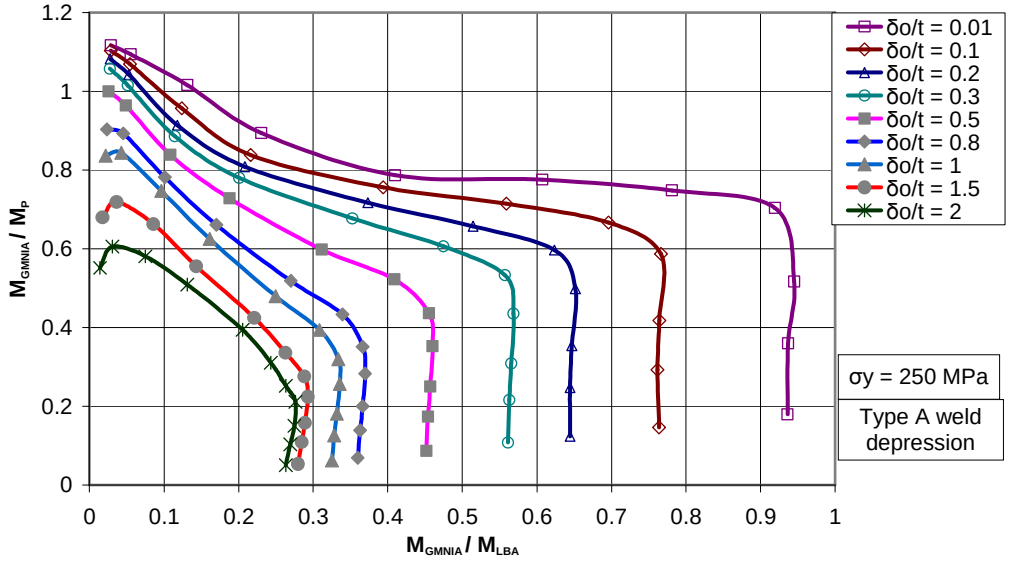

Figure 4-15: Alternative form of capacity curves for cylinders in bending with different imperfection amplitudes δ_o/t (Model B and changing r/t)

Assuming the failure is still controlled by plastic yield, with increasing values of r/t, the plastic zone before the collapse moment is reached becomes smaller, and the collapse mechanism forms before the yield strain spreads to the whole cross-section. In this situation, the collapse moment might be reached during the strain hardening stage, and the maximum extreme fibre stress at collapse moment is between the first yield stress and final plateau stress. So the critical strength is affected less by strain hardening for comparatively thinner cylinders than for very thick cylinders.

For thinner cylinders ($100 \le r/t < 500$), the failure is dominated by elastic-plastic buckling. The axial bifurcation buckling occurs after the first yield stress is reached but the yield of the full cross-section is far from being reached. The thinner the shell is, the sooner bifurcation buckling occurs after first yield and the less influence strain hardening has on the buckling strength. The values of M_k / M_p for the ideal elastic-plastic material Model A and hardening Mode B are thus closer with increasing r/t. For cylinders with $200 \le r/t < 500$, the difference in M_k / M_p between these two models is negligible.

For very thin cylinders with $r/t \ge 500$, the failure of the cylinder is controlled by elastic bifurcation buckling, and plasticity has no effect on the buckling behaviour at all. So the capacity curves of these cylinders for the two material models are identical.

It is concluded that only the buckling strength of very thick cylinders is affected much by the hardening of material.

4.5.3 Extraction of capacity curve parameters

Considering the definitions of elastic imperfection reduction factor α and plastic range factor β, and observing the results for the ideal elastic-plastic material model and hardening Model B, it is obvious that the parameter α is not affected by strain hardening of material and β is only slightly affected. The expressions for α and β

for the ideal elastic-plastic material are therefore still applicable for Model B. The expressions are expressed as follows:

$$\alpha = \frac{1}{1+2.00\left(\delta_o/t\right)^{0.8}} \tag{4.11}$$

$$1-\beta = \frac{0.77}{1+1.2\left(\delta_0/t\right)^{0.8}} \tag{4.12}$$

However, the interaction exponent η is affected by the hardening of the material and may be closely represented by

$$\eta = \frac{1}{1+0.22\left(\delta_0/t\right)^2} \tag{4.13}$$

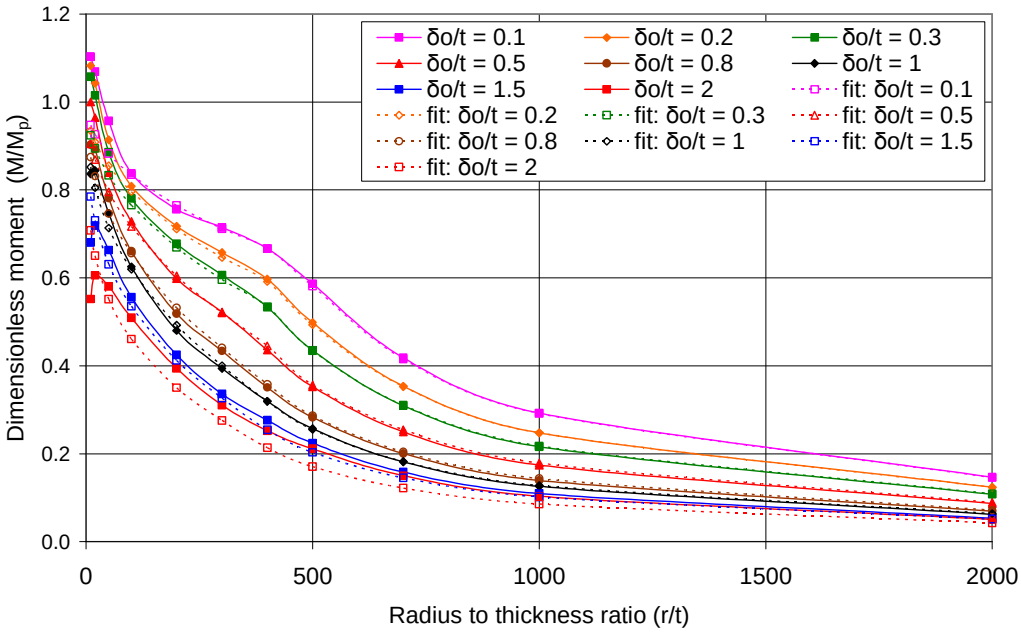

Figure 4-16: Calculated and best fitted capacity curves (Model B and changing *r/t*)

Results of using Eqs 4.11, 4.12 and 4.13 to represent the complete conventional capacity curves are shown in Fig. 4-16.

4.6 Buckling strength predictions for cylinders under pure bending with hardening Model C

4.6.1 The stress-strain relationship for hardening Model C

In this section, another hardening Model *C* was adopted to represent classical mild steel behaviour. Once the first yield stress is reached, the strain increases to ten times the first yield strain on a plastic plateau before it hardens, with a strain hardening modulus $h = 4000MPa$, producing a final stress that is ten times the initial yield stress. This huge hardening curve was used to explore the effects of both a yield plateau and the outcome for indefinite strain hardening. The tangent modulus E_T is again related to Young's modulus E and h by

$$\frac{1}{E_T} = \frac{1}{E} + \frac{1}{h}$$

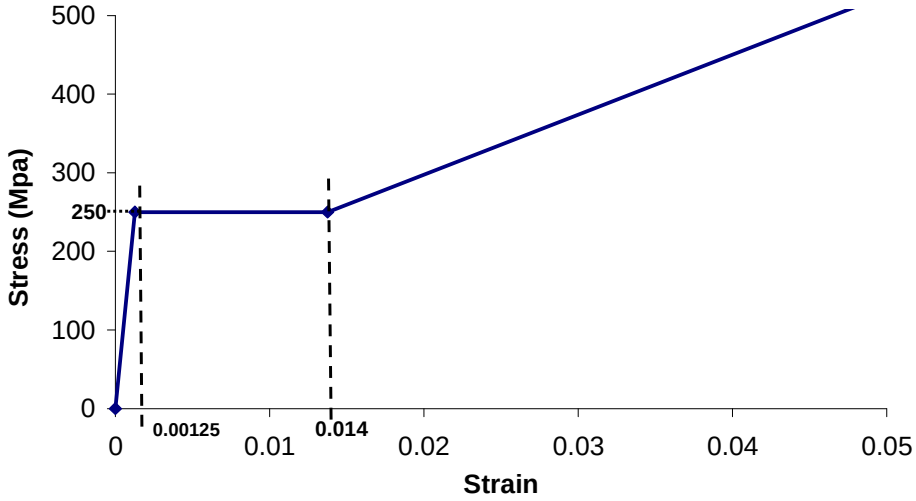

Figure 4-17: The stress- strain relationship for hardening Model C

The stress- strain relationship for hardening Model C is shown in Fig. 4-17.

4.6.2 Buckling strength prediction

The changing form of the moment-curvature curves with different radius to thickness ratios for hardening Model C are shown in Figs 4-18 and 4-19. Here, the geometric imperfection amplitude has been held constant at δ_o/t = 0.5. The behaviour

undergoes radical changes from bifurcation with a precipitous post-buckling fall at high radius to thickness ratios to a smooth rounded response due to ductile plasticity in thick cylinders. The moment and curvature are normalized as for the previous two models.

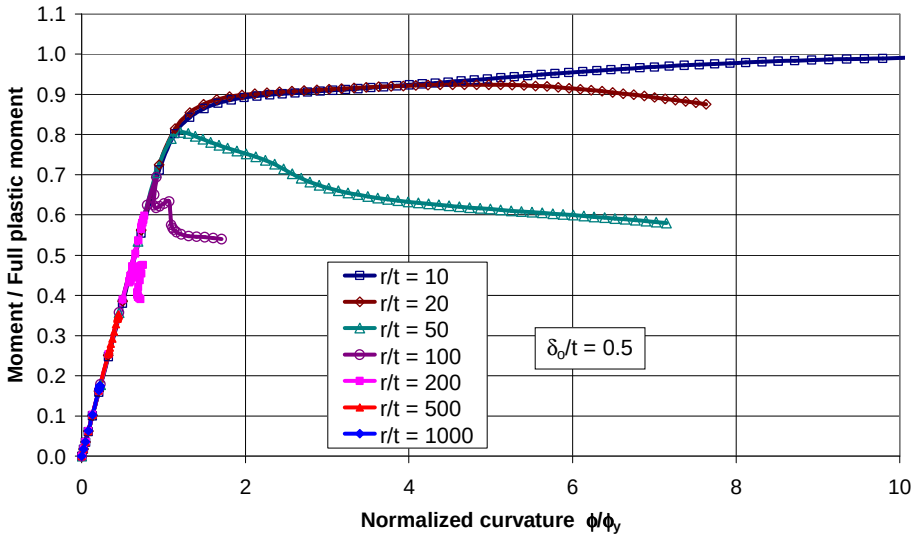

Figure 4-18: Typical moment-curvature curves for cylinders with different radius to thickness ratio (imperfection amplitude δ_o/t = 0.50)

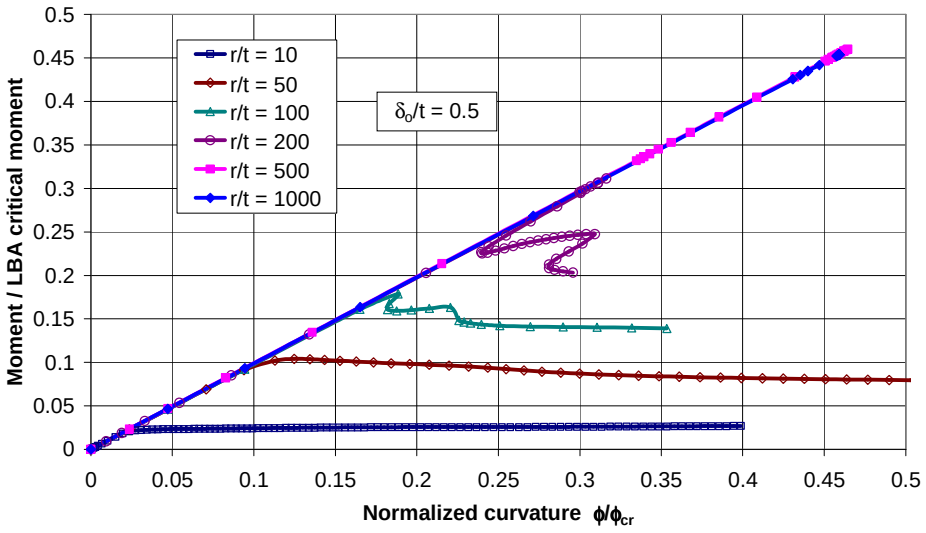

Figure 4-19: Typical moment-curvature curves for cylinders with different radius to thickness ratio (imperfection amplitude δ_o/t = 0.50)

For very thick shells, after first yield, the plasticity zone needs to develop very large strains to achieve a full plastic collapse. A cross-section made of ideal elastic-

plastic material can not quite reach M_p even at large curvatures as Fig. 4-20 (c) and Fig. 4-21 shows. Some strain-hardening is necessary for M_p to be reached and exceeded (Fig. 4-20d). The value of the plastic strain may exceed ten times the first yield strain before the geometrically nonlinear collapse moment is reached and thus strain hardening should have a strong effect on the buckling behaviour in very thick cylinders. The buckling strength can increase to some extent due to strain hardening depending on the specific *r / t* ratio.

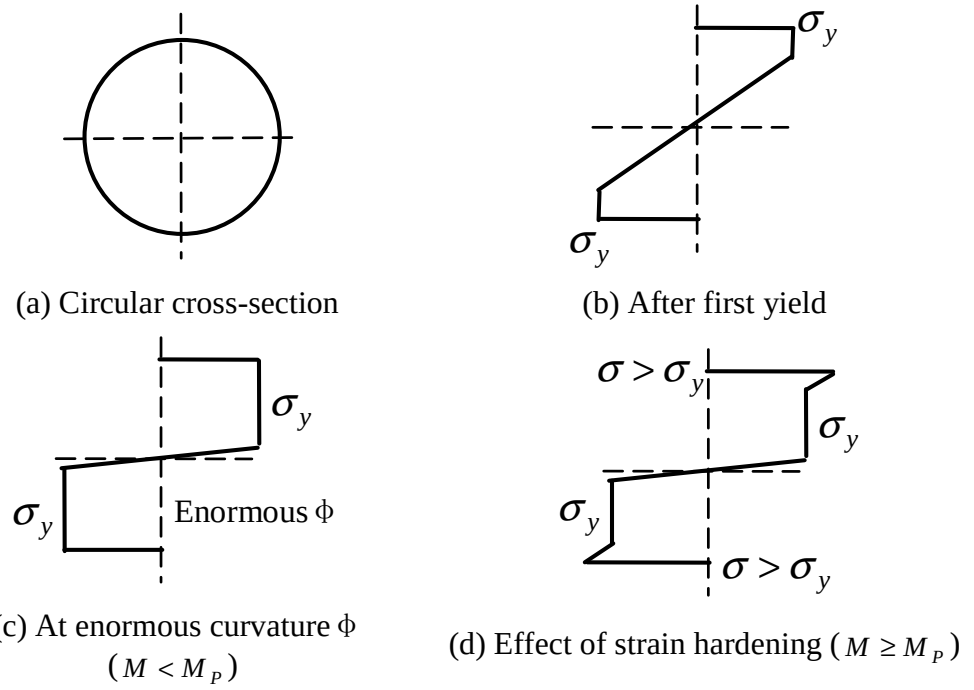

(a) Circular cross-section

(b) After first yield

(c) At enormous curvature ϕ ($M < M_P$)

(d) Effect of strain hardening ($M \geq M_P$)

Figure 4-20: Stress distribution of the circular cross-section for cylinders in global bending

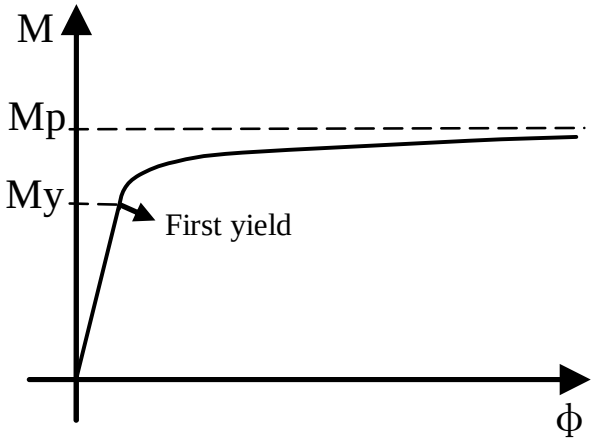

Figure 4-21: Relationship between the moment and curvature for cylinders in bending with ideal elastic-plastic material

For a thin shell, where the failure is dominated by either the yield or elastic-plastic bifurcation buckling, the collapse moment may occur during the development of plastic strain at constant yield stress. In this situation, the hardening of the material does not affect the collapse moment. The collapse moment derived for hardening Model C was consequently the same as for the ideal elastic-plastic material Model A.

For very thin shells, where the failure of the structure is dominated by elastic buckling without involving the effect of plasticity, the curves of these cylinders are exactly the same as the corresponding curves for the other two material models.

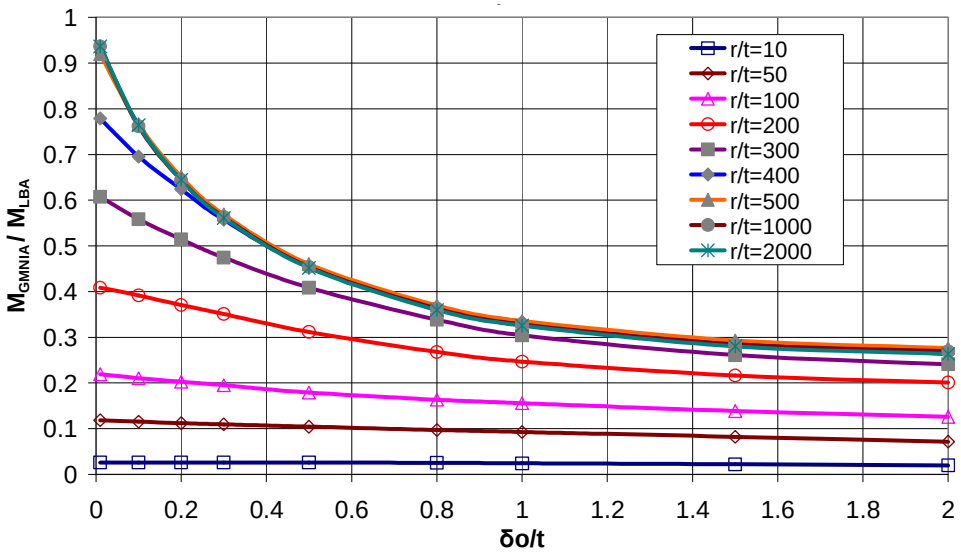

Figure 4-22: Imperfection sensitivity curves for cylinders with different radius to thickness ratios in bending

The imperfection sensitivity curves for hardening Model C with different radius to thickness ratios and imperfection amplitudes are shown in Fig. 4-22. The curves for comparatively thin cylinders are exactly the same as the corresponding curves for the ideal elastic-plastic model (Fig. 4-4) because plasticity has no effect on buckling behaviour. For quite thick cylinders, where the collapse moment is affected by both the imperfection amplitude and plasticity, the curves of these cylinders for Model A and Model C may be different, depending on the specific values of r/t.

The complete traditional buckling curves (capacity curves) and the alternative form of the capacity curves for cylinders in bending with weld depression geometric imperfections of different amplitudes are shown in Fig. 4-23 and Fig. 4-24.

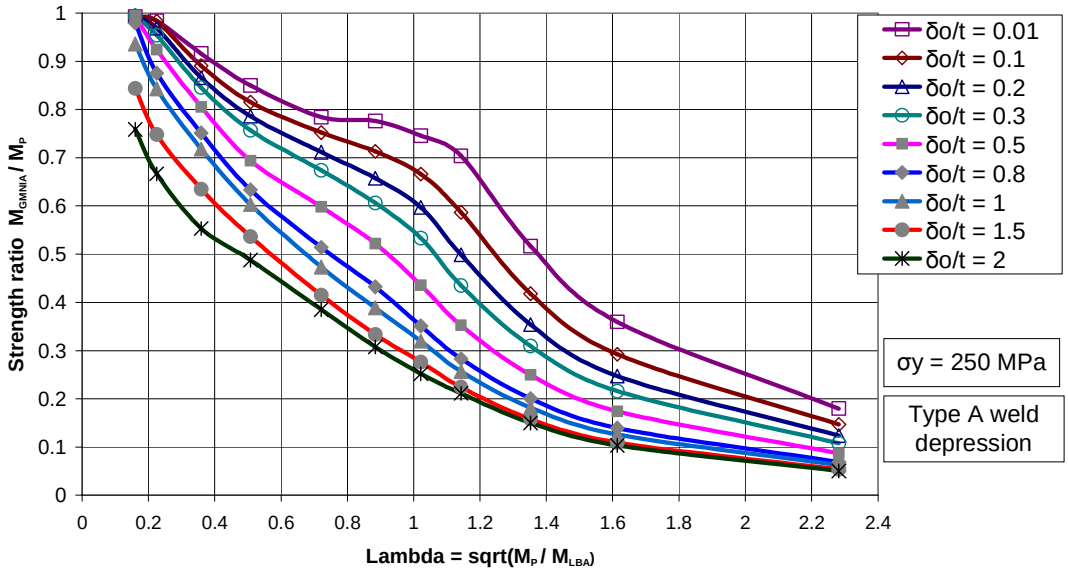

Figure 4-23: Buckling strength (capacity) curves for cylinders in bending with different imperfection amplitudes δ_o/t (Model C and with changing r/t)

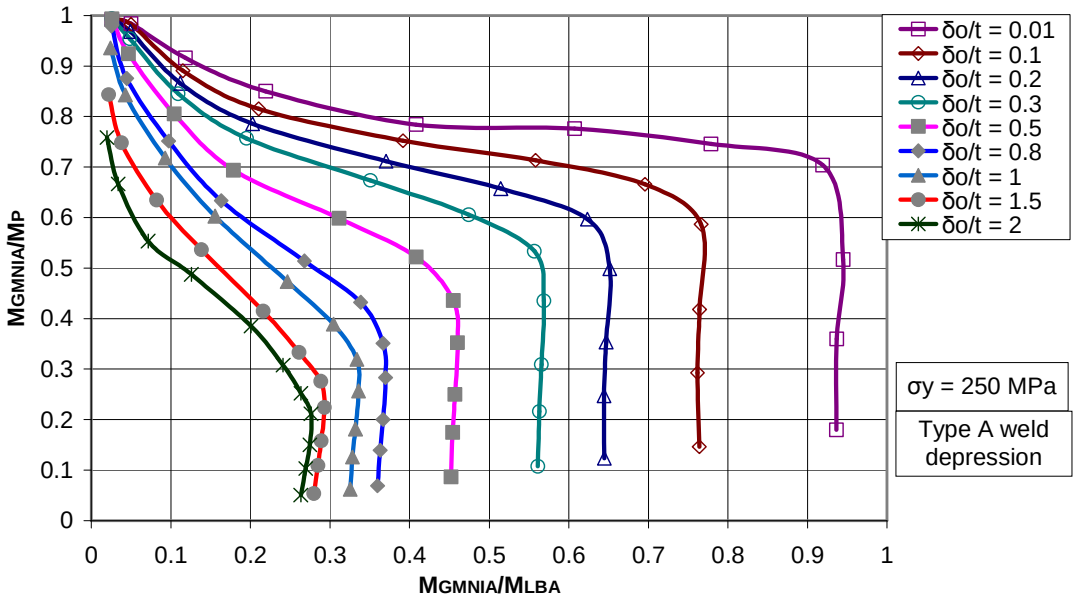

Figure 4-24: Alternative form of capacity curves for cylinders in bending with different imperfection amplitudes δ_o/t (Model C and with changing r/t)

Compared with the capacity curves for the ideal elastic-plastic material model (Figs 4-5 and 4-6), the values of M_k / M_p for hardening Model C increase remarkably for very thick shells ($10 \le r/t < 50$). This is especially so for very thick cylinders with deep imperfection amplitudes, which is due to the indefinite hardening

in hardening Model C. Plastic strains can develop considerably before reaching the collapse moment for very thick cylinders, so the high stress in the strain hardening stage can play an important role in increasing the collapse moment. By contrast, if the critical bending moment is reached before the strain hardening begins to intervene, the capacity curves for hardening Model C are precisely the same as for the ideal elastic-plastic material Model A.

4.6.3 Extraction of capacity curve parameters

The elastic imperfection reduction factor α and the plastic range factor β are not affected by the hardening of material. The expressions of α and β for ideal elastic-plastic material are still applicable for hardening Model C. They are expressed as:

$$\alpha = \frac{1}{1+2.00\left(\delta_o/t\right)^{0.8}} \tag{4.14}$$

$$1-\beta = \frac{0.77}{1+1.2\left(\delta_o/t\right)^{0.8}} \tag{4.15}$$

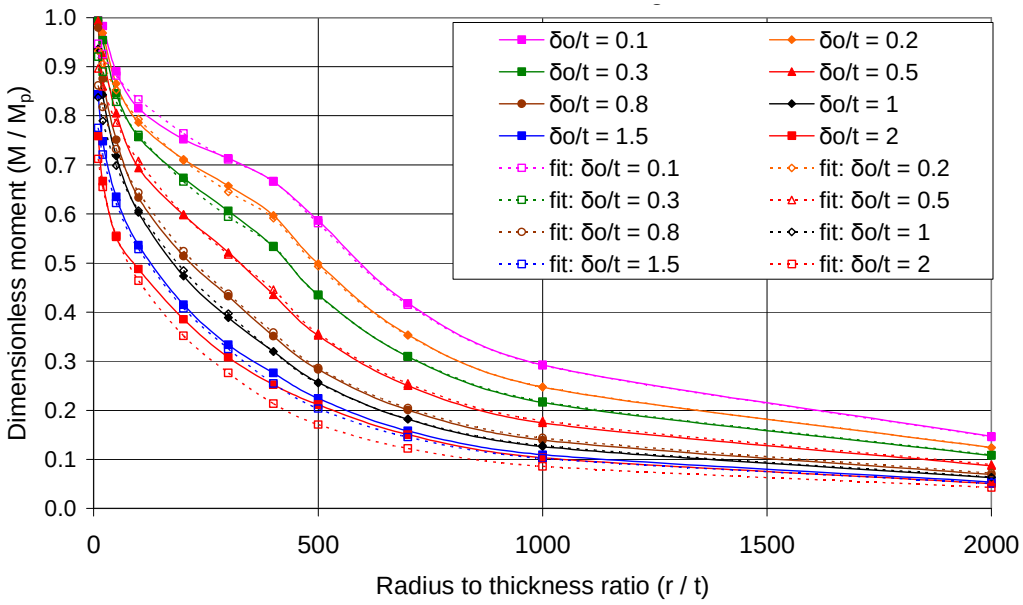

Figure 4-25: Calculated and best fitted capacity curves (Model C)

However, the interaction exponent η is affected by the hardening of material and may be closely represented by

$$\eta = \frac{1}{1+0.3(\delta_0 / t)^{1.5}} \tag{4.16}$$

Results of using Eqs 4-14, 4-15 and 4-16 to represent the complete conventional capacity curves are shown in Fig. 4-25.

4.7 Comparison of results for different material models

The relationship between normalized moment M_{GMNIA} / M_p and imperfection amplitude δ_0 / t for cylinders with $r/t = 10$ and material models is shown in Fig. 4-26. At a very small imperfection amplitude δ_o/t=0.01, the values of M_{GMNIA} / M_p for Models A and C are the same and close to 1. The corresponding value for Model B is larger than the other two. The results indicate that, after the first yield, the immediate strain hardening will increase the collapse moment considerably as Model B shows. On the contrary, subsequent strain hardening, after the plastic strains develops a lot at constant first yield stress, is not beneficial to improve the collapse strength as Model C shows.

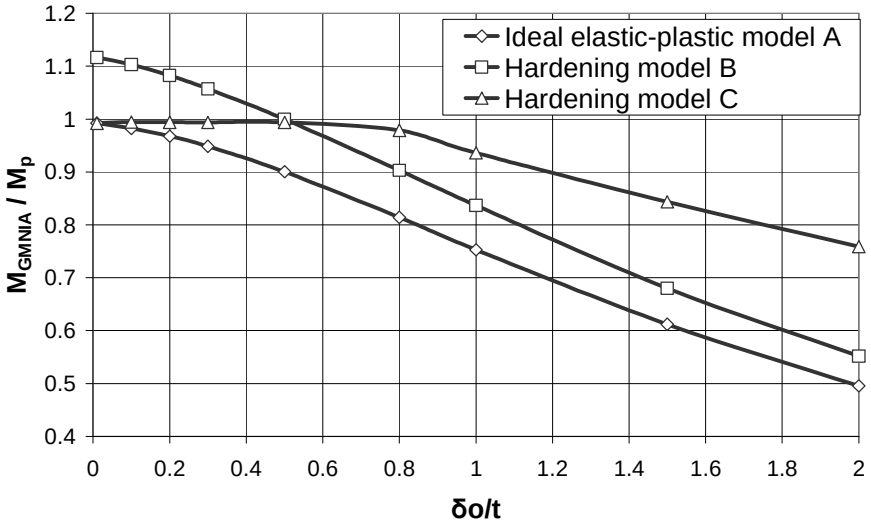

Figure 4-26: The dimensionless limit moment for different material models with different imperfection amplitudes δ_o/t ($r/t = 10$)

Also for $r/t = 10$, with increasing imperfection amplitudes, the difference of M_{GMNIA}/M_p between Models A and C increases steadily, especially for models with larger imperfection amplitudes. It indicates that the strain hardening in Model C began to affect the collapse strength with increasing values of imperfection amplitudes. Due to the high stress concentration at the central cross-section with the largest imperfection amplitude, the plastic strain develops quickly after the first yield stress is reached. This leads to a considerable plastic strain before the collapse moment is reached, so that the strain hardening in Model C affects the collapse moment. The peak stress at failure is increased leading to an increase in the collapse moment. The larger the imperfection amplitude is, the more significantly the strain hardening affects the buckling strength.

However, the difference of M_{GMNIA}/M_p for Models A and B changes little with increasing values of imperfection amplitude. That is because the plastic strain before the collapse load is reached is quite large, so that the whole strain hardening stage of Model B will be involved and affects the buckling behaviour, leading to the collapse moment occurring at a same value of yield stress. So for all imperfection amplitudes, the influence of the strain hardening of Model B is significant.

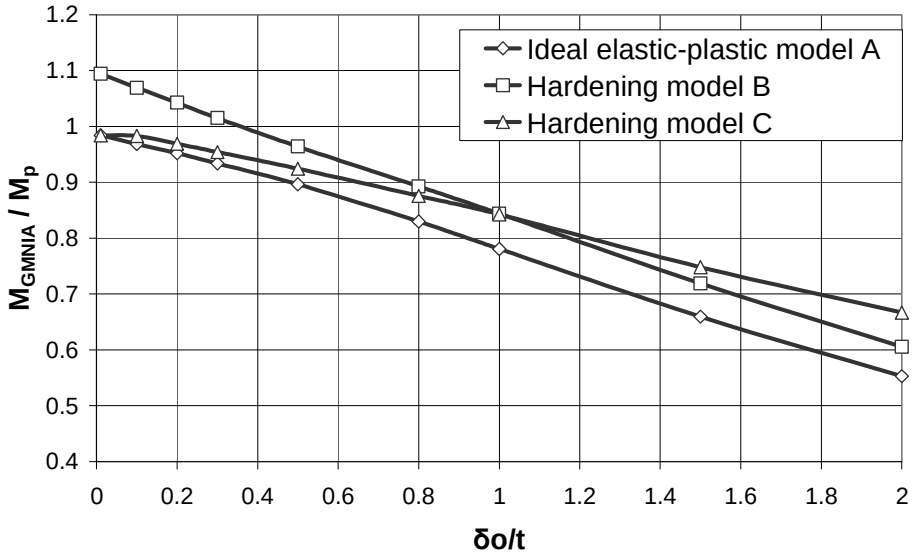

Figure 4-27: The dimensionless limit moment for different material models with different imperfection amplitudes δ_o/t ($r/t = 20$)

For a thinner shell with $r/t = 20$ (Fig. 4-27), the total plastic strain developed at the collapse moment decreases but the value might still be larger than ten times the first yield strain, so in Model C, strain hardening may affect the collapse moment except for cylinders with small imperfection amplitudes. However, this influence is less important than that for $r/t = 10$. The critical moment occurs at a lower yield stress compared with the shell with $r/t = 10$. This leads to the difference of M_{GMNIA}/M_p between Models C and A in Fig. 4-27 being smaller than that in Fig. 4-26. Similar to the shell with $r/t = 10$, the value of M_{GMNIA}/M_p for Models B and A is close for all imperfection amplitudes.

In the range $50 \le r/t < 200$ (Figs 4-28 and 4-29), the collapse moment for Model C is almost the same as that for Model A. With increasing r/t, the plastic zone of the cross-section that forms the plas1tic collapse mechanism becomes gradually smaller until local elastic-plastic bifurcation buckling occurs. The total plastic strain is smaller than ten times the first yield strain for these cylinders. In this situation, the strain hardening in Model C has no influence on the yield failure of thick cylinders or elastic-plastic bifurcation buckling of comparatively thin cylinders. For Model B, the collapse moment is reached during the strain hardening stage, and the influence of strain hardening decreases as the cylinder becomes thinner. So the moment ratio M_{GMNIA}/M_p is closer to the value for Model A as the cylinder becomes thinner.

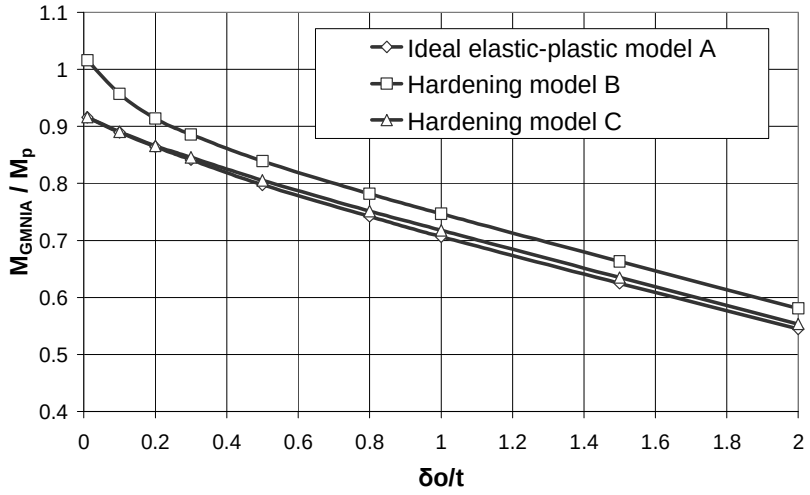

Figure 4-28: The dimensionless limit moment for different material models with different imperfection amplitudes δ_o/t ($r/t = 50$)

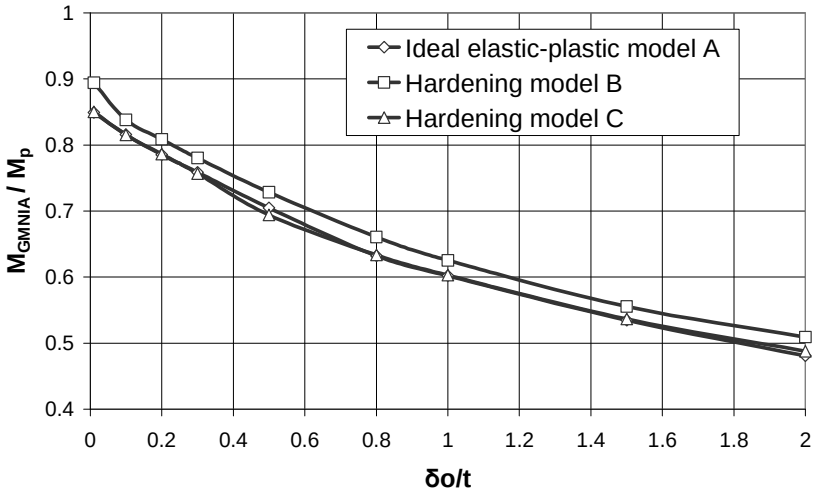

Figure 4-29: The dimensionless limit moment for different material models with different imperfection amplitudes δ_o/t ($r/t = 100$)

For a thinner shell with $r/t = 200$ (Fig. 4-30), the zones over which yield must spread to form a buckle is quite local and is easily achieved. Elastic-plastic bifurcation buckling occurs quickly once the first yield stress is reached. That is why the critical bending moments for Models B and A are almost indistinguishable. Though plasticity already affects the buckling behaviour and causes an obvious reduction in the buckling strength, the influence of strain hardening in Model B is negligible.

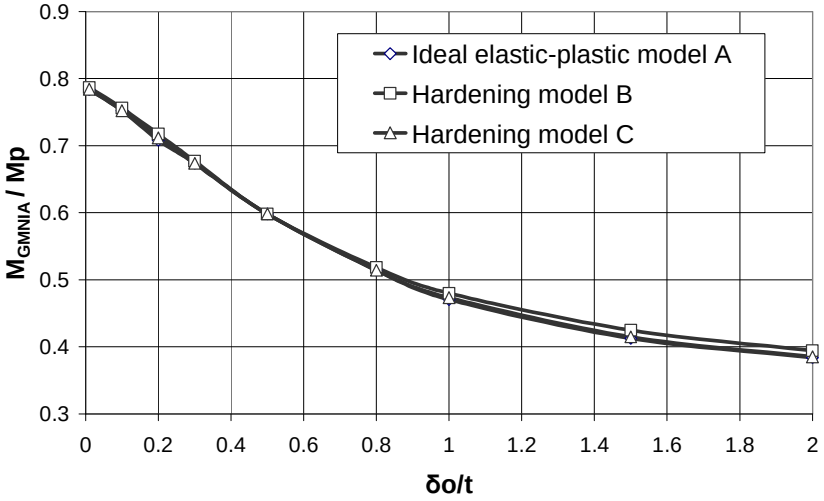

(e) $r/t = 200$

Figure 4-30: The dimensionless limit moment for different material models with different imperfection amplitudes δ_o/t ($r/t = 200$)

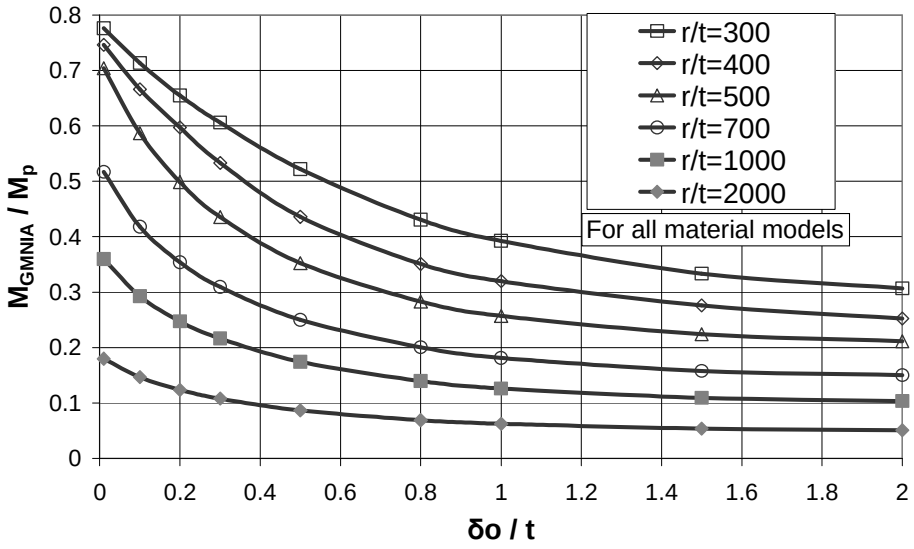

(f) $r/t > 200$

Figure 4-31: The dimensionless limit moment for different material models with different imperfection amplitudes δ_o/t

For cylinders with $r/t > 200$ (Fig. 4-31), the failure of the shell is dominated by either the elastic-plastic bifurcation buckling or elastic bifurcation buckling. The critical bending moments obtained for the three material models are very close. Dimensionless critical moment and imperfection amplitude relationship curves for different material models can be represented by a single curve for each value of r/t.

Another form of relationship curves linking the dimensionless moment M_{GMNIA}/M_{LBA} and imperfection amplitudes is shown in Fig. 4-32. For cylinders in the range $200 < r/t < 500$, strain hardening in Models B and C has a negligible effect on the critical bending moment. The critical moment is reached soon after first yield. Elastic-plastic bifurcation buckling occurs and the bifurcation buckling moment is affected by plasticity. This influence decreases as the cylinder becomes thinner. The critical moment is obviously reduced due to the effect of plasticity compared with the linear elastic critical moment M_{LBA}, especially for cylinders with small imperfection amplitudes.

For thin cylinders with $r/t > 500$, the failure is always controlled by elastic bifurcation buckling without the effect of plasticity. The relationship curves in Fig.

4-32 with different radius to thickness ratios and material models can be represented by a single curve. Precise extraction of the results leads to a classical “imperfection sensitivity curve”, as occurred in Fig. 4-7 for Model A. The elastic imperfection reduction factor α is given by Eq. 4.8.

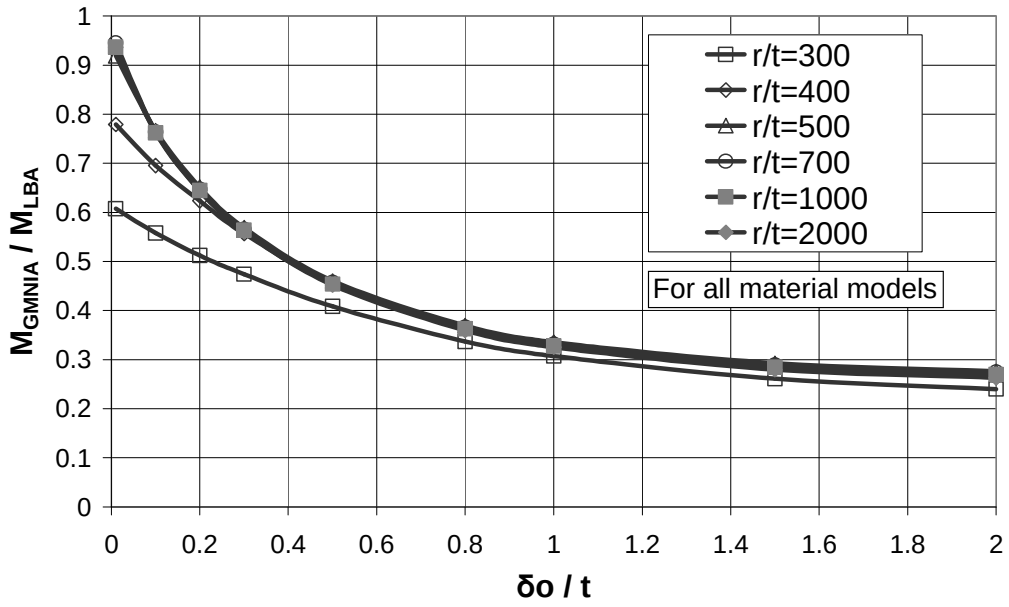

Figure 4-32: Imperfection sensitivity curve for cylinders with different radius to thickness ratios and material models

By comparing the results for the three different material models, it can be concluded that for very thin cylinders with $r/t \geq 500$, the elastic bifurcation buckling occurs and plasticity has no influence on the buckling strength. For thick cylinders with failure dominated by the plastic yield or elastic-plastic buckling, plasticity affects the buckling strength depending on the specific value of r/t. Strain hardening may increase the collapse moment for thick shells depending on how strain hardening is defined in stress-strain relationship curves. For cylinders with $r/t > 200$, the influence of any strain hardening on the collapse load is negligible.

4.8 Cylindrical shells under combined axial compression and global bending in the elastic-plastic range

4.8.1 Buckling of cylindrical shells under combined axial compression and global bending

Axial compression and global bending are two dominant loading conditions in practical cylindrical shells. The elastic-plastic imperfection sensitivity of axially compressed cylinders with weld depressions was studied by Rotter (1997, 2004, 2008). The buckling behaviour of medium-length cylindrical shells under pure global bending in the elastic-plastic range was studied in previous sections. These studies illustrate how the capacity curves of EN 1993-1-6 (2007) for shell buckling can be exploited to achieve a full characterisation of the ideal elastic-plastic buckling strength of imperfect cylindrical shells with a weld depression. However, it is not unusual for a cylindrical structure to be subjected to the combined action of both axial compression and global bending. Key examples are the tubular shells used in buildings, offshore platforms, pipelines, silos, tanks and other engineering structures. This next section presents FEM analysis of buckling behaviour of cylindrical shells under combined global bending and axial compression in the elastic-plastic range.

4.8.2 Aspects of finite element modeling

The bifurcation or plastic collapse of shells with radius to thickness ratios in the range $10 \le r/t \le 500$ were determined with geometric imperfections with amplitudes $\delta_0/t = 0.01$. The axi-symmetric imperfection adopted was Rotter and Teng's (1989) Type A weld depression, assumed to be a single local feature at middle of the cylinder, not interacting with other imperfections. The dimensions were all expressed in terms of the wall thickness *t*, and the length to radius ratio was kept at $L/r = 7$ for all reported calculations, which was same as those used for pure global bending analysis. The end boundaries were restrained to remain circular. These boundary conditions effectively prevent ovalization of these shells.

All the calculations reported here used an ideal elastic-plastic stress-strain relationship, obeying von Mises criterion, the normal flow rule and the flow theory

of plasticity in bifurcation calculations, with $E = 2.0 \times 10^5 MPa$, $\nu = 0.3$ and $\sigma_y = 250 MPa$.

An axial compressive stress was first applied to a prescribed value $\sigma = k\sigma_{cr}$ with $0 \le k \le 1$, where σ is the prescribed axial compressive membrane stress and σ_{cr} is the classical critical buckling stress for perfect cylinders under uniform axial compression. Then the compressive stress was fixed and a rotation θ was imposed at the ends of the shell and progressively incremented.

4.8.3 The moment-curvature curves

For very thick cylinders with $r/t = 10$, first yield occurs on the most compressed side of the cross-section. After first yield, the deformation of the structure develops quickly until the plastic limit load is reached. This represents a state of material rupture or unacceptably large plastic deformation, when stability phenomena do not intervene. The normalized moment-curvature curves for cylinders with $r/t = 10$ and $\delta_0 / t = 0.01$ with different values of prescribed axial compressive load are shown in Fig. 4-33. As the prescribed axial compressive load increases from a small value $\sigma = 0.1\sigma_{cr}$ to a large value $\sigma = 0.8\sigma_{cr}$, the plastic limit moment suffers a steady reduction. The obvious reason is that the prescribed axial compression load leads to an increase in the meridional stress on the compressed side, leading to an earlier occurrence of first yield. After the first yield, plastic deformations develop quickly to cause the plastic collapse.

For cylinders with $r/t = 200$ under pure global bending (Figs 4-2 and 4-3), the moment-curvature curve displays bifurcation buckling with a precipitous post-buckling fall. For cylinders with the same radius to thickness ratio under combined global bending and axial compression, the situation may be different. The normalized moment-curvature curves for cylinders with $r/t = 200$ and $\delta_0 / t = 0.01$ with different values of prescribed axial compressive stress are shown in Fig. 4-34. The curve for pure global bending is also shown in Fig. 4-34 as $\sigma / \sigma_{cr} = 0$.

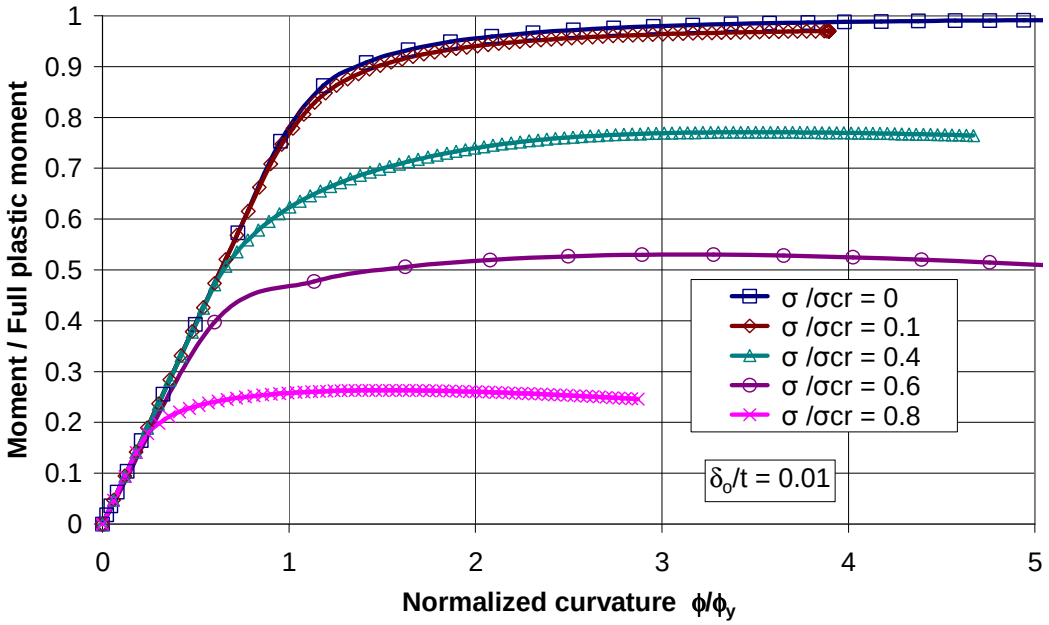

Figure 4-33: Moment-curvature curves for cylinders with different prescribed axial compression load ($r/t = 10$, imperfection amplitude $\delta_0/t = 0.01$)

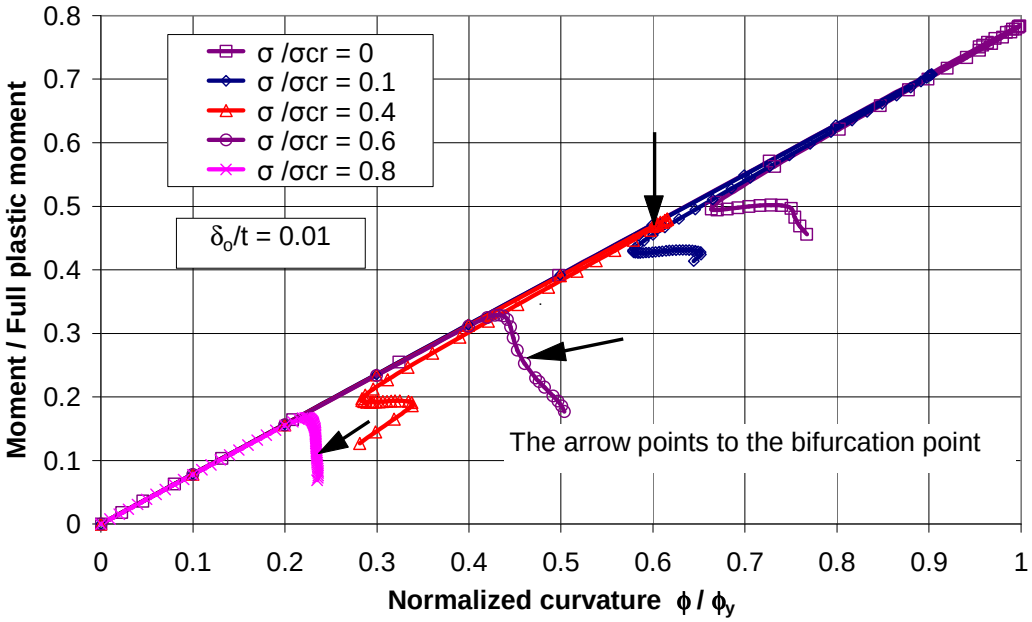

Figure 4-34: Moment-curvature curves for cylinders with different prescribed axial compression load ($r/t = 200$, imperfection amplitude $\delta_0/t = 0.01$)

When the prescribed axial compressive load is comparatively small ($\sigma = 0.1\sigma_{cr}$ or $\sigma = 0.4\sigma_{cr}$), the failure mode is still an elastic-plastic bifurcation buckling mode. The bifurcation point appears just before the limit moment point is reached and the moments at bifurcation and the peak point are quite close. The moment at bifurcation should be regarded as the collapse moment. After the peak point, the curve has a steep post-buckling fall followed by recovery and a second bifurcation leading to progressive falls in strength.

As the prescribed axial compressive load increases to a larger value as $\sigma = 0.6\sigma_{cr}$ and $\sigma = 0.8\sigma_{cr}$ (Fig. 4-34), snap-through buckling occurs at the limit point, and then a bifurcation point appears in the post-buckling path. The collapse of the structure is controlled by the snap-through buckling.

4.8.4 The nonlinear buckling modes for cylinders with $r/t = 200$

As Fig. 4-34 shows, the moment-curvature curves display different buckling behaviour as the prescribed value of axial compressive load changes. When a small prescribed axial load $\sigma = 0.1\sigma_{cr}$ is applied, the corresponding elastic-plastic bifurcation buckling mode and post-buckling mode is shown in Fig. 4-35(a) and (b).

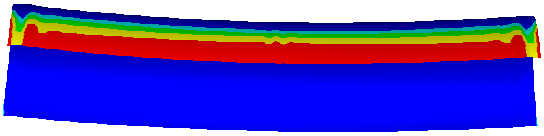

(a) Bifurcation buckling mode at bifurcation point

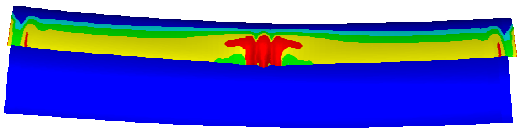

(b) Nonlinear post-buckling mode

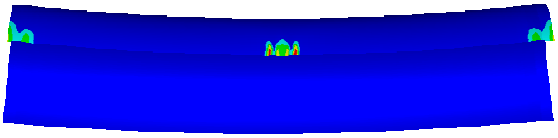

(c) Axial plastic strain at bifurcation point

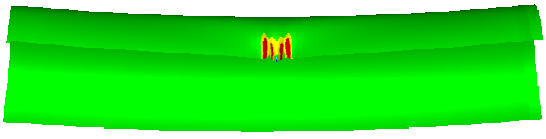

(d) Axial plastic strain at post-buckling stage

Figure 4-35: Buckling behaviour for prescribed compressive stress $\sigma = 0.1\sigma_{cr}$ ($r/t = 200$, $\delta_0/t = 0.01$)

Elastic-plastic bifurcation buckling occurs at the middle of the cylinder due to the effects of imperfection and geometric nonlinearity, which is similar to the nonlinear buckling mode under pure bending. The buckling stress is dominated by the compressive stress of the most compressed fibre caused by the global bending. The axial plastic strains at bifurcation point and post-buckling path (Fig. 4-35c and d) show that the buckling area is quite local, occupying only a tiny part of the whole cross-section.

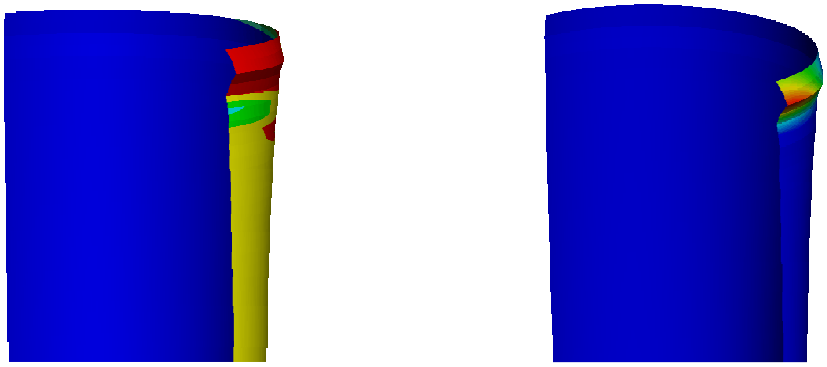

(a) Local Snap-through buckling mode **(b) Axial plastic strain at collapse load**

Figure 4-36: Local snap-through buckling mode at the ends of the cylinder for prescribed compressive load $\sigma = 0.8\sigma_{cr}$ ($r/t = 200$, $\delta_0/t = 0.01$)

The buckling behaviour is different when an axial compressive load $\sigma = 0.8\sigma_{cr}$ was prescribed. Firstly, a snap-through buckle occurs near the ends of the cylinder, due to the high stress concentration there. The buckling strength is dominated by the meridional membrane stress. Then a bifurcation point appears in the post-buckling path, leading to a secondary buckling mode, known as “elephant’s foot” buckling for thick cylinders (Fig. 4-36). However, this “elephant’s foot” bucking mode, caused by the axial compressive stress, is quite local and located at the compressed side of the cylinder. The buckling mode is similar to the nonlinear buckling mode for comparatively thick cylinders in uniform axial compression.

4.8.5 Interaction between axial compression and bending

Taking the collapse moment from each moment-curvature curve, the axial compression and bending interaction curves are shown in Fig. 4-37. For very thick

cylinders with radius to thickness ratio in the range $r/t \le 30$, the relationship curves are nonlinear, becoming linear when $r/t > 30$.

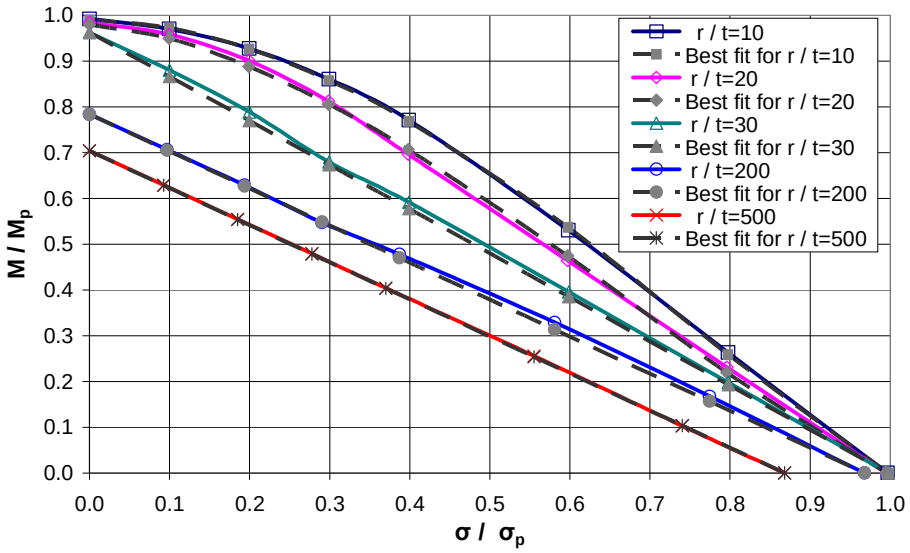

Figure 4-37: Collapse envelopes for cylinders under combined axial compression and global bending (imperfection amplitude δ_o/t = 0.01)

The interaction curves based on the ultimate capacity criterion can be closely approximated by a function of the form

$$a\left(\frac{M}{M_p}\right)^{\alpha} + b\left(\frac{\sigma}{\sigma_p}\right)^{\beta} = 1 \qquad (4.17)$$

in which a is a parameter to evaluate the buckling strength of cylinders under pure bending and is the reciprocal of the normalized collapse moment M/M_p for cylinders in pure bending; b is a parameter to evaluate the buckling strength of cylinders under pure axial compression and is the reciprocal of the normalized critical axial compressive stress σ/σ_p for cylinders under pure uniform axial compression. The values of a and b for cylinders with different radius to thickness ratios and $\delta_0/t = 0.01$ can be extracted easily from Fig. 4.37. For cylinders with different values of δ_0/t, the values of a and b can be extracted from the capacity curves for global bending (Figs 4-5 and 4-6) and uniform axial compression (Figs 2-13 and 2-14).

For thick cylinders with $r/t \le 30$, full plastic yield controls the collapse strength. The interaction curves for these cylinders are nonlinear in certain ranges. The reason is the plastic collapse mechanisms for these cylinders in two single loading conditions are quite different. For cylinders in uniform axial compression, the collapse occurs once the meridional membrane stress approaches the first yield stress. For cylinders in global bending, after the yield stress on the most compressed fire is reached, the plastic strain need to develop a lot before the collapse moment is reached. When consider the combined loading conditions, the collapse mechanism become a little complex.

In Fig. 4-37, because $\delta_0/t = 0.01$ is a very small imperfection, full plastic moment for pure global bending and yield stress for pure axial compression are almost achieved at the collapse load. Values of *a* and *b* representing the effect of imperfection amplitudes are thus very close l. The best fit equations in terms of Eq. 4.17 are given by:

For $r/t = 10$, $$1.008\left(\frac{M}{M_p}\right)^{0.81} + 1.003\left(\frac{\sigma}{\sigma_p}\right)^{1.83} = 1 \qquad (4.18)$$

For $r/t = 20$, $$1.016\left(\frac{M}{M_p}\right)^{0.8} + 1.005\left(\frac{\sigma}{\sigma_p}\right)^{1.60} = 1 \qquad (4.19)$$

For $r/t = 30$, $$1.039\left(\frac{M}{M_p}\right)^{0.98} + 1.0025\left(\frac{\sigma}{\sigma_p}\right)^{1.058} = 1 \qquad (4.20)$$

The indices α and β in Eq. 4.17 are shape parameters for the interaction curves. It can be seen when $r/t = 30$, the values of α and β are close to 1, and the interaction curve is very close to linear. So for thick cylinders with $r/t > 30$, the values of α and β are equal to 1. This is due to the close relationship of the buckling behaviour of comparatively thin cylinders under global bending and axial compression. For a comparatively thin cylinder under either uniform axial compression or global bending, the buckles are both caused by the axial compressive stress and the size of the typical buckle regimes is rather small. So a very small zone

with axial compressive stress reaching the critical value may be large enough to form an axial compressive buckle. The compressive stress within the buckling area for global bending is very close to uniform. So global bending actually increases the equivalent uniform axial compressive stress within the local buckling area. The interaction curves are thus linear. The relationship between parameters α or β and r/t is shown in Fig. 4-38.

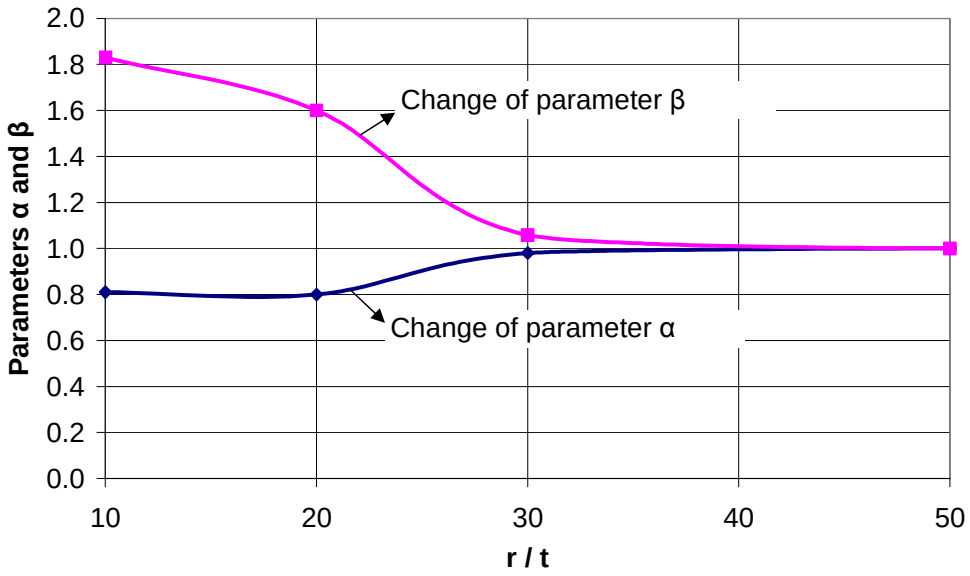

Figure 4-38: The relationship between parameters α or β and r / *t*

The thick cylinders in the range $r/t < 30$ with larger imperfection amplitudes are not included in this chapter. Because these cylinders are not practical in the design of cylindrical shell structures, it is not necessary to study the buckling behaviour of these cylinders further.

Due to the detrimental effect of the imperfection on the buckling strength, for cylinders in the range $r/t \geq 30$ with imperfection amplitude $\delta_0/t > 0.01$, local snap-through buckling, elastic-plastic buckling or elastic bifurcation buckling might occur at a reduced critical load than the corresponding buckling strength in Fig. 4-37. The buckling behaviours under global bending and axial compression should thus have a closer relationship. So interaction curves for these cylinders should be linear. The values of α and β are equal to 1.

Based on above description, for all cylinders in the range $r/t \geq 30$ with different imperfection amplitudes, the interaction curves can be replaced by:

$$a\left(\frac{M}{M_p}\right)+b\left(\frac{\sigma}{\sigma_p}\right)=1 \tag{4.21}$$

As the cylinder becomes thinner, the critical buckling strength is reached far from the full plastic moment (for global bending) or yield stress (for axial compression) being reached, and the values of a and b thence both increase continuously. The relationship of the parameters $1/a$ and $1/b$ with different radius to thickness ratios r/t is shown in Fig. 4-39. Similar curves for other imperfection amplitudes can be obtained easily from the capacity curves Figs 4-5 and 4-6 for global bending and Figs 2-13 and 2-14 for uniform axial compression.

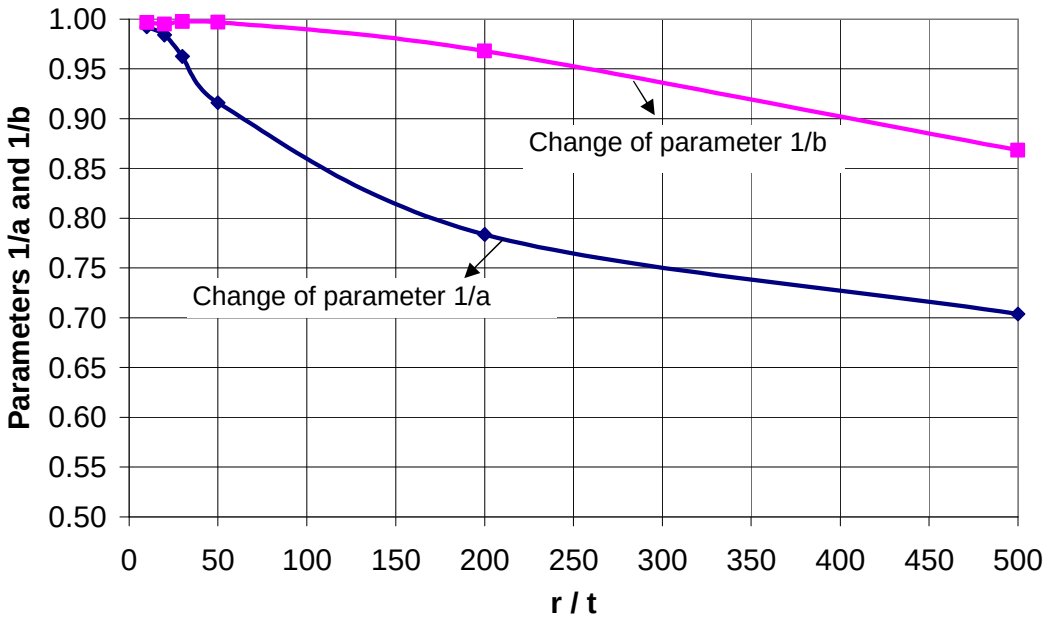

Figure 4-39: The relationship of the parameters $1/a$ and $1/b$ with different radius to thickness ratios r/t

4.8.6 Conclusions

The strength of cylindrical shells under combined axial compression and global bending in the elastic-plastic range has been studied. The buckling behaviour of cylinders with different radius to thickness ratios and prescribed axial compressive

loads were explored. Two different buckling modes “snap-through” buckling mode or bifurcation buckling mode might occur depending on the specific geometry and loading conditions. The axial compression and global bending interaction curves were derived and the best fit interaction expression in terms of Eq. 4.17 could fit the interaction curves quite well.

4.9 Conclusions

Geometrically and materially nonlinear analyses have been performed on thin cylindrical shells of moderate length, under either pure global bending or combined axial compression and global bending. The weld depression imperfection was adopted to explore the imperfection sensitivity of the buckling strength. The results have been mapped onto the shell buckling capacity curve of EN 1993-1-6 and a full characterisation achieved. This not only gave a fuller description of the elastic-plastic buckling strength of cylinders in global bending, but also showed how the capacity curve of the European shell buckling standard could be exploited to capture very complicated phenomena accurately.

Chapter 5 Buckling analysis of short cylinders of uniform thickness under uniform external pressure

5.1 Introduction and literature review

5.1.1 Buckling of cylindrical shells under uniform external pressure

The failure of elastic perfect cylinders under uniform external pressure is caused by circumferential buckling. It is a characteristic that cylinders under uniform external pressure develop relatively large buckles extending over the whole length of the shell (Greiner, 2004). This buckling pattern is quite different from that of cylinders under uniform axial compression. The effects of the cylinder length, of the restraining conditions at boundaries and of the length of the pressurised zone all have great influences on the critical buckling load.

The buckling behaviour of cylinders under uniform external pressure has been well studied by many researchers. In early studies, Southwell (1913), Batdorf (1947) and Nash (1954) studied this buckling problem based on an assumed simple one-term deflection function that satisfies the special boundary conditions. Following their works, Ho and Cheng (1963), Sobel (1964), etc. derived more accurate solutions by integrating the basic equations directly. Flügge (1973) obtained a comprehensive analytical solution for the critical buckling load. However, all the results above assumed a pre-buckling membrane stress state given by membrane theory.

In recent decades, solutions of the buckling strength of cylinders under uniform external pressure have been improved by many researchers. Yamaki (1984) derived both analytical and numerical results based on Flügge equations and Donnell equations. He also pointed out the importance of the pre-buckling bending effect for extremely short cylinders. Vodenitcharova (1996) presented a theoretical investigation based on Flügge's stability equations and studied the influence of 17 different homogeneous boundary conditions. More recently, Abdelmoula (2008) used an asymptotic method to determine the effects of boundary conditions on the

critical load and buckling shapes for cylinders under uniform external pressure with very large “Batdorf” length parameters, while quite short cylinders were not included.

In the European Standard for Shells EN 1993-1-6 (2007), the critical circumferential buckling stress is obtained by introducing an external buckling factor which takes the influence of different boundary conditions into account. For medium-length cylinders, the external pressure buckling factors is given by C_θ (Table 5-1), while for short cylinders, it is given by $C_{\theta s}$ (Table 5-2). However, the restraint of the meridional rotation at boundaries was not considered separately in these tables. This is correct for medium-length cylinders because the end rotation was proved to have little effect on the buckling strength, while for short cylinders, the rotations at the two ends of the shell may interact with each other, which may influence the buckle form and buckling strength significantly. In this situation, the meridional rotation may affect the form of the buckle greatly. However, the expressions in Table 5-2 for short cylinders take no account of meridional rotation at boundaries. So it is necessary to consider the effect of meridional rotation on the buckling strength of short, especially extremely short cylinders under uniform external pressure.

On the other hand, the classic buckling solution was based on the assumption of a pre-buckling membrane stress state, which is generally valid for medium-length and long cylinders, but for short cylinders any restraint of the boundaries affects the buckling mode and buckling strength greatly, so the influence of pre-buckling bending effect should be taken into account. Therefore, during the calculations, to derive more accurate solutions, the same boundary conditions should be adopted at the pre-buckling stage and buckling mode calculation stage, which corresponds to the real boundary conditions of practical structures where the pre-buckling membrane stress state is impossible to be achieved during the construction.

The reason to study the buckling behaviour of short cylinders under uniform external pressure is that the elastic buckling strength of these cylinders is usually very small and is directly related to the length (Eqs 5.1 and 5.2), which is different

from cylinders under uniform axial compression for which the elastic buckling strength is usually high and not directly related with the length of the cylinder (Eq. 1.1). It means the buckling strength of short cylinders under uniform external pressure is more sensitive to the boundary conditions. Tanks and silos are usually very thin so that plasticity seldom affects the buckling behaviour. Furthermore, in practice, the cylinder with quite a short length is not unusual. For some cylindrical shells of stepwise variable wall thickness under either uniform external pressure or wind loading, buckling occurs only in the upper thin strakes, while the lower thicker ones provide considerable restraint against both radial and axial displacements at the boundary between two strakes (ECCS EDR5, 2008). So elastic buckling is controlled by the buckling strength of the top thinner strakes. The length to radius ratio for the top thinner strakes is sometimes quite small.

In this chapter, the buckling behaviour of cylinders with $r/t = 250$ and different length to radius ratios under uniform external pressure was first analyzed comprehensively. Short, medium-length and long cylinders were all included. Next, the effect of meridional end rotations on the buckling strength of short cylinders was studied, with the assumption of a membrane pre-buckling stress state. Finally, the effect of pre-buckling edge rotations on the buckling strength of short cylinders was taken into account. Approximate equations based on the numerical results were derived for practical use.

5.1.2 Theoretical solutions for cylinders under uniform external pressure

For short, medium-length and long cylinders, in EN 1993-1-6 (2007) (also in Chapter 10, ECCS EDR5, Schmidt and Rotter, 2008), the critical circumferential buckling stress depends on different geometries and boundary conditions.

For medium-long cylinders which are defined by $20 \le \frac{w}{C_\theta} \le 1.63\frac{r}{t}$, the elastic critical circumferential stress should be obtained from (EN 1993-1-6, 2007) as:

$$\sigma_{\theta cr} = 0.92E\frac{C_\theta}{\omega}\frac{t}{r} \tag{5.1}$$

The external pressure buckling factor C_θ depends on the boundary conditions and should be taken from Table 5-1 (EN 1993-1-6, 2007).

Table 5-1: External pressure buckling factors for medium-length cylinders C_θ (EN 1993-1-6, 2007)

Case	Cylinder end	Boundary condition	External pressure factors C_θ
1	end 1	BC 1	1.5
	end 2	BC 1	
2	end 1	BC 1	1.25
	end 2	BC 2	
3	end 1	BC 2	1.0
	end 2	BC 2	
4	end 1	BC 1	0.6
	end 2	BC 3	
5	end 1	BC 2	0
	end 2	BC 3	
6	end 1	BC 3	0
	end 2	BC 3	

Equation 5.1 without C_θ arises from classical linear Donnell-type shell buckling theory and was first derived by Batdorf (1947) and later independently by Ebner (1952). It is derived for medium-length cylinders with simply-supported edges (BC2) and loaded by uniform external pressure. The circumferential buckling stress is related to the cylinder length directly, which contrasts with the classical buckling strength for meridionally compressed cylinders. This difference is caused by the different buckling modes in the two loading conditions. The meridional buckle for uniform external pressure is long, extending over the whole length of the cylinder, while the buckle for uniform axial compression is usually very local along the meridian and is far away from the boundaries.

For short cylinders which are defined by $\omega / C_\theta \le 20$, the elastic critical circumferential stress should be obtained from (EN 1993-1-6, 2007):

$$\sigma_{\theta cr} = 0.92E \frac{C_{\theta s}}{\omega} \frac{t}{r} \tag{5.2}$$

The external pressure buckling factor $C_{\theta s}$ depends on different boundary conditions and length parameter ω and should be taken from Table 5-2 (EN 1993-1-6, 2007). The expressions of $C_{\theta s}$ shown in Table 5-2 are approximations to numerical solutions and were developed by Schmidt and Greiner (1998). The value of $C_{\theta s}$ changes with the length parameter ω, but C_{θ} for medium-length cylinders is constant for a given boundary condition. It indicates that the buckling strength of short cylinders is sensitive to boundary conditions when the cylinder becomes shorter.

Table 5-2: External pressure buckling factors for short cylinders $C_{\theta s}$ (EN 1993-1-6, 2007)

Case	Cylinder end	Boundary condition	External pressure factors $C_{\theta s}$
1	end 1	BC 1	$C_{\theta s} = 1.5 + \frac{10}{\omega^2} - \frac{5}{\omega^3}$
	end 2	BC 1	
2	end 1	BC 1	$C_{\theta s} = 1.25 + \frac{8}{\omega^2} - \frac{4}{\omega^3}$
	end 2	BC 2	
3	end 1	BC 2	$C_{\theta s} = 1.0 + \frac{3}{\omega^{1.35}}$
	end 2	BC 2	
4	end 1	BC 1	$C_{\theta s} = 0.6 + \frac{1}{\omega^2} - \frac{0.3}{\omega^3}$
	end 2	BC 3	

Greiner (2004) gave the expression for short and medium-long cylinders as:

$$\sigma_{cr} = \frac{E}{m^2}\left[\frac{1}{\left(1+\left(m^2/\pi^2\right)(\ell/r)^2\right)^2} + \frac{(t/r)^2}{12\left(1-\nu^2\right)}\left(m^2+\pi^2\left(\frac{r}{\ell}\right)^2\right)^2\right] \tag{5.3}$$

Equation 5.3 is obtained based on the simply supported S3 boundaries at both ends. For very short cylinders, only the second term of Eq. 5.3 is relevant.

The critical buckling wave number for medium-long cylinders may be obtained by (Greiner, 2004):

$$m_{cr}^2 = C_M \frac{r}{l}\sqrt{\frac{r}{t}}\sqrt[4]{36\left(1-\upsilon^2\right)} \tag{5.4}$$

where C_M represents the effects of boundary conditions and can be found in Greiner (2004).

For quite short cylinders, the circumferential compressive buckling stress asymptotically approaches the plate buckling stress of an indefinitely long plate strip (see the results below). The equivalent formula for plates is (Schmidt & Greiner, 1998):

$$\sigma_{cr,pl} = E\left(\frac{r}{l}\right)\left(\frac{t}{r}\right)^{1.5}\left[\frac{0.904k}{(l/r)\sqrt{r/t}}\right] \tag{5.5}$$

where k is the buckling coefficient for the plate: $k = 2$ when external pressure includes the pressure on the end plates, and $k = 4$ for purely circumferential stress.

For long cylinders, the elastic critical circumferential stress should be obtained according to Eq. 5.6 (EN 1993-1-6, 2007):

$$\sigma_{\theta cr} = E\left(\frac{t}{r}\right)^2\left[0.275 + 2.03\left(\frac{C_\theta}{w}\frac{r}{t}\right)^4\right] \tag{5.6}$$

For very long cylinders, the circumferential buckling stress asymptotically approaches the value for a plane circular ring under a uniform radial load. The formula can be expressed as (Timoshenko and Gere, 1961):

$$\sigma_{\theta cr} = \frac{3Et^3}{12\left(1-\nu^2\right)r^3}\frac{r}{t} = 0.275E\left(\frac{t}{r}\right)^2 \tag{5.7}$$

It should be noted that the above expressions are all based on the assumption that the pre-buckling stresses are entirely membrane stresses and the meridional rotations at the ends are not considered. For short cylinders, these assumptions may cause inaccurate results, as will be seen later.

When a short cylinder is subjected to uniform external pressure, the stress distribution acting on the element, with consideration of meridional rotations in the pre-buckling state, together with the Poisson's ratio effect, is shown in Fig. 5-1. The nonlinear equilibrium equation at the pre-buckling stage is given by (Timoshenko and Gere, 1961)

$$D\frac{d^4w}{dx^4} + N_x\frac{d^2w}{dx^2} + \frac{Et}{r^2}w = p - \frac{\nu N_x}{r} \tag{5.8}$$

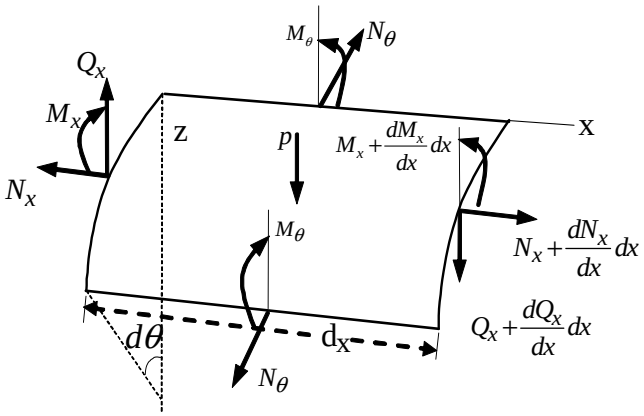

Figure 5-1: Stress distribution for cylindrical shells under uniform external pressure

Yamaki (1984) conducted a comprehensive study of this buckling problem and derived theoretical solutions based on the condition of either the pre-buckling bending effect being neglected or being considered. The effect of different boundary conditions was discussed. When considering the effect of pre-buckling bending deformations, his results were based on Donnell's basic equations, and the linear equilibrium equation at the pre-buckling state (without hydrostatic pressure) was given by

$$D\frac{d^4w}{dx^4} + \frac{Et}{r^2}w = p \tag{5.9}$$

Then the equations governing the incremental deformation are derived and the Galerkin method was used to determine the critical pressure.

In this chapter, finite element analyses were conducted to explore the effect of meridonal rotations and pre-buckling bending deformations on the buckling strength

using the finite element software ABAQUS. In ABAQUS, all shell elements use bending strain measures that are approximations to those of Koiter-Sanders shell theory (Budiansky and Sanders, 1963). The results were compared with Yamaki's results and results in EN 1993-1-6 (2007). It is expected that the external pressure buckling factor for short cylinders $C_{\theta s}$ given in EN 1993-1-6 (2007) can be improved in a more reasonable way.

5.2 Computational model for cylinders under uniform external pressure

5.2.1 Linear bifurcation buckling analysis (LBA)

The pre-bucking deformation of cylinders under uniform external pressure is very small compared with the geometry of the shell. The influence of geometric nonlinearity on the buckling strength is usually negligible. So only the linear bifurcation analysis (LBA) is required to derive the buckling strength. LBA procedure is an eigenvalue analysis and the buckling load is often obtained by solving an eigenvalue problem. More knowledge about eigenvalue problems can be found in many finite element books (Zienkiewicz and Taylor, 1971; Bathe, 1976; Hughes, 1987).

The boundary conditions adopted in eigenvalue buckling analysis in ABAQUS should be noted. A nonzero prescribed boundary condition in a general analysis step preceding the eigenvalue buckling analysis can be used to preload the structure, so that the effect of pre-buckling bending deformations due to the edge rotation can be involved. Nonzero boundary conditions prescribed in an eigenvalue buckling step will contribute to the incremental stress $\Delta\sigma$ and, thus, will contribute to the differential initial stress stiffness. Nonzero prescribed boundary conditions will be treated as constraints during the eigenvalue extraction. Therefore, unless the prescribed boundary conditions are removed for the eigenvalue extraction by specifying buckling mode boundary conditions, the mode shapes may be altered by these boundary conditions (Hibbitt, 2003).

5.2.2 Different form of boundary conditions

Table 5-3: Boundary conditions terminology for cylindrical shells

EN 1993-1-6 (2007)	Yamaki (1984)	δu (meridioanl displacement)	δv (circumferential displacement)	δw (radial displacement)	$\delta\beta$ (meridional rotation)
BC1f	S1	r	r	r	f
BC1f	S2	r	f	r	f
BC2f	S3	f	r	r	f
BC2f	S4	f	f	r	f
BC1r	C1	r	r	r	r
BC1r	C2	r	f	r	r
BC2r	C3	f	r	r	r
BC2r	C4	f	f	r	r
BC3		f	f	f	f

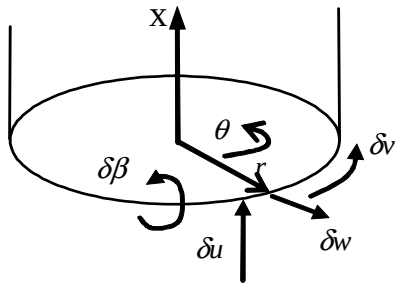

Figure 5-2: The degree of freedoms at ends of the cylinder

In EN 1993-1-6 (2007), the boundaries are differentiated in terms of BC1~BC3 for different restraints (Table 5-3), where f means free and r means restrained. The degrees of freedom at the ends of the cylinder for each defined boundary are shown in Table 5-3. Yamaki (1984) used terminology C1~C4 (Clamped) and S1~S4 (simply supported) to indicate these boundary conditions.

However, as stated in EN 1993-1-6 (2007), the circumferential displacement v is very closely linked to the radial displacement w that is normal to the surface, so separate conditions are not identified in EN 1993-1-6 for these two parameters. Yamaki's boundary conditions S2, S4, C2 and C4 are not considered separately in this study. Though rotational restrains at shell boundaries may be ignored in modelling for the plastic limit state (EN1993-1-6, 2007), it is still interesting to

explore the effects of rotational restraints on the elastic buckling strength due to the small elastic buckling strength of cylinders under uniform external pressure.

5.2.3 Finite element model

For the numerical analysis in this study, cylinders with radius to thickness ratios in the range $250 \le r/t \le 1000$ and different length to radius ratios were adopted. The commercial finite element program ABAQUS (Hibbitt et al, 2003) was used to calculate the critical buckling loads. Cylinders with $r/t = 250$ were chosen to explore the effects of meridional rotation and pre-buckling bending deformation on the buckling strength. The shell was assumed to be made of an isotropic material with Young's modulus $E = 2.0 \times 10^5 MPa$ and Poisson's ratio $\nu = 0.3$. The analyses for both 180° half cylinder model and whole shell model were first conducted. The results indicated that the 180° half cylinder model could capture the buckling strength accurately due to the symmetry of the geometry, integer values of the buckling modes and the loading conditions.

5.3 Mesh convergence study

5.3.1 General

As discussed above, the end boundary conditions could have a significant effect on the buckling strength of cylinders under uniform external pressure. For medium-length and long cylinders, the buckling strength is dominated by circumferential membrane stress without the influence of boundary conditions. With decreasing length, the bending stress caused by edge rotations near the boundaries gradually rises. For quite short cylinders, the buckling behaviour is similar to a long plate strip. In this situation, a very fine mesh, especially near the boundaries, is required to obtain the accurate results. From Eq. 5.4, it is obvious that the circumferential buckling wave number increases with decreasing length of a cylinder, which also indicates that a refined mesh is required to accommodate the small half wave-length of the buckle. It should be noted that this equation is only for medium-length cylinders and there are no known equations for short cylinders. So with decreasing length and increasing critical buckling wave number, the requirement of the mesh to

capture the accurate buckling strength is different. Due to the reasons above, it is necessary to conduct an initial mesh convergence study for this buckling problem in the numerical calculations.

A good approach for the mesh convergence study is to adopt a mesh which provides a close result to that from a further refined mesh. If the critical buckling load which is changed by less than 1% as a result of a further refinement of the mesh, the chosen mesh can be regarded as an acceptable result (Song, 2002). For the shell buckling problem studies, discretization into finite elements is sometimes discussed in terms of the number of elements or nodes per half-wavelength of the relevant bending or buckling deformations, which is usually adopted for cylinders under axial compression. However, for cylinders under axial compression, the end boundary conditions are not as important as in the current problem and the half-wave length of the local axisymmetrical meridional buckle is not related to the cylinder length (Eq. 2.13). While for short cylinders under uniform external pressure, no equations are known to describe the critical buckling wave number and the half-wave length around the circumference. So in the present study, a simple dimensionless length parameter $\varepsilon = a / r$, which is normalized by the radius of the shell, is adopted to describe the mesh size, where a is the size of one single element.

5.3.2 Mesh convergence ($r/t = 250$, BC1r and BC2f boundaries)

The results for cylinders with $r/t = 250$ and changing dimensionless length parameter ω using different mesh sizes are shown in Figs 5-3 and 5-4, where the external pressure buckling factor C_θ ($C_{\theta s}$ for short cylinders) represents the ratio of the critical buckling pressures and is expressed as $C_\theta = \sigma_{\theta cr} / \sigma_{\theta cr,D}$. The factors can be derived from either Eq. 5.1 or Eq. 5.2. The buckling strength $\sigma_{\theta cr}$ changes with changing pattern of mesh. The reference buckling strength $\sigma_{\theta crD}$ is based on the classical linear Donnell-type shell buckling theory and is given by Eq. 5.1 without C_θ.

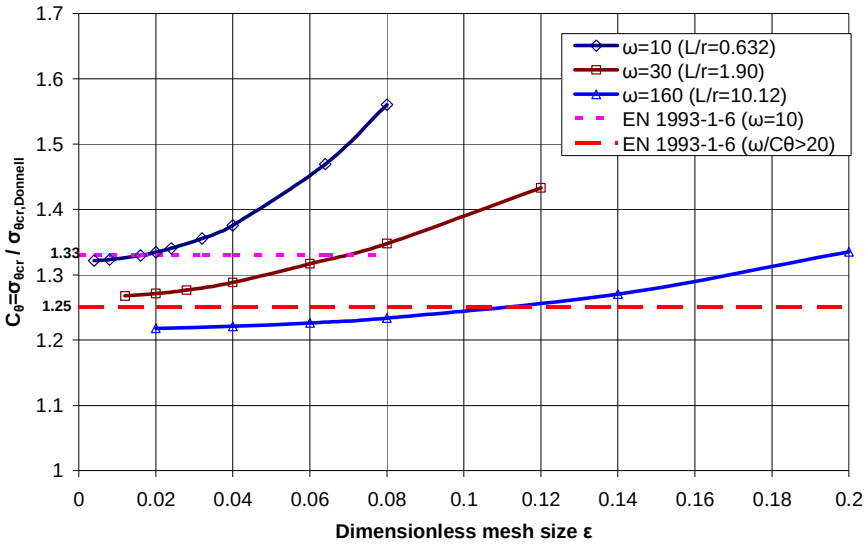

Figure 5-3: Mesh convergence study for cylinders with different length (*r / t=250*)

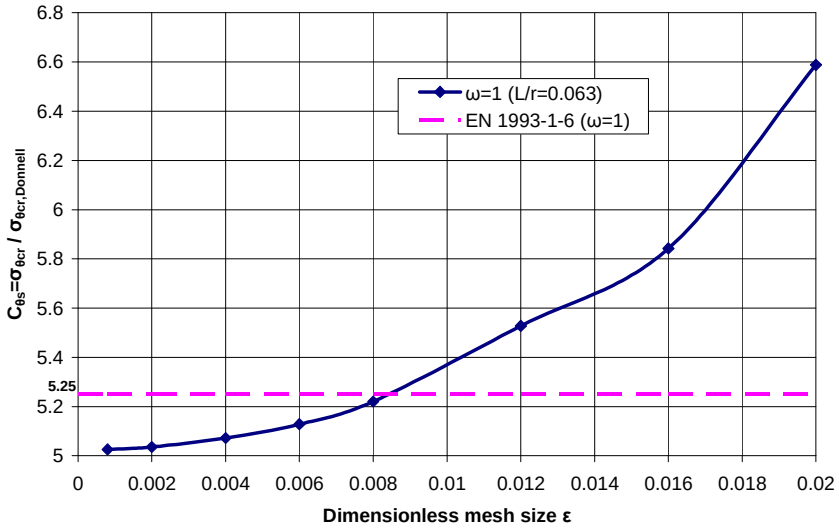

Figure 5-4: Mesh convergence study for very short cylinders (*r / t=250* and $\omega = 1$)

The results indicate that for medium-length cylinders ($\omega = 160$), the buckling strength does not depend on the mesh size significantly. The value of the buckling strength does not have sharp changes as the mesh size changes. The convergence can be achieved with a comparatively coarse mesh. The reason is obvious: the critical buckling wave number for these cylinders is small, so the half wavelength of one buckle is large so that fewer elements can accommodate the buckle and capture the buckling mode accurately. The influence of the boundaries can be represented by a constant buckling pressure factor (Table 5-1) for these cylinders.

But with decreasing length, due to the increasing effect of the boundaries and an increasing buckling wave number around the circumference, the half wavelength of one buckle may be quite small, so more elements in one buckle are required to capture the accurate buckling mode and buckling strength. The external pressure buckling factors convergence to larger values when the cylinder becomes shorter ($\omega = 10$ and $\omega = 1$ in Figs 5-3 and 5-4). The value of the buckling factor $C_{\theta s}$ depends strongly on the length parameter ω (Table 5-2).

For a very short cylinder with $\omega = 1$(Fig. 5-4), the results indicate that the element size should be refined to a very small value to achieve the convergence. The value $C_{\theta s} = 5.25$ according to EN 1993-1-6 (2007) is slightly larger than the asymptotic value.

If the element size is refined enough, for medium-length cylinders, the external pressure buckling factor C_θ obtained from numerical results is slightly larger or smaller than the value 1.25 defined in Table 5-1 for BC1 and BC2 boundaries ($\omega = 30$ and $\omega = 160$). That is because the number of the buckling waves around the circumference has a continuous change with changing length of the shell, so does the factor C_θ. This can be observed in next section (Fig. 5-5).

For short cylinders, if the element size is infinite small, the external pressure buckling factor $C_{\theta s}$ obtained from numerical results would be smaller than the results according to the expressions defined in Table 5-2. These equations are approximations to numerical solutions developed by Schmidt and Greiner (1998). It indicates that the element size for short cylinders does influence the buckling strength significantly and should be carefully checked during the finite element analysis.

It is obvious that the required value of ε to achieve convergence changes with the length of the cylinder. It is quite difficult to derive a general rule for the requirement of the mesh. The purpose of the above study is to show the importance of the mesh convergence study on this shell buckling problem. All the results below are obtained based on careful mesh convergence studies.

5.4 Buckling strength of cylinders under uniform external pressure with membrane pre-buckling stresses

Next the linear critical stress for cylinders with different boundary conditions at the two ends was calculated. The relationship between the dimensionless critical circumferential buckling stress $C_\theta = \sigma_{\theta cr} / \sigma_{\theta cr,Donnell}$ and the length parameter L / r is shown in Fig. 5-5.

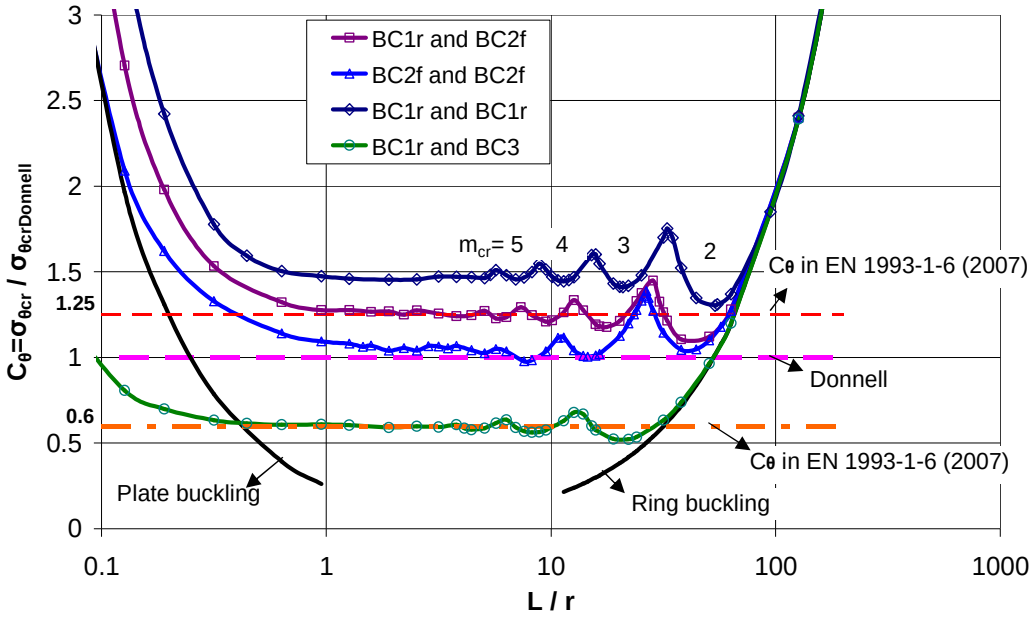

Figure 5-5: Critical circumferential buckling stress according to linear buckling theory with membrane pre-buckling stresses (*r / t=250*)

The results in Fig. 5-5 are based on the classical membrane pre-buckling stress field assumption. This assumption is correct for medium-length and long cylinders. Because the buckling is caused by the uniform membrane stress which is far form the ends for these cylinders, so the stress distribution near the end does not affect the buckling behaviour. By contrast, this assumption is incorrect for short cylinders. The pre-buckling edge rotations cause non-uniform pre-buckling stress distribution near the ends for short cylinders, which affects the buckling behaviour and must be taken into account to obtain more accurate solutions. This effect is discussed in Section 5.6.

The buckling behaviours for short, medium-length and long cylinders are illustrated comprehensively in Fig. 5-5. The finite element predictions, Eqs 5.5 and 5.7 for plate buckling and ring buckling respectively, and the expressions of external pressure buckling factors in EN 1993-1-6 (2007) are all shown in this figure. The buckling behaviour does correspond well to previous descriptions of short, medium-length and long cylinders under uniform external pressure (Yamaki, 1984; Greiner, 2004).

The boundary conditions play a significant role in predicting the buckling strength. In Fig. 5-5, for BC1 boundary, the meridional end rotation is restrained, while for BC2 boundary, the meridional rotation is free. The result of adopting these boundaries corresponds well with the predictions of EN 1993-1-6 (2007). The influence of the meridional rotation at boundaries on the buckling strength is discussed in next section.

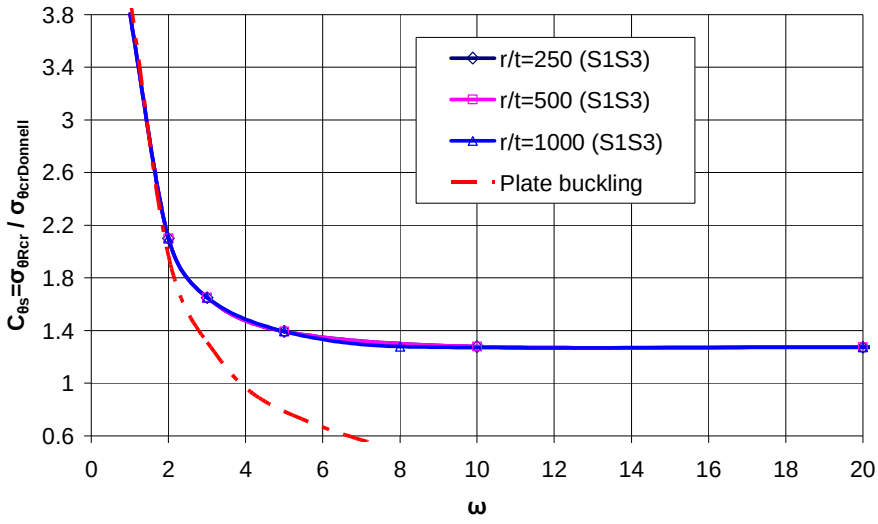

Figure 5-6: Critical circumferential buckling stress for short cylinders with membrane pre-buckling stresses

If the length of the cylinder is characterised in terms of the dimensionless length parameter ω, the critical load changes with ω for short cylinders with different radius to thickness ratios as shown in Fig. 5-6. By contrast, if the length of the cylinder is characterised in terms of dimensionless length parameter Ω, the critical load changes with Ω for medium-length and long cylinders with different radius to thickness

ratios as shown in Fig. 5-7. So in the following calculations, only short cylinders with $r/t = 250$ are needed to obtain general results if these are interpreted using the length parameter ω. The conclusions obtained are correct for other cylinders with different radius to thickness ratios.

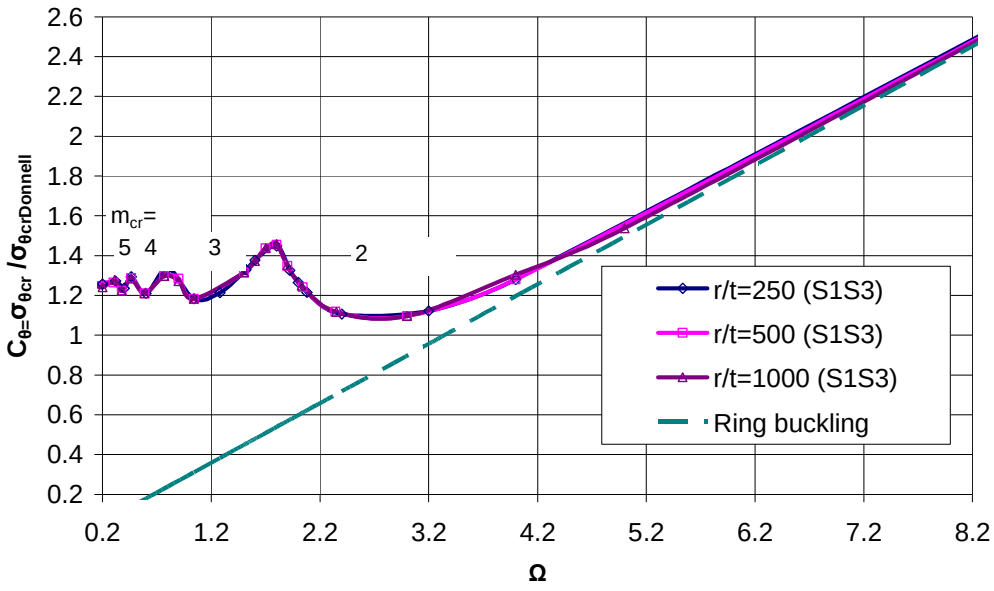

Figure 5-7: Critical circumferential buckling stress for long cylinders with membrane pre-buckling stresses

5.5 Effect of meridional end rotation $\delta\beta$ on buckling strength of short cylinders with membrane pre-buckling stresses

In EN 1993-1-6 (2007), the meridional end rotational restraint is not considered separately for short cylinders under uniform external pressure. One single expression of the external pressure factor $C_{\theta s}$ is given for each pair of boundaries (Table 5-2). However, the meridional rotation $\delta\beta$ does influence the buckling strength of short cylinders due to the restraint of boundaries. This influence will be explored next based on the boundaries given in Table 5-3. To compare the results with those in EN 1993-1-6 (2007), the membrane pre-buckling stress state was still assumed.

The buckling pressure factors $C_{\theta s}$ for short cylinders with BC2 and BC2 boundaries and with a membrane pre-buckling stress state are shown in Fig. 5-8. The meridional end rotation was restrained at either one end or both ends of the shell.

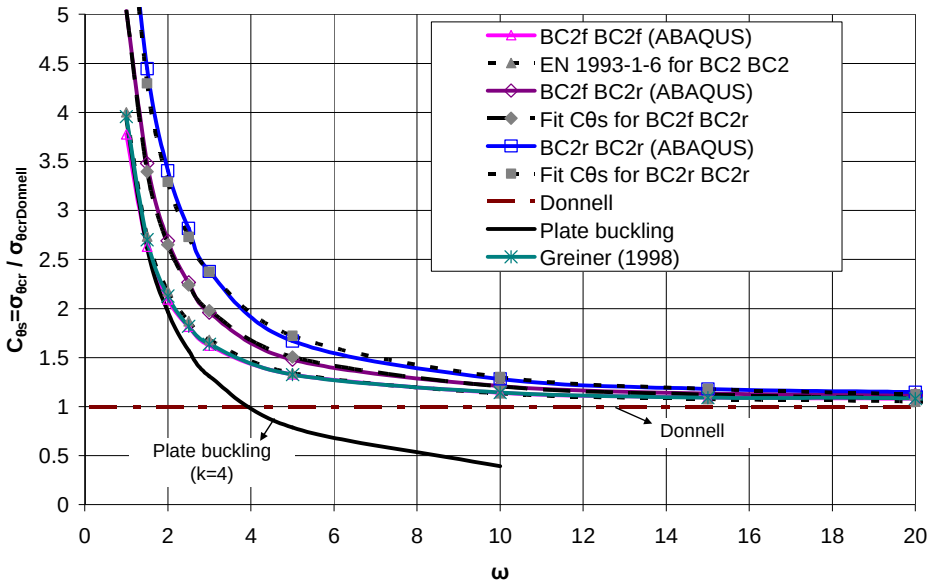

Figure 5-8: External pressure buckling factors for short cylinders with membrane pre-buckling stresses (*r / t=250*, BC2 and BC2)

The results indicate that restraint of the meridional end rotation could increase the buckling strength considerably for short cylinders, and especially for extremely short cylinders. Restraint of one end or both ends could cause different results. The curve for BC2f and BC2f boundaries fits well with Greiner's result (Eq. 5.3) for short and medium cylinders. The curve also fits well with the expression for $C_{\theta s}$ (Table 5-2) for BC2 and BC2 boundaries. This conclusion indicates that the expression in EN 1993-1-6 (2007) for BC2 and BC2 boundaries was obtained based on the boundaries where the meridional end rotation of BC2 was free. The curve asymptotically approaches the value of Eq. 5.5 for plate buckling.

The following expressions for $C_{\theta s}$ could be adopted into EN 1993-1-6 to include the effect of meridional end rotation for BC2 and BC2 boundaries:

BC2f and BC2f: $$C_{\theta s} = 1.0 + \frac{3}{\omega^{1.35}} \text{ (EN 1993-1-6, 2007)} \quad (5.10)$$

BC2f and BC2r: $$C_{\theta s} = 1.0 + \frac{4}{\omega^{1.30}} \quad (5.11)$$

BC2r and BC2r: $$C_{\theta s} = 1.0 + \frac{5.5}{\omega^{1.25}} \quad (5.12)$$

These equations would enhance the description given in EN 1993-1-6 (2007).

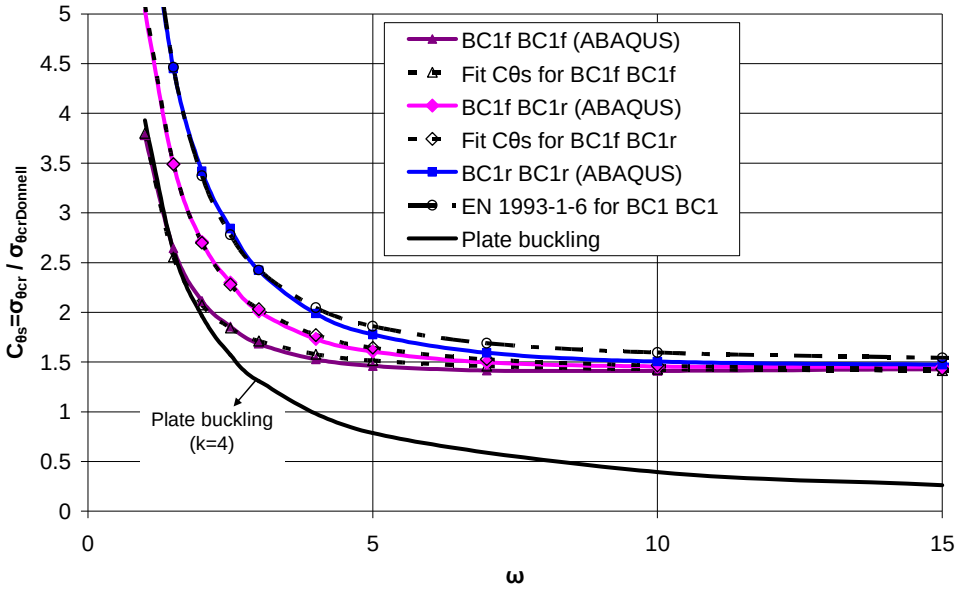

Figure 5-9: External pressure buckling factors for short cylinders with membrane pre-buckling stresses (*r / t=250*, BC1 and BC1)

The buckling pressure factors $C_{\theta s}$ for short cylinders with BC1 and BC1 boundaries and with a membrane pre-buckling stress state are shown in Fig. 5-9. The curve for BC1f and BC1f asymptotically approaches the value of Eq. 5.5 for plate buckling. The curve for BC1r and BC1r fits well with the expression for $C_{\theta s}$ (Table 5-2) for BC1 and BC1 boundaries. This outcome indicates that the expression in EN 1993-1-6 (2007) for BC1 and BC1 boundaries was obtained by assuming that the meridional end rotation in BC1 boundary was restrained and that a membrane pre-buckling stress state was assumed.

The following expressions for $C_{\theta s}$ could be adopted into EN 1993-1-6 to include the effect of meridional end rotation for BC1 and BC1 boundaries:

BC1f and BC1f: $$C_{\theta s} = 1.4 + \frac{3}{\omega^2} - \frac{0.6}{\omega^3} \tag{5.13}$$

BC1f and BC1r: $$C_{\theta s} = 1.4 + \frac{7}{\omega^2} - \frac{3.5}{\omega^3} \tag{5.14}$$

BC1r and BC1r: $$C_{\theta s} = 1.5 + \frac{10}{\omega^2} - \frac{5}{\omega^3} \text{ (EN 1993-1-6, 2007)} \qquad (5.15)$$

The buckling pressure factors $C_{\theta s}$ for short cylinders with BC1 and BC2 boundaries and with a membrane pre-buckling stress state are shown in Fig. 5-10. The curve for BC1f and BC2f asymptotically approaches the value of Eq. 5.5 for plate buckling. The curve for BC1r and BC2f (also for BC1f and BC2r) fits the expression of $C_{\theta s}$ in EN 1993-1-6 (2007) for BC1 and BC2 boundaries.

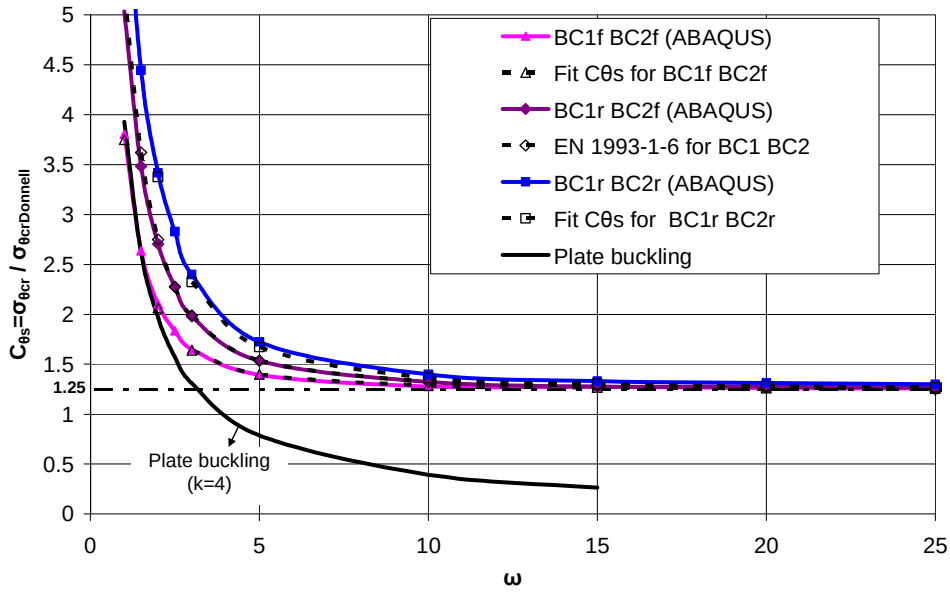

Figure 5-10: External pressure buckling factors for short cylinders with membrane pre-buckling stresses (*r / t=250*, BC1 and BC2)

The following expressions for $C_{\theta s}$ could be adopted into EN 1993-1-6 to include the effect of meridional end rotation for BC1 and BC2 boundaries:

BC1f and BC2f: $$C_{\theta s} = 1.25 + \frac{4}{\omega^2} - \frac{1.5}{\omega^3} \qquad (5.16)$$

BC1r and BC2f: $$C_{\theta s} = 1.25 + \frac{8}{\omega^2} - \frac{4}{\omega^3} \text{ (EN 1993-1-6, 2007)} \qquad (5.17)$$

BC1r and BC2r: $$C_{\theta s} = 1.25 + \frac{12}{\omega^2} - \frac{7}{\omega^3} \qquad (5.18)$$

The buckling pressure factors $C_{\theta s}$ for short cylinders with BC1 and BC3 boundaries and a membrane pre-buckling stress state are shown in Fig. 5-11. The curve for BC1r and BC3 fits well with the expression of $C_{\theta s}$ in EN 1993-1-6 (2007) for BC1 and BC3, and the curve asymptotically approaches the value of Eq. 5.5 for plate buckling.

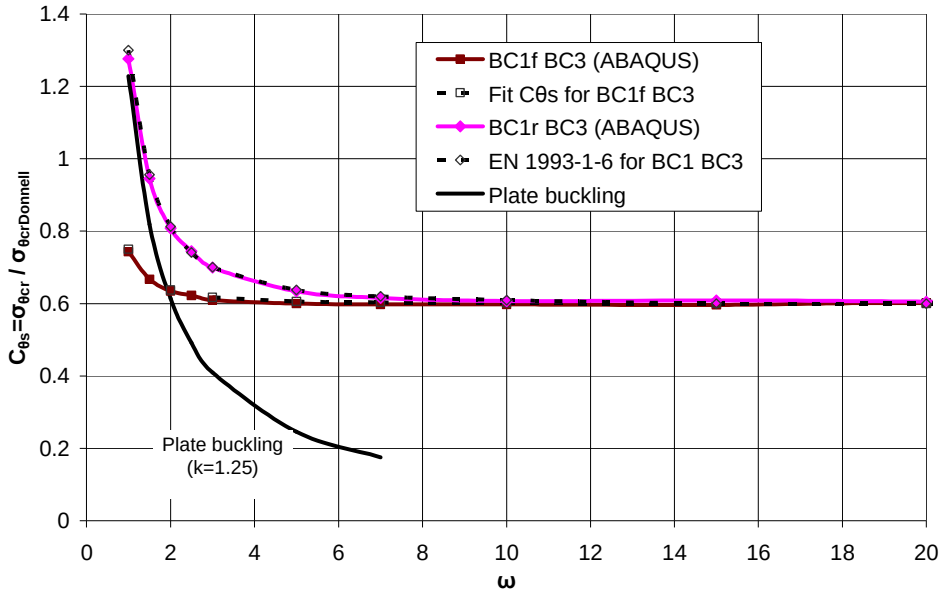

Figure 5-11: External pressure buckling factors for short cylinders with membrane pre-buckling stresses (*r / t=250*, BC1 and BC3)

The following expressions for $C_{\theta s}$ could be adopted into EN 1993-1-6 to include the effect of meridional end rotation for BC1 and BC3 boundaries:

BC1f and BC3: $$C_{\theta s} = 0.6 + \frac{0.15}{\omega^2} \tag{5.19}$$

BC1r and BC3: $$C_{\theta s} = 0.6 + \frac{1}{\omega^2} - \frac{0.3}{\omega^3} \text{ (EN 1993-1-6, 2007)} \tag{5.20}$$

Table 5-4 summarizes the approximate expressions for external pressure buckling factors for short cylinders with membrane pre-buckling stresses including the influence of meridional end rotation. It is clear that that the boundary conditions, for which $C_{\theta s}$ fits the current expressions in EN 1993-1-6 (2007), are BC1r and BC1r, BC1r and BC2f, BC2f and BC2f, and BC1r and BC3 respectively. It may be

concluded that in EN 1993-1-6 (2007), the expressions for the buckling pressure factors for short cylinders were obtained based on the assumption that the meridional end rotation is restrained for the BC1 boundary and are free for the BC2 boundary.

Table 5-4: External pressure buckling factors $C_{\theta s}$ for short cylinders (with membrane pre-buckling stress state)

Case	Boundary condition based on EN 1993-1-6 (2007)	Yamaki's boundary conditions (1984)	Fitted expressions of $C_{\theta s}$
1	BC1f and BC1f	S1S1	$C_{\theta s} = 1.4 + \frac{3}{\omega^2} - \frac{0.6}{\omega^3}$
	BC1f and BC1r	S1C1	$C_{\theta s} = 1.4 + \frac{7}{\omega^2} - \frac{3.5}{\omega^3}$
	BC1r and BC1r	C1C1	$C_{\theta s} = 1.5 + \frac{10}{\omega^2} - \frac{5}{\omega^3}$ (EN 1993-1-6, 2007)
2	BC1f and BC2f	S1S3	$C_{\theta s} = 1.25 + \frac{4}{\omega^2} - \frac{1.5}{\omega^3}$
	BC1r and BC2f	C1S3(S1C3)	$C_{\theta s} = 1.25 + \frac{8}{\omega^2} - \frac{4}{\omega^3}$ (EN 1993-1-6, 2007)
	BC1r and BC2r	C1C3	$C_{\theta s} = 1.25 + \frac{12}{\omega^2} - \frac{7}{\omega^3}$
3	BC2f and BC2f	S3S3	$C_{\theta s} = 1.0 + \frac{3}{\omega^{1.35}}$ (EN 1993-1-6, 2007)
	BC2f and BC2r	S3C3	$C_{\theta s} = 1.0 + \frac{4}{\omega^{1.30}}$
	BC2r and BC2r	C3C3	$C_{\theta s} = 1.0 + \frac{5.5}{\omega^{1.25}}$
4	BC1f and BC3	S1BC3	$C_{\theta s} = 0.6 + \frac{0.15}{\omega^2}$
	BC1r and BC3	C1BC3	$C_{\theta s} = 0.6 + \frac{1}{\omega^2} - \frac{0.3}{\omega^3}$ (EN 1993-1-6, 2007)
Note: As described in EN 1993-1-6 (2007), the circumferential displacement v is very closely linked to the displacement w normal to the surface, so separate conditions are not identified for these two parameters. The boundary conditions S2, S4, C2, C4 used by Yamaki are not necessarily considered separately.			

5.6 Influence of pre-buckling bending deformation (linear elastic pre-buckling stress state)

The above calculations were all derived based on the assumption of a pre-buckling membrane stress state. The reason for adopting this assumption for most of research to date is described in ECCS EDR5 (2008) as follows:

> *In the early development of the analysis of the buckling of shells, it was difficult to produce algebraic buckling solutions for conditions in which the pre-buckling stress state was anything other than a uniform membrane stress state (see, for example Timoshenko and Gere, 1961; Flügge, 1973). The boundary conditions required to achieve purely membrane pre-buckling stress state are rather special, and these usually involve no restraint at the boundary against displacements normal to the shell surface (e.g. radial displacements at the end of a cylinder, normal displacements at the end of a cone). Such boundary conditions are generally unrealistic, but they do produce simple pre-buckling stress states. By contrast, the buckling modes generally require radial constraint of the displacements at the ends of a buckled zone (otherwise the buckling strength is very low), so in the historical development of this field, different boundary conditions were adopted for the incremental displacements in the bifurcation mode from the boundary conditions used in the pre-buckling stress analysis. The formulas resulting from this methodology are referred to as the "classical" expressions (ECCS EDR5, 2008).*

The buckling strength of cylinders under uniform external pressure will be examined next including the effect of pre-buckling bending deformations arsing from a realistic representation of the actual boundary conditions. The aspects of computational analysis are the same as previous calculations. But the same boundary conditions are adopted in the pre-buckling deformation calculation and the buckling mode calculation, in which way the influence of the pre-buckling bending deformation is included.

Yamaki (1984) obtained theoretical solutions based on Donnell basic equations. The pre-buckling deformation and incremental buckling mode deformation were assumed in different forms. Different boundary conditions S1~S4 and C1~C4 (Table 5-3) were all considered. Finite element predictions of buckling strength are

compared with Yamaki's results for S1S1 and C1C1 boundary conditions in Fig. 5-12. When $\omega > 4$, the numerical results are precisely the same as Yamaki's results. But for quite short cylinders with $\omega \leq 4$, Yamaki's predicted analytical results have a higher estimate of the critical load, which is probably due to the pre-buckling meridional stress caused by the lateral pressure being neglected. When the cylinder has S1 or C1 boundaries at both ends, the longitudinal extension is restrained by the boundaries, and meridional stress is thus caused and affects the buckling strength.

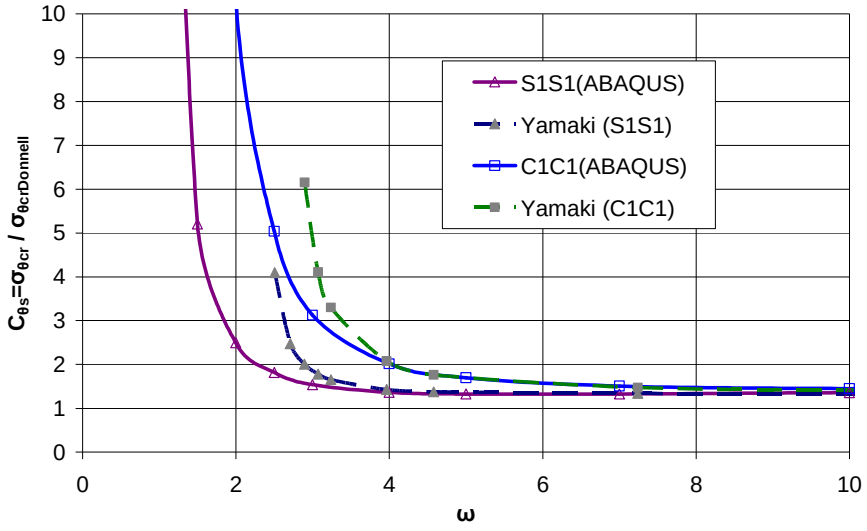

Figure 5-12: External pressure buckling factors for short cylinders with linear elastic pre-buckling stress state (*r / t=250*)

The buckling strength of cylinders with BC2 and BC2 boundaries at the two ends and with a linear elastic pre-buckling stress state is shown in Fig. 5-13. Compared with the results with assumption of a membrane pre-buckling stress state (Fig. 5-8), for quite short cylinders, the curve in Fig. 5-13 for BC2f and BC2f does not fit the expression for $C_{\theta s}$ in Table 5-2 for BC2 and BC2 boundaries any more. The buckling strength increases considerably when the cylinder becomes shorter due to the restraint of the boundaries. The following fitted expressions for $C_{\theta s}$ could be adopted into EN 1993-1-6 to include the effect of pre-buckling bending deformation:

$$\text{BC2f and BC2f:} \qquad C_{\theta s} = 1 + \frac{12}{\omega^2} - \frac{36}{\omega^3} + \frac{56}{\omega^4} \tag{5.21}$$

BC2f and BC2r: $$C_{\theta s} = 1 + \frac{20}{\omega^2} - \frac{70}{\omega^3} + \frac{138}{\omega^4} \quad (5.22)$$

BC2r and BC2r: $$C_{\theta s} = 1 + \frac{40}{\omega^2} - \frac{181}{\omega^3} + \frac{380}{\omega^4} \quad (5.23)$$

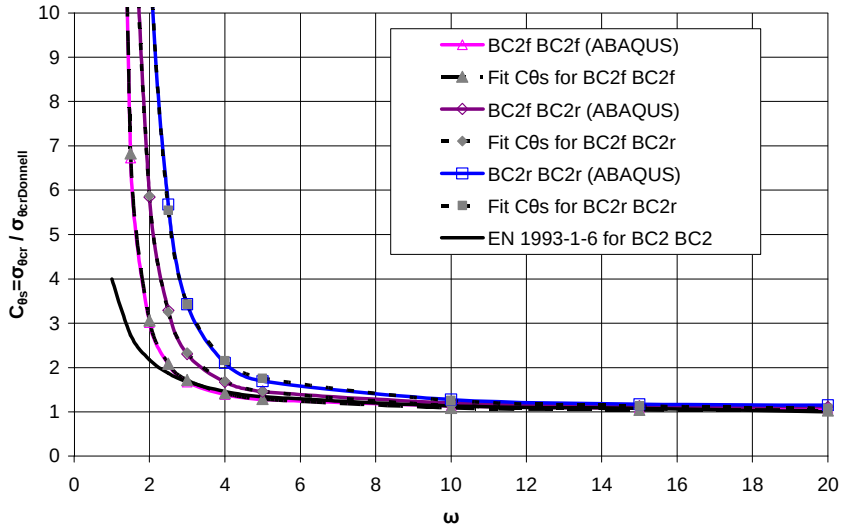

Figure 5-13: External pressure buckling factors for short cylinders with linear elastic pre-buckling stress state (*r / t=250*, BC2 and BC2)

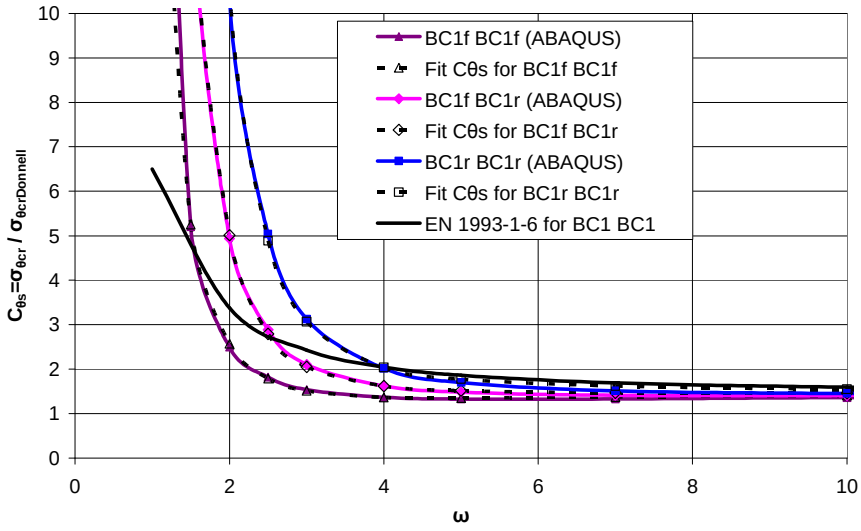

Figure 5-14: External pressure buckling factors for short cylinders with linear elastic pre-buckling stress state (*r / t=250*, BC1 and BC1)

The buckling strength of cylinders with BC1 and BC1 boundaries at the two ends and with a linear elastic pre-buckling stress state is shown in Fig. 5-14. The

following fitted equations for $C_{\theta s}$ could be adopted into EN 1993-1-6 to include the effect of pre-buckling bending deformation:

$$\text{BC1f and BC1f:} \quad C_{\theta s} = 1.45 - \frac{7}{\omega^2} + \frac{22}{\omega^3} + \frac{2}{\omega^4} \tag{5.24}$$

$$\text{BC1f and BC1r:} \quad C_{\theta s} = 1.45 + \frac{1.5}{\omega^2} - \frac{16}{\omega^3} + \frac{83}{\omega^4} \tag{5.25}$$

$$\text{BC1r and BC1r:} \quad C_{\theta s} = 1.45 + \frac{17}{\omega^2} - \frac{100}{\omega^3} + \frac{278}{\omega^4} \tag{5.26}$$

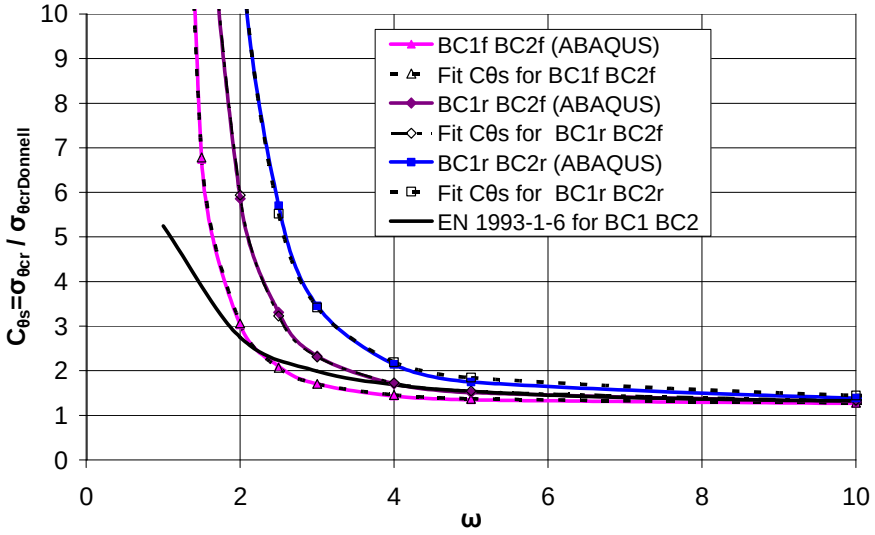

Figure 5-15: External pressure buckling factors for short cylinders with linear elastic pre-buckling stress state (*r / t=250*, BC1 and BC2)

The buckling strength of cylinders with BC1 and BC2 boundaries at the two ends and with a linear elastic pre-buckling stress state is shown in Fig. 5-15. The following fitted expressions for $C_{\theta s}$ could be adopted into EN 1993-1-6 to include the effect of the pre-buckling bending deformations:

$$\text{BC1f and BC2f:} \quad C_{\theta s} = 1.25 + \frac{4}{\omega^2} - \frac{12}{\omega^3} + \frac{37}{\omega^4} \tag{5.27}$$

$$\text{BC1r and BC2f:} \quad C_{\theta s} = 1.25 + \frac{13}{\omega^2} - \frac{54}{\omega^3} + \frac{131}{\omega^4} \tag{5.28}$$

BC1r and BC2r: $$C_{\theta s} = 1.25 + \frac{32}{\omega^2} - \frac{158}{\omega^3} + \frac{362}{\omega^4} \quad (5.29)$$

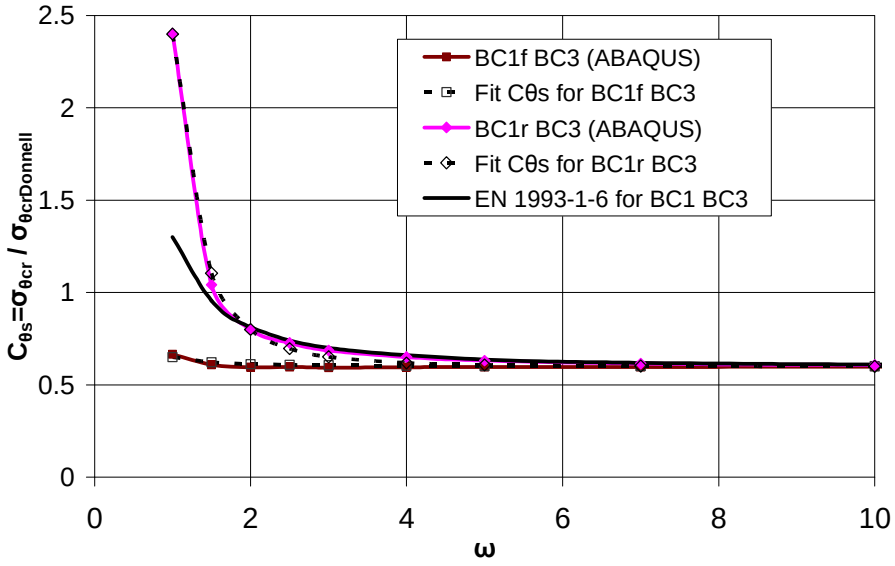

Figure 5-16: External pressure buckling factors for short cylinders with linear elastic pre-buckling stress state (*r / t=250*, BC1 and BC3)

The buckling strength of cylinders with BC1 and BC3 boundaries at the two ends and with a linear elastic pre-buckling stress state is shown in Fig. 5-16. The following fitted expressions for $C_{\theta s}$ could be adopted into EN 1993-1-6 to include the effect of the pre-buckling bending deformations:

BC1f and BC3: $$C_{\theta s} = 0.6 + \frac{0.05}{\omega^2} \quad (5.30)$$

BC1r and BC3: $$C_{\theta s} = 0.6 + \frac{1}{\omega^2} - \frac{0.3}{\omega^3} \quad (5.31)$$

Table 5-5 summarizes the approximate expressions for the external pressure buckling factor $C_{\theta s}$ for short cylinders, including the influence of pre-buckling bending deformations.

Table 5-5: External pressure buckling factors for short cylinders
(linear elastic pre-buckling stress state)

Case	Boundary condition based on EN 1993-1-6 (2007)	Yamaki's boundary conditions	Fitted expressions of $C_{\theta s}$
1	BC1f and BC1f	S1S1	$C_{\theta s}=1.45-\frac{7}{\omega^2}+\frac{22}{\omega^3}+\frac{2}{\omega^4}$
	BC1f and BC1r	S1C1	$C_{\theta s}=1.45+\frac{1.5}{\omega^2}-\frac{16}{\omega^3}+\frac{83}{\omega^4}$
	BC1r and BC1r	C1C1	$C_{\theta s}=1.45+\frac{17}{\omega^2}-\frac{100}{\omega^3}+\frac{278}{\omega^4}$
2	BC1f and BC2f	S1S3	$C_{\theta s}=1.25+\frac{4}{\omega^2}-\frac{12}{\omega^3}+\frac{37}{\omega^4}$
	BC1r and BC2f	C1S3(S1C3)	$C_{\theta s}=1.25+\frac{13}{\omega^2}-\frac{54}{\omega^3}+\frac{131}{\omega^4}$
	BC1r and BC2r	C1C3	$C_{\theta s}=1.25+\frac{32}{\omega^2}-\frac{158}{\omega^3}+\frac{362}{\omega^4}$
3	BC2f and BC2f	S3S3	$C_{\theta s}=1+\frac{12}{\omega^2}-\frac{36}{\omega^3}+\frac{56}{\omega^4}$
	BC2f and BC2r	S3C3	$C_{\theta s}=1+\frac{20}{\omega^2}-\frac{70}{\omega^3}+\frac{138}{\omega^4}$
	BC2r and BC2r	C3C3	$C_{\theta s}=1+\frac{40}{\omega^2}-\frac{181}{\omega^3}+\frac{380}{\omega^4}$
4	BC1f and BC3	S1BC3	$C_{\theta s}=0.6+\frac{0.05}{\omega^2}$
	BC1r and BC3	C1BC3	$C_{\theta s}=0.6+\frac{1}{\omega^2}-\frac{0.3}{\omega^3}$

The ratio of the buckling stresses $\zeta=\sigma_{b\theta cr}/\sigma_{m\theta cr}$ is shown in Fig. 5-17, where $\sigma_{b\theta cr}$ means the buckling stress based on the linear elastic pre-buckling stress assumption and $\sigma_{m\theta cr}$ means the buckling stress based on the membrane pre-buckling stress assumption.

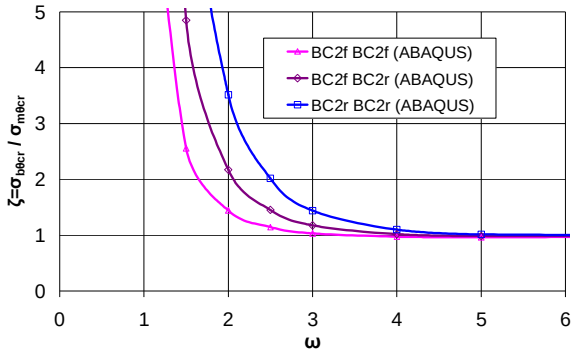

(a) BC2 and BC2

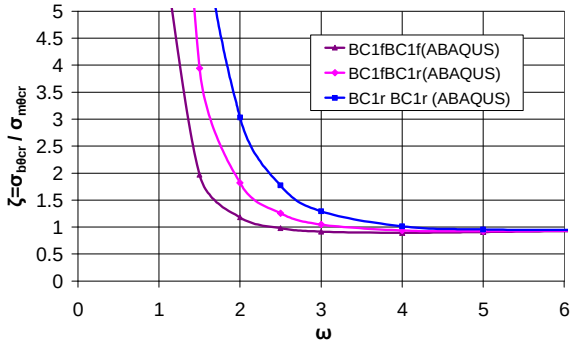

(b) BC1 and BC1

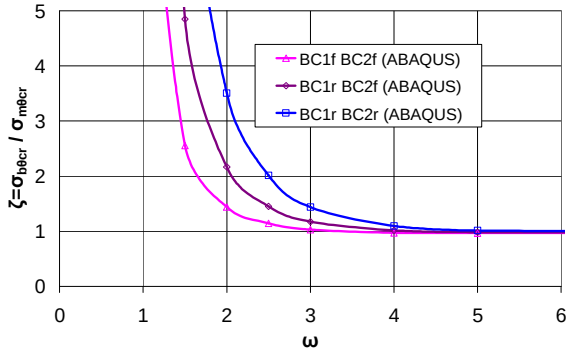

(c) BC1 and BC2

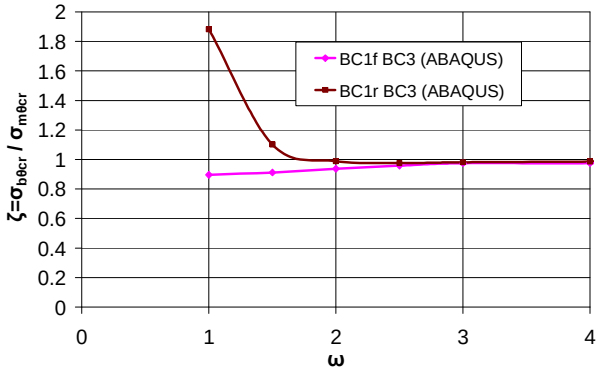

(d) BC1 and BC3

Figure 5-17: Comparison of the external pressure buckling factors using membrane and linear elastic pre-buckling conditions (*r / t=250*)

A comparison of the buckling stresses using the two different pre-buckling boundary conditions is shown in Fig. 5-18. Compared with the results with membrane pre-buckling stress condition, for extremely short cylinders with $\omega < 3$, pre-buckling bending deformations increase the buckling strength considerably as the cylinder becomes shorter, except for the BC1f and BC3 boundary conditions. When $3 \le \omega \le 5$, the value of $\sigma_{b\theta cr}$ can be either larger or smaller than $\sigma_{m\theta cr}$ depending on the specific boundary conditions. This is caused by the complicated influence of pre-buckling stresses on the buckling strength. When $\omega > 5$, the maximum relative error of the two buckling stresses is less than 6% for almost all the cases, and $\sigma_{b\theta cr}$ is slightly smaller than the value of $\sigma_{m\theta cr}$. The error gradually disappears as the length becomes longer. It can be concluded that the results based on the membrane pre-buckling stress assumption are accurate for shells with $\omega > 5$.

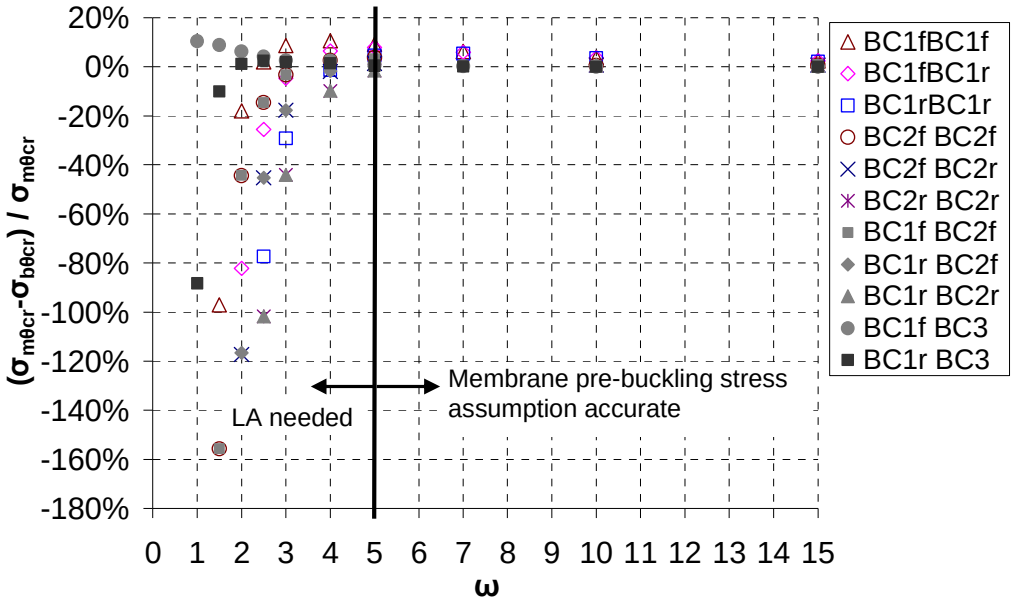

Figure 5-18: Comparison of the buckling strength using different pre-buckling boundary conditions (*r / t=250*)

5.7 Conclusions

The linear elastic bifurcation buckling behaviour of cylindrical shells under uniform external pressure was studied. The boundary conditions have an important

effect on the buckling strength of short cylinders. The influence of the meridional rotation $\delta\beta$ and the pre-buckling stress state on the buckling strength was explored.

The meridional rotation $\delta\beta$ has a significant influence on the buckling strength for short cylinders, but this influence is not considered separately in EN 1993-1-6 (2007). The results indicate that the restraint of meridional end rotation could increase the buckling strength of short, especially extremely short cylinders.

The classical solutions are based on the assumption of a pre-buckling membrane stress state which is satisfactory for medium-long and long cylinders but not accurate for short cylinders. This assumption requires no restraint at the boundaries against displacements normal to the shell surface in the pre-buckling stage, which is not practical for short cylinders. The results indicate that pre-buckling bending deformations have a significant influence on the buckling strength for very short cylinders, while for cylinders with $\omega > 5$, this effect is negligible.

Chapter 6 Buckling analysis of cylinders of uniform thickness under wind pressure

6.1 Introduction

Cylindrical shells subjected to non-uniform wind pressure display different buckling behaviours compared with cylinders under uniform external pressure. As the length parameter changes, quite different and complex buckling behaviours may be observed, but the buckling of cylinders under uniform external pressure is always caused by circumferential buckling and is affected little by geometry except the very short cylinders.

In Chapter 12 of the European Recommendations on Shell Buckling, (Greiner, Guggenberger, and Schneider, 2008), it states that three different stability failure modes for stocky, intermediate aspect ratio and slender cylinders could be observed respectively (Fig. 6-1). In stocky cylinders, the radial compression in the stagnation zone causes circumferential compressive stresses that result in circumferential buckling which is similar to cylinders under uniform external pressure (Fig. 6-1a). The axial and shear components can be neglected for these cylinders. In slender cylinders, the buckling caused by axial compressive stress may occur on the leeward meridian, either in the base area or in the lower half of the shell (Fig. 6-1c). For very thin and slender cylinders (Fig. 6-1c), the buckling may occur in upper half the cylinder at the windward area, which is caused by axial compressive stress. In intermediate aspect ratio cylinders (Fig. 6-1b), the buckling is caused by the interaction of circumferential compression and axial compression generated by the external pressure in the stagnation zone. The buckling occurs in the windward area (near the mid-height) with a significant geometrically nonlinear effect caused by circumferential ovalization (Greiner and Derler, 1995).

However, the equations for buckling given in ECCS EDR5 (2008) are not differentiated in terms of the linear elastic buckling mode or nonlinear buckling mode as shown in Fig. 6-1. The results of Greiner (1998) and Pircher (2004) showed that for intermediate and long cylinders, the linear buckling mode and nonlinear

buckling mode are quite different. Therefore the linear buckling behaviour and nonlinear buckling behaviour are explored separately in this chapter to obtain a better understanding of the buckling behaviour of cylinders under wind pressure. The analyses focus on silos and tanks of practical geometry.

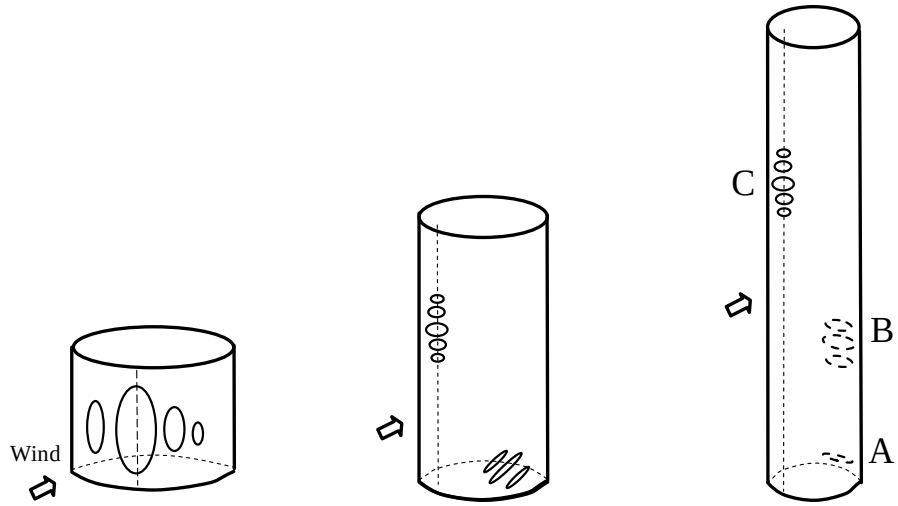

(a) Stocky cylinder (b) Intermediate aspect ratio cylinder (C) slender cylinder

Figure 6-1: Buckling modes in cylinders with different aspect ratios under wind pressure (after ECCS EDR5, 2008)

6.2 Literature review and objective

Cylinders under uniform external pressure have been well studied by many researchers. The failure of elastic perfect cylinders under uniform external pressure is caused by circumferential buckling. It is a characteristic that cylinders under uniform external pressure form relatively large buckles extending over the whole length of the shell (Greiner, 1998). For cylinders under wind pressure, Greiner and Derler (1995) investigated the imperfection sensitivity of wind-pressured cylindrical shells based on numerical analyses by considering various types of imperfection shapes. The results indicate that short shells are most sensitive to pre-buckling deformations in the form of the eigenmode and long shells are most sensitive to local imperfections in the form of a rectangular or ring shape. Their results also indicate that material plasticity has no effect for short and thin cylinders and just has a moderate effect for medium thin cylinders.

Schneider (2001) presented the results of materially and geometrically nonlinear analyses of the pressure-bearing capacity of slender wind-pressured cylindrical shells with $h/r > 15$. He obtained different buckling modes for slender cylinders under wind pressure and explored the effect of ring stiffeners. However, his models are restricted to the ranger $r/t < 350$ and so are only meant to chimneys.

Picher (2004) studied the buckling behaviour of a medium-length thin-walled cylinder under wind pressure and the influence of a weld-induced axisymmetric imperfection on the buckling of a medium-length silo. His results indicate that the position of the weld imperfection in the upper half of the shell is most influential and this influence is similar to the buckling behaviour in axial compression. However, the geometry of his model was restricted to moderate thin and intermediate long cylinders.

Portela and Godoy (2005) studied the buckling of cylindrical steel tanks with either a conical roof or a dome roof under wind pressure using a computational method. Their results showed the effect of conical roof on the buckling capacity of a tank and proved that the bifurcation pressures are similar to the case for a tank under uniform pressure around the circumference.

Jaca and Godoy (2007) used a lower bound approach to the buckling analysis of tanks subjected to wind pressures based on a reduced energy model. The classical bifurcation buckling analysis is an upper bound to experimental and nonlinear computational results. His results were limited to tanks that are open at the top.

The researches above usually focused on one specific aspect of this wind buckling problem, and the geometries were usually restricted to a certain limited range. There is no systematic discussion of how the buckling behaviour changes as the geometry of the cylinders changes, of the relationship between the linear buckling behaviour and nonlinear buckling behaviour for different geometries.

Furthermore, the relationship of the buckling strengths of cylinders under uniform external pressure and wind pressure is significant. In EN 1993-1-6 (2007), for stocky cylinders, the peak of non-uniform pressure distribution is related to a fictitious

equivalent uniform pressure which was developed and verified by wind-tunnel tests by Resinger and Greiner (1981, 1982) for isolated cylinders of stocky shape. In this chapter, the idea of relating the buckling strengths of cylinders under uniform external pressure and wind pressure is explored further through numerical analysis. Linear bifurcation analysis (termed LBA) and geometrically nonlinear analysis (termed GNA) were all performed. The influence of geometric nonlinearity on the buckling behaviour was investigated. The cylinders are not restricted to stocky cylinders. The influences of material plasticity and imperfections on buckling behaviour were also investigated. The aim of this chapter is to present a comprehensive understanding of the buckling behaviour of cylinders under wind pressure.

6.3 Wind pressures on cylindrical shells

6.3.1 Brief introduction of related elementary fluid dynamics

In fluid mechanics, Bernoulli equation is a well-known equation governing fluid motion under a fairly stringent set of restrictions. It is expressed as (Munson, et al., 1998):

$$p + \frac{1}{2}\rho V^2 + \gamma z = \text{constant along the streamline.} \tag{6.1}$$

in which p is the static pressure at any point, V is the fluid speed at that point, ρ is the density of the fluid, γ is the specific weight, z is called elevation head related to the potential energy of the particle.

This equation can be interpreted in terms of work-energy principle. As the fluid moves, the work done on a particle by all forces acting on the particle is equal to the change of the kinetic energy of the particle (Munson, et al., 1998). The terms γz and p in Eq. 6.1 are related with the work done by the weight and pressure forces respectively and $\frac{1}{2}\rho V^2$ is related with the kinetic energy of the particle. The Bernoulli equation can be associated with stagnation and dynamic pressures. These pressures arise from the conversion of kinetic energy in a flowing fluid into a

"pressure rise" as the fluid is brought to rest (Munson, et al., 1998). The sum of the static pressure p, hydrostatic pressure γz and dynamic pressure $\frac{1}{2}\rho V^2$ is termed the total pressure p_T.

$$p + \frac{1}{2}\rho V^2 + \gamma z = p_T = \text{ constant along the streamline.} \tag{6.2}$$

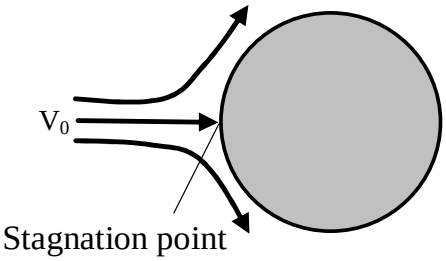

Figure 6-2: Stagnation point on a circular body in flowing fluids

At stagnation point shown in Fig. 6-2, the velocity of the fluid is zero. Therefore the stagnation pressure which is the static pressure at the stagnation point equals to the total pressure. Apply Bernoulli equation for both the stagnation point and other points along the streamline and the elevation effects are neglected, the stagnation pressure at stagnation point is expressed as:

$$p_{stagnation} = p + \frac{1}{2}\rho V^2 \tag{6.3}$$

in which p and V are static pressure and wind velocity at any other points along the streamline. If the static pressure at other points can be neglected and the velocity is regarded as constant along the streamline, then

$$p_{stagnation} = \frac{1}{2}\rho V^2 \tag{6.4}$$

6.3.2 Wind pressure

Wind pressure is one of the most common types of pressures for any structure. Wind induced pressures are important considerations in design of structures. The types of wind pressure have been studied by many researchers and specified in many

national standards and codes. A few of them are Davenport (1967, 1972), Cermak (1971, 1977), Hunt (1975), Surry (1977), Kareem (1978, 1982, 1984), Reinhold (1982), Mehta (1979, 1984), Australian (SAA, 1983), British (BSI, 1972), Canadian (NRCC, 1980), US. (ANSI, 1982).

In this chapter, only the distribution of wind pressure on cylindrical shells will be discussed. Wind fluctuates randomly in space and time. When wind encounters a structure, these fluctuating phenomena causes wind pressures on structures also fluctuating. Fluctuating wind pressures are converted to static pressures for simplicity in use in professional practice (Mehta, 1985). Mehta (1985) discussed the parameters that are used to determine the wind pressures including the occurrence of free-field wind speed and wind-structure interaction effects. The wind velocity and velocity pressure are composed of a mean and a fluctuating component which depends on many factors such as wind climate, probabilities of occurrence of wind speed, height variation of the wind. The mean wind velocity at a height above the terrain depends on the terrain roughness and orography and the basic wind velocity (EN 1991-1-4, 2005). Wind-structure interaction effects include the influence of gustiness in wind, dynamic characteristics of the structure, consideration of shape and size of the structures (pressure and drag coefficients), the orientation of the structure and the interaction of a structure with adjacent structures.

Because the wind pressure are affected by many indeterminate factors, determination of wind velocity and corresponding wind pressure for specific structures is quite complex. Mehta (1985) derived an equation to calculate the wind pressure by:

$$p = kV^2GC \tag{6.5}$$

in which p is the pressure, V is the free-field wind speed, G is the gust related factor, C is the pressure or drag coefficient, and k is a constant related to the mass density of air. Wind velocity V affects the wind pressure significantly. Based on the work of Scrutton and Rogers (1971) on cylindrical structures at high Reynolds numbers (8.4×10^6) and related to the Australian Wind Code AS1170 Pt II, wind velocity and wind pressure are given by

$$V_z = 1.35V\left(\frac{z}{z_g}\right)^k \quad (z < z_g) \tag{6.6}$$

$$q_z = 0.6\times10^{-3}V_Z^2 \tag{6.7}$$

where V_z is the wind speed at height z, V is the wind speed at gradient height z_g.

6.3.3 Wind pressure distribution on cylindrical shells

Wind pressure on cylindrical shells has also been studied by many researchers and specified in many national standards and codes. A few of them are Vickery (1974), Davenport (1975), Cook (1980), Farell (1981), Cheung and Melbourne (1983), Trahair (1983), Sabransky (1984), Holmes (1985), Engineering Sciences Data Item ESDU 80025 (1980), Data Item 81017 (1981), Australian (SAA, 1983), BS EN 1991-1-4 (2005), EN 1993-4-1 (2007), etc.

Kareem (1985) introduced several aspects of wind tunnel modelling. Basic requirements for simulating natural winds such as Reynolds number, Rossby number, mean velocity and turbulence characteristics can be measured based on wind tunnel modelling. The local pressure fluctuations in wind tunnel tests are monitored through the use of sensitive pressure transducers with high frequency response. Rigid "Lucite" models with pressure ports at selected locations are used for such studies (Kareem, 1985).

Kwok (1985) studied specific wind pressure distribution on circular cylindrical structures and summarized related research about wind pressures on storage bins, silos and tanks. However, most experimental results of many researchers mentioned in his paper are not directly relevant to the wind pressure on storage bins, silos and tanks. An expression for wind distribution around the circumference of the shell that mentioned in Kwok's paper is proposed by Holmes (1985) based on the data obtained from isolated silos.

Rotter (1985) derived Fourier coefficient for common pressure patterns. In his paper, it mentioned two types of wind pressure represented by Rish (1967) and Rogers (1971). However, most researches derived the wind pressure distribution by

assuming one Reynolds number and did not discuss the effect of different Reynolds numbers. Their results are based on the experimental data tested in smooth flow conditions and they are of limited use in the design of shells in turbulent shear flow. The reason is the inability to achieve high Reynolds number flow comparable to full scale supercritical Reynolds number flow conditions (Kwok, 1985).

In EN 1991-1-4 (2005), the external pressure coefficients around circumference is derived based on the Reynolds number and the end-effect factor. The Reynolds number is related with kinematic velocity and geometry of the structure and is defined as:

$$R_e = \frac{b \cdot V(z_e)}{\nu} \tag{6.8}$$

where b is diameter, ν is kinematic viscosity of the air ($\nu = 15 \cdot 10^{-6} m^2 / s$) and $V(z_e)$ is peak wind velocity.

The laminar flow and turbulent flow are defined according to the Reynolds number. The famous Moody chart (Moody, 1944) clearly shows the laminar, transition, and turbulent flow regimes as Reynolds number increases. Due to the influence of neighboring structures, the wind velocity can be quite different. The pressure patterns are determined according to what specific Reynolds number is obtained in specific conditions.

A wind tunnel studied by Macdonald in the late 1980s provided the extensive wind data that Rotter (2001b) used to devise a much better pattern of wind pressures for the silo, which depends on the aspects ratio of the silo and is adopted in EN 1993-4-1 Annex C. For an isolated closed roof structure, the circumferential variation of the pressure distribution (positive inward) is given by (Fig. 6-3):

$$\begin{aligned} C_P = &-0.54 + 0.16(d_c / H) + \{0.28 + 0.04(d_c / H)\}\cos(\theta) + \{1.04 - 0.20(d_c / H)\}\cos(2\theta) \\ &+ \{0.36 - 0.05(d_c / H)\}\cos(3\theta) - \{0.14 - 0.05(d_c / H)\}\cos(4\theta) \end{aligned} \tag{6.9}$$

Where d_c is the diameter of the cylinder and H is the overall height of the complete structure (The cylinders studied here have no support). For silos with H/d_c less than 0.50, the value for $H/d_c = 0.50$ should be adopted.

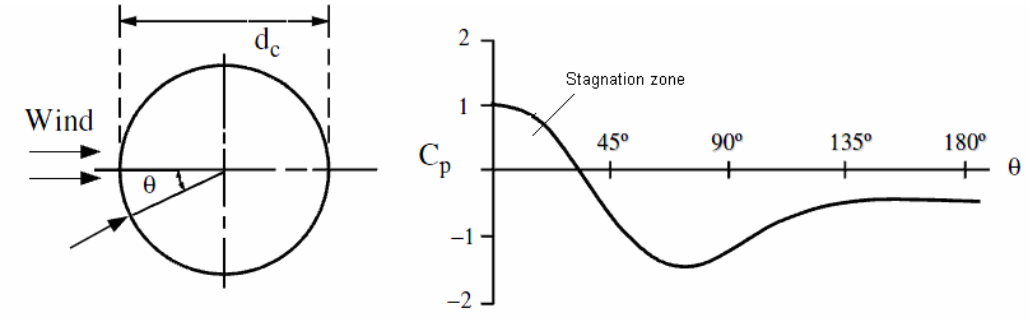

Figure 6-3: Wind pressure variation around half circumference in an isolated silo (EN 1993-4-1, 2007)

This is the only expression considering the effect of the aspect ratios of the silo and will be adopted throughout this chapter. For one of a group of closely spaced similar structures, the wind pressure distribution based on relatively little data (Vickery and Ansourian, 1974) can be approximated by:

$$C_P = 0.20 + 0.6\cos(\theta) + 0.27\cos(2\theta) - 0.05\cos(3\theta) - 0.13\cos(4\theta) + 0.13\cos(6\theta) - 0.09\cos(8\theta) + 0.07\cos(10\theta) \quad (6.10)$$

Some different types of wind distribution around the circumference of the cylinders are shown in Fig. 6-4. In this Figure, Holmes's curve was based on the data obtained from isolated silos with height to diameter ratio in the range $0.5 \le h/d \le 2.0$. Rish's curve assumed an internal suction of 0.607 times the stagnation pressure. Roger's curve was derived based on a high Reynold number (8.4×10^6) and was related to Australian Wind Pressure Code, AS1170 Pt II. The conditions he used, such as the geometry of the model or whether it is for an isolated cylinder or one of the group cylinders, are unknown. The curve for EN 1991-1-4 (2005) was derived based on the calculated Reynolds number and the rules in the code. The model was based on an isolated cylinder with $r/t = 500$ and $L/r = 3$. The value of the fundamental basic wind velocity at Edinburgh is found from NA to BS EN 1991-1-4 (2005).

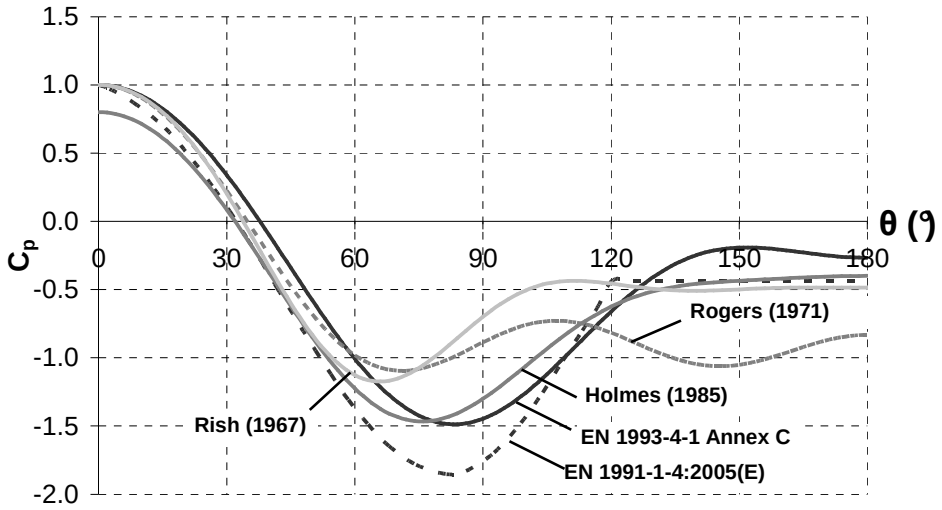

Figure 6-4: Different types of wind distribution around the circumference of cylindrical shells

The curves in Fig. 6-4 for EN 1993-4-1 (2007) are derived using Eq. 6.9 based on an isolated cylinder with $r/t = 500$ and $L/r = 3$. It can be seen the wind distribution in the stagnation zone for all curves are close. But the distributions outside the stagnation zone are quite different, especially near the maximum pressure point. The reason may be the pressure at leeward side is more prone to be affected by the factors such as test methods, test models, the types of wind pressure, etc. This difference shows the difficulty to have a general standard for the wind pressure distribution.

It is noted that the maximum stagnation pressure coefficient at the centre of the windward area did not reach 1.0 in Holmes's test results, which is due to the special velocity profile of the wind tunnel (Resinger and Greiner, 1982). Greiner (1998) stated that due to friction effects of ground surface, the pressure coefficient reaches not more than 0.80 in practical cases. This has to be considered in comparing the buckling test data, but not for the design of tanks, where the maximum stagnation pressure coefficient 1.0 is adopted. For one of a group of cylinders, the rule in the code can be adopted to calculate the peak wind velocity and the Reynolds numbers to derive corresponding wind distribution.

The wind distribution coefficients around the circumference of a cylindrical shell with $r/t = 500$ and different L/r according to EN 1993-4-1 (2007) are shown in Fig. 6-5. It is obvious that the wind distribution varies a lot as the aspect ratio changes,

especially for short cylinders, slight changes in the length to radius ratio may change the type of wind distribution noticeably. However, for intermediate long and slender cylinders, the wind distribution changes slightly with the increase of length.

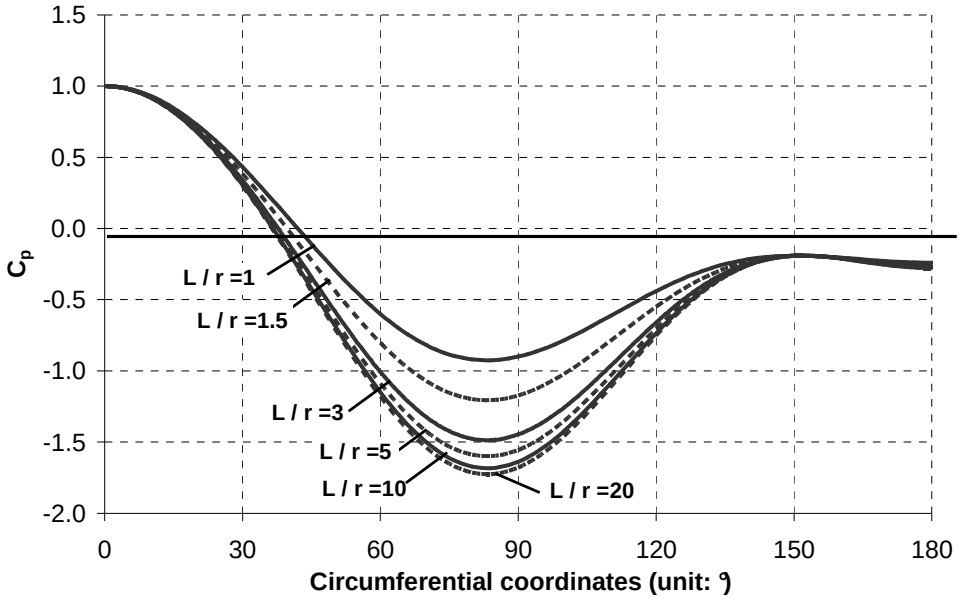

Figure 6-5: Wind distribution coefficient around the circumference for cylindrical shells with different *L / r* according to EN 1993-4-1 (2007)

Comparing all the types of wind distribution, it may conclude that most results of previous researches are derived from experimental data tested in smooth flow conditions with low Reynolds numbers. Their models are usually stocky cylinders with low height to radius ratios. There are limitations in general applications. The rule in EN 1991-1-4 (2005) provides a more reasonable method to derive wind distribution around the circumference of cylinders by considering many factors, but it is quite complex and difficult to adopt in practical application. The wind distribution equation adopted in EN 1993-4-1(2007) based on the extensive experimental data that not only considers the influence of geometrical model but also is easy to apply generally, and so it is adopted throughout this chapter to study the buckling behaviour of cylinders under wind pressure.

6.3.4 Membrane stresses for cylinders under wind pressure

The membrane stresses for circular cylinders under wind pressure are shown in Fig. 6-6. For cylinders with different aspect ratios, the dominant membrane stress

that controls buckling may be quite different depending on the specific buckling mode. For stocky cylinders, several long vertical buckles are formed at the stagnation zone (Fig. 6-1a), which is similar to the buckling mode for cylinders under uniform external pressure. The dominant buckling stress is circumferential membrane stress. For intermediate long cylinders, buckling may occur in either the upper half of the windward meridian or the leeward zone (Fig. 6-1b). The buckling is caused by the combination of circumferential membrane stress and meridional membrane stress. For slender cylinders, different buckling modes may occur as shown in Fig. 6-1c. These buckling modes are mainly caused by meridional membrane stress.

However, Fig. 6-1 does not describe in detail which buckling mode corresponds to which specific condition, especially for intermediate aspect ratio and slender cylinders. Furthermore, whether the buckling modes are linear buckling mode or nonlinear buckling mode are also not clear. These questions are discussed next.

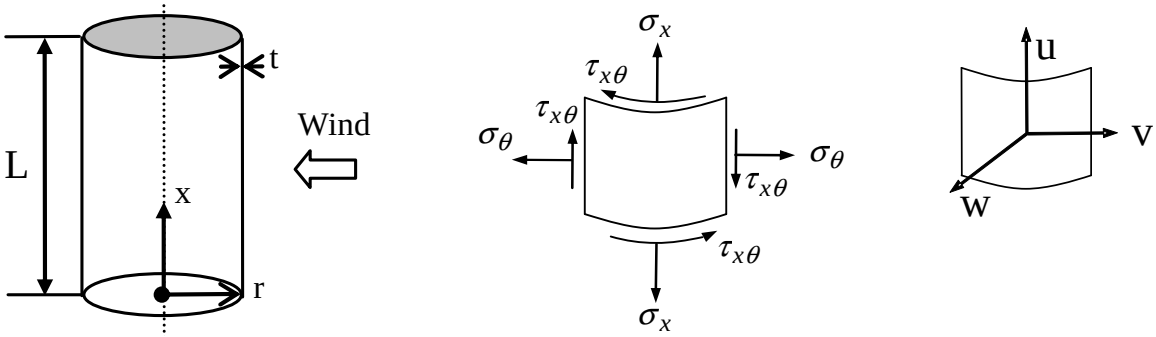

Figure 6-6: Structure model, membrane stress and displacement

6.4 Linear elastic bifurcation analysis (LBA)

6.4.1 Review of linear bifurcation buckling analysis

Linear bifurcation analysis (LBA) is a small displacement stability analysis that assumes a perfect geometry, linear elastic material behaviour and no change in geometry (small displacement theory) before the infinitesimal displacements of the secondary path. It is based on the stresses derived from a linear elastic analysis (LA). This procedure is an eigenvalue analysis and the buckling pressure is obtained by solving an eigenvalue problem. In general the result from LBA cannot be justified

for practical structures because shell structures are quite sensitive to geometric nonlinearity and geometric imperfections while linear bifurcation analysis (LBA) ignores these effects (Rotter, 2002). However, LBA analysis determines the elastic critical buckling resistance R_{cr}, which is a very important reference pressure for all analyses, since the pressure is not only important in determining the capacity curves of the Eurocode (EN 1993-1-6, 2007), it always gives a good first estimate of the elastic buckling strength, and this pressure is unique, always calculable when compressive stresses occur in the structure, and can usually be represented by a relatively simple equation following a parametric numerical study (Rotter, 2002).

6.4.2 Computational aspects of finite element analysis

Linear bifurcation analysis (LBA) for cylinders under wind pressure was performed using the finite element program ABAQUS (Hibbit et al, 2002). The analyses focused on silos and tanks of practical geometry. Tanks lie in the range $0.1 < L/r < 4$ and $500 < r/t < 2000$. Silos are generally in the range $0.5 < L/r < 8$ and $200 < r/t < 1000$. Some models with geometries slightly outside the above ranges are also included. The shell was made of an isotropic material with Young's modulus $E = 2.0 \times 10^5 MPa$ and Poisson's ratio $\nu = 0.3$. When material plasticity was included, an ideal elastic-plastic model with yield stress $\sigma_y = 250 MPa$ was adopted. At the top of the shell, a ring stiffener with enough stiffness was adopted to keep the top circular. At the bottom of the shell, all the displacements were restricted, the meridional rotation was free, and the other rotations were restricted. The distribution of the wind pressure around the circumference was adopted according to Fig. 6-3 (EN 1993-4-1, 2007). An isolated cylinder was considered, so the circumferential variation of the pressure distribution is determined according to Eq. 6.9. The wind pressure does not vary up the height of the shell.

6.4.3 Linear bifurcation analysis for cylinders with $r/t = 200$

The linear buckling behaviour of cylinders with $r/t = 200$ in the range $0.5 \le L/r \le 8$ was analysed.

6.4.3.1 Linear critical buckling modes

The linear buckling modes for cylinders under wind pressure with different length to radius ratios are shown in Fig. 6-7. When the length parameter L/r is small, as shown in Fig. 6-7(a), (b), (c) for $L/r = 0.5$, $L/r = 1$ and $L/r = 4$ respectively, the linear buckling modes are similar to cylinders under uniform external pressure. The buckles form in the windward zone extending over the whole length of the shell and the governing stress component is circumferential compression in the stagnation zone. This buckling mode is here called Mode A as shown in Fig. 6-8a. The number of the critical buckling waves around the circumference is larger for shorter cylinders. When L/r changes from $L/r = 0.5$ (Fig. 6-7a) to $L/r = 4$ (Fig. 6-7c), the critical circumferential buckling wave number decreases and the half wavelength around the circumference extends further.

When L/r increases to a larger value, $L/r = 6$ for example, the buckling mode becomes a new pattern of mode caused by the combination of circumferential compressive stress and meridional membrane stress. Several fold-like buckles are formed around the circumference, and a main long buckle forms at the windward meridian extending over almost the whole length of the shell. The main buckle is quite similar to the buckle for cylinders under uniform external pressure. However, unlike short cylinders that have several circumferential compressive buckles formed around the circumference, for intermediate aspect ratio cylinders, several fold-like buckles are formed following the main buckle and gradually eclipse toward the bottom of the cylinder until the buckles disappear. This buckling mode is here called Mode B as shown in Fig. 6-8(b). Examples of this buckling mode are shown in Fig. 6-7(d) and (e) for $L/r = 6$ and $L/r = 7$.

With increasing L/r, the shear buckling mode with comparatively large buckles up the meridian (Mode B) changes to a more local shear buckling mode here termed Mode C (Fig. 6-8b). The buckling mode for $L/r = 8$ (Fig. 6-7f) shows this buckling mode. Several small fold-like buckles form at the bottom of the leeward zone extending over a limited area of the shell. The buckles are arranged neither horizontally nor vertically, and primarily occur under shear membrane stress near the base.

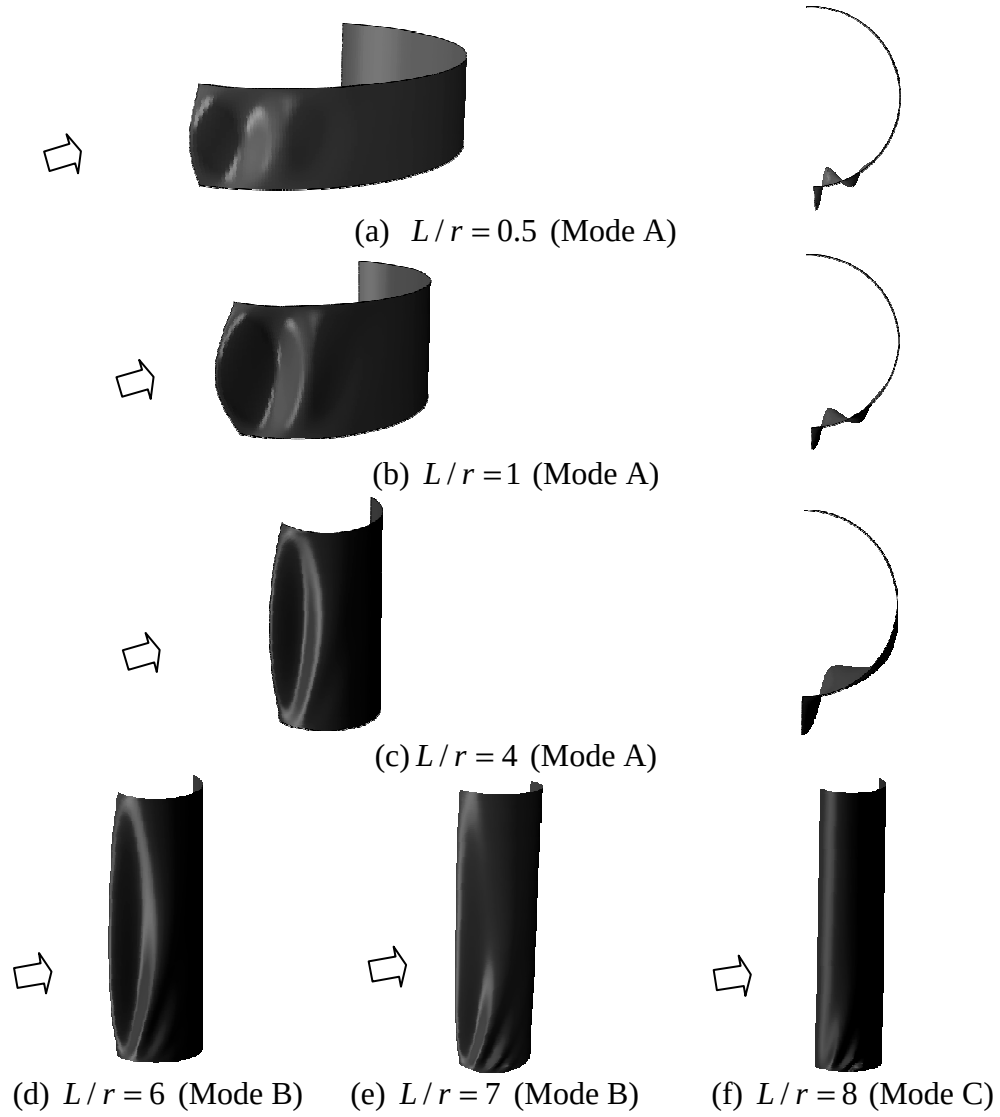

(a) $L/r = 0.5$ (Mode A)

(b) $L/r = 1$ (Mode A)

(c) $L/r = 4$ (Mode A)

(d) $L/r = 6$ (Mode B) (e) $L/r = 7$ (Mode B) (f) $L/r = 8$ (Mode C)

Figure 6-7: Linear critical buckling modes for cylinders under wind pressure ($r/t = 200$)

The three different linear critical buckling modes Mode A, Mode B and Mode C discussed above are shown in Fig. 6-8. Cylinders with Mode A are here categorized as stocky cylinders and cylinders with Modes B and C are here categorized as intermediate aspect ratio cylinders.

The ranges of L/r, in which each of the corresponding linear critical buckling modes in Fig. 6-8 occur, are shown in Table 6-1. The category is determined according to the pattern of the linear buckling mode which is caused by the corresponding pre-buckling membrane stress induced in the cylinder. But it should be noted that the boundaries between different buckling modes are difficult to be

determined accurately, because the transition of the buckling mode from one pattern to another is difficult to identify clearly. More accurate categories may be defined using geometric nonlinear analysis (GNA).

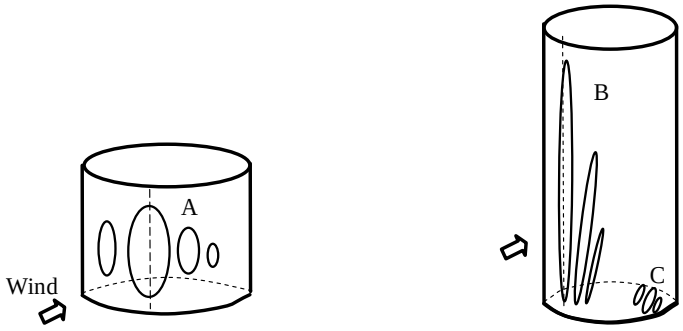

(a) Stocky cylinder (b) Intermediate aspect ratio cylinder

Figure 6-8: Linear buckling modes for cylinders with different aspect ratios under wind pressure

Table 6-1: Linear buckling modes for cylinders with different length to radius ratios ($r/t = 200$)

$r/t = 200$	$0.5 \le L/r < 6$	$6 \le L/r < 7.5$	$7.5 \le L/r <$?
Buckling modes	Mode A	Mode B	Mode C

6.4.3.2 Membrane stress distribution derived from LA analysis

To investigate the membrane stress distribution in the cylinder under wind loading, linear analysis termed LA was performed. The linear critical pressure derived from linear bifurcation analysis (LBA) was applied as the reference pressure on each shell. The meridional membrane stress distribution up the windward generator, the meridional membrane stress distribution around the circumference at the bottom edge and the circumferential membrane stress distribution up the windward generator are shown in Figs 6-9 to 6-11, respectively. The axial coordinate is normalized by the height of the cylinder as x/h. The vertical coordinate is denoted as x, and with x equal to zero at the bottom of the shell. The meridional membrane stress and circumferential membrane stress are indicated as $\sigma_{x,m}$ and $\sigma_{\theta,m}$

respectively. A positive value of the stress resultant is tensile while a negative value means a compressive membrane stress resultant.

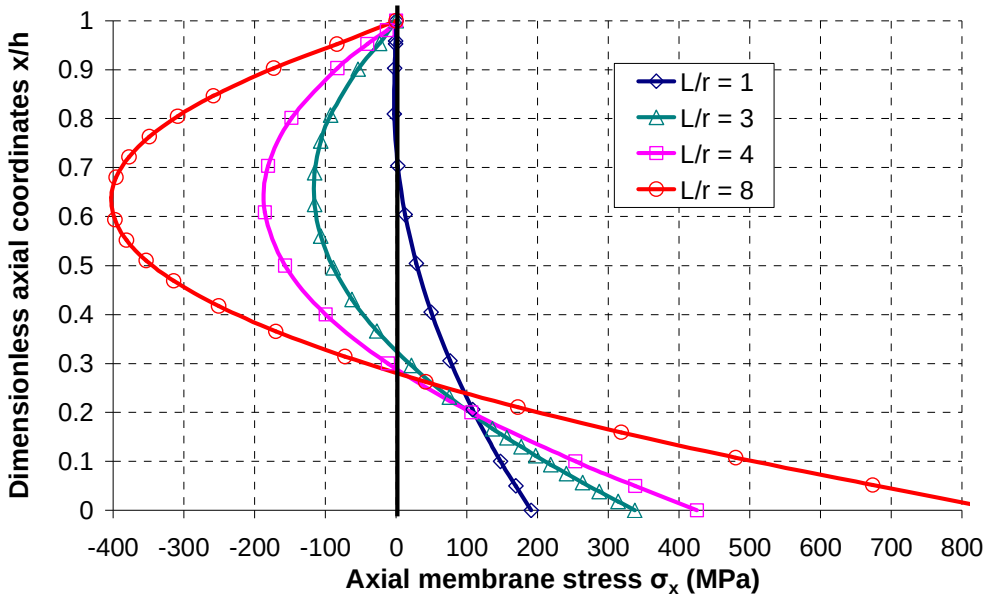

Figure 6-9: Meridional membrane stress distribution up the windward generator

When the cylinder is short, $L/r = 1$ in Fig. 6-9, the meridional membrane stress distribution up the windward generator is similar to a propped cantilever beam in the longitudinal direction. At the top of the cylinder, the value of the meridional membrane stress is very small because the top edge is axially free. The high tensile membrane stress near the bottom is caused due to the restraint of the boundary at the base. The high value of tensile membrane stress may cause local yield when plasticity influences the failure of the structure or may lead to failure of the base holding down detail.

Also for $L/r = 1$, the maximum meridional compressive membrane stress at the bottom edge occurs at an angle of eighty degrees or so to the windward generator (Fig. 6-10). This stress does not cause buckling due to the restraint of boundaries. By contrast, circumferential compressive membrane stress is large up the windward generator (Fig. 6-11). The circumferential buckling resistance is small for cylinders under external pressure. As a result, circumferential compressive buckling is caused by $\sigma_{\theta,m}$. It can also be noted that tensile membrane stress could be large near the sides of the shell (Fig. 6-11). The cylinder behaves in the way as the cylinder under

uniform external pressure. The linear buckling mode for $L/r=1$ is shown in Fig. 6-7(b).

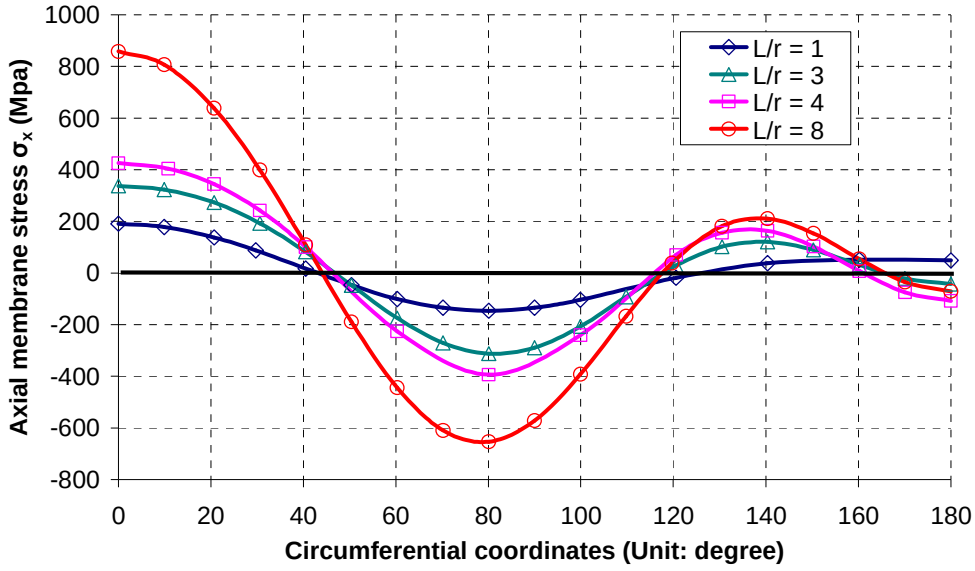

Figure 6-10: Meridional membrane stress distribution around the circumference of bottom edge

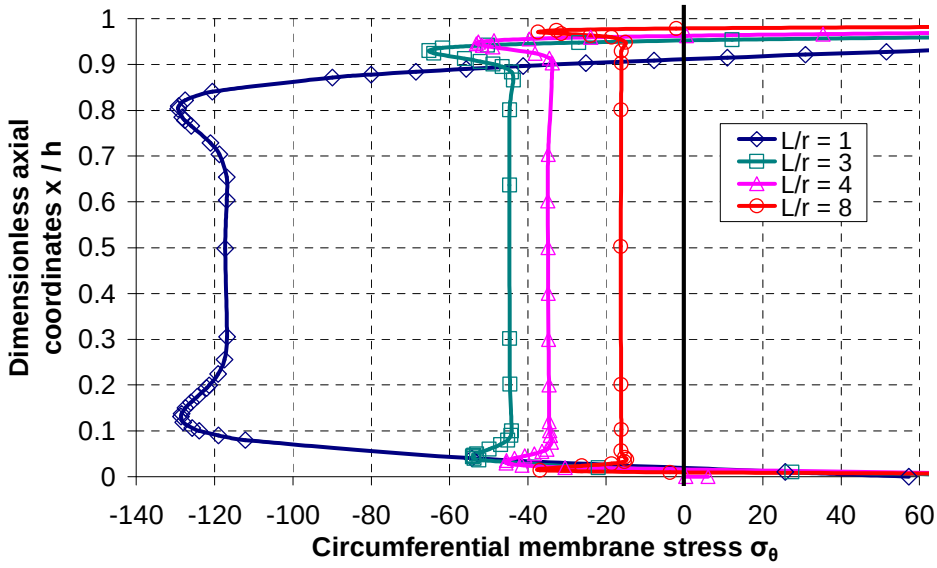

Figure 6-11: Circumferential membrane stress distribution up the windward generator

With an increase of L/r ($L/r=3,\ 4$), which also leads to slight changes in the pressure pattern, the maximum tensile meridional membrane stress occurs at the bottom of windward generator. However, the meridional compressive membrane stress increases noticeably in the upper part of the cylinder and the maximum value

occurs at $x/h = 0.62$ (Fig. 6-9). The meridional membrane stress around the circumference at the bottom has a similar distribution as for $L/r = 1$, but the maximum value induced in the shell increases. The increased compressive stress still does not cause buckling, due to the restraint of boundaries. By contrast, the maximum circumferential compressive membrane stress up the windward generator decreases considerably (Fig. 6-11), but it is still the dominant stress to control the buckling due to the small circumferential compressive resistance.

With a further increase of L/r, such as $L/r = 8$, under the corresponding linear critical pressure, the magnitudes of the maximum meridional tensile membrane stress at the bottom of the windward generator and the maximum meridional compressive membrane stress in the upper half of the windward generator increase quickly (Fig. 6-9). The maximum meridional compressive membrane stress around the circumference at the bottom edge also increases steadily with an increase of L/r (Fig. 6-10). By contrast, the maximum circumferential compressive membrane stress on the windward meridian decreases quickly with an increase of L/r (Fig. 6-11).

For cylinders of moderate aspect ratio, buckling is caused by the interaction of meridional compressive membrane stress and circumferential compressive membrane stress, and a mixed buckling mode with several fold-like buckles occurs. The cylinder with $L/r = 7$ (Fig. 6-7e) shows this buckling mode.

When the cylinder is long enough ($L/r = 8$), high meridional compressive membrane stress and the shear membrane stress at the bottom edge at the side affect the buckling behaviour significantly, causing a more local shear buckling mode in that area. The buckles are formed at around eighty degrees or so to the windward generator, corresponding to the position of the maximum meridional compressive membrane stress around the bottom edge.

The radial displacement up the windward generator for cylinders with different values of L/r under the linear critical buckling pressure is shown in Fig. 6-12. The inward radial displacement is defined as a positive value.

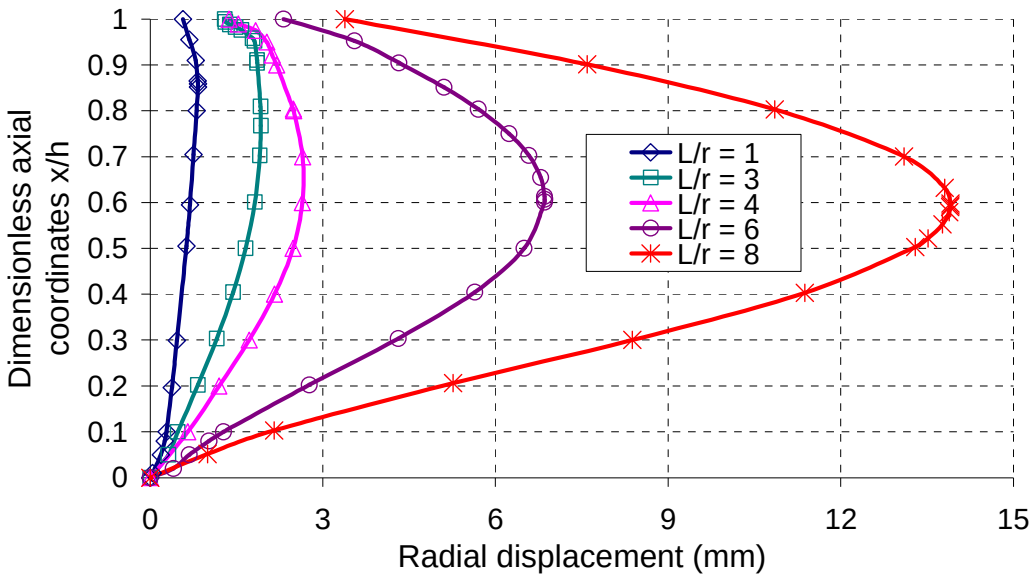

Figure 6-12: Radial displacement up the windward generator under the linear critical buckling pressure

When $L/r = 1$, the maximum radial displacement is small. The stress induced in the shell can be derived accurately based on the undeformed shape of the cylinder. For longer cylinders, the pattern of radial displacement up the windward generator does not follow a linear pattern any more, neither does the stress distribution. In this situation, the solution should be obtained based on the full shell theory. However, almost the same results can be obtained by using the semi-membrane theory (Greiner, 1983), and in many cases even the membrane theory alone gives sufficient accuracy.

The maximum radial displacement occurs at around $x/h = 0.62$ for comparatively long cylinders with $L/r \geq 3$, which is the position where the maximum meridional compressive membrane stress on the windward generator occurs for these cylinders. So the cross-section at this position may have a considerable ovalization which reduces the axial buckling resistance greatly. In this situation, geometric nonlinearity may influence both the buckling mode and buckling strength significantly, as can be seen later.

The top edge of the cylinder has a small radial displacement. That is because the ring stiffener at the top of the cylinder cannot restrain the radial displacement completely under the asymmetric wind pressure even though the stiffness of the ring

is already very large, but the results are acceptable according to the rule in ECCS EDR5 (2008) which requires the bending stiffness of the ring stiffener be large enough to limit the ovalization of the ring stiffened cross-sections under the wind action to 2% (Schneider et al., 2002). The minimum requirement of the bending stiffness of the ring stiffener is another complex problem which is discussed in Chapter 8.

From the linear membrane stress analysis described above, it may be concluded that for stocky cylinders, the circumferential buckling mode is caused by circumferential compressive membrane stresses. The pre-buckling deformation is small. For intermediate aspect ratio cylinders, the pattern of the membrane stress distribution changes a lot as the length changes. The meridional compressive stress either in the stagnation area or at the sides increases significantly and may influence the buckling behaviour greatly. The linear buckling mode is either shear buckling with a main long buckle on the windward meridian or local shear buckling with local small fold-like buckles at the bottom of the side meridian. More accurate predictions of the buckling mode and buckling strength should be obtained by geometrically nonlinear analysis with consideration of the noticeable influence of pre-buckling deformations.

6.4.3.3 Relationship of the linear critical buckling pressures for cylinders under wind pressure and uniform external pressure

The linear critical buckling pressures for cylinders under both uniform external pressure and wind pressure were calculated. The relationship between the dimensionless buckling pressure ratio $q_{cr,LBA}/q_{cr,D}$ for each load case and the length to radius ratio L/r is shown in Fig. 6-13, where $q_{cr,LBA}$ is the linear critical buckling pressure for cylinders under either wind loading or uniform external pressure derived from ABAQUS. For cylinders under asymmetric wind pressure, the value of $q_{cr,LBA}$ is given as the critical maximum stagnation pressure. The reference critical buckling pressure $q_{cr,D}$ is the value for uniform external pressure using the classical linear Donnell-type shell buckling theory applied to a medium-length cylinder with simply-supported edges and is defined as:

$$q_{cr,D} = 0.92E(t/r)^2/\omega \qquad (6.11)$$

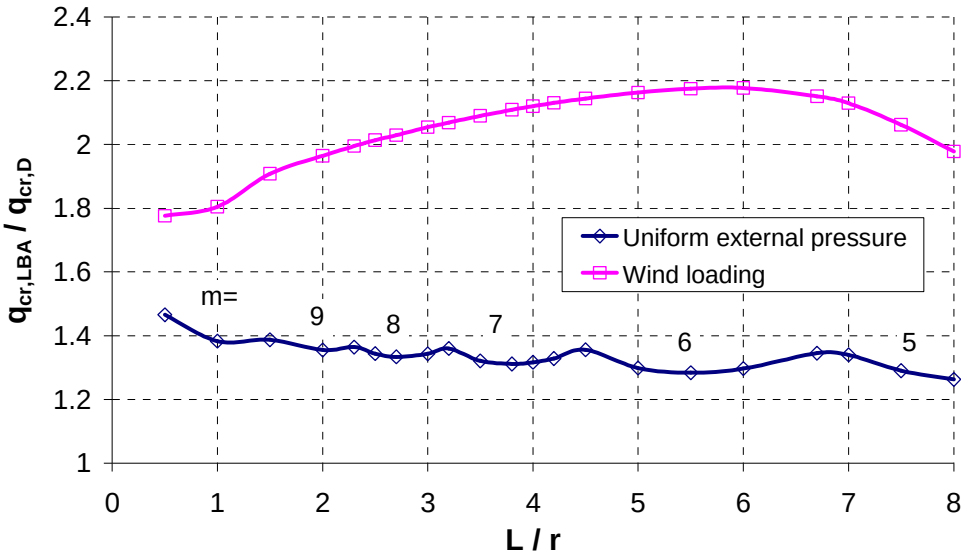

Figure 6-13: Linear critical buckling pressures for cylinders under wind pressure and uniform external pressure ($r/t = 200$)

For cylinders under uniform external pressure, the buckling curve has several cusps, which corresponds to progressive changes of the buckling wave number around the circumference as shown in Fig. 6-13.

For cylinders under wind pressure, in the range $0.5 \le L/r \le 6$, the dimensionless pressure ratio $q_{cr,LBA}/q_{cr,D}$ increases continuously as L/r increases. In this range, the linear buckling mode is a circumferential compressive buckling mode, which is similar to cylinders under uniform external pressure. If the cylinder is short enough, the half wavelength of one buckle is short enough, and then the pressure amplitude is almost uniform within one single buckle. In this situation, the linear critical maximum stagnation pressure is only a little larger than the corresponding critical value for uniform external pressure.

When $L/r > 6$, the value of $q_{cr,LBA}/q_{cr,D}$ for wind loading decreases with increasing values of L/r. This is due to the change of the linear buckling mode. The buckling mode for these cylinders changes to shear buckling caused by a complex pre-buckling membrane stress state.

It is natural to try to relate the linear buckling pressures of cylinders under the two loading conditions (Resinger and Greiner, 1981, 1982; EN 1993-1-6, 2007; ECCS EDR5, 2008). The relationship between the dimensionless buckling pressure ratio $q_{w,LBA}/q_{u,LBA}$ and the length to radius ratio L/r is shown in Fig. 6-14, where $q_{w,LBA}$ is the linear critical maximum stagnation pressure for cylinders under wind pressure, which is derived from the finite element predictions. The linear critical pressure for cylinders under uniform external pressure $q_{u,LBA}$ can be derived from either finite element predictions or the equations given in EN1993-1-6 (2007).

The value of $q_{w,LBA}/q_{u,LBA}$ is always larger than 1, so the wind pressure at buckling is always greater than the uniform buckling pressure. When the shell is short, the ratio is close to 1. That is because, for extremely short cylinders, a large number of circumferential waves are formed within the stagnation zone, and the response at the leading generator of the windward zone is similar to that for uniform external pressure. The half wavelength of the buckle around the front of the windward generator is quite short so that the pressure within this buckle zone is close to uniform. The calculated critical buckling pressures under the two different loading conditions are thus close.

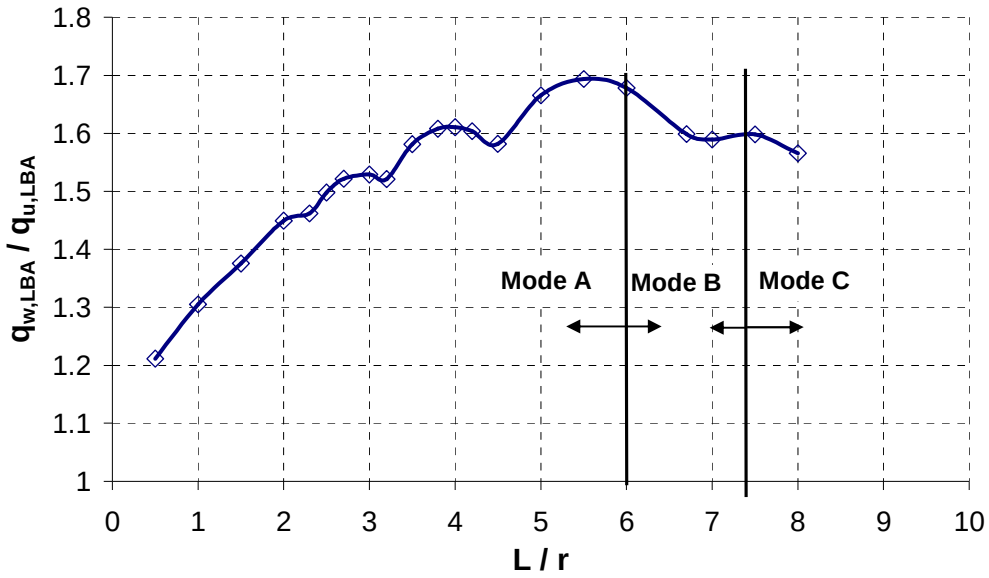

Figure 6-14: Relationship between the linear critical pressure ratio $q_{w,LBA}/q_{u,LBA}$ and the length parameter L/r ($r/t = 200$)

However, if the shell is longer, the critical circumferential buckling wave number around the circumference decreases with increasing value of L/r, and the half wavelength of one buckle around the circumference becomes longer. The magnitude of the stagnation pressure within the buckle around the front of the windward generator cannot be regarded as uniform. The critical maximum stagnation pressure is then larger than the corresponding value for uniform external pressure to provide an "equivalent uniform pressure" to cause buckling within the stagnation zone. The idea of relating the peak of non-uniform pressure distribution in the stagnation zone to a fictitious equivalent uniform pressure was introduced by Resinger and Greiner (1981, 1982) for isolated stocky cylinders (Fig. 6-15). In ECCS EDR5 (2008), the shell buckling design for stocky cylinders under wind loading is based on the following rules:

> *Cylindrical shells with radially fixed boundaries at both ends are here treated using the buckling stress design procedure of EN 1993-1-6 for circumferential (hoop) compression if the following condition is met:*
>
> $$w = \frac{\ell}{\sqrt{rt}} \geq \left(\frac{C_\theta}{15}\right)\left(\frac{r}{t}\right)$$
>
> *in which C_θ is a factor that accounts for the boundary conditions .*
>
> *The non-uniform distribution of pressure q_w resulting from external wind loading on cylinders may, for the purposes of shell buckling design, be substituted by an equivalent uniform external pressure:*
>
> $$q_{eq} = k_w q_{w,\max}$$
>
> *where $q_{w,\max}$ is the maximum stagnation pressure and k_w is a reduction factor:*
>
> $$k_w = 0.46\left(1 + 0.1\sqrt{\frac{C_\theta}{\omega}\frac{r}{t}}\right)$$
>
> *with the value of k_w not outside the range $0.65 \leq k_w \leq 1$, and with C_θ taken from Table 10.3 in Chapter 10 in ECCS EDR5 (2008) according to the boundary conditions.*

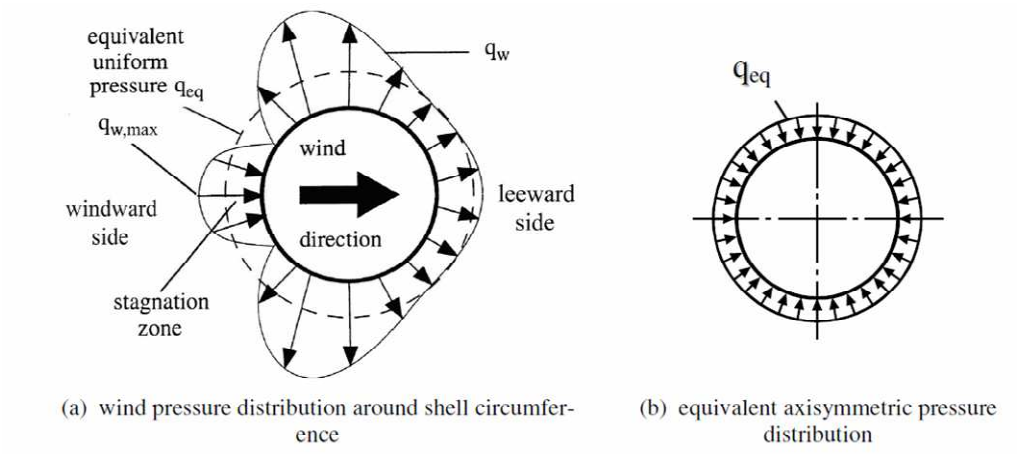

Figure 6-15: Wind pressure distribution for an isolated cylinder and equivalent uniform external pressure (figure taken from Chapter 12 of ECCS EDR5, 2008)

If the number of the waves in the stagnation zone is small, the adjacent suction zone has a stabilizing effect (Greiner, 1998). So for stocky cylinders, with an increase of the length, the non-uniform wind pressure distribution leads to a continuous increase of $q_{w,LBA}/q_{u,LBA}$ as long as the linear buckling modes are similar to those for uniform external pressure. The maximum value of $q_{w,LBA}/q_{u,LBA}$ is 1.70 at $L/r = 5.5$. The curve has several waves, which are caused by the progressive changes of the buckling wave number under uniform external pressure with changing L/r.

After the maximum point in Fig. 6-14, the value of $q_{w,LBA}/q_{u,LBA}$ decreases steadily with further increase of L/r. That is because, for longer cylinders, the buckling strength is no longer dominated by circumferential compressive membrane stress alone, but the interaction of axial membrane stress and circumferential membrane stress. The linear critical buckling mode for these cylinders under wind loading is no longer similar to that for uniform external pressure, but a more complex buckling behaviour caused by a complex pre-buckling membrane stress state. The boundary between Mode A and Mode B is here defined at $L/r = 6$, because the maximum value of linear critical pressure $q_{w,LBA}$ is reached at $L/r = 6$ (Fig. 6-13).

6.4.4 Linear bifurcation analysis for cylinders with $r/t = 500$

The linear buckling behaviour of cylinders with $r/t = 500$ in the range $0.5 \le L/r \le 12$ was analysed next.

6.4.4.1 Linear critical buckling modes

The linear buckling modes for cylinders with different length to radius ratios under wind pressure are shown in Fig. 6-16. The linear buckling modes are the circumferential compressive buckling mode in the range $0 < L/r \le 8$, corresponding to Mode A in Fig. 6-8(a). The circumferential buckling is caused by circumferential compressive membrane stress with a negligible influence of the meridional membrane stress.

(a) $L/r = 2$ (Mode A) (b) $L/r = 8$ (Mode A) (c) $L/r = 9$ (Mode B) (d) $L/r = 10$ (Mode C)

Figure 6-16: Linear critical buckling modes for cylinders under wind pressure ($r/t = 500$)

When $L/r = 9$, some fold-like buckles are formed following the main buckle and the linear buckling mode changes to the global shear buckling mode (Mode B in Fig. 6-8b). When $L/r = 10$, the linear buckling mode changes to the local shear buckling mode (Mode C in Fig. 6-8b). The transition between these linear buckling modes is similar to that for $r/t = 200$.

6.4.4.2 Relationship of the linear critical pressure for cylinders under wind pressure and under uniform external pressure

The relationship between the dimensionless buckling pressure ratio $q_{cr,LBA}/q_{cr,D}$ and the length parameter L/r is shown in Fig. 6-17. By comparing the results for

cylinders with $r/t = 500$ and $r/t = 200$, it may be concluded that for cylinders with different radius to thickness ratios under uniform external pressure, the dimensionless pressure ratio $q_{cr,LBA}/q_{cr,D}$ changes similarly as the length changes. The cusps correspond to the progressive changes of the buckling wave number around the circumference.

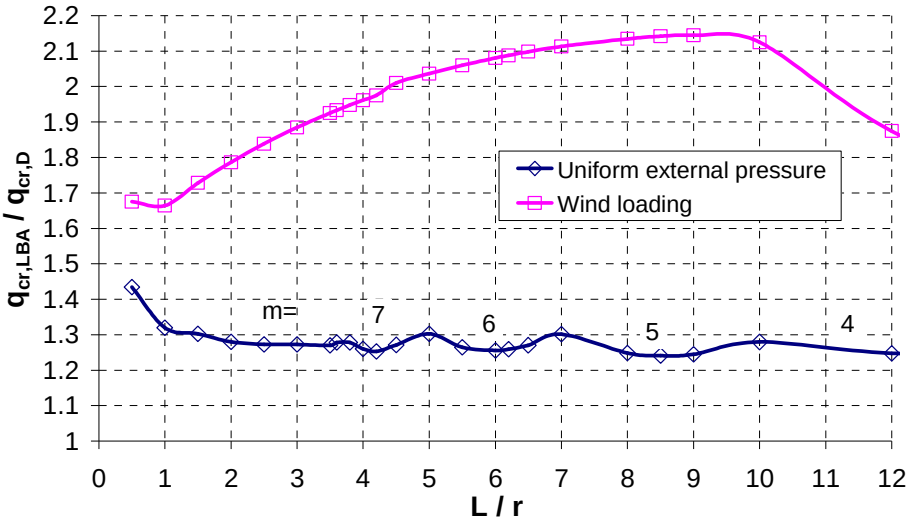

Figure 6-17: Linear critical buckling pressure for cylinders under wind pressure and uniform external pressure ($r/t = 500$)

The dimensionless pressure ratio $q_{cr,LBA}/q_{cr,D}$ increases steadily with increasing L/r in the range $0.5 \le L/r \le 9$, and the maximum value is reached at $L/r = 9$, which is different from the value for $r/t = 200$. This pattern of the linear buckling modes changes at different values of L/r depending on the radius to thickness ratio. When $L/r > 9$, the value of $q_{cr,LBA}/q_{cr,D}$ decreases with increasing value of L/r, which is due to the change of linear buckling modes as noted before.

The relationship between the dimensionless buckling pressure ratio $q_{w,LBA}/q_{u,LBA}$ and the length parameter L/r for cylinders with $r/t = 500$ is shown in Fig. 6-18. The curve has a similar characteristic as for $r/t = 200$. The buckling pressure ratio $q_{w,LBA}/q_{u,LBA}$ increases steadily as L/r increases and the maximum value 1.72 is reached at $L/r = 8.5$, which is close to the maximum value 1.70 for $r/t = 200$. After the maximum point, the buckling pressure ratio $q_{w,LBA}/q_{u,LBA}$ decreases with a

further increase of L/r. The boundary between Mode A and Mode B is defined here as $L/r = 9$ because the linear critical pressure reaches the maximum value at $L/r = 9$ in Fig. 6-17.

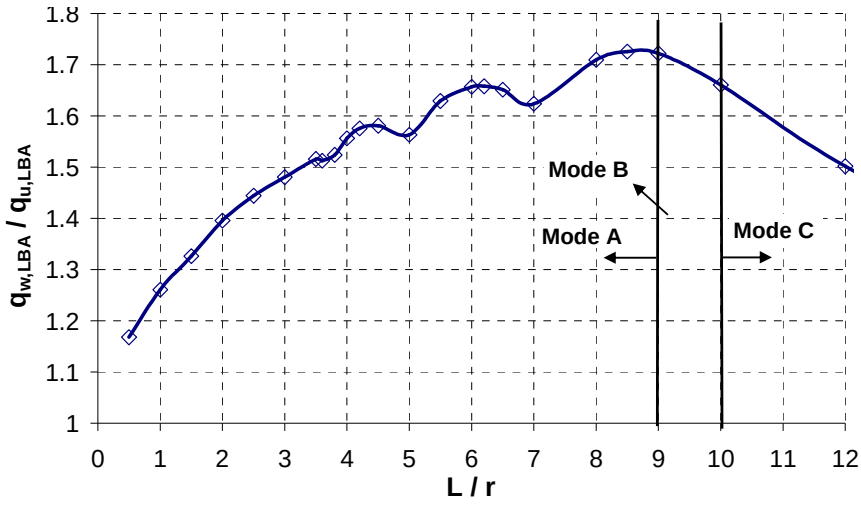

Figure 6-18: Relationship between the linear critical pressure ratio $q_{w,LBA}/q_{u,LBA}$ and the length parameter L/r ($r/t = 500$)

6.4.5 Linear buckling strength for thin cylinders with different geometries under wind pressure and uniform external pressure

Similar curves as Figs 6-14 and 6-18 for cylinders with different radius to thickness ratios can be obtained. The curves can be brought together by using the length parameter Ω which was shown in Chapter 3 to be the relevant dimensionless length parameter for medium-length and long cylinders under global bending. The relationship between the linear elastic critical pressure ratio $q_{w,LBA}/q_{u,LBA}$ and the length parameter Ω is shown in Fig. 6-19 for four values of the radius to thickness ratio.

For cylinders with $r/t = 200$, the value of $q_{w,LBA}/q_{u,LBA}$ is very slightly smaller than the corresponding value of the other thinner cylinders for the same value of Ω. This small discrepancy may be caused by many factors, such as the wind distribution around the circumference, the pre-buckling stress distribution and the effect of the boundary conditions. However, this discrepancy disappears when the shell becomes

thinner. The geometry of practical tanks and silos is usually very thin and the radius to thickness ratio often lies in the range $500 \le r/t \le 2000$. For thin cylinders within this range or other much thinner cylinders, the curves can all be represented accurately by the curve for $r/t = 500$.

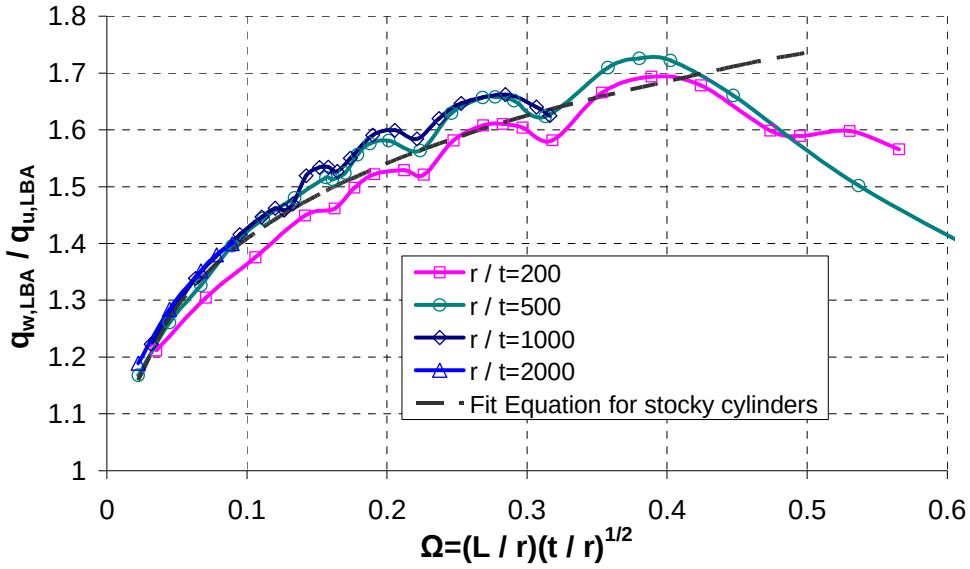

Figure 6-19: Relationship between the linear elastic critical pressure ratio $q_{w,LBA} / q_{u,LBA}$ and the length parameter Ω

An approximate expression can be found to represent the curves in Fig. 6-19 for short thin cylinders. The power function Eq. 6.12 was chosen here to fit the numerical results and the least squares best-fitting procedure was conducted to determine the parameters a and b.

$$q_{w,LBA} / q_{u,LBA} = a\Omega^{b} \tag{6.12}$$

As a result, Eq. 6.13 accurately represents these buckling curves for short thin cylinders. This equation is shown as the dashed line in Fig. 6-19. It fits the accurate numerical predictions very well and provides a lower bound to the numerical results for cylinders with $r/t \ge 500$.

$$q_{w,LBA} / q_{u,LBA} = 1.90\Omega^{0.13} \tag{6.13}$$

By using Eq. 6.13 and the general buckling resistance equations for short cylinders under uniform external pressure given in EN 1993-1-6 (2007), the linear

critical buckling pressure for cylinders under wind loading can be predicted directly. For thin cylinders with $r/t \geq 500$, the predicted results might be slightly conservative for some cylinders, because the fitted equation is a lower bound result without considering the progressive changes in the circumferential buckling wave number. For cylinders with $r/t < 500$, the calculated results using the fitted equation might overestimate the result slightly as shown in Fig. 6-19.

In using Eq. 6.13, the length parameter Ω should be limited to the range in which cylinders have similar linear buckling modes under wind pressure and uniform external pressure. By observing the curves in Fig. 6-19, it is seen that the range $0 < \Omega \leq 0.4$ is an appropriate range for 6.13. As a result, the linear buckling pressures of short cylinders under wind pressure and uniform external pressure can be related by a simple equation with a clear application condition.

The upper limit of $\Omega = 0.4$ corresponds to different values of the length to radius ratio for different r/t as shown in Fig. 6-20.

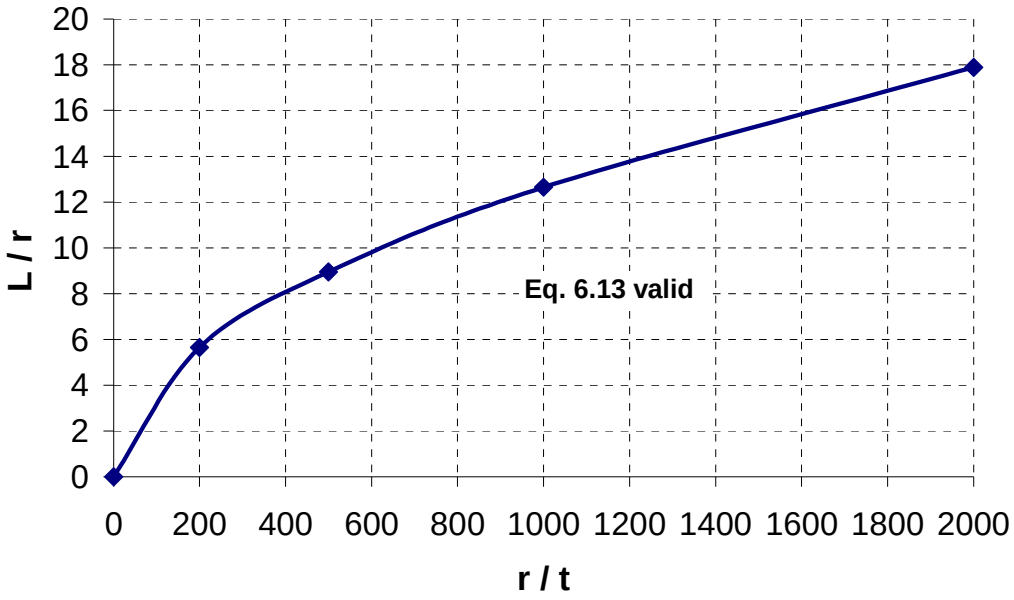

Figure 6-20: The upper limit of *L / r* for different *r / t* to apply Eq. 6.13

6.5 Geometrically nonlinear analysis for cylinders under wind loading

6.5.1 Overview of geometrically nonlinear buckling analysis (GNA) for cylinders under wind loading

A shell may be subjected to either bifurcation buckling or snap-through buckling. The methodology of the LBA procedure covers only bifurcation buckling (ECCS EDR5, 2008). When large deformation occur before the linear elastic critical load is reached or where snap-through buckling may occur, the pre-buckling deformation and stresses may play an important role in affecting the buckling behaviour. The final critical load might be much smaller than the value derived from LBA. Due to the effects of geometric nonlinearity, the nonlinear buckling mode may be quite different from the linear buckling mode, depending on the specific geometry. In this situation, geometrically nonlinear analysis should be adopted to obtain accurate buckling strength predictions.

For cylinders under uniform external pressure, the geometrically nonlinear load-displacement relationship curve in the pre-buckling stage is close to linear, and the pre-buckling deformations are quite small and have little influence on the post-buckling behaviour, which leads to very similar critical buckling pressure predictions for both LBA and GNA.

However, the situation for cylinders in wind loading might be quite different. For stocky cylinders, the buckling behaviour is similar to cylinders under uniform external pressure, the critical pressures derived from LBA and GNA are thus close. But for intermediate aspect ratio cylinders, pre-buckling geometric nonlinearity influences the buckling behaviour significantly. The critical buckling pressures and buckling modes derived from LBA and GNA may be quite different depending on the specific geometry. This discrepancy is mainly caused by the significant influence of meridional compressive stress as the shell becomes longer, so it is helpful to use the buckling resistance for pure uniform axial compression as a reference value. The “classical elastic buckling strength” for a perfect thin-walled cylinder under pure axial compression is given by

$$\sigma_{cl} = 0.605E\frac{t}{r} \tag{6.14}$$

The ovalization of the cross-section leads to an increase in the local radius of curvature of the shell structure, so to calculate the reference value of the buckling resistance in axial compression after ovalization, the radius r in Eq. 6-14 should be replaced by the local increased radius, which causes an obvious reduction to the buckling resistance. Assuming $w << r_0$, the local radius up the windward meridian can be obtained approximately according to the following equation (Karamanos, 2002):

$$\rho \cong r_0 + w_1 + 2\frac{w_1 - w_0}{\Delta\varphi^2} \tag{6.15}$$

in which r_0 is the original radius, w_0 is the radial displacement at the centre of stagnation zone indicating as $\varphi = 0$, w_1 is the radial displacement at position with an increased angle $\Delta\varphi$.

Due to the complexity of the nonlinear buckling behaviour for cylinders under wind loading, the following discussions focus on geometrically nonlinear finite element analysis. The same geometries, boundary conditions and loading conditions as for LBA were used. The aim is to give a comprehensive understanding of the nonlinear buckling characteristics of cylinders with different geometric parameters under wind loading.

6.5.2 Geometrically nonlinear analysis for cylinders with $r/t = 200$

The nonlinear buckling behaviour of cylinders with $r/t = 200$ in the range $0.5 \le L/r \le 8$ was analysed next.

The load-radial displacement curves are shown in Fig. 6-21. The radial displacement means the maximum radial displacement up the windward generator. The imposed pressure is normalized by the linear critical maximum stagnation pressure $q_{w,LBA}$ which was derived from linear bifurcation analysis (LBA).

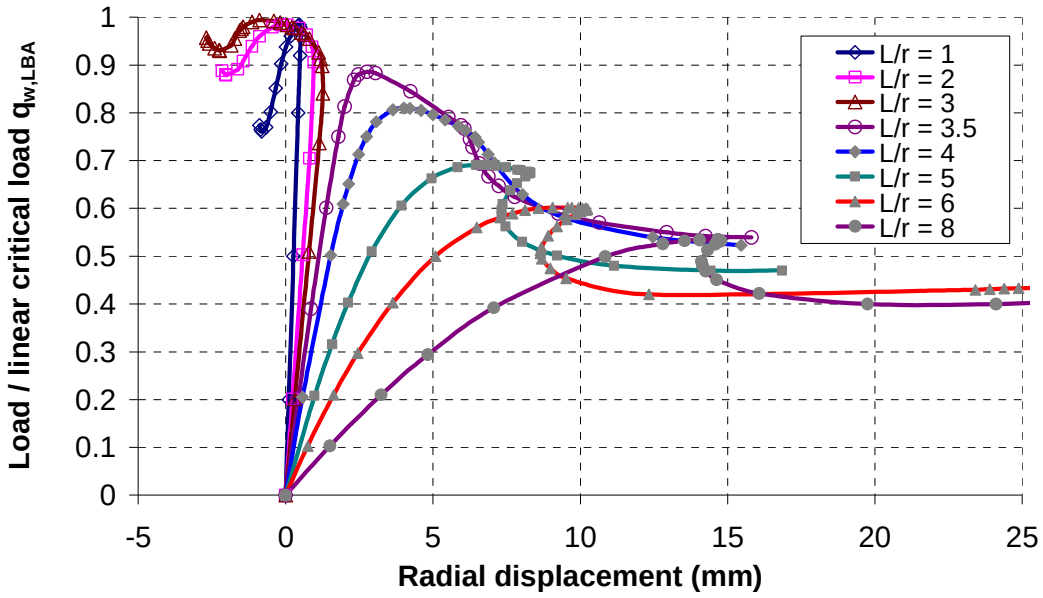

Figure 6-21: Relationship between the dimensionless pressure ratio and the maximum radial displacement up the windward meridian ($r/t = 200$)

For stocky cylinders with $L/r \leq 3$, snap-through buckling occurs and an instability point appears just after the limit load has been reached. The instability point is defined by the point where the maximum load is reached or the appearance of a negative eigenvalue in the load-displacement path. The pre-buckling deformation is small before the limit load is reached. The nonlinear critical pressure is close to the linear elastic critical pressure for stocky cylinders, which corresponds to the conclusion that geometric nonlinearity has little effect on the buckling strength of cylindrical shells under uniform external pressure. In the first stages of deformation, the shell can bear large pressures with little inward radial deformation and the load-displacement relationship is close to linear. Then the inward radial deformation decreases and outward radial displacement increases gradually until the limit point is reached. At the limit point, the membrane tangent stiffness is reduced to zero. After the limit point, the outward radial displacement increases with decreasing load.

The nonlinear buckling modes for cylinders with $L/r = 1$ and $L/r = 3$ are shown in Fig. 6-22(a) and (b). The buckling mode is the circumferential compressive buckling mode, which is similar to cylinders under uniform external pressure.

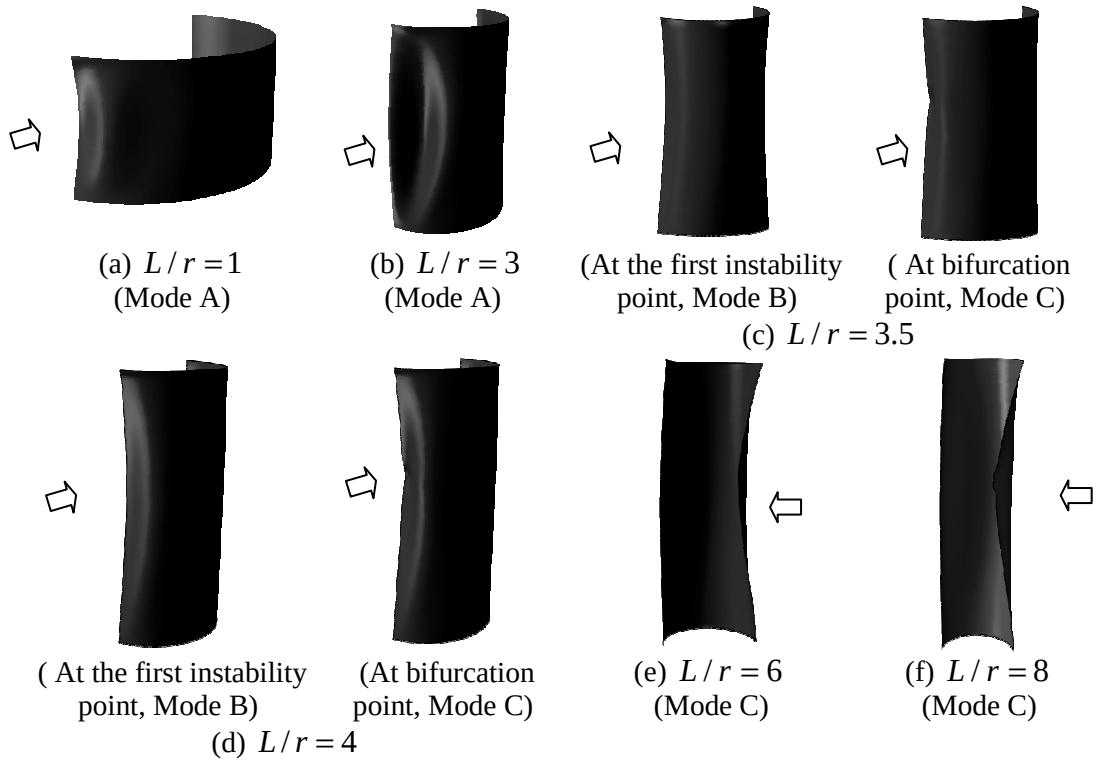

Figure 6-22: Nonlinear buckling modes for cylinders under wind pressure ($r/t=200$)

For intermediate aspect ratio cylinders ($L/r \geq 3.5$ in Fig. 6-21), the load-displacement curves are different from short cylinders and the curves display different buckling characteristics depending on the specific value of L/r . When $L/r=3.5$ and $L/r=4$, in the first stages of deformation, the shell can bear large loads with comparatively small inward radial deformation until a first critical stability point occurs indicating the occurrence of snap-through buckling. The pre-buckling deformation is naturally larger than for stocky cylinders. The relationship of load and radial displacement is close to linear, becoming nonlinear when it approaches the snap-through buckling point. This buckling is an axial long wavelength buckling mode and occurs in a large zone around the upper part of the windward meridian caused by the interaction of axial compression and circumferential compression.

After the snap-through buckling point, the load decreases quickly but with accelerated inward radial deformation until a second bifurcation point appears leading to a more aggressive fall in strength. This triggers local bifurcation buckling into a short wavelength pattern with a maximum inward displacement at

about $x/h = 0.62$ .The location of the buckling area with maximum inward displacement corresponds to the position of the maximum meridional compressive membrane stress in the upper part of the cylinder as shown the curves for intermediate aspect ratio and long cylinders in Fig. 6-9. This local bifurcation buckling is caused mainly by the large meridional compressive membrane stress in the upper part of the windward meridian.

When $L/r = 3.5$ and $L/r = 4$, the relationship of the load and radial displacement is close to linear at the beginning but becomes nonlinear when the curve approaches the snap-through buckling point. Geometric nonlinearity in the pre-buckling stage affects the buckling strength. The buckling pressure ratio $q_{w,GNA}/q_{w,LBA}$ equals 0.89 and 0.81 respectively, where $q_{w,GNA}$ is the nonlinear critical buckling pressure. After the snap-through buckling, the radial displacement increases quickly accompanied by ovalization of the cross-section. The local increased radius ρ due to ovalization reduces the buckling resistance to axial compressive stress. Furthermore, the axial compressive membrane stress in the upper part of the cylinder induced by wind pressure increases quickly with increasing values of L/r (Fig. 6-9). As a result, local meridional compressive buckling is triggered at a reduced load in the upper half of the shell.

The first figure of Fig. 6-22(c) shows the snap-through buckling mode for $L/r = 3.5$ at the first instability point, and the second figure shows the buckling mode at the subsequent bifurcation point when bifurcation buckling occurs. The nonlinear buckling mode for $L/r = 4$ (Fig. 6-22d) shows a similar buckling behaviour as for $L/r = 3.5$. For these cylinders, the buckling strength is controlled by snap-through buckling.

For larger values of L/r, pre-buckling ovalization of the cross-section plays a more important role in affecting the buckling behaviour. By observing the load-displacement curves for cylinders in the range $5 \le L/r \le 8$ (Fig. 6-21), it is known that in the pre-buckling stage, the load-displacement curves become more nonlinear for these cylinders. The shell may have a large inward radial deformation even under low pressure. In this situation, the ovalization of the cross-section is more significant.

The local radius of curvature due to ovalization of the cross-section becomes larger, leading to a more noticeable reduction to the buckling resistance under axial compression.

Furthermore, the meridional compressive membrane stress in the upper part of the cylinder induced by wind pressure increases continuously with increasing values of L/r (Fig. 6-9). So for longer cylinders, after the snap-through buckling point, local axial compressive buckling is triggered more quickly due to the large axial compressive membrane stress and reduced axial compressive resistance in the upper part of the cylinder.

If the cylinder is long enough, snap-through buckling is superseded by bifurcation buckling. The local axial compressive buckling mode caused by the axial compressive membrane stress occurs in the upper part of cylinder first. Cylinders with $L/r = 6$ and $L/r = 8$ display this nonlinear buckling mode, as shown in Fig. 22 (e) and (f). For these cylinders, buckling occurs quite locally with considerable inward radial displacement. The small meridional buckles with a short wavelength pattern are difficult to detect clearly. For cylinders where bifurcation buckling was first detected, the buckling strength is controlled by bifurcation buckling.

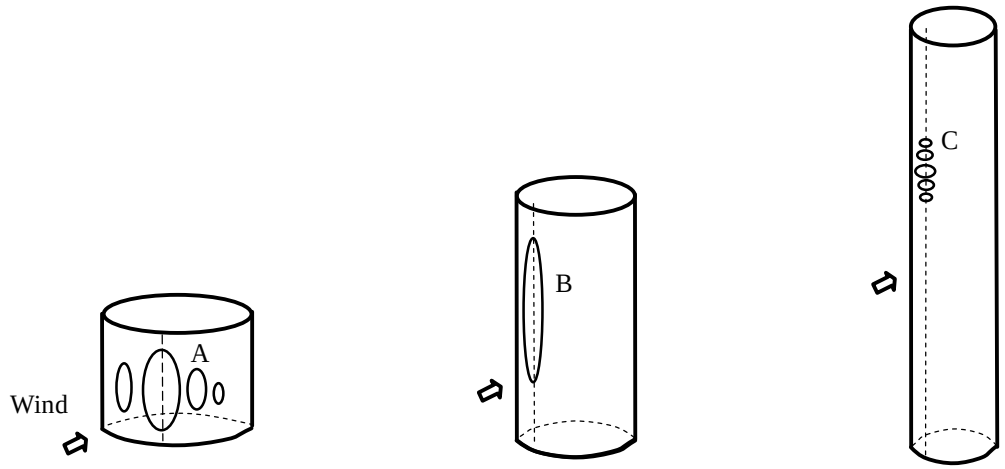

(a) Stocky cylinder (b) Intermediate aspect ratio cylinder (c) Slender cylinder

Figure 6-23: Nonlinear buckling modes for cylinders with different aspect ratios under wind pressure

The three different nonlinear critical buckling modes termed here Mode A, Mode B and Mode C, corresponding to the circumferential compressive buckling mode, snap-through buckling mode and local bifurcation buckling mode respectively, are shown in Fig. 6-23. The categorisation here is based on the different nonlinear critical buckling modes. The cylinders with Mode A are categorized as stocky cylinders. The cylinders with buckling strength controlled by the snap-through buckling mode pattern Mode B are categorized as intermediate long cylinders. The cylinders with buckling strength controlled by the bifurcation buckling mode pattern Mode C are categorized as slender cylinders.

6.5.3 Geometrically nonlinear analysis for cylinders with $r/t = 500$

The nonlinear buckling behaviour of cylinders with $r/t = 500$ in the range $0.5 \le L/r \le 12$ was analysed next. The pressure-deflection curves between the dimensionless buckling pressure ratio and the radial displacement are shown in Fig. 6-24. The radial displacement is the maximum radial displacement up the windward meridian.

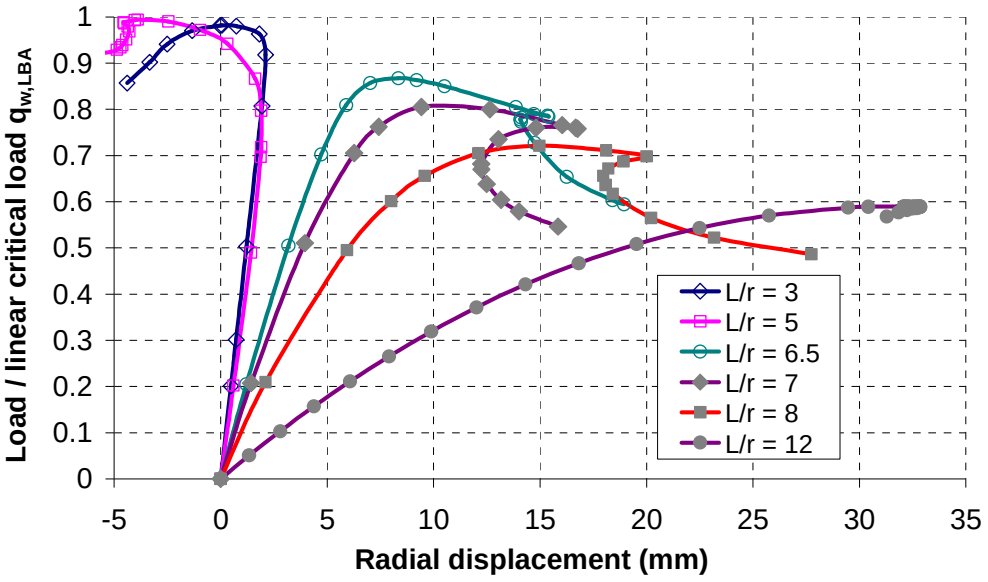

Figure 6-24: Relationship between the dimensionless pressure ratio and the maximum radial displacement up the windward meridian ($r/t = 500$)

The curves in Fig. 6-24 show a similar buckling behaviour to that for $r/t = 200$. For short cylinders, circumferential compressive buckling is caused by circumferential compressive membrane stress. For intermediate long cylinders, snap-through buckling occurs, followed by a bifurcation buckling due to the effect of pre-buckling ovalization of the cross-section. With increasing values of L/r, bifurcation buckling occurs earlier after the snap-through buckling until the snap-through buckling is surpassed finally. Either snap-through buckling or bifurcation buckling may dominate the buckling behaviour, depending on the specific geometry of the shell.

The nonlinear buckling modes for cylinders with different length to radius ratios are shown in Fig. 6-25. The buckling modes are similar to the buckling modes of stocky, intermediate long cylinders for $r/t = 200$.

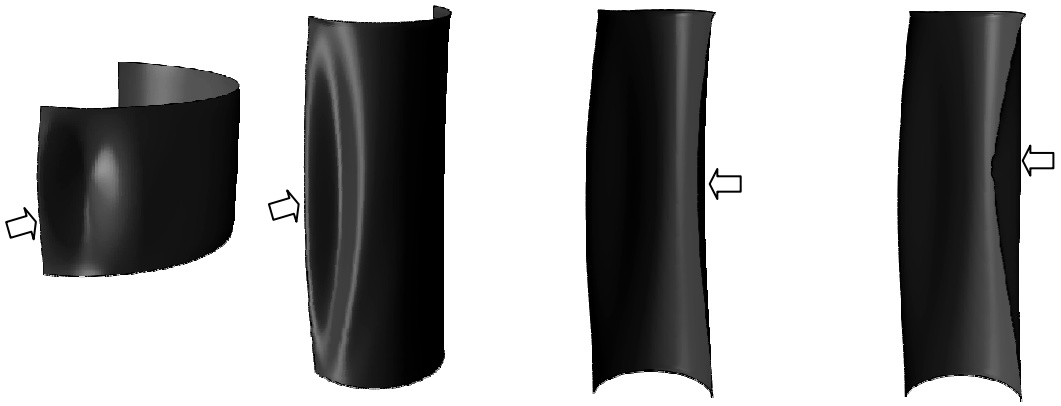

(a) $L/r = 1$ (Mode A) (b) $L/r = 5$ (Mode A) (At the first instability point, Mode B) (At the bifurcation point, Mode C)

(c) $L/r = 6.5$

Figure 6-25: Nonlinear buckling modes for cylinders under wind pressure ($r/t = 500$)

The length boundary between stocky and intermediate aspect ratio cylinders are defined at the point where the buckling mode starts to change from Mode A to Mode B. It also means that geometric nonlinearity starts to affect the buckling behaviour significantly. When $r/t = 200$, it is $L/r = 3$. When $r/t = 500$, it is $L/r = 6$. The boundaries for other thinner cylinders with $r/t > 500$ can also be determined accordingly. The boundary between stocky and intermediate aspect ratio cylinders for cylinder with different geometric parameters is shown in Fig. 6-26. It is clear that

geometric nonlinearity starts to affect the buckling behavior ar a larger value of L/r in thinner cylinders.

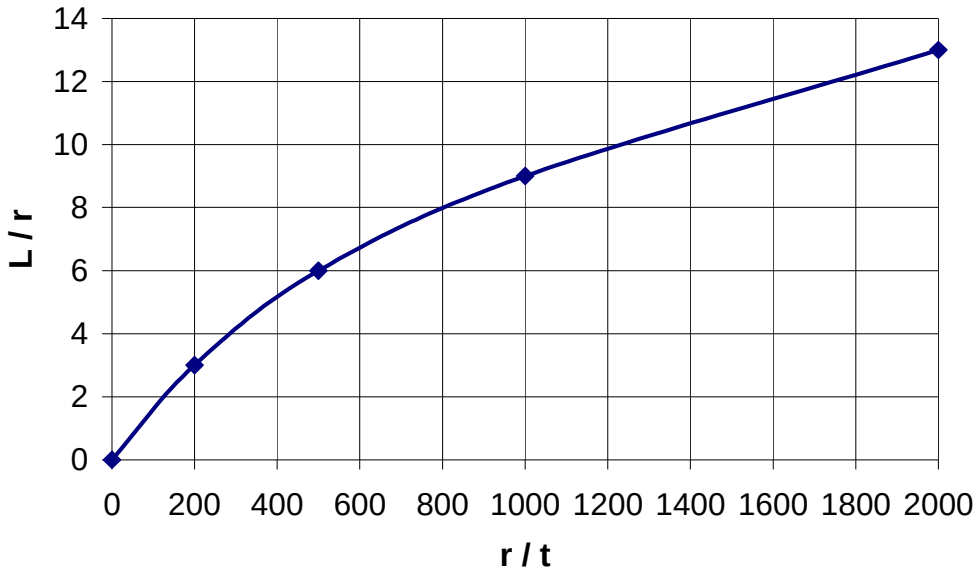

Figure 6-26: Boundary between stocky and intermediate aspect ratio cylinders for cylinders with different geometries determined from GNA

6.5.4 Comparison of the results from LBA and GNA for cylinders under uniform external pressure and wind pressure

6.5.4.1 Comparison of the linear and nonlinear critical buckling pressures for cylinders under wind loading

The effect of geometrically nonlinearity is best seen by examining the ratio of the GNA buckling pressure $q_{w,GNA}$ to the LBA buckling pressure $q_{w,LBA}$. The relationship between the dimensionless buckling pressure ratio $q_{w,GNA}/q_{w,LBA}$ and the dimensionless length parameter Ω for cylinders with different radius to thickness ratios is shown in Fig. 6-27.

For short cylinders, the values of $q_{w,GNA}/q_{w,LBA}$ are close to 1, indicating that geometric nonlinearity has a negligible effect on the buckling strength. Buckling is caused mainly by circumferential compressive membrane stress. The pre-buckling deformation is usually very small before circumferential compressive buckling

occurs (Figs 6-21 and 6-24) and the load-displacement relationship is close to linear at pre-buckling stage, so pre-buckling deformations have little influence on the buckling strength.

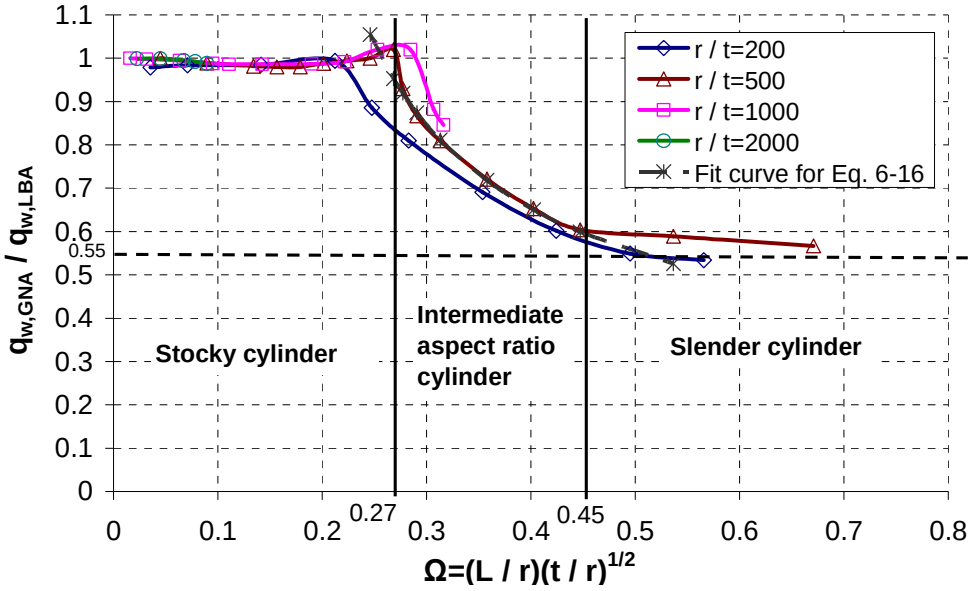

Figure 6-27: Relationship between the dimensionless critical buckling pressure $q_{w,GNA} / q_{w,LBA}$ and dimensionless length parameter Ω

For intermediate aspect ratio cylinders, pre-buckling deformations have a detrimental effect on the buckling strength, causing a reduction to the critical buckling pressure. It is observed that geometric nonlinearity affects the buckling strength from $\Omega = 0.21$ for cylinders with $r/t = 200$. For thinner cylinders with $r/t = 500$, it affects from a larger value $\Omega = 0.27$. However, for thinner cylinders with $r/t > 500$, it affects from only a slightly larger value of Ω than for $r/t = 500$. The value $\Omega = 0.27$ can therefore be chosen conservatively as the boundary between stocky and intermediate aspect ratio cylinders for thin cylinders with $r/t \geq 500$. Once the buckling behaviour is influenced by geometric nonlinearity, the buckling pressure ratio $q_{w,GNA} / q_{w,LBA}$ decreases greatly with a small increase in Ω.

Greater reductions in the buckling strength are caused by geometric nonlinearity as the cylinder becomes longer. The nonlinear load-displacement curves in Figs 6-21 and 6-24 describe this nonlinear buckling behaviour as the length changes.

However, when the length parameter Ω increases to a certain value, as shown in Fig. 6-27 in the range $\Omega > 0.45$, the pressure ratio $q_{w,GNA} / q_{w,LBA}$ decreases only slightly with a further increase of Ω. The constant value of 0.55 can be chosen as a conservative estimate of $q_{w,GNA} / q_{w,LBA}$ for thin cylinders in this range.

Based on above descriptions, for cylindrical shells under wind loading, the nonlinear buckling behaviour can be divided into three stages. First, when $0 < \Omega \le 0.27$, cylindrical shells are categorized as stocky cylinders, the values of $q_{w,GNA} / q_{w,LBA}$ are close to 1. A small reduction in the buckling strength might be caused by the slight influence of pre-buckling geometric nonlinearity but this effect is negligible. It should be noted that for thick cylinders with $r/t < 500$ in the range $0.20 < \Omega \le 0.27$, adoption of linear elastic buckling pressure may overestimate the buckling strength for some shells (Fig. 6-27). Thin shells with $r/t \ge 500$ are more practical in the design of thin silos and tanks, so $0 < \Omega \le 0.27$ is a proper definition of stocky cylinders for a wide range of thin cylindrical shells.

Shells in the range $0.27 < \Omega \le 0.45$ are categorized as intermediate aspect ratio cylinders. The relationship between the buckling pressure ratio $q_{w,GNA} / q_{w,LBA}$ and the length parameter Ω can be represented by an approximate equation as:

$$q_{w,GNA} / q_{w,LBA} = \frac{0.54}{5.43\Omega^{0.14} - 3.95} \tag{6.16}$$

Equation 6.16 is shown as the dashed line in Fig. 6-27. It fits the numerical results for cylinders with $r/t = 500$ in the range $0.27 < \Omega \le 0.45$ quite well. For thin cylinders with $r/t > 500$, it may underestimate the nonlinear buckling strength slightly. That is because the influence of geometric nonlinearity on the buckling strength depends slightly on the length parameter Ω.

For cylinders in the range $\Omega \ge 0.45$, the values of buckling pressure ratio $q_{w,GNA} / q_{w,LBA}$ can be defined as a constant value 0.55, which is a conservative approximation for thin cylinders with $r/t \ge 500$. Even for cylinders with $r/t < 500$, the value $q_{w,GNA} / q_{w,LBA} = 0.55$ is close to the accurate numerical predictions.

However, more calculations are needed to explore the nonlinear buckling behaviour of slender cylinders further.

6.5.4.2 Comparison of the nonlinear buckling pressures for cylinders under uniform external pressure and wind loading

The nonlinear buckling pressures for cylinders with different aspect ratios under wind pressure and uniform external pressure can be related through the dimensionless length parameter Ω (Fig. 6-28). As geometric nonlinearity has a negligible influence on the buckling strength of cylinders under uniform external pressure, the value of $q_{u,GNA}$ is very close to the value $q_{u,LBA}$, so $q_{u,GNA}$ can be obtained through the well known buckling equations for uniform external pressure.

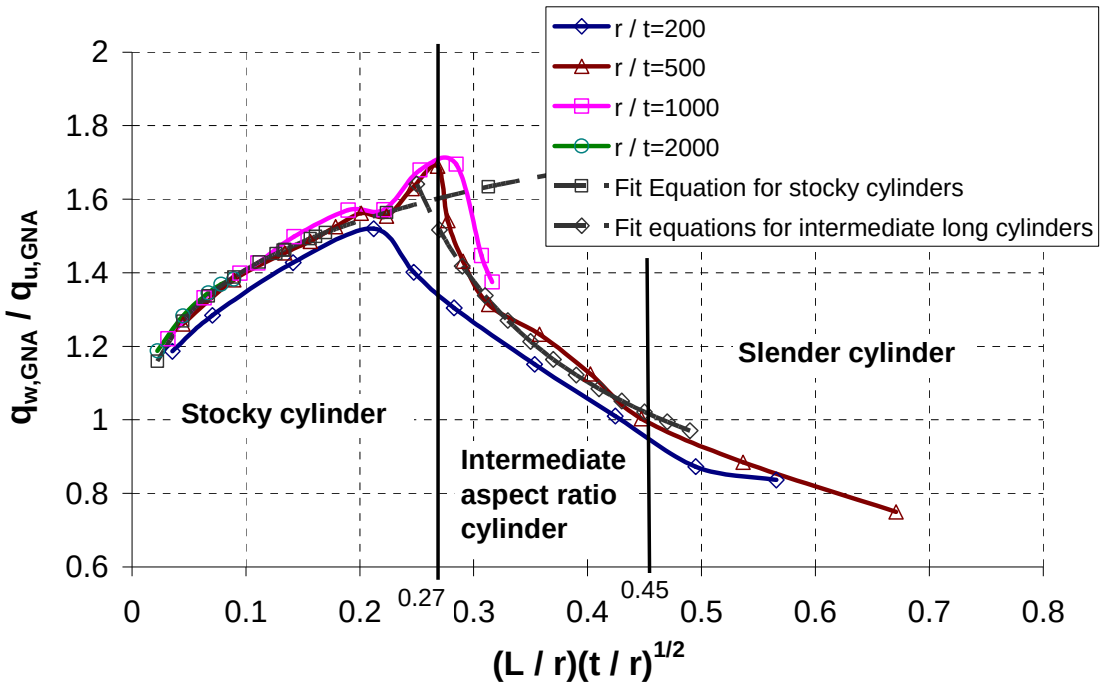

Figure 6-28: Relationship between the buckling pressure ratio $q_{w,GNA} / q_{u,GNA}$ and the dimensionless length parameter Ω

The dashed line of the best fit Eq. 6.13 for stocky cylinders is shown in Fig. 6-28. It indicates that Eq. 6.13 also describes the relationship between the nonlinear buckling pressure ratio $q_{w,GNA} / q_{u,GNA}$ and the length parameter Ω quite well for short

cylinders with $r/t \geq 500$ in the range $0 < \Omega \leq 0.27$, which is different from the condition $0 < \Omega \leq 0.4$ determined from LBA.

For cylinders in the range $0.27 < \Omega \leq 0.45$, the GNA relationship curves in Fig. 6-28 seem difficult to describe. However, it is noted that Eq. 6.13 is accurate to describe the relationship between $q_{w,LBA}/q_{u,LBA}$ and Ω, and the reduction in the buckling strength under wind loading due to geometric nonlinearity is described well by Eq. 6.16. So the buckling pressure ratio $q_{w,GNA}/q_{u,GNA}$ can be calculated directly in terms of the product of Eqs 6.13 and 6.16 as

$$q_{w,GNA}/q_{u,GNA} = (1.90\Omega^{0.13}) \bullet (\frac{0.54}{5.43\Omega^{0.14} - 3.95}) \tag{6.17}$$

The dashed line of the best fit equations for intermediate aspect ratio cylinders in Fig. 6-28 indicates that Eq. 6.17 gives an accurate prediction of $q_{w,LBA}/q_{u,LBA}$ for cylinders with $r/t = 500$ in the range $0.27 < \Omega \leq 0.45$. In this way, cylinders in the range $0 < \Omega \leq 0.45$, which covers most practical silos and tanks, the nonlinear buckling strength for cylinders under wind pressure $q_{w,GNA}$ is related to the critical value for uniform external pressure $q_{u,GNA}$ by the length parameter Ω in a simple way.

For cylinders in the range $\Omega > 0.45$, the relationship curves of $q_{w,GNA}/q_{u,GNA}$ and Ω is more complex to describe due to the progressive changes in both the linear buckling mode and the nonlinear buckling mode with changing length under wind pressure. The nonlinear buckling pressure $q_{w,GNA}$ can be related to $q_{u,GNA}$ referring to the curves in Fig. 6-28. However, the length to radius ratios for these cylinders are very large and not practical for the design of silos and tanks, and thus outside the scope of this chapter.

The relationship between the buckling pressure ratio $q_{w,GNA}/q_{u,GNA}$ and the length parameter Ω is summarized in Table 6-2. It shows that the idea of relating the buckling strength under wind loading to the buckling strength under uniform external pressure is a very useful and simple way to describe the complex buckling behaviour

of cylinders for a wide range of shells under wind loading. The cylinders are categorized as stocky, intermediate aspect ratio and slender cylinders according to the length parameter Ω.

Table 6-2: Relationship between the buckling pressure ratio $q_{w,GNA} / q_{u,GNA}$ and the length parameter Ω for cylinders in different aspect ratios

Category	$\Omega = (L/r)(t/r)^{1/2}$	$q_{w,GNA} / q_{u,GNA}$
Stocky cylinders	$0 < \Omega \le 0.27$	$1.90\Omega^{0.13}$
Intermediate aspect ratio cylinders	$0.27 < \Omega \le 0.45$	$(1.90\Omega^{0.13}) \bullet (\frac{0.54}{5.43\Omega^{0.14} - 3.95})$
Slender cylinders	$\Omega > 0.45$	Figure 6-28

6.6 Mesh Convergence study

The results above are based on careful mesh division after a mesh convergence study. In this section, the significant effect of the finite element mesh on the buckling strength evaluation is explored through linear bifurcation analysis (LBA). The aim is to show the importance of mesh division in the finite element analysis of cylinders under asymmetric wind pressure. Different mesh divisions are required to obtain accurate buckling predictions depending on the specific geometric parameters of the shell.

Cylinders under wind pressure may display different buckling behaviours as described above. The linear critical buckling modes for stocky, intermediate aspect ratio and slender cylinders are quite different. Whether a particular mesh can capture an accurate result is usually determined by the number of the elements in one half-wavelength of the relevant bending or buckling deformations. The buckling modes for cylinders with different geometries may be quite different, which makes the mesh requirement different.

By observing the buckling modes shown in Fig. 6-7, it is noted that for short cylinders, only one buckle forms in the meridional direction extending over the whole length of the cylinder, and several buckles are formed around the circumference, so fewer elements down the meridian could accommodate the single buckle and capture accurate results. The element size down the meridian could thus be large. The requirement of the mesh around the circumference can be determined by considering the number of circumferential buckling waves around the circumference of cylinders with same geometries under uniform external pressure.

For intermediate aspect ratio and slender cylinders, the buckling mode is indeterminate. The buckles are formed toward the bottom of the cylinder as the length of the shell increases, local buckling may occur in a small zone near the bottom boundary and the half-wavelength of one buckle is quite small. To have enough elements to accommodate the local buckle, the element size should be small enough near the buckling zone. Considering that buckling occurs locally near the bottom boundary, the mesh is only required to be refined enough in the zone near the bottom, and the other parts of the shell can have a comparatively coarse mesh since only the pre-buckling stresses near the buckling zone need to be accurate.

The meshes are described in terms of the number of nodes in one linear elastic bending half-wavelength λ_b in both meridional and circumferential directions, λ_b, as given by (Rotter and Teng, 1989):

$$\lambda_b \approx 2.444\sqrt{rt} \tag{6.18}$$

Cylinders with radius to thickness ratio $r/t = 200$ and length to radius ratio $L/r = 6$ and $L/r = 8$ are studied next. The results are summarised in Table 6-3.

The number of elements in one half-wavelength in both the circumferential and meridional directions is represented as m and n respectively. The mesh is uniform around the circumference, so m is constant around the circumference. The mesh up the meridian is determined with consideration of the linear buckling mode. The mesh near the bottom is refined more than in the upper part of the cylinder. The value of n

in Table 6-3 represents the largest number of elements in one half-wavelength near the bottom of the cylinder.

Table 6-3: Results of mesh convergence study

L/r	Number of nodes in one half wavelength		Linear critical buckling pressure	Linear critical buckling modes
6	m	11	0.11804	A
	n	6		
	m	11	0.11802	A
	n	12		
8	m	11	0.08406	B
	n	2		
	m	11	0.08215	C
	n	4		
	m	11	0.08095	C
	n	8		
	m	16	0.08041	C
	n	20		

When $L/r = 6$, the linear buckling mode is circumferential compressive buckling mode as shown in Fig. 6-7(d). So a relatively coarse mesh can capture accurate buckling modes and buckling pressures. The buckling behaviour is affected little by changing the size of the mesh. In Table 6-3, it can be seen that even if the number of elements near the bottom boundary is doubled, the buckling mode and buckling strength are almost identical. So for stocky cylinders, the buckling strength is not sensitive to the mesh.

For longer cylinders with $L/r = 8$, the linear buckling behaviour is sensitive to the mesh. When $m = 11$ and $n = 2$, the linear buckling mode is a shear buckling mode with comparatively long buckles up the meridian as shown in Fig. 6-29 (a). If the mesh near the bottom is refined to $m = 11$ and $n = 8$, the shear buckling mode with quite local buckles near the bottom occurs as shown in Fig. 6-29 (c). The buckling mode has an obvious change as the mesh becomes finer.

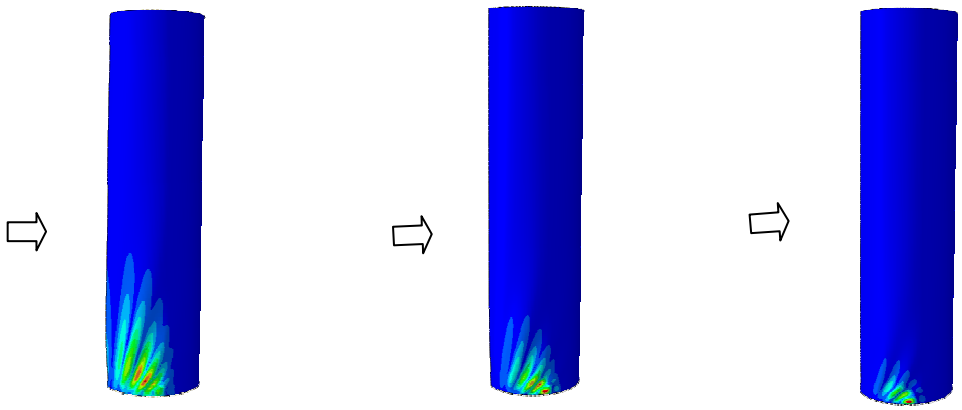

(a) m=11, n=2 (b) m=11,n=4 (c) m=11,n=8

Figure 6-29: Linear critical buckling modes for cylinders with $r/t = 200$ and $L/r = 8$ with different meshes

The reason for the above phenomenon is the influence of the membrane stress distribution in these cylinders under wind pressure. As discussed before, the meridional compressive membrane stress near the bottom of the side meridian increases greatly with an increasing value of L/r (Fig. 6-10). For moderately long cylinders, the meridional membrane stress, together with the circumferential compressive stress, causes local shear buckling near the bottom of the cylinder. If the cylinder is slender enough, local meridional compressive buckling may be caused by meridional compressive stress alone, which is not discussed further in this chapter.

The above description indicates the importance of the meridional membrane stress in affecting the buckling behaviour as the shell becomes longer. It is known that under axial compressive buckling, the buckle is in a short wavelength pattern and is quite local and small, so only with a quite good mesh near the bottom is this local axial compressive buckling captured. By contrast, if the mesh is not refined enough, the real local buckling mode may be lost due to the incapability of the elements in one half-wavelength to accommodate the buckle. Other incorrect buckling modes may be captured instead of the real buckling mode.

For a further refined mesh with $m = 16$ and $n = 20$, the buckling mode and buckling pressure have no obvious changes compared with the mesh with $m = 11$ and $n = 8$. A good mesh that was finally adopted in this study was the one which provides almost identical results to those from a further refined mesh. The buckling

pressure is changed by less than 1% as a result of halving the mesh size (Song, 2004). So the mesh with $m = 11$ and $n = 8$ is accurate enough for the model with $r/t = 200$ and $L/r = 8$.

However, it should be mentioned that the aim of the above mesh convergence study is just to show the importance of the mesh on the buckling behaviour predictions for cylinders under wind loading. All the results were based on linear bifurcation analysis. When geometric nonlinearity is involved, the nonlinear buckling mode is different from the linear buckling mode, depending on the specific geometry. For example, for an intermediate long cylinder, the nonlinear buckling mode is the local axial compressive buckling mode in the upper part of the cylinder. The mesh near the buckling zone should be refined enough to obtain an accurate result and the mesh near the bottom is thus not important. So there is no general rule for the mesh that should be used for a specific model and different meshes may be required as the geometry of the shell changes.

It may be concluded that the requirement of the mesh is different depending on the specific buckling behaviour of the cylinder. Sometimes the linear or nonlinear buckling mode cannot be anticipated in advance due to the complex mechanical behaviour of shells under asymmetrical loading conditions. In this situation, a fairly refined mesh for the whole model should be used to predict the buckling mode. Then more sophisticated meshes may be used based on the first prediction of the buckling mode until accurate and reliable results are derived.

6.7 Geometrically and materially nonlinear analysis (GMNA)

In some situations, yielding of the material plays an important role in affecting the buckling behaviour. For some structures, large-scale plasticity of the material occurs, and the material undergoes strains well into the plastic range. There may also be large overall changes in geometry during the process of the deformation. Some shell structures are subjected to loading which they resist by combinations of bending and stretching action over relatively small areas of the shell. In these cases the material can be strained locally well into the plastic range even though the overall distortion of the structure is relatively small. For some shell structures, the buckling behaviour

can change drastically as soon as a relatively small region begins to enter the plastic range (Calladine, 1983).

For cylinders under wind pressure, plasticity only affects the buckling strength of comparatively thick cylinders. The relationship between the buckling pressure ratio $q_{w,GNA} / q_{w,LBA}$ or $q_{w,GMNA} / q_{w,LBA}$ and the dimensionless length parameter Ω is shown in Fig. 6-30. An ideal elastic-plastic material with yield stress $\sigma_y = 250MPa$ was adopted.

For thin cylinders with $r/t = 500$ under wind loading, the buckling strength predictions from GMNA and GNA analyses are identical for all values of Ω (Fig. 6-30), indicating that plasticity has no effect on the buckling behaviour. The buckling behaviour is the same as the elastic buckling behaviour. That is because the elastic buckling strength is small for these thin cylinders so that the yield stress is not reached before elastic buckling occurs. For thinner cylinders, the elastic buckling strength becomes smaller, and elastic buckling occurs earlier. So plasticity has no influence on the buckling behaviour for all thin cylinders with $r/t \geq 500$.

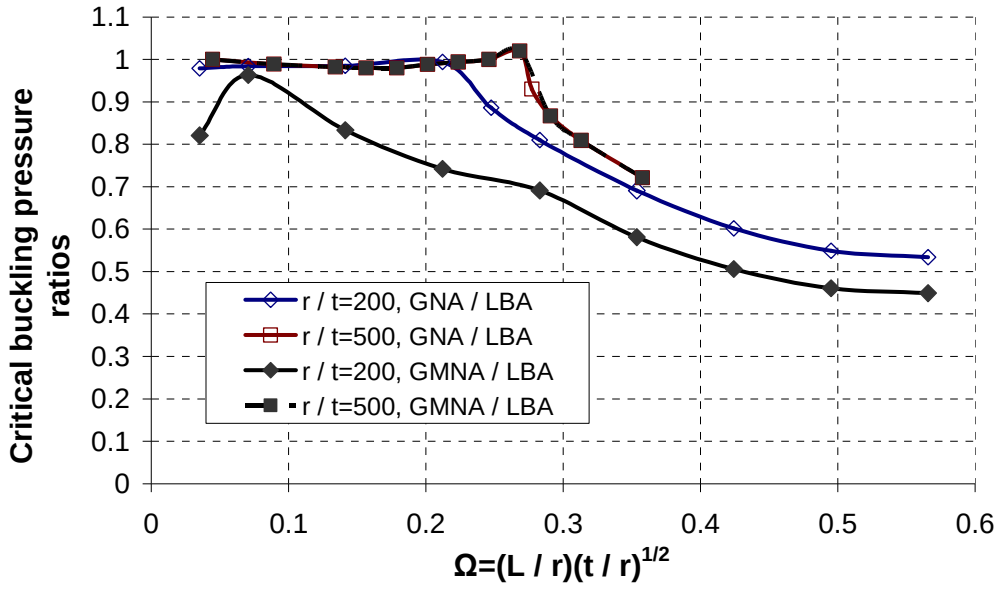

Figure 6-30: Relationship between the dimensionless buckling pressure ratio $q_{w,GNA} / q_{w,LBA}$ or $q_{w,GMNA} / q_{w,LBA}$ and the dimensionless length parameter Ω

For comparatively thick cylinders with $r/t = 200$, plasticity influences the buckling behaviour and causes a reduction in the buckling strength (Fig. 6-30). Yield occurs in different patterns depending on the specific value of L/r . For a stocky cylinder with $L/r = 0.5$, yield occurs in the zone near the bottom edge at some angel from windward generator as shown in Fig. 6-31(a). It is caused by the high meridional membrane stress and circumferential membrane stress in that area. Before global circumferential compressive buckling occurs, the large bending and stretching stresses induced by the restraint of the boundary may cause local yield of the shell wall. However, these stress components are concentrated near the bottom boundary and decrease quickly up the meridian, so the bending and stretching action is resisted over a relatively small area near the bottom edge leading to the local yield.

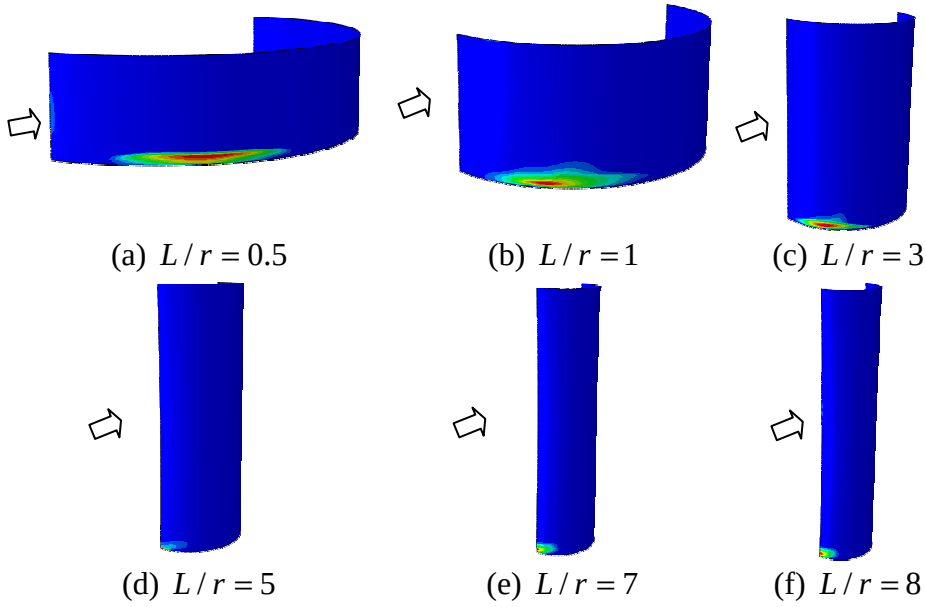

Figure 6-31: Equivalent plastic strain under critical buckling pressure for cylinders with different L/r under wind pressure ($r/t = 200$)

With increasing values of L/r , the plastic zone at the critical buckling pressure moves gradually toward the bottom edge of the windward generator. That is because for longer cylinders, high tensile membrane stress near the bottom edge of the windward area induced by the wind pressure increases quickly with an increase of L/r , which can be seen in Figs 6-9 and 6-10. The high local bending and stretching stresses in this area cause this local yield.

6.8 Geometrically nonlinear imperfection sensitivity analysis

6.8.1 Literature review

The buckling behaviour of imperfect cylinders is one of the most important aspects of the buckling behaviour of thin shells. An imperfection is one of the most important causes of the big discrepancy between experimental and simple theoretical strengths. This phenomenon was first investigated by Koiter (1945) in his PhD thesis, followed by Donnell and Wan (1950), Hutchinson (1965), Yamaki (1984) and many others. The key problem for the design process is to identify and characterise appropriate practically relevant geometric imperfections, including both their form and amplitude (Rotter, 1985; Teng, 2004).

The imperfection sensitivity of cylinders under axial compression and uniform external pressure has been widely studied by many researchers, which has been described in previous chapters. But for cylinders under wind loading, there are few related papers discussing the buckling behaviour of imperfect cylinders. This section focuses on the imperfection sensitivity of cylinders under wind loading. For cylindrical shells with different geometries and different nonlinear buckling modes, the appropriate form and amplitude of imperfection are adopted.

Greiner and Derler (1995) studied the effect of imperfections in cylinders with $r/t = 500$ under wind loading based on six types of pattern: 3 local shapes including a square one, a rectangular one and a ring shaped axisymmetric one; 1 global shape with an ovalization of 0.5% of the shell diameter; 1 combined shape by adding the local rectangular shape to the global ovalization; 1 structure-dependent shape with buckling mode either at the bifurcation point or at the post-buckling minimum. Their results indicated that long shells respond most sensitively to local pre-buckling patterns of rectangular shape or ring shape and the worst case is produced by adding a further global ovalization to the local shape. Long shells are not at all sensitive to eigenmode like imperfection shapes because the nonlinear buckling mode is quite different from the linear buckling mode. On the contrary, short cylinders are most sensitive to eigenmode imperfections.

Pircher (2004) investigated the influence of a weld-induced axisymmetric imperfection on the buckling of a medium-length silo. His results indicated that the weld imperfection in the upper half of the shell is quite influential on the buckling strength of medium long cylinders and this influence is similar to the buckling behaviour under axial compression. He also compared the influences of several types of imperfection including the global eigenmode imperfection, a small dent on the windward meridian and a small axisymmetric weld imperfection in the upper half of the cylinder. He concluded that the weld imperfection is the most detrimental imperfection among the imperfection shapes studied.

Schneider (2005) studied the imperfection sensitivity of very slender thicker cylinders under wind loading. There are two failure modes for his model. Relative stocky shells display leeward buckling in the base area and very slender shells display leeward local buckling in the lower half of the leeward meridian. He concluded that imperfections in the form of these two collapse modes for the perfect shells are in general more detrimental imperfections than idealised buckling mode forms.

The previous results indicate that the imperfection might be quite influential on the buckling strength of cylinders under wind pressure. Furthermore, stocky, intermediate long and slender cylinders may respond most sensitively to different types of imperfection. However, the ECCS EDR5 (2008) Chapter 12 “Cylindrical shells under wind loading” (Greiner, Guggenberger and Schneider, 2008) says nothing about the imperfection sensitivity of cylinders under wind loading, so it is necessary to explore the buckling behaviour of imperfect cylinders under wind loading to provide more knowledge for this problem.

6.8.2 Imperfection forms

Koiter (1945) first identified that the buckling strength of an axially compressed cylindrical shell is extremely sensitive to initial geometric imperfections and the imperfections in the form of perfect shell buckling eigenmode would be very deleterious. For stocky cylinders under wind loading, the nonlinear buckling mode is quite similar to the linear buckling mode. So an imperfection in the form of the

eigenmode can be quite detrimental to the buckling strength, which was verified by Greiner and Derler (1995). However, when the nonlinear buckling mode is different from the linear buckling mode, this conclusion is not always correct. The worst and practically relevant imperfections should be determined according to a systematic study considering the specific geometric parameters, loading condition, etc.

Following Koiter's research, because of the huge range of potential imperfection shapes (Yamaki, 1984), and the poor relationship of simple forms to measured imperfections (Ding et al, 1996; Teng et al., 2005), there has long been a debate concerning the "worst" form of imperfection and the "practically relevant" form (Rotter, 2004). One of the simplest solutions to this controversy is adoption of a circumferential weld depression imperfection (Rotter and Teng, 1989), which is seen in practical civil engineering constructions and which is often either the worst or close to the worst (Song et al., 2004) when measured using accepted stick measurements (EN 1993-1-6, 2007). This axisymmetric imperfection in a circular cylindrical shell structure is formed during construction when rolled steel plates are formed in a series of individual strakes and joined together by circumferential welds (Rotter and Teng, 1989).

Picher (2004) verified the noticeable reduction in the buckling strength due to a weld-induced axisymmetric imperfection in the upper half of the cylinder for cylinders under wind loading. However, the buckling strength of intermediate and slender cylinders is quite sensitive to the position of the weld depression. The weld-depression imperfection may have no effect on the buckling strength when the imperfection is far away from the buckling area. So it cannot simply be said that the weld-induced axisymmetric imperfection is the most detrimental imperfection for cylinders under wind loading.

An imperfection in the form of the nonlinear buckling mode can cause a significant reduction in the buckling strength (Song, 2004, Schneider, 2005). This type of the imperfection is always dependent on the real nonlinear buckling mode of the perfect cylinder and should be always detrimental. This imperfection will be used in this study for intermediate long cylinders. But this pattern of imperfection is not definitely the most practically relevant one.

As to the amplitude of the imperfection, the rules in ECCS EDR5 (2008) about dimple tolerances based on gauge measurements are adopted. The gauge has been devised with a length related to the size of buckles that are expected to form under specific load cases. When circumferential compressive stresses or shear stresses occur, measurements of the depth $\Delta w_{0\theta}$ should be made in circumferential direction using the gauge of length $\ell_{g\theta}$ given by:

$$\ell_{g\theta} = 2.3(\ell/r)^{1/2}(t/r)^{1/4} r \text{ , but } \quad \ell_{g\theta} \le r \tag{6.19}$$

in which ℓ is the meridional length of the shell segment (ECCS EDR5, 2008).

For a stocky cylinder under wind loading, buckling is caused by circumferential stress with several buckle waves around circumference extending over the whole length. It is appropriate to adopt Eq. 6.19. For an intermediate aspect ratio cylinder, the buckling mode is either the snap-through buckling mode followed by a bifurcation buckling mode or just the bifurcation buckling mode. In the first situation, a large buckle forms down the windward meridian before snap-through buckling occurs, adoption of $\ell_{g\theta}$ is reasonable. In the second situation, though the bifurcation buckling mode is an axial compressive short wavelength pattern, it is accompanied by significant ovalization of the cross-section. The pre-buckling deformation around circumference is large before bifurcation buckling occurs, so it is reasonable to adopt $\ell_{g\theta}$ rather than ℓ_{gx}, since the latter is defined according to the meridional compressive stress.

Table 6-4: Recommended values for dimple tolerance parameter $U_{0,\max}$ (EN 1993-1-6, 2007)

Fabrication tolerance quality class	Description	Value of $U_{0,\max}$
Class A	Excellent	0.006
Class B	High	0.01
Class C	Normal	0.016

The equivalent amplitude of the dimple $\Delta w_{0\theta}$ can be assessed in terms of the dimple parameter $U_{0\theta}$ given by:

$$U_{0\theta} = \Delta w_{0\theta} / \ell_{g\theta} \tag{6.20}$$

The value of $U_{0\theta}$ should satisfy $U_{0\theta} \le U_{0,\max}$, where $U_{0,\max}$ is the dimple tolerance parameter for the relevant fabrication tolerance quality class and is given in Table 6-4. In this study, the dimple tolerance parameter $U_{0\theta} = U_{0,\max} = 0.01$ corresponding to fabrication tolerance quality class "High" has been adopted.

6.8.3 Imperfection sensitivity for cylinders with different length to radius ratios under wind loading ($r/t = 500$)

The eigenmode imperfection and nonlinear buckling mode imperfection were considered for stocky and intermediate long cylinders respectively. The relationship between the dimensionless buckling pressure and the radial displacement for stocky cylinders with $r/t = 500$ under wind pressure with eigenmode imperfection is shown in Fig. 6-32. The pressure is normalized by the linear critical buckling pressure $q_{w,LBA}$ for perfect cylinders. The radial displacement is the maximum radial displacement up the windward meridian. The equivalent amplitude of the imperfection is derived from Eqs 6.19 and 6.20, depending on the specific geometric parameters.

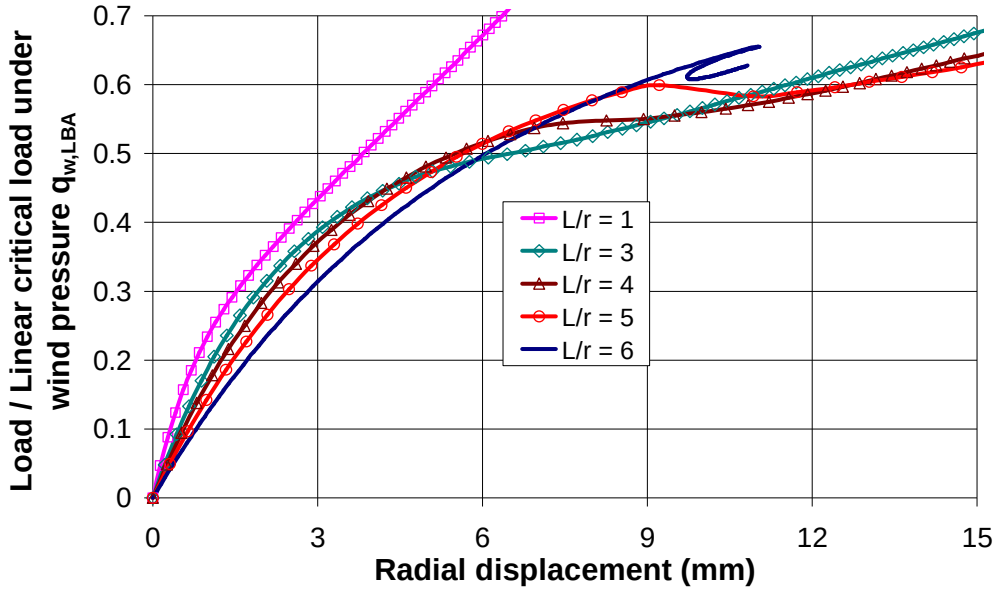

Figure 6-32: Relationship between the dimensionless pressure ratio and the radial displacement for stocky cylinders with eigenmode imperfection under wind loading (*r / t=500*)

For an imperfect cylinder with $L/r = 6$, the nonlinear critical load $q_{w,GNIA}$ is 0.655 times the linear critical pressure $q_{w,LBA}$. The nonlinear critical pressure $q_{w,GNA}$ for a perfect cylinder with $L/r = 6$ is 1.02 times the linear critical pressure $q_{w,LBA}$ (Fig. 6-27). It is clear that an eigenmode imperfection caused a considerable reduction to the buckling strength. Bifurcation buckling occurs at the limit load point with a steep post-buckling fall in strength and is then followed by a recovery with increased strength and radial deformation.

For a stocky cylinder with $L/r = 5$, Figure 6-32 shows that snap-through buckling occurs first at an instability point. The nonlinear critical pressure $q_{w,GNIA}$ is 0.599 times the linear critical pressure $q_{w,LBA}$. This snap-through buckling has a softening post-buckling response leading to a small fall in strength but is quickly followed by a recovery with increased strength and radial deformation. The strength exceeds the first limit load and increases continuously with considerably large radial deformations. The pressure at the first snap-through buckling point could be regarded as the critical buckling pressure.

For more stocky cylinders with $L/r < 5$, no distinct maximum point like snap-through buckling point or bifurcation buckling point could be detected in the load-displacement curves, which means that no distinct point indicating loss of stability could be observed during the deformation. The transition from the pre-buckling stage of the load-displacement curve into the post-buckling stage was gentle. The "post-buckling" load-deflection path merges with the "pre-buckling" load-deflection path. In this situation, according to ECCS EDR5 (2008), the largest tolerable deformation on the loading path before reaching a bifurcation load or a limit load can be regarded as a criterion to define the critical load. But how much tolerable deformation is permitted has no clear definition. Alternatively, the critical load can be determined by the change of slope of the load deflection curve rather than any fall in load carried. But this might make a safe but a very uneconomical estimate of the failure load (Doerich, 2007). In this study, the nonlinear critical buckling pressures for imperfect cylinders are defined according to the second rule (the infection point in the load-displacement curve).

The relationship between the dimensionless buckling pressure ratio and the radial displacement for stocky and intermediate long cylinders with $r/t = 500$ under wind pressure with imperfections in the form of the nonlinear buckling mode is shown in Fig. 6-33. The equivalent amplitudes of the imperfection are determined according to Eqs 6.19 and 6.20 for each value of L/r.

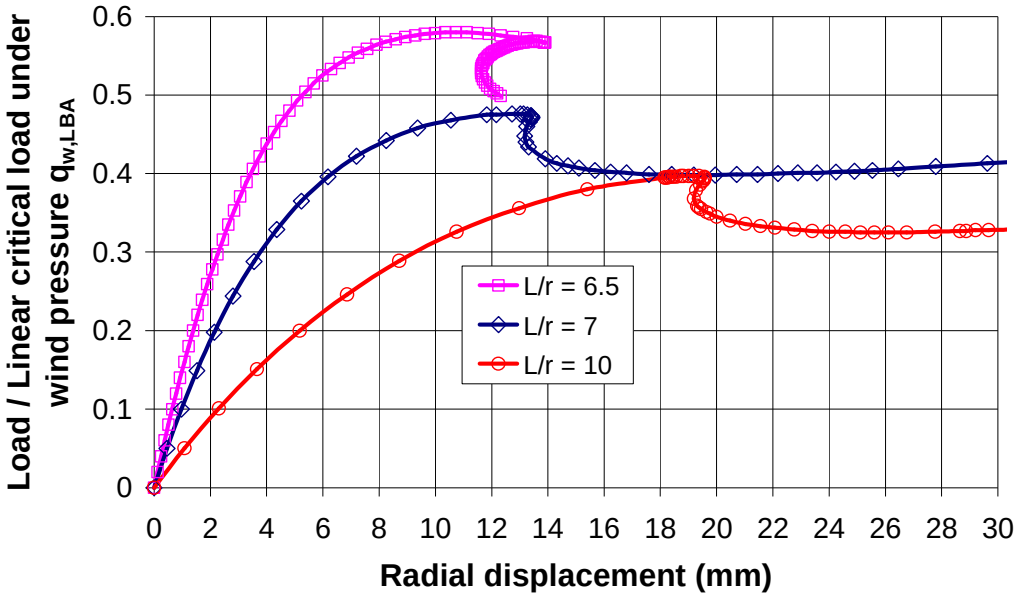

Figure 6-33: Relationship between the dimensionless pressure and the radial displacement for cylinders under wind loading with nonlinear buckling mode imperfection (*r / t=500*)

For an imperfect cylinder with $L/r = 6.5$, snap-through buckling occurs first at a limit instability point. The nonlinear critical buckling pressure $q_{w,GNIA}$ is 0.58 times the linear critical buckling pressure $q_{w,LBA}$. Compared with the nonlinear critical buckling pressure $q_{w,GNA}$ for perfect cylinders which is 0.897 times the linear critical buckling pressure $q_{w,LBA}$, it can be seen the imperfection causes an obvious reduction in the buckling strength. Then this snap-through buckling has a softening post-buckling response with accelerated inward radial displacement. This initial instability then triggers bifurcation buckling at a level of 0.567 times the linear critical buckling pressure $q_{w,LBA}$, leading to a progressive loss in strength.

For more slender cylinders with $L/r \geq 7$, snap-through buckling occurs just before the bifurcation point, and the two types of buckling modes, snap-through

buckling and bifurcation buckling, are almost identical. The load-displacement curves are different from the corresponding curves for perfect cylinders in Fig. 6-24. The load-displacement curves for $L/r = 7$ and $L/r = 8$ in Fig. 6-24 show two obvious different instability points indicating the occurrence of the snap-through buckling and local meridional bifurcation buckling respectively. So it can be concluded that the imperfection in the form of the nonlinear buckling mode could accelerate the occurrence of bifurcation buckling for longer cylinders. The imperfection causes a larger pre-buckling deformation and leads to more ovalization of the cross-section, causing more reduction to the meridional buckling resistance. Meridional bifurcation buckling is dominated by the meridional membrane stress, so the imperfection leads to an earlier occurrence of meridional bifurcation buckling.

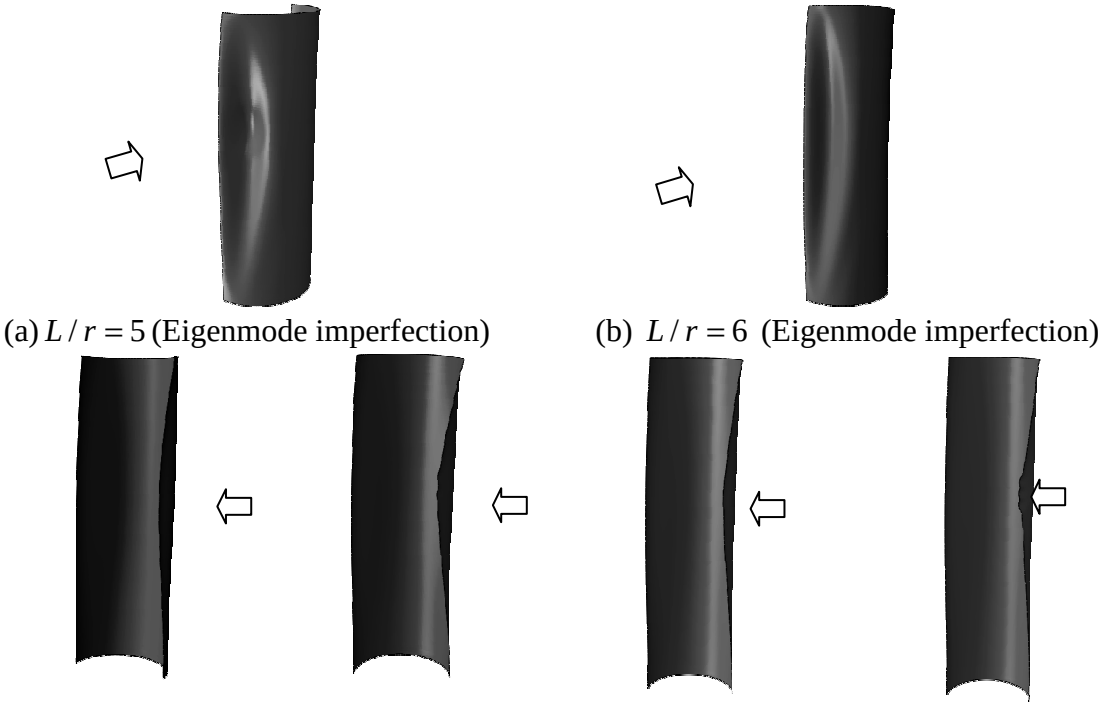

Figure 6-34: Nonlinear buckling modes for imperfect cylinders with different types of imperfection under wind loading ($r/t = 500$)

The nonlinear buckling modes for imperfect cylinders with different L/r are shown in Fig. 6-34. For cylinders with $L/r = 5$ and $L/r = 6$, an imperfection in the form of the eigenmode was adopted. The nonlinear buckling modes are

circumferential buckling modes which are the same as for perfect cylinders. For cylinders with $L/r = 6.5$ and $L/r = 8$, imperfections in the form of the nonlinear buckling mode were adopted. The dominant buckling mode is either snap-through buckling or bifurcation buckling. The characteristic of each of these buckling modes was described in previous sections.

The relationship between the critical buckling pressure ratio $q_{w,GNIA}/q_{w,LBA}$ and L/r with two different types of imperfection is shown in Fig. 6-35.

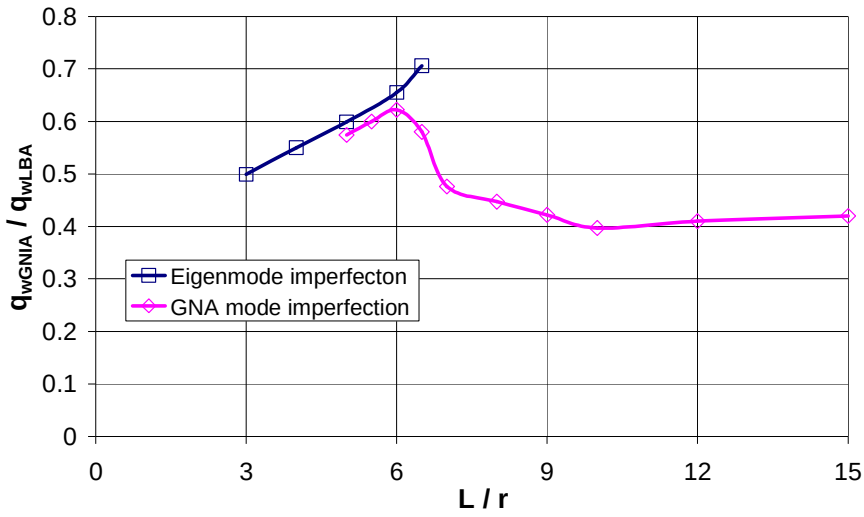

Figure 6-35: Critical buckling pressure ratio $q_{w,GNIA}/q_{w,LBA}$ for cylinders under wind loading ($r/t = 500$)

For stocky cylinders with $L/r \le 6$, both eigenmode imperfections and nonlinear buckling mode imperfections cause a considerable reduction in the buckling strength. The influence of the imperfection is more significant for shorter cylinders. Because the nonlinear buckling mode imperfection is closer to the real failure mode than the eigenmode imperfection, it causes a more serious reduction in the buckling strength. However, this difference is small.

For intermediate aspect ratio cylinders with $L/r > 6$, the imperfection in the form of the nonlinear buckling mode has a more detrimental effect on the buckling strength than the eigenmode imperfection. The value of the buckling pressure ratio

$q_{w,GNIA} / q_{w,LBA}$ with the nonlinear buckling mode imperfection decreases quickly with increasing values of L/r after the maximum point at $L/r = 6$.

When $L/r > 6$, the linear critical buckling mode and the nonlinear critical buckling mode are totally different as described earlier. An imperfection in the form of the nonlinear buckling mode is always similar to the failure mode and thus always has a detrimental effect on the buckling strength. By contrast, the buckling pressure ratio $q_{w,GNIA} / q_{w,LBA}$ with an eigenmode imperfection has a steady increase as L/r increases due to the inconsistency between the failure mode and the imperfection mode.

For cylinders with nonlinear buckling mode imperfections in the range $L/r > 7$, the buckling pressure ratio $q_{w,GNIA} / q_{w,LBA}$ decreases slightly with an increase of L/r (Fig. 6-35) until a minimum value is reached at $L/r = 10$. The value of $q_{w,GNIA} / q_{w,LBA}$ then increases slightly with further increase in L/r.

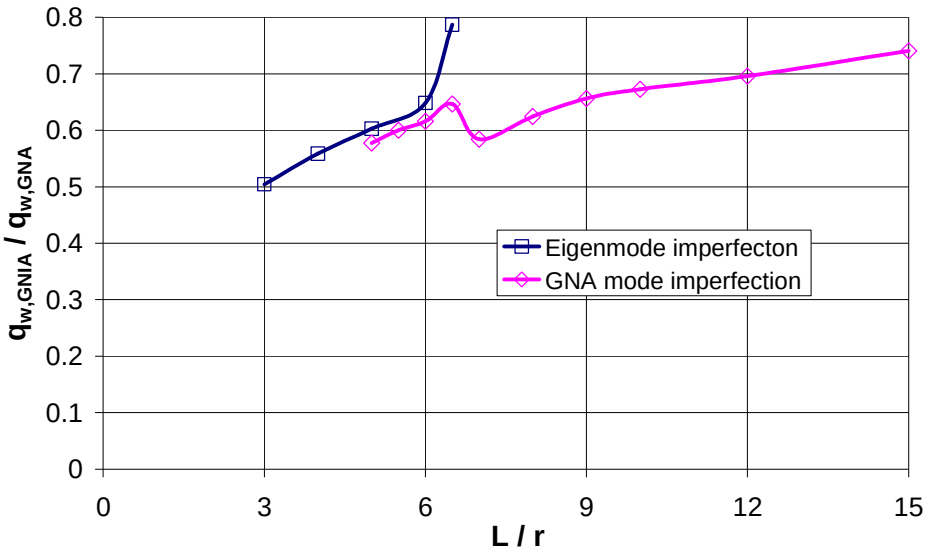

Figure 6-36: Critical buckling pressure ratio $q_{w,GNIA} / q_{w,GNA}$ for cylinders under wind loading ($r/t = 500$)

The relationship between the buckling pressure ratio $q_{w,GNIA} / q_{w,GNA}$ and L/r is shown in Fig. 6-36. For cylinders with a nonlinear buckling mode imperfection, after

the minimum point at $L/r = 7$, $q_{w,GNIA}/q_{w,GNA}$ increases continuously as L/r increases. The cause is the dual influence of imperfection amplitude and pre-buckling deformation for these cylinders.

For cylinders in the range $6 < L/r \le 7$, snap-through buckling with a long buckle down the windward meridian dominates the buckling behaviour. The load-displacement curve in the pre-buckling stage is close to linear, and the nonlinear pre-buckling deformation in these cylinders is comparatively small (Fig. 6-24), so the buckling strength of these shells may respond sensitively to a change in the imperfection amplitude. Larger imperfection amplitudes correspond to larger values of L/r. So with an increase in L/r, more reductions in the buckling strength are caused by larger imperfection amplitudes.

For cylinders in the range $L/r > 8$, as Fig. 6-24 shows, the load-displacement curve along the pre-buckling path is quite nonlinear. The pre-buckling deformation could be large and increases with increasing values of L/r. The cylinders that have large pre-buckling deformations may display less imperfection sensitivity. Large pre-buckling deformations may alleviate the effect of imperfections to some extent. So for these cylinders, though the calculated imperfection amplitude according to Eqs 6.19 and 6.20 increases as L/r increases, the imperfection caused a smaller reduction to the buckling strength. That is why the value of $q_{w,GNIA}/q_{w,GNA}$ increases as L/r increases (Fig. 6-36).

To study the imperfection sensitivity of the buckling strength to the nonlinear buckling mode imperfection, first, geometric nonlinear analysis (GNA) should be performed. The incremental mode at the first instability point from GNA provides an initial imperfection form. The maximum radial displacement $w_{\max}$, which is the maximum radial displacement around the circumference at the first instability point, could be extracted from the results of the GNA analysis. Geometric nonlinear imperfect analysis (GNIA) is then performed. The maximum amplitude of the imperfection used for GNIA is set at the deformation of the initial nonlinear buckling mode multiplied by a “Scaling factor”. This scaling factor should be determined in the “imperfection” command in ABAQUS. The objective here is to study the effect

of an imperfection of amplitude $\Delta w_{0\theta}$, which is the equivalent amplitude of the imperfection obtained by circumferential gauge measurement, on the buckling strength. So to achieve this objective, the value of $\Delta w_{0\theta} / w_{\max}$ should be adopted as the scaling factor in the "imperfection" command.

The values of scaling factor for cylinders with different L/r is shown in Table 6-5. It can be seen that the scaling factor shows up the relationship between the equivalent amplitude of imperfection $\Delta w_{0\theta}$ and the maximum radial displacement $w_{\max}$. The maximum radial displacement $w_{\max}$ for $L/r = 5$ and $L/r = 6$ is large because the nonlinear critical buckling pressures for the two models are close to linear buckling pressures. The maximum inward radial deformation occurs under a large value of critical buckling pressure.

When $L/r = 6.5$, snap-through buckling occurs and the critical buckling load is lower than the linear buckling pressure. The maximum inward deformation occurs up the windward generator at a smaller load leading to a smaller value of $w_{\max}$ than shorter cylinders. Because the nonlinear buckling pressure $q_{w,GNA}$ for perfect cylinders with $L/r = 6.5$ has a clear reduction compared with the linear buckling pressure $q_{w,LBA}$ ($\Omega = 0.3$ in Fig. 6-27), the value of $q_{w,GNIA} / q_{w,GNA}$ at $L/r = 6.5$ (Fig. 6-36) is still larger for shorter cylinders.

Table 6-5: The load scale factor for nonlinear buckling mode imperfection

L/r	Equivalent amplitude of the imperfection $\Delta w_{0\theta}$ (mm)	The maximum radial displacement $w_{\max}$ (mm)	Scaling factor $\Delta w_{0\theta} / w_{\max}$
5	5.44	9.787	0.556
6	5.96	12.97	0.459
6.5	6.20	5.281	1.296
7	6.43	8.52	0.755
8	6.88	12.04	0.571
9	7.30	16.21	0.45
10	7.69	22.63	0.34

However, when $L/r = 7$, due to the more significant influence of imperfections on the buckling strength, the nonlinear buckling pressure $q_{w,GNIA}$ has a considerable reduction from the value for perfect cylinders $q_{w,GNA}$, leading to a smaller value of $q_{w,GNIA}/q_{w,GNA}$ than for $L/r = 6.5$ (Fig. 6-36).

But with a continuous increase of L/r ($L/r > 7$), pre-buckling ovalization of the cross-section becomes more and more important and large pre-buckling deformations occur before buckling occurs, though the value of the buckling pressure becomes smaller. The scaling factor becomes smaller and the influence of imperfections decreases.

6.8.4 The effect of imperfection amplitude on the buckling strength

The above discussion of the imperfection sensitivity of cylinders under wind loading is based on the equivalent imperfection amplitude obtained from Eqs 6.19 and 6.20. It explores the imperfection sensitivity of cylinders with different length to radius ratios. Next, the imperfection sensitivity of a cylinder with fixed L/r and different imperfection amplitudes was investigated. From previous conclusions, it is known that stocky cylinders respond most sensitively to eigenmode imperfections, and intermediate long cylinders respond most sensitively to imperfections in the form of the nonlinear buckling mode (not the eigenmode imperfection), so a typical stocky cylinder with $L/r = 3$ and a typical intermediate long cylinder with $L/r = 7$ are studied here. The radius to thickness ratio $r/t = 500$ is adopted throughout the analyses.

The relationship between the buckling pressure ratio and the radial displacement for cylinders with $L/r = 3$ and an eigenmode imperfection is shown in Fig. 6-37, where $\Delta w_{0\theta}$ is the equivalent imperfection amplitude changing from $0.1\Delta w_{0\theta}$ to $1.0\Delta w_{0\theta}$. It shows that small imperfection amplitudes lead to a reduction in the buckling strength and a snap-through buckling point was recorded in the load-displacement curve. The critical load could be well defined at the limit point. But when the imperfection amplitude is large, no distinct limit point can be detected. In

this situation, the critical buckling pressure may be chosen as the point of infection in the load-displacement curve (Yamaki, 1984).

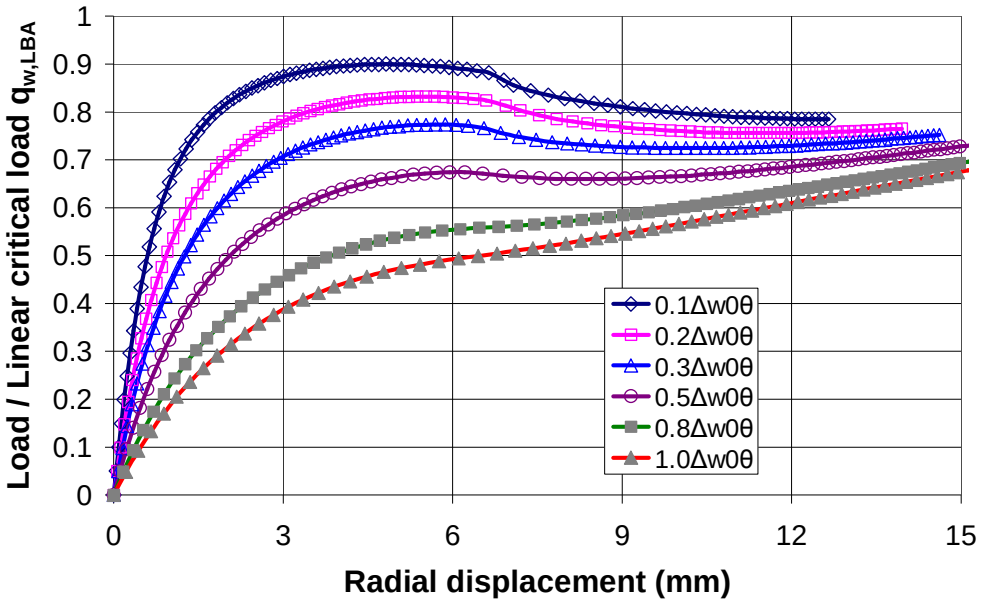

Figure 6-37: Relationship between the pressure ratio and the radial displacement for cylinders with eigenmode imperfection under wind pressure ($r/t = 500, L/r = 3$)

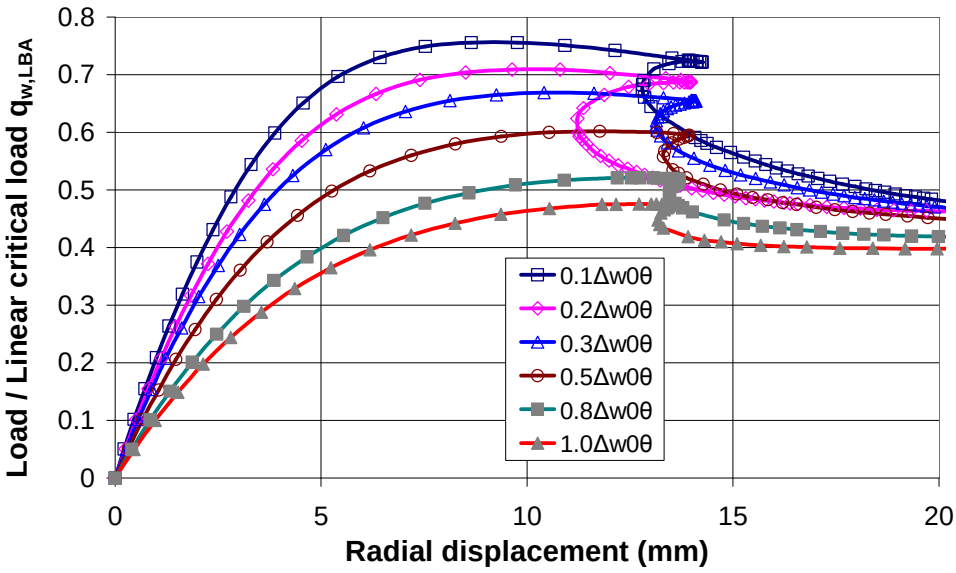

Figure 6-38: Relationship between the pressure ratio and the radial displacement for cylinders with nonlinear buckling mode imperfection under wind pressure ($r/t = 500, L/r = 7$)

The relationship between the buckling pressure ratio and the radial displacement for cylinders with $L/r = 7$ and a nonlinear buckling mode imperfection is shown in Fig. 6-38. The imperfection amplitude is varied over the range $0.1\Delta w_{0\theta} \le \Delta w \le 1.0\Delta w_{0\theta}$.When the imperfection amplitudes is small ($\Delta w < 0.5\Delta w_{0\theta}$), snap-through buckling occurs first, then the buckle develops and bifurcation buckling is triggered. There is a clear distinction between snap-through buckling and bifurcation buckling. After the imperfection amplitude exceeds $\Delta w = 0.8\Delta w_{0\theta}$, snap-through buckling is superseded by bifurcation buckling, and the two types of buckling mode are undistinguishable. The instability point can always be recorded for any value of the imperfection amplitude. Larger imperfection amplitudes cause more reduction in the buckling strength leading to an earlier occurrence of bifurcation buckling.

The imperfection sensitivity curves for stocky cylinders with eigenmode imperfections and intermediate long cylinders with nonlinear buckling mode imperfections are shown in Fig. 6-39. The imperfection causes a continuous reduction in the buckling strength with increasing values of imperfection amplitude.

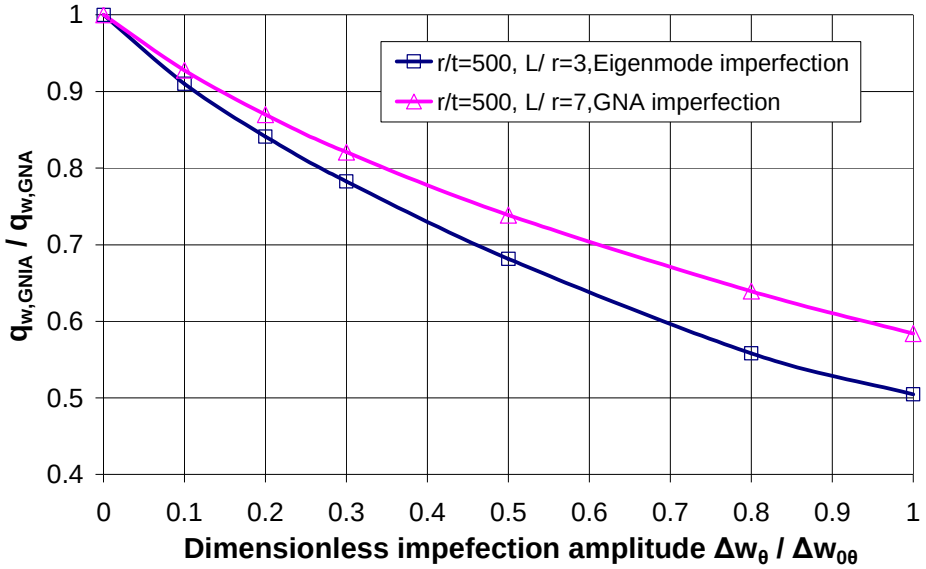

Figure 6-39: Imperfection sensitivity curves for cylinders with different types of imperfection and imperfection amplitude ($r/t = 500$)

6.9 Conclusions

The buckling behaviour of cylinders under wind pressure was studied in this chapter. The analyses focused on silos and tanks of practical geometry. The linear buckling behaviour and the nonlinear buckling behaviour were both explored. Cylinders may display different buckling behaviours depending on their geometry. For stocky cylinders, the linear buckling mode and the nonlinear buckling mode are both the circumferential compressive buckling mode, which is caused by the circumferential compressive membrane stress. For intermediate aspect ratio cylinders, the linear buckling mode and the nonlinear buckling mode are often quite different.

The idea of relating the peak of the non-uniform pressure distribution in the stagnation zone to a fictitious equivalent uniform pressure introduced by Resinger and Greiner (1981, 1982) for isolated stocky cylinders is quite useful. The linear critical pressure and the nonlinear critical pressure under wind loading can both be related to the critical pressure for uniform external pressure using empirical equations with good precision.

Finite element mesh division may affect the accuracy of the results greatly, depending on the specific geometry of the model, especially when local buckling modes occur. Sometimes a bad mesh may produce a totally incorrect buckling mode and buckling strength. So mesh convergence studies should be performed very carefully for any studied model to derive the correct buckling mode and buckling strength.

Imperfection sensitivity is a complex problem for cylinders under wind loading, because the nonlinear buckling mode is indefinite for cylinders with different aspect ratios. The failure modes may change greatly with a change in the geometric parameters. The imperfection sensitivity depends on the failure mode. For stocky cylinders, the nonlinear buckling mode is the circumferential compressive buckling mode, which is similar to the linear buckling mode, so the shell responds most sensitively to both the eigenmode imperfection and the nonlinear buckling mode imperfection. For intermediate aspect ratio cylinders, the nonlinear buckling mode is different from the linear buckling mode, so these cylinders respond most sensitively

to an imperfection in the form of the nonlinear buckling mode. But it should be noted that the nonlinear buckling mode imperfection is not definitely the most practical form. To find a most practical and detrimental imperfection form is a difficult problem. This chapter just gives an initial investigation of the imperfection sensitivity of cylinders under wind loading. More sophisticated work is required to explore this very complicated problem further in future research.

Chapter 7 A study of cylindrical shells with stepwise varying wall thickness under external pressure

7.1 Cylindrical shells of stepwise varying wall thickness

Cylindrical shells of stepwise variable wall thickness are widely used for cylindrical containment structures of moderate length, such as vertical-axis tanks and silos. The thickness changes because the stress resultants are much larger at lower levels. The increase of internal pressure and axial compression in the shell is addressed by increasing the wall thickness (API 650, 2007). Each shell is built up from a number of individual strakes of constant thickness. The thickness of the wall increases progressively from top to bottom. Figure 7-1 shows a typical example of tank structure taken from ECCS EDR5 (2008).

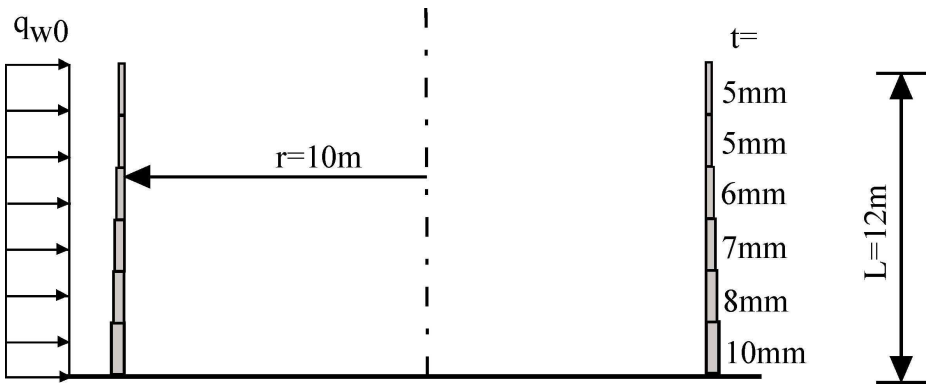

Figure 7-1: Typical example of tank structure (taken from ECCS EDR5, 2008)

The thickness of the wall of these cylindrical vessels is generally very thin and the strength is often controlled by elastic buckling failure. The buckling behaviour of a cylindrical shell with uniform wall thickness under uniform external pressure has been extensively studied by many researchers (e.g. Batdorf, 1947; Ebner, 1952; Flügge, 1973; Yamaki, 1984; Greiner, 2004). However, the buckling behaviour of cylinders of stepwise variable wall thickness has not been understood completely and has drawn little attention to date. This may be partly because the formulation of rules for any pattern of thicknesses is difficult.

In the European Standard for Shells EN 1993-1-6 (2007) and the European Recommendations on Shell Buckling ECCS EDR5 (2008), stepped wall cylinders under circumferential compression are transformed, first into a three-stage cylinder and thence into an equivalent uniform thickness cylinder, based on the research of Resinger & Greiner (1974), (1976) and Greiner (1981). This two-stage process leads to a complicated calculation that requires a chart that is tricky to use, and where the mechanics is somewhat hidden. The process is rather awkward for the practical design of silos and tanks.

This chapter introduces a new "weighted smeared wall method", which is proposed as a much simpler method to deal with stepped-wall cylinders with any thickness variation. The method is based on an idea proposed by Trahair et al. (1983) for stepped wall cylinders under external pressure. Buckling predictions are made for a wide range of geometries using the new hand calculation method and compared with both accurate predictions from finite element calculations using ABAQUS and those of the current Eurocode rules. The comparison shows that the weighted smeared wall method is a very effective, accurate and informative method of capturing the buckling behaviour of stepped wall cylinders for a wide range of shells. It is much easier to use than the current method of DIN 18800 (1990), EN 1993-1-6 (2007) or ECCS EDR5 (2008).

7.2 Buckling behaviour of cylinders under external pressure

7.2.1 Buckling behavior of cylinder under uniform external pressure

The buckling strength of a cylinder of uniform thickness under uniform external pressure or wind loading was studied in previous chapters. The buckling mode for a moderately long cylinder of uniform thickness under wind loading is shows in Fig. 7-2. The buckling phenomena for practical cylindrical shells of stepwise variable wall thickness under external pressure are shown in Fig. 7-3.

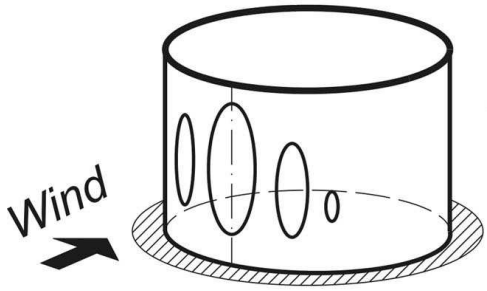

Figure 7-2: Buckling mode in a moderately long cylinder of uniform thickness under wind loading (ECCS EDR5, 2008)

Figure 7-3: Buckling phenomenon of thin cylinders under external pressure (photographs courtesy by Prof. J.M. Rotter)

The buckling strength of a cylinder under uniform external pressure is governed by the geometry of the cylinder. It drops rapidly as the buckle becomes longer, so longer cylinders have a lower critical buckling pressure. The buckling strength is also affected by the thickness of the cylinder: thinner cylinders have lower critical buckling pressures.

The theoretical radial buckling pressure of a constant thickness cylinder can be obtained by minimising (Batdorf, 1947; Brush and Almroth, 1975; Trahair et al, 1983):

$$p_{cr} = E\left(\frac{\pi}{\omega}\right)^2\left(\frac{t}{r}\right)^2\left(\alpha+\frac{1}{\alpha}\right)^2\left[\frac{1}{12\left(1-\nu^2\right)}+\left(\frac{\omega}{\pi}\right)^4\left(\frac{\alpha}{\alpha+\frac{1}{\alpha}}\right)^4\right] \tag{7.1}$$

where $\alpha = \frac{\pi}{m\omega}\sqrt{\frac{r}{t}}$, r is the radius of the shell, t is the thickness of the shell wall, E is Young's modulus, ν is Poisson's ratio, m is the number of complete buckles around the circumference and ω is the dimensionless length parameter which is defined as:

$$\omega = \frac{\ell}{\sqrt{rt}} \tag{7.2}$$

in which ℓ is the half wave-height of the buckle, which is equal to the whole height of a cylinder of uniform thickness.

For medium length cylinders, which are defined in EN 1993-1-6 (2007) by:

$$20 < \frac{\omega}{C_\theta} < 1.63\frac{r}{t} \tag{7.3}$$

For medium length cylinders, the critical buckling wave number is given by (Greiner, 2004):

$$m_{cr}^2 = \frac{\pi r}{\omega t}\sqrt[4]{36\left(1-\nu^2\right)} \tag{7.4}$$

The circumferential buckling pressure for medium length cylinders is defined by classical equation as (EN 1993-1-6, 2007):

$$p_{cr,Donnell} = 0.92E(t/r)^2/\omega \tag{7.5}$$

which is based on classical linear Donnell-type shell buckling theory .

Using the boundary condition terminology of Singer and Yamaki (1984), Eqs 7.1~7.5 all use classical simply-supported boundaries S3 at both ends. The main useful boundary conditions are defined in Table 7-1, where *r* means restrained and *f* means free. The effect of different boundary conditions may be taken into account by modifying the buckling external pressure by the factors C_θ (EN 1993-1-6, 2007), as indicated in Table 7-2 for medium-length cylinders.

Table 7-1: Boundary condition terminology for cylindrical shells (Yamaki, 1984)

Boundary condition	δu (meridioanl displacement)	δv (circumferential displacement)	δw (radial displacement)	$\delta\beta$ (meridional rotation)
S1	r	r	r	f
S3	f	r	r	f
C1	r	r	r	r
C3	f	r	r	r

Table 7-2: External pressure buckling factors for medium-length cylinders C_θ (Original in EN 1993-1-6, 2007))

Case	Boundary conditions	External pressure factors C_θ
1	S1 and S1	1.5
2	S1 and S3	1.25
3	S3 and S3	1.0
4	S1 and F (Free end)	0.6

Restraint of meridional rotation has no effect on the buckling strength of medium-length cylinders, so S1 and C1, S3 and C3 are not differentiated in Table 7-2. For quite short cylinders, the factor is not constant but depends on the dimensionless length parameter ω, which can be found in EN 1993-1-6 (2007).

7.2.2 Buckling of cylinders of stepwise variable wall thickness under uniform external pressure

For cylinders of stepwise variable wall thickness, the top thinnest parts are always involved in the buckling mode. The buckling strength may reduce when the lower thicker strakes are also involved because the increasing length can reduce the strength of the potential buckle, but at the same time the increased thickness of the lower strakes may increase the potential buckling pressure. The simultaneous change of length and thickness leads to two opposite trends, so it is not easy to determine how large the weakest buckle should be in a stepwise varying thickness wall cylinder. A change in the wall thickness distribution can easily result in a different critical buckling mode. This is the reason why the current codified method (EN 1993-1-6, 2007) is rather complicated.

In the experimental study of Fakhim et al. (2009), buckling modes with buckles extending over the whole height of the shell were observed in shorter shells, while in longer shells, buckling modes with buckle waves only in the top parts were observed.

An important characteristic of this buckling mode is that the bottom of a buckle will always be at a change of plate thickness because the buckling pressure falls as the length increases. This statement is only strictly valid if the base of the buckle is deemed to be pinned, which is of course untrue. But the approximation is relatively good because the real buckle is slightly longer, taking in part of the restraining underlying course and longer buckles have lower strengths, but the restraint of the underlying course increases the buckling pressure again, so these two effects partially counteract each other. The later part of this chapter provides an effective and accurate correction to account for the restraining effects of the underlying course beneath the buckle.

The illustrative example in Chapter 11 of ECCS EDR5 (2008) (Greiner and Rotter, 2008), shown in Fig. 7-4, is quite helpful in giving an initial understanding of the buckling behaviour of step-wise variable wall thickness cylinders under external pressure. It shows the buckling modes for three cylindrical tanks with identical upper strakes, but with different total heights under uniform external pressure. The modes

indicate that the variation of the wall thickness results in buckles developing only in the same group of upper strakes, while the lower ones provide considerable restraint against both radial and axial displacements at the boundary between two strakes (ECCS EDR5, 2008). The height of the buckle does not depend on the thicknesses used throughout the whole wall if the buckling mode in the top parts is already critical.

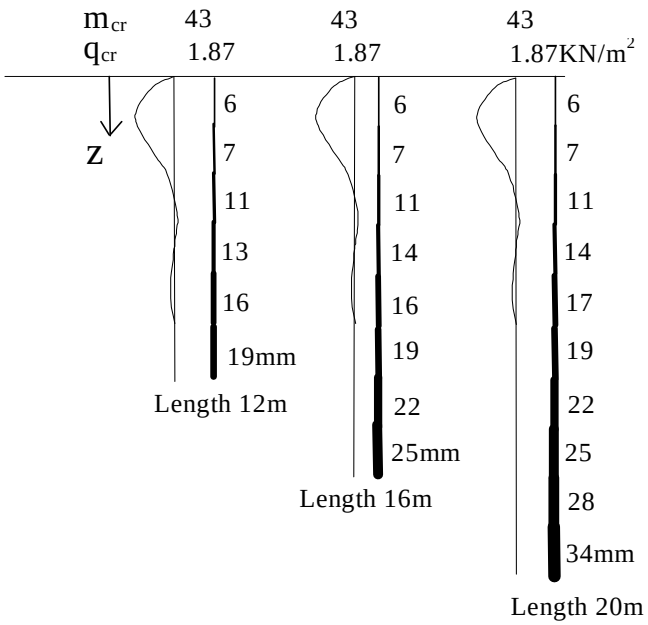

Figure 7-4: Buckling modes of cylindrical tanks of 40m diameter and different wall heights under uniform external pressure (Original in Greiner and Rotter, 2008)

But for a specific structure being designed, it is not impossible to identify in advance which parts of the wall will participate in the critical buckle, due to the dual effects of length and thickness described above.

So for a given cylinder composed of several parts with strakes of stepwise varying thickness, determination of the critical buckle height is an initial step in studying the buckling behaviour. It should be noted that the top uniform thinnest parts will always be involved in the possible buckling modes (Fig. 7-4). The critical buckling mode may extend over one or more strakes below the thinnest one or may extend over the whole wall. This corresponds physically to the fact that the thinner upper parts are restrained by the thicker lower parts. The design method in EN 1993-1-6 (2007), in

ECCS EDR5 (2008), in Trahair's method and the weighted smeared wall method derived in this chapter all rely on this concept.

7.3 Current design method of EN 1993-1-6 (2007) and ECCS EDR5 (2008) due to Greiner (1981)

In DIN 18800 (1990), EN 1993-1-6 (2007) and ECCS EDR5 (2008), for stepped wall cylinders under circumferential compression, the cylinder is transformed into an equivalent cylinder of uniform thickness based on the research of Resinger & Greiner (1974) and (1976) and Greiner (1981). Greiner's method (1981) for stepped wall cylinders under uniform circumferential compression was developed based on linear bifurcation analyses of cylinders under uniform external pressure.

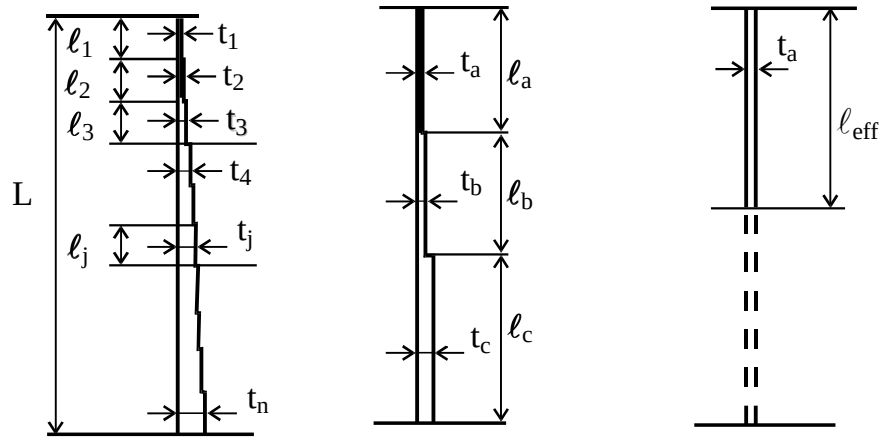

(a) Cylinder of stepwise variable wall thickness **(b) Equivalent cylinder comprising three sections** **(c) Equivalent single cylinder with uniform wall thickness**

Figure 7-5: Transformation of stepped cylinder to equivalent cylinder (Greiner and Rotter, 2008)

For cylinders consisting of more than three sections with different wall thickness (Fig. 7-5a), the design method first replaces the multiple sections by an equivalent three-section-cylinder (Fig. 7-5b). The fictitious equivalent lengths ℓ_a, ℓ_b, ℓ_c and equivalent thicknesses t_a, t_b, t_c are determined by categorization rules:

> *The length of its upper section, ℓ_a, should extend to the upper edge of the first section that has a wall thickness greater than 1,5 times the smallest wall thickness t_1, but should not comprise more than half the total length L of the*

cylinder. The length of the two other sections ℓ_b *and* ℓ_c *should be obtained as follows:*

$$\ell_b = \ell_a \text{ and } \ell_c = L - 2\ell_a \qquad \text{if } \ell_a \le L/3$$

$$\ell_b = \ell_c = 0.5(L - \ell_a) \qquad \text{if } L/3 \le \ell_a \le L/2$$

The fictitious wall thicknesses t_a, t_b *and* t_c *of the three sections should be determined as the weighted average of the wall thickness over each of the three fictitious sections:*

$$t_a = \frac{1}{l_a}\sum_a l_j t_j, \qquad t_b = \frac{1}{l_b}\sum_b l_j t_j, \qquad t_c = \frac{1}{l_c}\sum_c l_j t_j$$

The commentary on this procedure in Chapter 11, ECCS EDR5 (2008), written by Greiner and Rotter (2008), gives the following explanations:

It is important to note that the meridional dimension of the buckling mode often extends only over one or more of the upper (thinner) courses instead of the whole cylinder. This corresponds physically to the thinner upper courses being restrained by the thicker lower courses. Thus, often the lowest courses may not take part in the critical buckling mode at all.

The thickness ratio of 1.5 turned out to be an approximate criterion to describe this restraining effect, so that $t_j / t_1 \le 1.5$ *could be used to roughly define the portion of the cylinder length comprising the buckling mode. Averaging of the wall thickness with respect to the buckling behaviour is, therefore, restricted to the corresponding length* ℓ_a*. However, the averaging in the areas of* ℓ_b *and* ℓ_c *is mainly used for estimating the stiffness of these parts with respect to their restraining effects on the upper part.*

Then the three-section-cylinder is replaced by an equivalent single cylinder of effective length ℓ_{eff} and of uniform wall thickness $t = t_a$ (Fig. 7-5c) using a complicated set of charts (Fig. 7-6). The effective length of the cylinder ℓ_{eff} is determined by:

$$\ell_{eff} = \ell_a / \kappa \tag{7.6}$$

in which κ is a dimensionless factor indicating the effect of the stiffness of the lower parts of the cylinder and can be extracted from Fig. 7-6. However, the curves in Fig. 7-6 are not well defined. No equations are known that describe these curves. If the geometry of the tank or silo being designed lies in the zone between one curve and another, it is quite difficult to capture an accurate value of the parameter κ. So it is clear that this method in EN 1993-1-6 (2007) is quite complex in practical use for the design of stepped wall cylinders, and only with difficulty can accurate estimates be obtained for the buckling pressure of a stepped-wall cylinder.

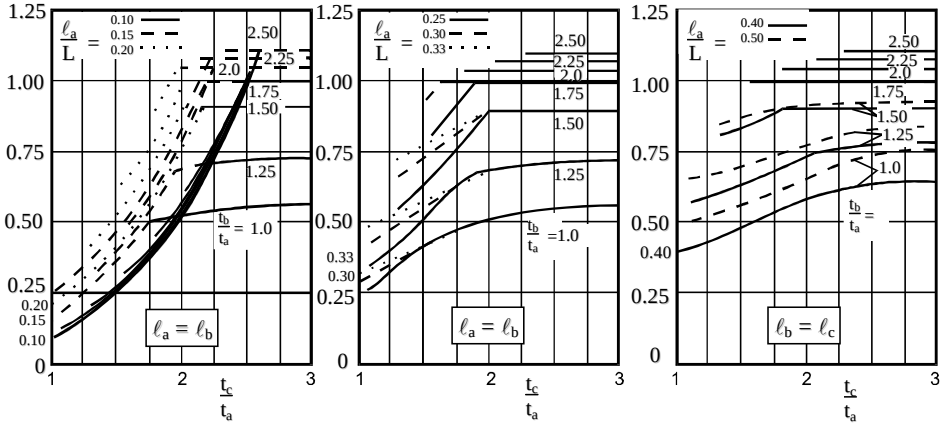

Figure 7-6: Factor κ for the determination of l_{eff} (Greiner and Rotter, 2008)

After transformation, the general buckling formula Eq. 7.7 (Greiner and Rotter, 2008) for cylinders of uniform thickness under uniform external pressure is then used to calculate the buckling pressure for the equivalent cylinder:

$$q_{Rcr} = 0.92 C_\theta E \frac{r}{\ell_{eff}} \left(\frac{t_a}{r} \right)^{2.5} \tag{7.7}$$

in which C_θ is the external pressure buckling factor which is derived from the boundary conditions at ends of the buckle. When the cylinder has uniform thickness, the factor C_θ is given in Table 7-2. By contrast, in cylinders with stepwise varying thickness, the possible axial restraint of lower boundary may not have a significant effect on a cylinder with varying thickness strakes (Greiner and Rotter, 2008) which is significantly restrained by the thicker lower courses. In the following calculations, S3 boundaries at both ends of the buckle are assumed when using Greiner's method.

7.4 The weighted smeared wall method for non-uniform walls

For a shell wall with both circumferentially and axially varying stiffness, Trahair et al. (1983) adopted a buckling mode with sinusoidal deformation in both directions and evaluated the corresponding “effective thickness” of the components within the buckle. This evaluation of an equivalent thickness corresponding to the buckling mode is termed here the “weighted smeared thickness” and is approximated by “smearing out” the thickness changes by replacing them with an equivalent thickness in the buckling mode. Then the potential buckling modes can be checked using the corresponding effective thickness to find the critical buckling mode with lowest buckling strength. The weighted smeared wall method derived in this chapter is based on this concept.

It should be noted that the original idea of Trahair et al. (1983) was only published in a small sub-section of a design guide on silos in Australia with no derivation given. It has not been widely used to date. It was written specifically for corrugated silo walls with vertical stiffeners. It has never been verified either by classical equations or finite element studies. It assumes a half sine wave for the buckle shape in the vertical direction, but this is not precise (Fig. 7-4).

The equivalent thickness is derived as an appropriate weighted value based on energy principles (Brush and Almroth, 1975). The weighted smeared thickness is found by considering the contribution of each part of the wall to the energy involved in the buckling mode, and this can then be equated to the energy of the destabilising pressures. This is equivalent to a single term Galerkin procedure or a first estimate of Rayleigh-Ritz evaluation.

For cylinders with stepwise variable thickness under uniform external pressure, the buckling behaviour may be accurately approximated by assuming a buckling mode shape that is close to the critical form as:

$$w = A\sin\left(\frac{\pi z}{\ell}\right)\sin(m\theta) \tag{7.8}$$

where A is the amplitude, z and θ are meridional and circumferential coordinates. It is assumed that the meridional and circumferential deformations are negligible compared with the radial displacement so that the buckling displacement and curvature are only related with radial deformation.

In silos and tanks formed from rolled plates, the thickness of the cylinder is constant around the circumference. Owing to the symmetry of the assumed deformation at the buckled area, the twist of the shell surface maybe neglected, and the strain energy due to bending is expressed as:

$$U_b = \frac{r}{2}\iint D(z)(\kappa_x^2 + \kappa_\theta^2 + 2\nu\kappa_x\kappa_\theta)dzd\theta \tag{7.9}$$

where $D(z) = \dfrac{Et_z^{\,3}}{12(1-\nu^2)}$ is the flexural stiffness of the cylinder.

The strain energy due to stretching of the middle surface is expressed as:

$$U_m = \frac{r}{2}\iint C(z)(\varepsilon_x^2 + \varepsilon_\theta^2 + 2\nu\varepsilon_x\varepsilon_\theta)dzd\theta \tag{7.10}$$

where $C(z) = \dfrac{Et_z}{1-\nu^2}$ is the membrane stiffness of the cylinder.

It should be noted that the thickness t_z varies up the meridian, so the integral with respect to z must be performed.

The total strain energy of a deformed shell equals to the sum of bending energy and stretching energy as:

$$U = U_b + U_m \tag{7.11}$$

The changes of the curvature in the axial and circumferential plane are expressed as:

$$\kappa_x = -w_{,xx} = A\left(\frac{\pi}{\ell}\right)^2 \sin\left(\frac{\pi z}{\ell}\right)\sin(m\theta) \tag{7.12}$$

$$\kappa_\theta = \frac{-w_{,\theta\theta}}{r^2} = A\frac{m^2}{r^2}\sin\left(\frac{\pi z}{\ell}\right)\sin(m\theta) \tag{7.13}$$

The increment bending energy during buckling is derived by substituting Eqs 7.12 and 7.13 into Eq. 7.9:

$$\Delta U_b = A^2\frac{Er}{24(1-\nu^2)}\left[\left(\frac{\pi}{\ell}\right)^4 + \left(\frac{m}{r}\right)^4 + 2\nu\left(\frac{\pi}{\ell}\right)^2\left(\frac{m}{r}\right)^2\right]\int_0^{\ell}\int_0^{\pi/m}\left[t_z^3\sin^2\left(\frac{\pi z}{\ell}\right)\sin^2(m\theta)\right]dzd\theta \tag{7.14}$$

The circumferential strain before buckling ε_0 is given by:

$$\varepsilon_0 = \frac{p_{cr}r}{Et_z} \tag{7.15}$$

The circumferential force intensity may also be obtained by:

$$N_{cr} = p_{cr}r = \frac{Et_z}{1-\nu^2}(\varepsilon_\theta + \nu\varepsilon_z) \tag{7.16}$$

where the strains ε_z and ε_θ are meridional strain and circumferential strain after buckling, respectively.

From Eqs 7.15 and 7.16, the pre-buckling strain and the strains after buckling in meridional and circumferential directions are related by:

$$(1-\nu^2)\varepsilon_0 = \varepsilon_\theta + \nu\varepsilon_z \tag{7.17}$$

Observing that:

$$\varepsilon_\theta = \varepsilon_0 + \frac{w}{r} \tag{7.18}$$

The meridional strain ε_z is found as:

$$\varepsilon_z = -\nu\varepsilon_0 - \frac{w}{\nu r} \tag{7.19}$$

The strain energy due to stretching of the middle surface is then obtained by substituting Eqs 7.18 and 7.19 into Eq. 7.10 as:

$$U_m = \frac{Er}{2}\int_0^{\ell}\int_0^{\pi/m}(t_z\varepsilon_0^2)dzd\theta + \frac{A^2E}{2r\nu^2}\int_0^{\ell}\int_0^{\pi/m}\left[t_z\sin^2\left(\frac{\pi z}{\ell}\right)\sin^2(m\theta)\right]dzd\theta$$
$$+ A\int_0^{\ell}\int_0^{\pi/m}\left[p_{cr}r\sin\left(\frac{\pi z}{\ell}\right)\sin(m\theta)\right]dzd\theta \tag{7.20}$$

The first term in Eq. 7.20 which involves only the pre-buckling strain ε_0 is the pre-buckling stretching energy. So the increment energy due to stretching of the middle surface during buckling is:

$$\Delta U_m = \frac{A^2E}{2r\nu^2}\int_0^{\ell}\int_0^{\pi/m}\left[t_z\sin^2\left(\frac{\pi z}{\ell}\right)\sin^2(m\theta)\right]dzd\theta + A\int_0^{\ell}\int_0^{\pi/m}\left[p_{cr}r\sin\left(\frac{\pi z}{\ell}\right)\sin(m\theta)\right] \tag{7.21}$$

The total increment of the strain energy during buckling is then obtained by:

$$\Delta U = \Delta U_b + \Delta U_m = A^2B\int_0^{\ell}\int_0^{\pi/m}\left[t_z^3\sin^2\left(\frac{\pi z}{\ell}\right)\sin^2(m\theta)\right]dzd\theta$$
$$+ \frac{A^2E}{2r\nu^2}\int_0^{\ell}\int_0^{\pi/m}\left[t_z\sin^2\left(\frac{\pi z}{\ell}\right)\sin^2(m\theta)\right]dzd\theta + A\int_0^{\ell}\int_0^{\pi/m}\left[p_{cr}r\sin\left(\frac{\pi z}{\ell}\right)\sin(m\theta)\right] \tag{7.22}$$

where $B = \frac{Er}{24(1-\nu^2)}\left[\left(\frac{\pi}{\ell}\right)^4 + \left(\frac{m}{r}\right)^4 + 2\nu\left(\frac{\pi}{\ell}\right)^2\left(\frac{m}{r}\right)^2\right]$

The work done by the circumferential forces during buckling is:

$$\Delta\Omega = rp_{cr}\left[\int_0^{\ell}\int_0^{\pi/m} w dzd\theta + \int_0^{\ell}\int_0^{\pi/m}\frac{1}{2}\left(w_{,\theta}\right)^2 r dzd\theta\right]$$
$$= A\int_0^{\ell}\int_0^{\pi/m}\left[p_{cr}r\sin\left(\frac{\pi z}{\ell}\right)\sin(m\theta)\right]dzd\theta + \frac{1}{8}A^2m\pi\ell r^2p_{cr} \tag{7.23}$$

Equating expressions 7.22 and 7.23, the expression of the critical buckling pressure in terms of the integration of the thickness t_z is obtained:

$$p_{cr} = \frac{8B}{m\pi\ell r^2}\int_0^{\ell}\int_0^{\pi/m}\left[t_z^3 \sin^2\left(\frac{\pi z}{\ell}\right)\sin^2(m\theta)\right]dzd\theta + \frac{4E}{m\pi\ell\nu^2 r^3}\int_0^{\ell}\int_0^{\pi/m}\left[t_z \sin^2\left(\frac{\pi z}{\ell}\right)\sin^2(m\theta)\right]dzd\theta \tag{7.24}$$

During buckling, the total strain energy is dominated by bending energy and stretching energy is small compared with the bending energy, so the calculation is simplified by considering only the first term in Eq. 7.24 to find an equivalent thickness. The effectiveness of this simplification is verified later. The equivalent uniform thickness t_{eq} then replaces the awkward integration in terms of the variable thickness t_z, and is found as a weighted average value of the thickness of each strake:

$$t_{eq}{}^3 = \left(\frac{4m}{\pi\ell}\right)\int_0^{l}\int_0^{\pi/m} t_z{}^3 \sin^2(m\theta)\sin^2\left(\frac{\pi z}{\ell}\right)d\theta dz \tag{7.25}$$

The form of Eq. 7.25 differs from Trahair's equation (1983) for the equivalent thickness which was expressed as:

$$t_{eq} = \left(\frac{4m}{\pi\ell}\right)\int_0^{l}\int_0^{\pi/m} t_z \sin^2(m\theta)\sin^2\left(\frac{\pi z}{\ell}\right)d\theta dz \tag{7.26}$$

The buckling pressure predictions using Eq. 7.25 were verified in this study to be closer to the accurate finite element predictions than Eq. 7.26, so Eq. 7.25 is adopted throughout the following calculations.

As the thickness of the cylinder is constant around the circumference, the equivalent thickness needs no integration in the circumferential direction and Eq. 7.25 reduces to:

$$t_{eq}^3 = \left(\frac{2}{\ell}\right)\int_0^{l} t_z{}^3 \sin^2\left(\frac{\pi z}{\ell}\right)dz \tag{7.27}$$

For a buckling mode that extends over *n* strakes of constant thickness, Eq. 7.27 reduces to the sum of the integrals for each the individual strakes and can be expressed as a simple summation:

$$t_{eq}^3 = \left(\frac{1}{\ell}\right)\sum_{i=1}^{n}\left[t_i^3\left(\mathrm{H}_i - \mathrm{H}_{i-1}\right)\right], i = 1,2,\cdots n. \tag{7.28}$$

in which $\mathrm{H}_i = \left(h_i - \frac{\ell}{2\pi}\sin\frac{2\pi h_i}{\ell}\right)$.

The distance from the top of the cylinder to the bottom of the i^{th} strake is defined as h_i, which is indicated in Fig. 7-7 (for $i = 1$, $h_0 = 0$ and $\mathrm{H}_0 = 0$). It should be recognized that ℓ is the height of the potential buckle being considered, which corresponds to an integer number of strakes.

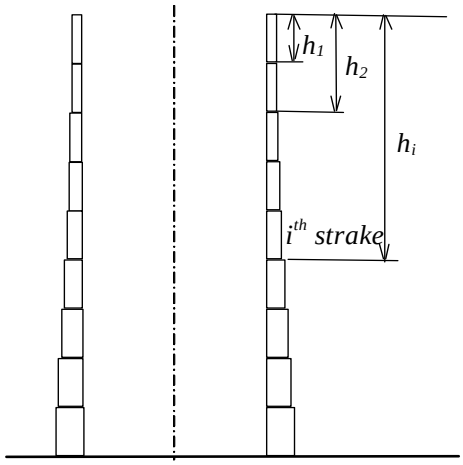

Figure 7-7: The definition of parameter h_i

As noted above, the chief difficulty in determining the buckling strength of a stepped wall cylinder is to find the critical buckling mode: that with the lowest buckling pressure. In EN 1993-1-6 (2007), by transforming stepped cylinders into an equivalent cylinder of uniform thickness, the critical buckling mode and buckling strength can be obtained by analysing the uniform equivalent cylinder. But this method is very complex to use. By using the weighted smeared wall method, this problem can be solved in a different and much easier way.

First, different buckle heights for possible buckling modes must be examined. The half wavelength ℓ can extend over just the top thinnest strakes only, or a longer part of the wall ending at a change of thickness, or over the whole height of the cylinder. For each potential buckling height, there are many different possible modes in the

circumferential direction, so the minimum pressure amongst these modes must be found for this potential buckling height.

The equivalent thickness t_{eq} for each potential buckling mode is found using Eq. 7-28. If the equivalent cylinder is of medium length (Eq. 7.3), Eq. 7.5 may be used directly to assess the buckling pressure. The critical buckling wave number m_{cr} may be found using Eq. 7.4. If instead the potential buckling mode corresponds to a short cylinder (Eq. 7.3), Eq. 7.1 must be minimised with respect to *m* to find the buckling pressure and mode. However, this situation seems to be rare in typical designs. The above calculations are easily set out in a spreadsheet. The buckling mode with the lowest buckling pressure is then found as the final critical buckling mode for this pattern of wall thicknesses.

This method assumes a half sine wave in the vertical direction for the buckle shape, but this is not realistic (Fig. 7-4). The validity of this simple treatment is verified here by studying several different patterns of wall thickness variation, covering the full range of potential modes.

7.5 Weighted smeared wall method applied to a varied wall thickness distribution

A verification of the weighted smeared wall method was undertaken using four models, which lead to a total of 1756 separate tank designs. The verification begins with Model 1, which has reference geometry of a defined set of wall thicknesses taken from Annex A of the API standard 650 (2007). Different distributions of wall thickness (here termed “designs”) were devised by scaling the ratios of the thickness changes from one strake to another in the reference geometry. It may first be noted that the top strakes have a high radius to thickness ratio, which can be retained throughout all the modified designs derived for Model 1.

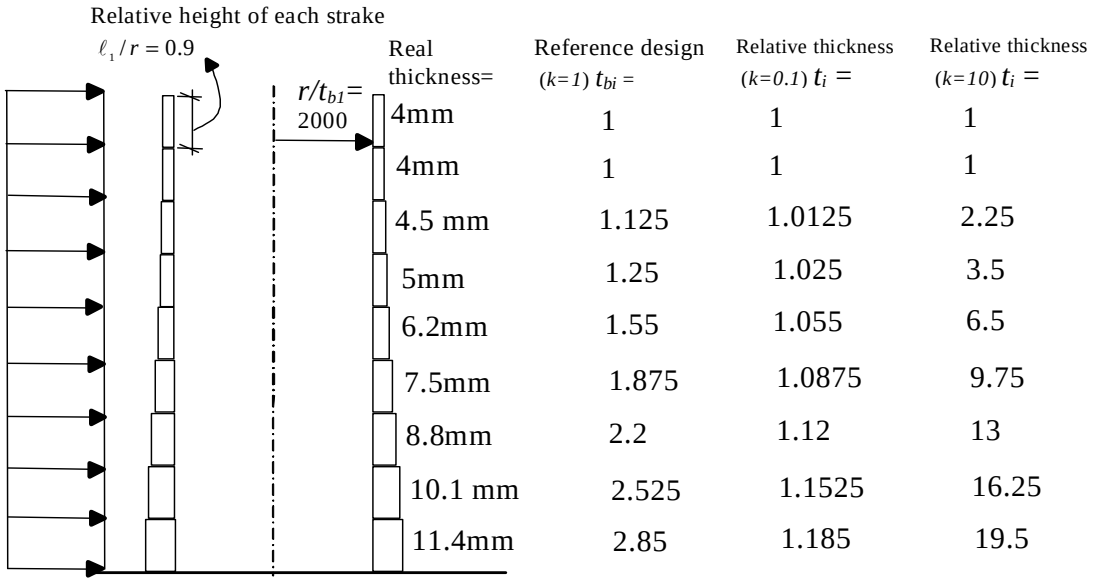

Figure 7-8: Wall thickness distribution of Model 1 defined according to Annex A of the API standard 650 (2007)

The large set of designs devised in this way can produce the full range of buckling modes from buckling over the full height to buckling only in the top strakes, simply by changing the ratio of the plate thicknesses at each step. The thickness of the thinnest strakes t_{b1} is used as the reference thickness. The thickness of the next strake is taken as the thickness of the thinnest strake plus k times the difference between its reference value and that of the thinnest strake so that $k = 1$ corresponds to the API 650 reference design, $k = 0$ corresponds to a uniform wall and large k gives large lower strake thicknesses causing the buckles to be only in the thinnest strake. The adjusted thickness of the i^{th} strake in any given adjusted design is determined as:

$$t_i = t_{b1} + k\left(t_{bi} - t_{b1}\right) \tag{7.29}$$

This device systematically transforms a reference design from API650 (2007) into a large range of designs, all of which have quite different buckling modes. The different designs depend only on the value of k, so this parameter should be noted for the discussion which follows.

Different patterns of wall thickness distribution can be realized by adjusting the values of the factor *k* in Eq. 7.29, which can be changed from a small value 0.1 to a very large value 10 or more (Fig. 7-8).

The relative thicknesses of the strakes in three example designs are shown in Fig. 7-8. The thickness of each strake has been made dimensionless relative to the thinnest top strakes. The relative thickness of the reference design is indicated as t_{bi}, where i is the number of the strake.

7.6 Buckling predictions using the weighted smeared wall method

For Model 1 with varying patterns of wall thickness distribution under uniform external pressure, the weighted smeared wall method described above was used to determine the buckling behavior. For a given pattern of wall thickness distribution (*k* may take any value), the buckling mode may take any form because the critical buckling mode for this thickness distribution is not known in advance. The buckle can extend only over the top uniform thinnest strakes, or over several upper strakes of mixed thickness, or over all strakes. In principle, all different potential buckling heights should be checked.

The equivalent thickness for each potential buckling mode is found using Eq. 7-28 (Fig. 7-9). For all patterns of wall thickness, the equivalent thickness always increases as the assumed buckle height rises because the lower strakes are always thicker than those above. A low value of k can be seen to give only small changes in the equivalent thickness, but high values produce large changes.

The critical circumferential buckling mode m_{cr} for a set of assumed buckling modes is shown in Fig. 7-10. Using Eq. 7.4 and minimizing Eq. 7.1 produces the same results ($k = 0.1$ in Fig. 7-10). For all patterns of wall thickness, the critical circumferential buckling wave number m_{cr} decreases as the buckling height rises. This is natural because the complete buckling mode tends to be approximately square,

so taller buckles also have longer circumferential wavelengths (low modes). The wave number m_{cr} is always lowest for a full height buckle.

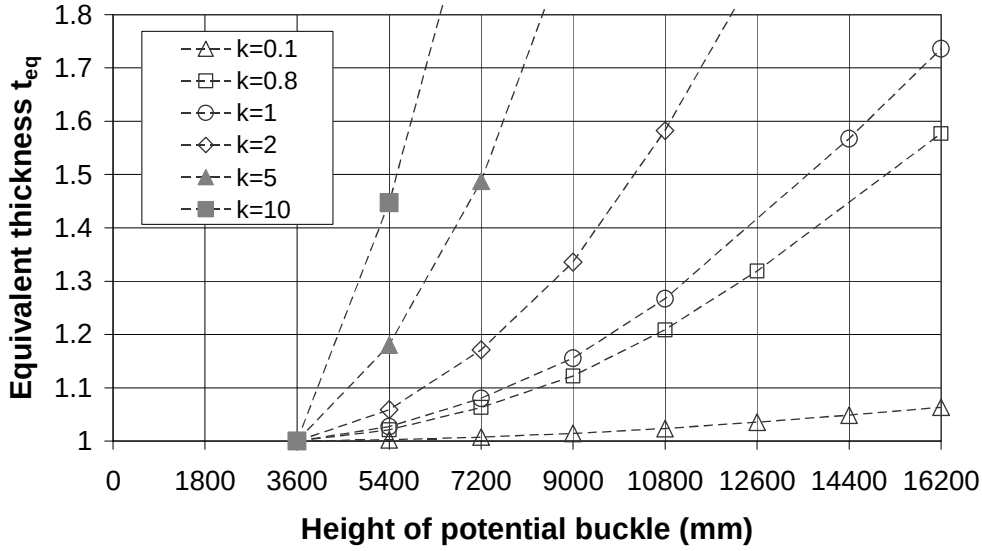

Figure 7-9: Equivalent thickness t_{eq} against the potential buckling height with different wall thickness distributions

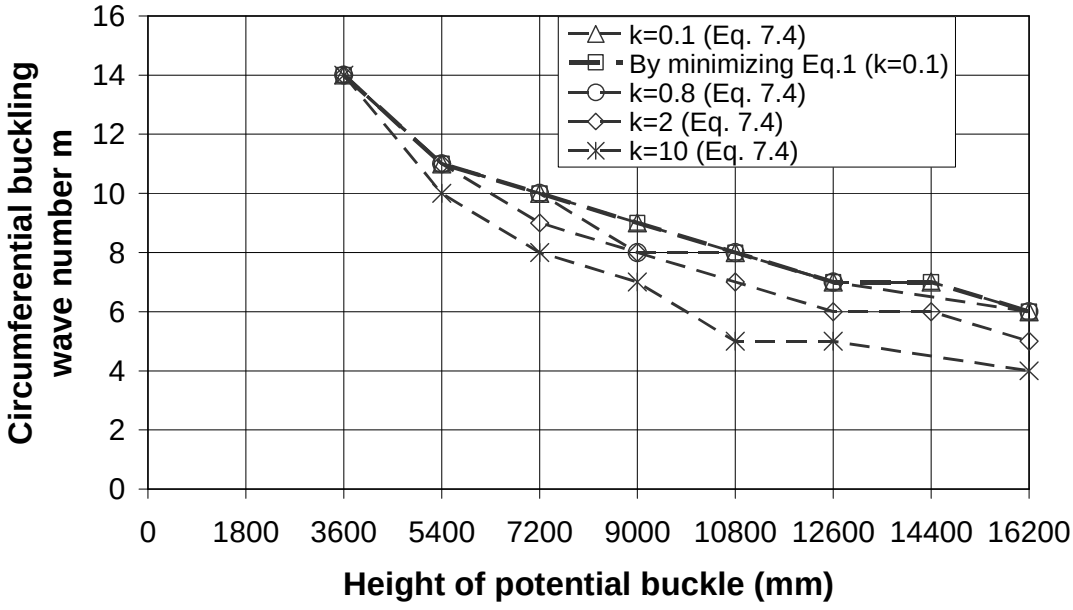

Figure 7-10: Critical circumferential buckling wave number *m* against the potential buckling height with different wall thickness distributions

A larger value of *k* corresponds to a more pronounced change in the wall thickness at each step, and corresponds to a larger value of equivalent thickness for a given buckle height, leading to a smaller wave number.

The equivalent thickness increases with the potential buckle becomes longer. Thicker cylinders have a higher potential buckling pressure. But long length decreases the buckling resistance meantime. So the two factors must be considered at the same time to determine the lowest buckling pressure.

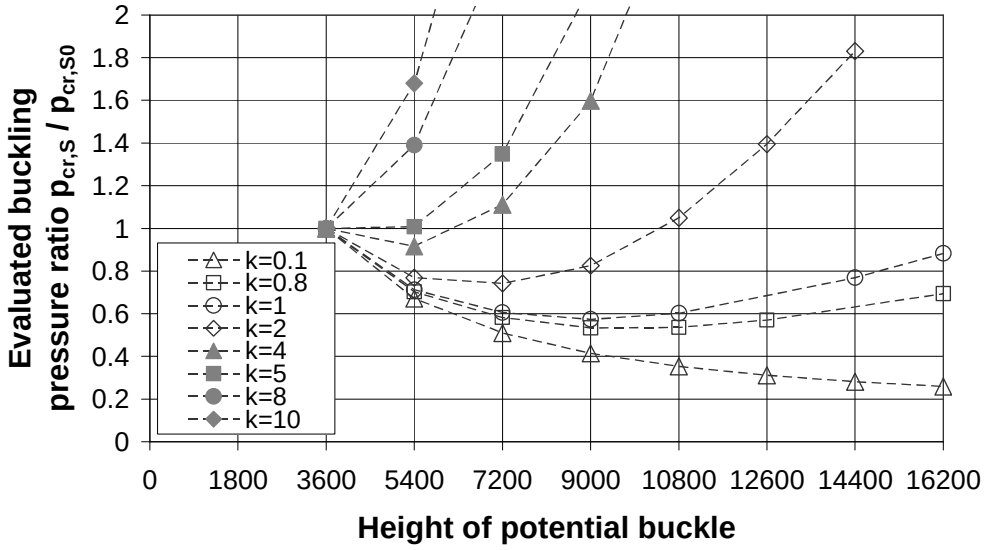

Figure 7-11: Evaluated dimensionless critical buckling pressure against the potential buckling height with different wall thickness distributions

The buckling pressures $p_{cr,S}$ for all potential buckling modes are evaluated using Eq. 7-5 (Fig. 7-11). The relationship between the evaluated dimensionless critical buckling pressure ratio $p_{cr,S} / p_{cr,S0}$ and the potential assumed buckling height is shown in Fig. 7-11, with different values of *k* to give different wall thickness distributions. The buckling pressures were all made dimensionless by using a reference value $p_{cr,S0}$ which is the buckling pressure when the buckling occurs only in the top thinnest strakes. It is invariant for all patterns of wall thickness distribution. The final critical buckling mode for a given pattern of wall thickness distribution is the one with the lowest buckling pressure for all possible heights and all possible circumferential modes (the minimum of each curve).

When k=0.1, the step changes in wall thickness are slight, after checking the buckling pressure for all possible buckling heights, the critical buckling mode with lowest buckling pressure is found to occur when the buckle extends over the whole height of the cylinder. When k=10, the step changes in wall thickness are large, the critical buckling mode is found to occur when the buckle extends over just the top two thinnest strakes. When the value of k is moderate, the critical buckling mode may occur in any strakes of mixed thickness. The results indicate that the critical buckling mode and buckling strength for a stepped wall cylinder is influenced a lot by the patterns of wall thickness distribution.

It may be noted that not all possible buckle heights need to be investigated. For a given wall thickness distribution, the shortest buckle gives a buckling pressure. In general, the buckling pressure falls as the buckle height increases, but as soon as an increase in buckling pressure with increased height is formed, the critical mode has been passed. This may be automatically stated by saying that the curves in Fig. 7-11 each have a single valued minimum.

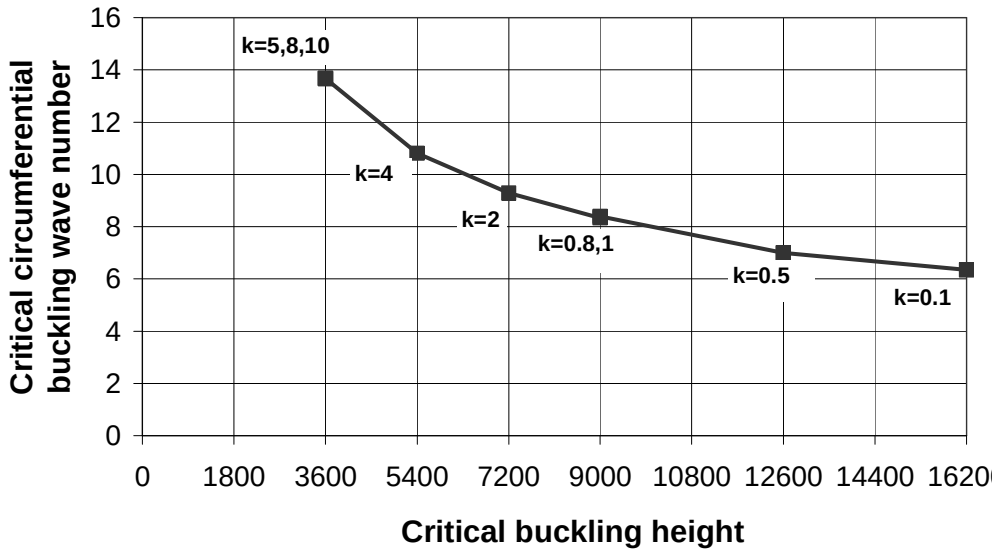

Figure 7-12: Critical circumferential buckling wave number *m* against the critical buckling height with different wall thickness distributions

The critical circumferential buckling wave number m_{cr} corresponding to the critical buckling mode (with lowest buckling pressure) can take any value between 6

and 14 in this example depending on the specific pattern of wall thickness distribution as shown in Fig. 7-12.

7.7 Comparison of the weighted smeared wall method, Greiner's method in EN 1993-1-6 (2007) and finite element predictions

7.7.1 Comparison of the buckling modes using the weighted smeared wall method and finite element predictions

To establish the validity of the weighted smeared wall method, accurate predictions of the buckling behaviour of stepped wall cylinders were performed using the finite element software ABAQUS. The wall thickness patterns shown in Fig. 7-8 were adopted for computational simulation. Exploiting the symmetry of the buckling modes, a 180° half cylinder model was used to obtain accurate results. At the base, all translations were restrained but the meridional rotation was free, corresponding to a practical boundary condition defined as S1 in Table 7-1 (Yamaki, 1984). A ring stiffener with enough flexural stiffness was used at the top to maintain circularity. The restraint provided by the ring stiffener is close to an S3 boundary. The shell was made of isotropic material with Young's modulus E=2.0$\times 10^5$MPa and Poisson's ratio $\nu = 0.3$.

The finite element predictions of critical buckling mode for Model 1 with different patterns of wall thickness distribution are shown in Fig. 7-13. The number of strakes in each buckle is indicated as n. The critical buckling modes in the finite element predictions (Fig. 7-13) are very similar to those of the weighted smeared wall method (Fig. 7-12), but some differences are also clear. Based on the assumption of S3 boundaries at both ends, the weighted smeared wall method gives the shape of the buckle as a half sine vertical wave. By contrast, the finite element predicted shape includes the restraining effect of the strakes below the buckle. This difference will later be seen to cause a small discrepancy in the buckling strength predictions depending on the specific wall thickness distribution.

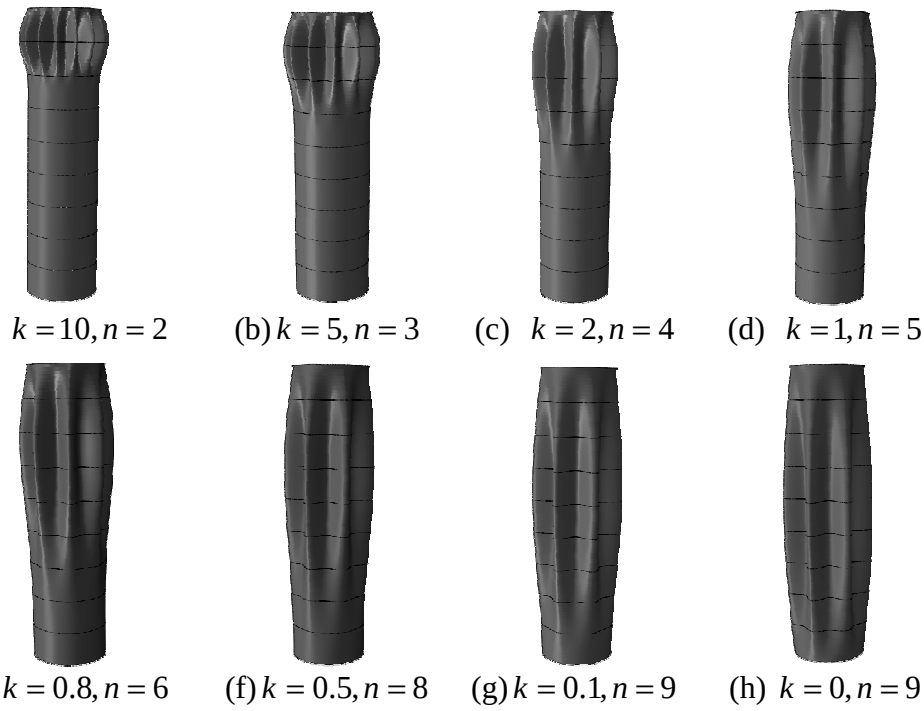

(a) $k = 10, n = 2$ (b) $k = 5, n = 3$ (c) $k = 2, n = 4$ (d) $k = 1, n = 5$

(e) $k = 0.8, n = 6$ (f) $k = 0.5, n = 8$ (g) $k = 0.1, n = 9$ (h) $k = 0, n = 9$

Figure 7-13: Finite element predictions of critical buckling mode for stepped wall cylinders with different patterns of wall thickness distribution under uniform external pressure

7.7.2 Comparison of the buckling pressure predictions using the three different methods

The buckling pressures p_{cr} derived from the three methods were next compared: the weighted smeared wall method, Greiner's method and finite element predictions. The buckling pressures were all made dimensionless using Eq. 7.5 with an adopted thickness of the thinnest strakes but the length equals to the critical buckle height for each case. The relationship between the buckling pressure ratio ϕ (Eq. 7.30) and the wall thickness distribution factor *k* is shown in Figs 7-14 and 15.

$$\phi = p_{cr} / p_{cr,D} \tag{7.30}$$

The buckling pressure ratio ϕ is always larger than 1.0 because the reference pressure $p_{cr,D}$ has been calculated using the thinnest strakes thickness t_1.

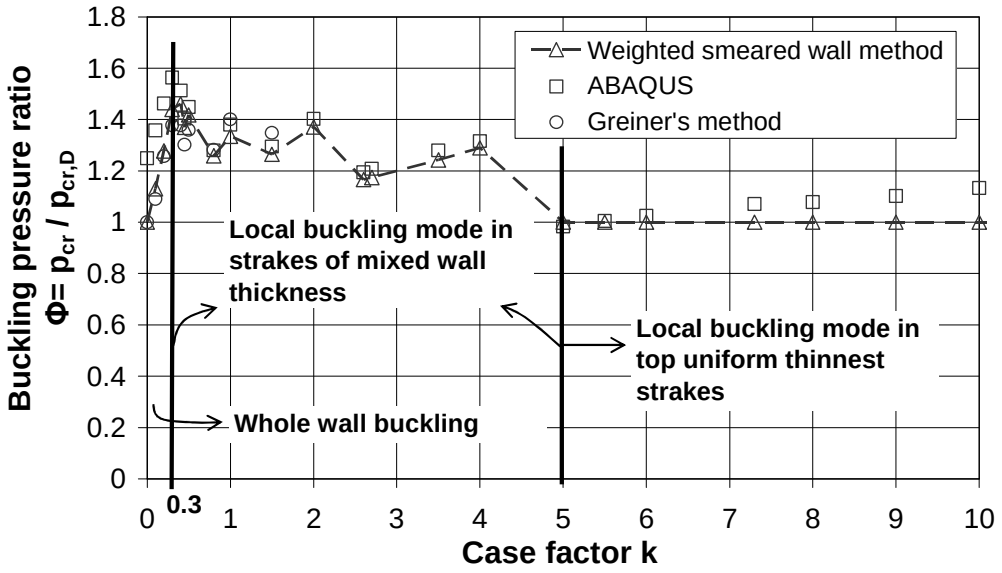

Figure 7-14: Relationship between the buckling pressure ratio ϕ and the wall thickness distribution factor *k*

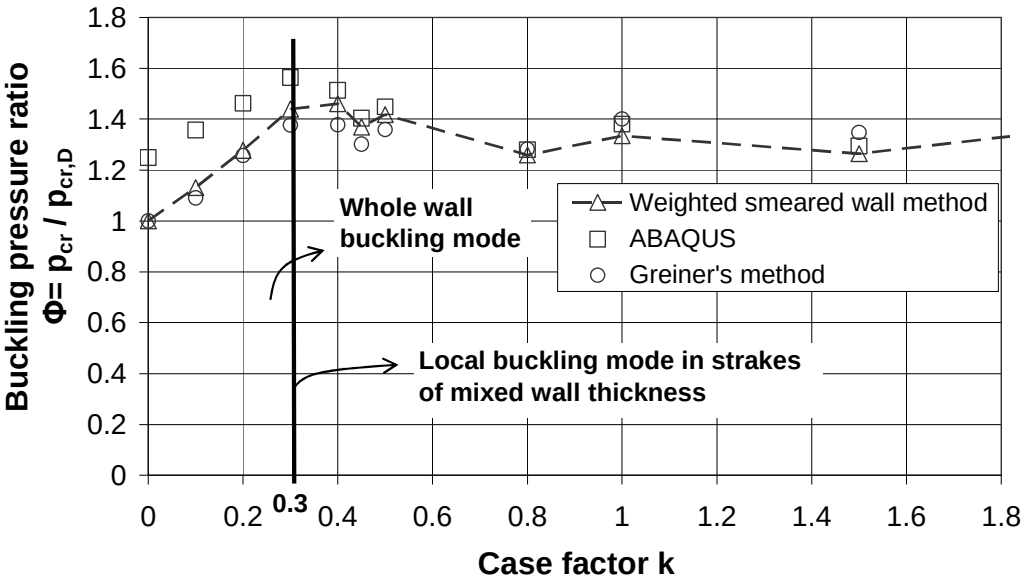

Figure 7-15: Detail of Fig. 7-14 for small values of factor *k*

The buckling behaviour can be divided into three categories, according to the patterns of the vertical buckling mode with changing values of *k*. Small values of *k* correspond to the whole wall buckling mode. The buckling pressure ratio ϕ increases steadily with an increase of *k* due to the increasing thicknesses of lower strakes. Then the buckling mode changes to local buckling modes with the buckle in strakes of

mixed thicknesses. The values of ϕ fluctuate with increasing values of *k*, which is due to the changing number of strakes in the buckle and changing critical circumferential buckling wave number.

When *k* is large ($k \geq 5$), the local buckling mode in the top thinnest strakes occurs. The buckling pressure from the weighted smeared wall method is then constant as *k* increases, because the flexural restraint of the strake below the thinnest one is ignored. However, the real critical pressure is slightly increased by the restraint provided by the thicker strake below the buckle so that an increase in *k* causes a steady slight increase in the critical pressure.

When the whole wall buckling mode occurs ($k \leq 0.3$), Greiner's method and the weighted smeared wall method give very similar predictions, but they are smaller than those from finite element analysis. That is because both Greiner's method and the weighted smeared wall method arise from assumption of a classical S3 base boundary, which ignores the axial restraint at the base of the shell. By contrast, the finite element predictions have used a practical S1 base boundary that includes the axial restraint there. If S3 base boundary was adopted at in the finite element model, the buckling pressure predictions from the three methods in this range have verified to be all close.

When the shell is uniform ($k = 0$), the bottom strake is involved in the buckling mode to the maximum extent and the buckling pressure is significantly affected by the boundary condition at the base. Both the weighted smeared wall and Greiner's methods produce their greatest underestimates. But as *k* increases, the bottom strake becomes thicker and it restrains the buckling mode. The base boundary then has less effect on the buckling pressure, and the predictions from the three methods are then all close.

When local buckling occurs in strakes of mixed thicknesses ($0.3 < k < 5$), all three methods give very close results in the range $0.3 < k \leq 1.5$. The accuracy of Greiner's method depends strongly on the calculation of the effective length of the transformed equivalent uniform thickness cylinder. The effective length is determined by the factor κ which is quite difficult to extract accurately from Fig. 7-6. For $k > 1.5$, the

wall thicknesses are outside the scope of Greiner's method. The weighted smeared method can then be used for a wider range of wall thicknesses and its predictions are close to accurate numerical values.

7.7.3 The influence of the boundary condition at bottom of the shell

The above finite element predictions are based on the practical S1 and S3 boundaries at both ends, where the axial displacement at the bottom of the shell was restrained, but in weighted smeared wall method and Greiner's method, classical S3 boundary conditions at both ends were assumed. The different boundary condition at the base causes a discrepancy of the buckling strength using the three different methods when the whole wall buckling mode occurs. It is clear that the whole wall buckling mode is restrained greatly by the base boundary and a change in the base boundary may affect the buckling strength significantly.

For shells of uniform thicknesses, the meridional displacement at the bottom of the shell has a strong influence on the buckling strength under uniform external pressure. The buckling strength for classic S3 boundaries can be simply multiplied by an external buckling factor (Table 7-2) to involve the influence of meridional restraint at boundaries on the buckling strength. If S1 and S3 boundaries at two ends are adopted, the external pressure factor is 1.25.

In the following analysis, the influence of axial displacement restraint at the base of the shell on the buckling strength of stepped wall cylinders under uniform external pressure is explored. Yamaki's S3 boundary was adopted at the bottom of the shell in the finite element analysis, which is same as the boundary adopted in the weighted smeared wall method and Greiner's method.

When whole wall buckling mode occurs, corresponding to a small value of k, the finite element prediction of the buckling strength agrees well with those from the weighted smeared wall method and Greiner's method (Fig. 7-16). It may concludes that the weighted smeared wall method is effective in capturing the buckling strength accurately for all thickness distributions if a classic S3 boundary was adopted at the base of the cylinder.

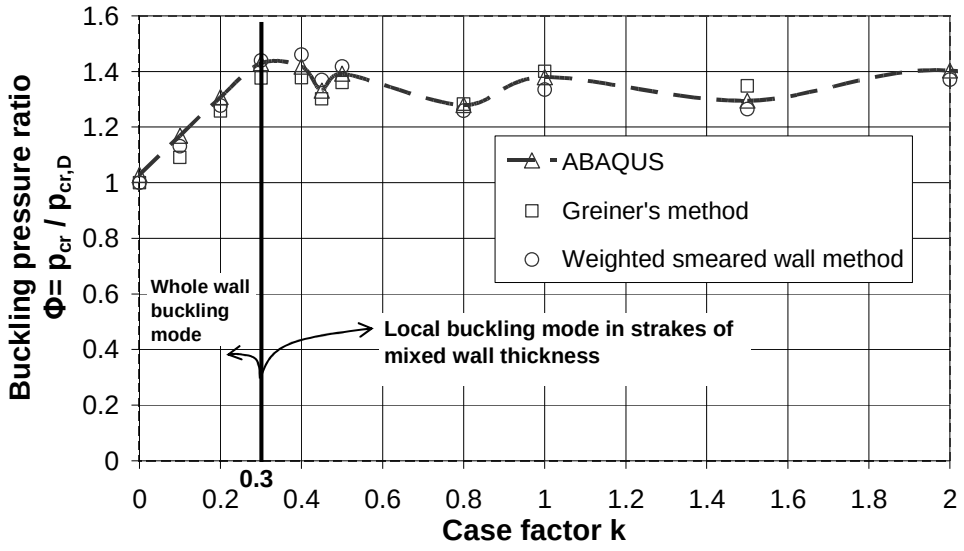

Figure 7-16: Relationship between the buckling pressure ratio ϕ and the wall thickness distribution factor *k* with S3 boundary at the bottom

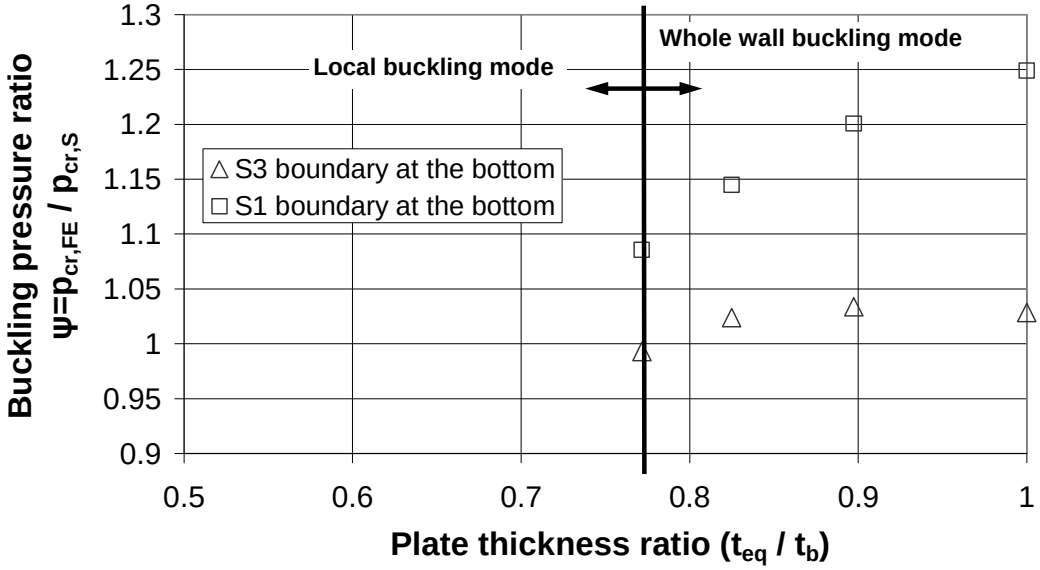

Figure 7-17: Whole wall buckling: discrepancy between FE and smeared wall buckling pressures for all models

The relationship between the critical buckling pressure ratio $\psi = p_{cr,FE} / p_{cr,S}$ and the plate thickness ratio t_{eq} / t_b when whole wall buckling mode occurs is shown in Fig. 7-17. The S1 or S3 boundary was adopted at the bottom separately while the S3 boundary at the top is unchanged. The buckling pressure derived from ABAQUS

is indicated as $p_{cr,FE}$ while the corresponding value obtained from the weighted smeared wall method is indicated as $p_{cr,S}$. The value of $p_{cr,S}$ is invariant without consideration of the changing bottom boundary. The thickness ratio t_{eq}/t_b measures the weight of the equivalent thickness t_{eq} compared with the thickness of the thickest bottom strake t_b.

When S3 boundary was adopted at the base, the buckling pressure ratio ψ is close to 1 for all patterns of wall thickness distribution, corresponding to the results in Fig. 7-16.

When S1 boundary was adopted at the base, for uniform thickness cylinder, corresponding to $k=0$ and $t_{eq}/t_b=1$, the buckling pressure ratio ψ equals to 1.25 which is the constant external buckling factor defined in Table 7-2. With an increase of k, according to previous descriptions, the buckling pressure prediction from the weighted smeared wall method is closer to the accurate finite element prediction as the bottom strake become thicker, and thus the value of ψ decreases with decreasing value of t_{eq}/t_b.

When local buckling in strakes of mixed thickness occurs, the buckling mode is restrained directly by the strake below the buckle and the boundary at the base of the shell has little effect on the buckling behavior. The buckling pressures using the two different bottom boundaries have no difference in the range $t_n/t_{n+1}<0.9$ as shown in Fig. 7-18, where t_n is the thickness of the n^{th} strake at the bottom of the buckle and t_{n+1} is that of the strake below it. The difference of the buckling pressure in the range $t_n/t_{n+1}>0.9$ is caused by the discrepancy of the buckling modes derived from the weighted smeared wall method and finite element predictions when buckling mode changes from the whole wall buckling mode to the local buckling mode. However, the errors using either S1 or S3 boundary at the base are small.

It concludes from the above results that the base boundary only influences the buckling behaviour significantly when whole wall buckling occurs. This influence is disappeared with the bottom strake becomes thicker. Considering S1 boundary at the

base is a more practical boundary in the design of silos and tanks, the later finite element predictions for other models all adopt S1 boundary at the base.

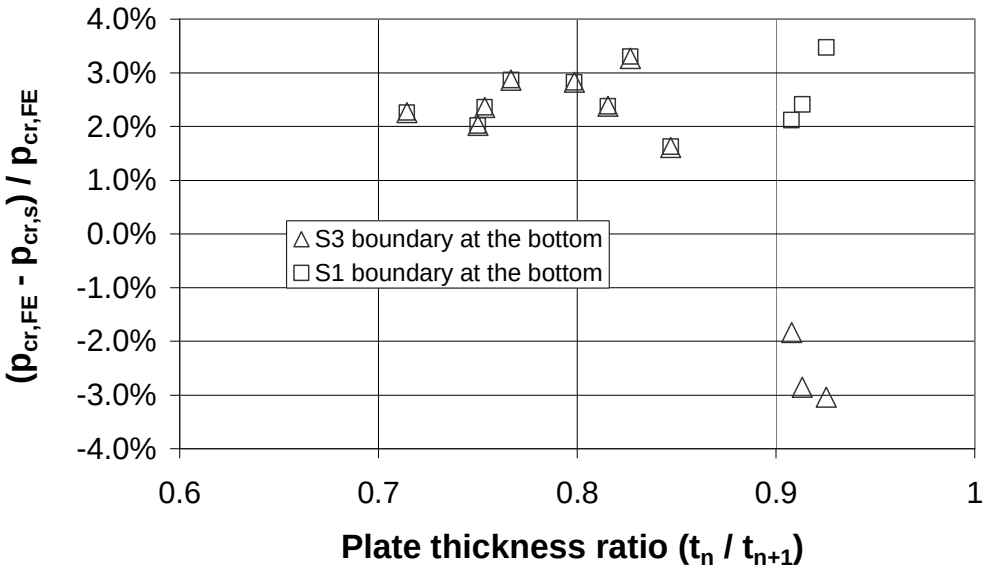

Figure 7-18: Mixed thickness buckling: discrepancy between FE and smeared wall buckling pressures for all models

7.8. The buckling pressure predictions for different models using the weighted smeared wall method

The above results were all for Model 1 (Fig. 7-8) defined according to the Annex A of the API standard 650 (2007). To obtain a more comprehensive check of the weighted smeared method, three more models with different geometries were explored further. The key geometric parameters for each model are shown in Table 7-3 and 4: the relative thickness t_{bi}, the largest radius to thickness ratio, the reference height of each strake, the total number of strakes, the number of the top stakes of uniform thickness and the adjusted thickness of each strake. All three models were modified using the factor *k* in the same way to produce a range of designs.

Table 7-3: The relative thickness of the basic case for different geometric models

Basic case	t_{b1}	t_{b2}	t_{b3}	t_{b4}	t_{b5}	t_{b6}	t_{b7}	t_{b8}	t_{b9}	t_{b10}	t_{b11}	t_{b12}	t_{b13}
Model 1	**1**	**1**	**1.125**	**1.25**	**1.55**	**1.875**	**2.2**	**2.525**	**2.85**	**-**	**-**	**-**	**-**
Model 2	**1**	**1**	**1**	**1**	**1.125**	**1.25**	**1.5**	**2**	**2.5**	**3**	**3.5**	**4**	**5**
Model 3	**1**	**1**	**1.125**	**1.25**	**1.55**	**1.875**	**2.2**	**2.525**	**2.85**	**-**	**-**	**-**	**-**
Model 4	**1**	**1.063**	**1.125**	**1.25**	**1.55**	**1.875**	**2.2**	**2.525**	**2.85**	**-**	**-**	**-**	**-**

Table 7-4: The geometric parameters of different models based on the basic case

Model name	Reference largest radius to thickness ratio r/t_1	Reference height of each strake	Total number of strakes	The number of the top strakes of uniform thickness	The adjusted thickness of each stakes (t_i)
Model 1	**2000**	**1800**	**9**	**2**	$t_i = t_{b1} + k(t_{bi} - t_{b1})$
Model 2	**2000**	**1500**	**13**	**4**	$t_i = t_{b1} + k(t_{bi} - t_{b1})$
Model 3	**1000**	**1000**	**9**	**2**	$t_i = t_{b1} + k(t_{bi} - t_{b1})$
Model 4	**500**	**300**	**9**	**1**	$t_i = t_{b1} + k(t_{bi} - t_{b1})$

The relationship between the buckling pressure ratio ϕ and the wall thickness distribution factor k for Model 2 is shown in Fig. 7-19 and has the same characteristics as Figs 7-14 and 15 for Model 1. The buckling behaviours can be divided into the same three categories according to the patterns of the buckling mode. The key difference is that, for Model 2, the buckling mode changes to the local buckling mode in strakes of mixed thicknesses at a smaller value $k = 0.13$, and to the local buckling mode only in the top thinnest strakes at the larger value $k = 8$. This difference is caused by many factors, including the plate thickness ratio t_{eq} / t_b which is a critical factor to determine whether the whole wall buckling mode occurs or not, and the geometric parameter of the top uniform thinnest strakes which determines the requirement of the flexural restraint provided by the next strake below the top thinnest ones to restrain the buckling mode in just the top uniform thinnest strakes.

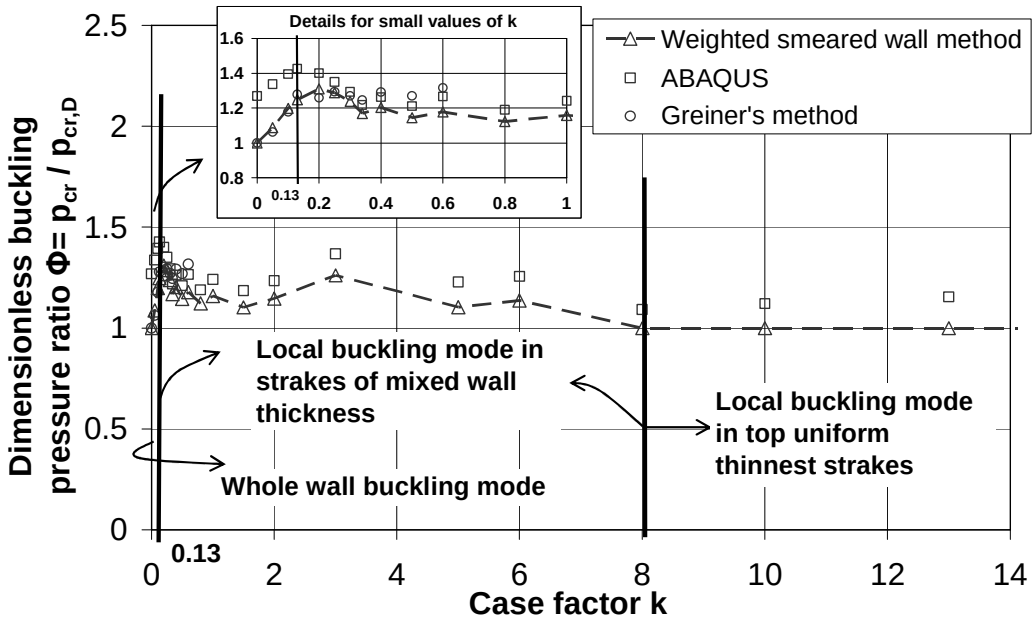

Figure 7-19: Relationship between the buckling pressure ratio ϕ and the wall thickness distribution factor *k* (Model 2)

The values of *k*, in determining the boundary between the whole wall buckling mode and the local buckling mode in strakes of mixed wall thickness, and the boundary between the local buckling mode in strakes of mixed wall thickness and the local buckling mode in the top uniform thinnest strakes for Model 3 (Fig. 7-20), are close to the corresponding values for Model 1 due to the similar the wall thickness distributions up the height (Table 7-3) though the geometric parameters of the two models in Table 7-4 are different.

The maximum value of the buckling pressure ratio ϕ for Model 4 is obvious larger than other models when local buckling in strakes of mixed thicknesses occurs (Fig. 7-21). It can be noted that there is only a single thinnest strake for Model 4, and the ratio of the length of the top thinnest strakes to the whole length of the shell is smallest. The contribution of the thinnest part to the energy involved in the buckling mode is smallest. But the relative thickness t_1 of the top thinnest strake is always adopted to calculate the reference buckling pressure $p_{cr,D}$, so the value of $p_{cr,D}$ may underestimate the buckling pressure most significantly.

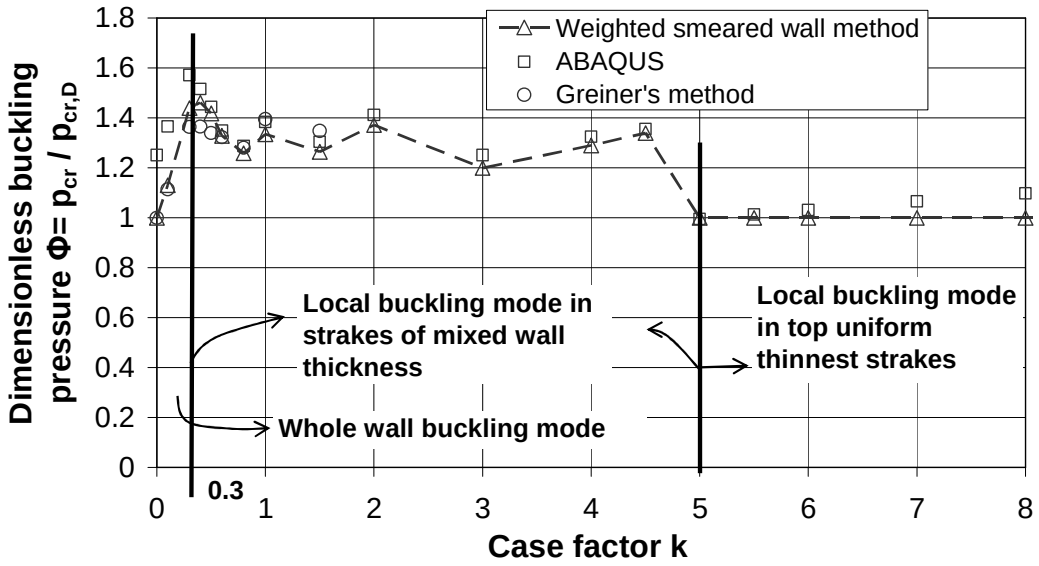

Figure 7-20: Relationship between the buckling pressure ratio ϕ and the wall thickness distribution factor *k* (Model 3)

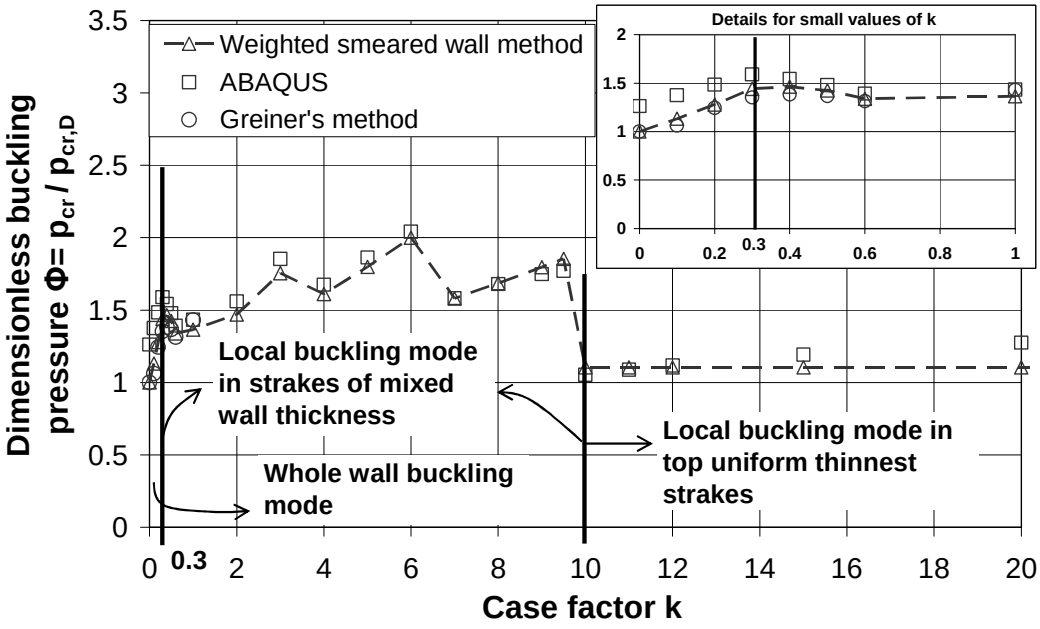

Figure 7-21: Relationship between the buckling pressure ratio ϕ and the wall thickness distribution factor *k* (Model 4)

7.9 Exploitation and enhancement of the weighted smeared wall method based on accurate finite element predictions

The analyses described above used three different methods to predict the buckling pressures of stepped wall cylinders under uniform external pressure. The weighted smeared wall method sometimes slightly underestimates or overestimates the buckling pressure. The neglect of the flexural restraint of the strake below the buckle may have different influences on the buckling predictions according to the specific buckling mode as described above. A remedy for this phenomenon is described here. The S1 boundary at the base of the shell was adopted in the finite element predictions.

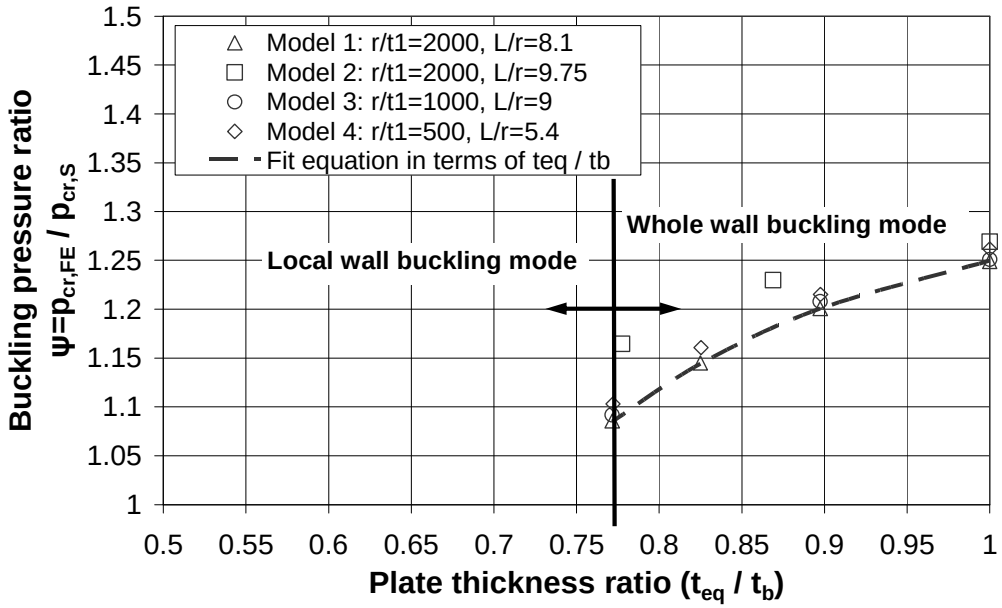

Figure 7-22: Whole wall buckling: discrepancy between FE and smeared wall buckling pressures for all models

Similar as Fig. 7-17 for Model 1, the relationship between the buckling pressure ratio ψ and the plate thickness ratio t_{eq}/t_b for different models defined in Tables 7-3 and 7-4 when whole wall buckling mode occurs is shown in Fig. 7-22.

For different models with different geometries, the values of ψ have similar changes with t_{eq}/t_b. When $t_{eq}/t_b = 1$, corresponding to a uniform thickness cylinder, the ratio ψ is close to the constant external buckling factor C_θ=1.25 (Table

7-2) for all models which shows that this effect is entirely due to axial restraint at the base.

The weighted smeared wall method may present a lower prediction for Model 2 than other models. Model 2 is composed of more strakes up the height and has a more distinctive change of the wall thickness distribution up the height, and it has four uniform thinnest strakes at top, which is different from other three models. The equivalent thickness in weighted smeared wall method is calculated based on the weighted value of the wall thickness of each strake up the height. So the total number of the strakes of the cylinder and the number of uniform thinnest strakes at top might influence the accuracy of the results. How much is this effect is an interesting question to explore in the future. However, it can be noted that whatever the specific pattern of the wall thickness distribution is, when $t_{eq}/t_b = 1$, the value of ψ should be close to the factor 1.25, and it is true for other geometries that are not included here. In another aspect, the pressure parameter ψ changes similarly as the thickness parameter t_{eq}/t_b changes for all models. It concludes that the relationship curves of ψ and t_{eq}/t_b should have small discrepancy for all models.

An improved modified value for the buckling pressure $p_{cr,M}$ can then be obtained as:

$$p_{cr,M} / p_{cr,S} = -1.08 + 4.4\left(\frac{t_{eq}}{t_b}\right) - 2.07\left(\frac{t_{eq}}{t_b}\right)^2 \tag{7.31}$$

By using Eq. 7.31 which is shown as the dot line in Fig. 7-22, more accurate evaluation of the buckling pressure based on the weighted smeared wall method for stepped wall cylinders under uniform external pressure can be obtained when whole buckling mode occurs. It leads to a conservative close estimate of the buckling strength with error less than 1% for most results, except a few for Model 2.

For local buckling modes involving strakes of mixed thickness, the weighted smeared wall method slightly underestimates the buckling pressure in most cases as shown in Fig. 7-23, where t_n is the thickness of the n^{th} strake at the bottom of the

buckle and t_{n+1} is that of the strake below it. When the buckling mode involves one more strake below the top zone in Models 2 and 4, a slightly larger error occurs, but it is less than 7% for most results. For Model 1, based on the practical design of API 650, the largest error is around 3 percent. Thus for practical designs, the weighted smeared wall method gives directly good estimates of the buckling pressure.

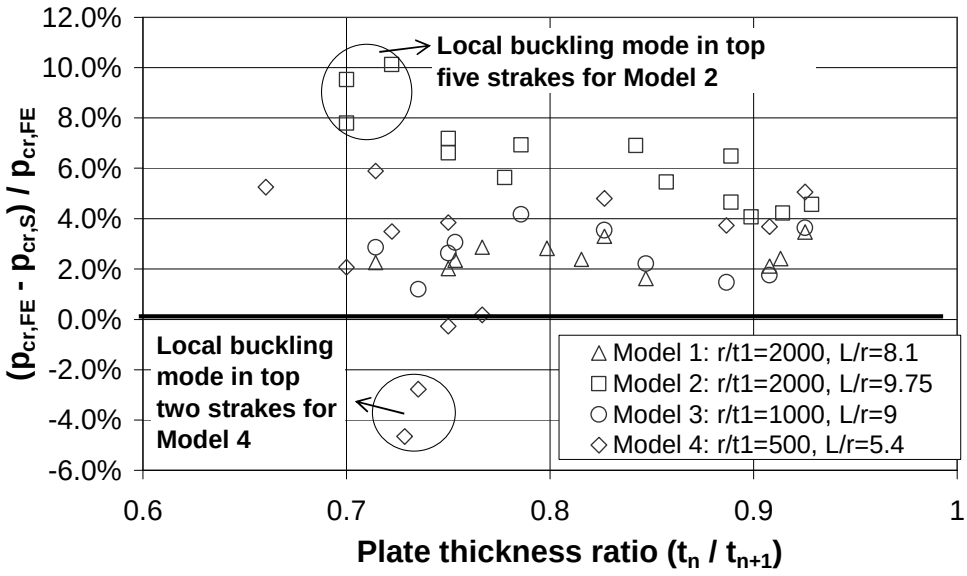

Figure 7-23: Mixed thickness buckling: discrepancy between FE and smeared wall buckling pressures for all models

When the wall thickness distribution factor *k* is large enough, the third buckling mode termed local buckling mode in the top thinnest strakes occurs. The buckling pressure $p_{cr,S}$ predicted from the weighted smeared wall method is invariant with changing plate thickness ratio t_1 / t_2, where t_1 is the top strake thickness and t_2 the thickness of the next strake below it. By contrast, the accurate finite element prediction $p_{cr,FE}$ increases continuously as t_2 becomes larger, which leads to the buckling pressure ratio $\psi = p_{cr,FE} / p_{cr,S}$ steadily rises as the thickness t_2 of the strake below it increases (Fig. 7-24). The reference thickness of the top section (thinnest and uniform thickness) t_1 can be any value, and here $t_1 = 1$.

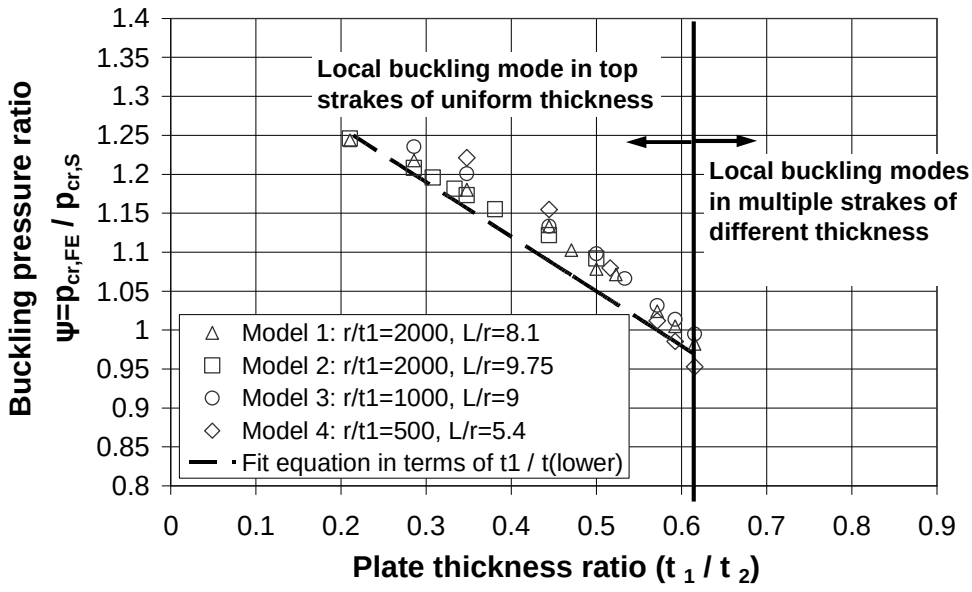

Figure 7-24: Top zone buckling: discrepancy between FE and smeared wall buckling pressures for all models

A modified buckling pressure $p_{cr,M}$ can be obtained using the thickness ratio t_1 / t_2 as:

$$p_{cr,M} / p_{cr,S} = 1.4 - 0.7(t_1 / t_2) \tag{7.32}$$

Adoption of Eq. 7.32 which is shown as the dot line in Fig. 7-24 gives a slightly conservative buckling pressure for all models with a maximum error around 5% for Model 4.

From above analyses, it can be seen that the weighted smeared wall method provides a much easier way than the method in EN1993-1-6(2007) to evaluate the buckling pressure of cylinders of stepwise variable wall thicknesses under uniform external pressure. It estimates the critical buckling mode and buckling pressure that are close to FE predictions. The whole wall buckling mode, local buckling only in the top thinnest strakes and local buckling in strakes of mixed thickness may all occur depending on the specific wall thickness distribution. This study has produced a new design method that can give accurate results for a wide range of shell walls and is much easier to use than that in EN 1993-1-6 or ECCS EDR5.

7.7 Cylinders of stepwise wall thickness under wind loading

Thin-walled tanks and silos are in danger of buckling under wind loading when they are empty or only partially filled. The phenomena of this buckling behaviour can be found for cylindrical shells with any geometry. An example of the buckling phenomena for cylindrical shells under wind loading in practical shell structures is shown in Fig. 7-3. For stocky cylinders, the buckling is like cylinders under uniform external pressure. For intermediate and slender cylinders, the buckling behaviour is affected by geometric nonlinearity, which was discussed in detail in Chapter 6.

7.7.1 Existing provisions in EN 1993-1-6 (2007) and ECCS EDR5 (2008)

For stocky cylinders of stepwise variable wall thickness under wind loading, the following rules are set out in ECCS EDR5 (2008) as the buckling stress design procedure:

> *The buckling check for cylinders with stepwise variable wall thickness under wind pressure should be carried out by using the procedure given in EN 1993-1-6 (2007) and Chapter 11, ECCS EDR5 (2008) for cylinders of stepwise wall thickness under uniform external pressure and by replacing the wind pressure with an equivalent uniform external pressure according to the following equation:*
>
> $$q_{eq} = k_w q_{w,\max}$$
>
> *Where $q_{w,\max}$ is the maximum stagnation pressure and k_w is a reduction factor.*
>
> *The following condition of the cylindrical shells with radially fixed boundaries at both ends should be met:*
>
> $$m_{cr} \geq 10$$
>
> *with m_{cr} being the critical buckling wave-number in circumferential direction of the stepped cylinder under uniform external pressure.*
>
> *The equivalent uniform external pressure should be determined using the following reduction factor k_w:*

$$k_w = 0.46\left(1 + 0.037 m_{cr}\right) \le 1$$

The critical buckling wave number m_{cr} depends on the ratio of equivalent plate thickness t_c / t_a which controls the meridional height of the buckle. The expression of m_{cr} can be found in EN 1993-1-6 (2007).

Further commentary on this procedure in ECCS EDR5 (2008) Chapter 12 (Greiner, Guggenberger and Schneider, 2008), gives the following explanations:

The design procedure for buckling of cylinders with stepwise varying wall thickness under wind pressure (Greiner, 1981) was developed in close relationship to the development of procedures for cylinders with stepped wall thicknesses under uniform external pressure.

The procedure for non-uniform pressure was to replace the wind pressure by an equivalent uniform pressure. Since the determination of the equivalent uniform pressure depends on the number of buckling waves in the zone of circumferential compression, the main challenge of the investigation was to identify the buckling wave number for a given pattern of wall thicknesses in the stepped-wall cylinder. In this sense the approach is a plausible extension of the method derived for a cylinder with constant wall thickness.

One thing about the definition of stocky cylinders in EN 1993-1-6 (2007) should be mentioned. It is not easy to use because it requires the buckling mode to be predicted before it can be determined whether the cylinder is stocky or not, and the buckling mode probably should depend on whether the cylinder is stocky or not. So it would be better to search for a geometric criterion that depends on the length, radius and thickness to decide when it should be stocky.

The rule for stepped wall cylinders under wind loading in EN1993-1-6(2007) is related closely to the rule for stepped wall cylinders under uniform external pressure. The factor κ is also unavoidably adopted from Fig. 7-6. So the same complexity and difficulties exist for the practical use of this method for wind loaded cylinders as for cylinders in uniform external pressure.

7.7.2 The effect of geometric nonlinearity

As described in previous sections, for cylinders of stepwise wall thickness under uniform external pressure, the buckle may extend over several upper strakes of the cylinder. The lower parts may not be involved in the buckling mode and just provide some restraint against buckling in the upper part. For a stepped wall cylinder under wind pressure, the whole geometry may correspond to an intermediate or slender cylinder according to the definition for cylinders of uniform thickness, but the buckling behaviour may correspond to that of a stocky cylinder because local buckling occurs only in several upper strakes.

For cylinders under symmetric uniform external pressure, geometric nonlinearity rarely affects the buckling behaviour. But for cylinders under unsymmetrical wind loading, geometric nonlinearity may have a significant effect on intermediate and slender cylinders (Chapter 6). Geometrically nonlinear analysis is sometimes necessary to see whether geometric nonlinearity affects the buckling strength.

Model 1 was next used to study the buckling behaviour of stepped wall cylinders under wind loading. The linear critical buckling modes for Model 1 with different wall thickness distributions under wind loading are shown in Fig. 7-25. When k is large enough, local buckling occurs only in the top two strakes. When k is zero (uniform thickness of the shell) or is small enough, the buckle extends over the whole height of the cylinder. When k lies between these two extremes, the linear critical buckling mode may occur in any strakes with mixed thickness. The buckling modes are all circumferential buckling modes. Under wind loading, a large buckle forms in the windward area, extending over the height of the strakes in the buckle. The buckling pressure is here related to the stagnation pressure.

The buckling behaviour of stepped wall cylinders under wind loading was found to be quite similar to that of cylinders under uniform external pressure. Even the change of the buckling mode (the number of the strakes in buckling) with the change of k agrees well for the two loading conditions, as can be seen by comparing Figs 7-13 and 7-25.

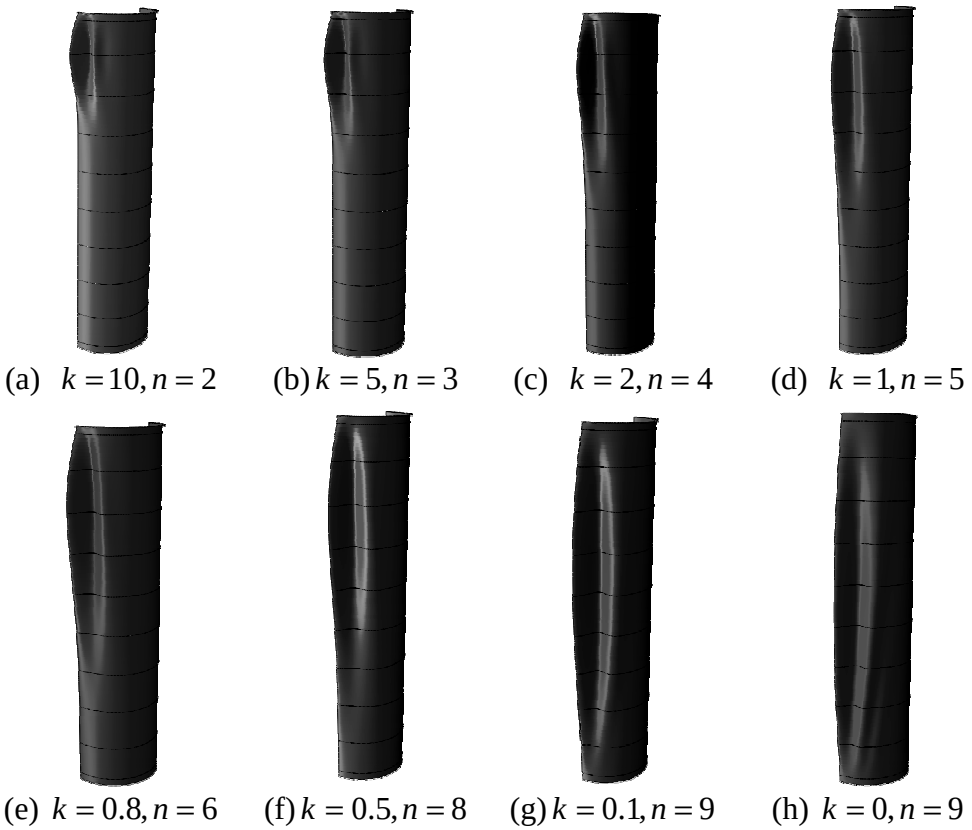

Figure 7-25: Linear critical buckling modes for stepped wall cylinders with different patterns of wall thickness distribution under wind pressure (Model 1)

Figure 7-26: Nonlinear buckling mode for Model 1 with uniform thickness (*k*=0)

The buckling modes in Fig. 7-25 show the linear critical buckling modes. To study the effect of geometric nonlinearity, the cylinder with *k*=0 corresponding to a uniform thickness cylinder was investigated, because cylinders with longer buckles (Fig. 7-25h) are more easily affected by geometric nonlinearity. The nonlinear critical buckling mode for Model 1 with *k*=0 under wind pressure is shown in Fig. 7-

26. The nonlinear critical buckling mode is the same as the linear critical buckling mode in Fig.7-25(h). The critical nonlinear buckling pressure is 0.991 times the linear critical buckling pressure. So when k=0, the linear and nonlinear buckling pressure are almost identical.

It may be concluded that the nonlinear buckling behaviour for all cases, with any value of k, is very similar to the linear buckling behaviour for Model 1. Geometric nonlinearity has little effect on the buckling behaviour. Since Model 1 is the most general geometry in a practical stepped wall cylindrical structure, it may be concluded that geometric nonlinearity plays a comparatively small role in the buckling behaviour for a wide range of practical cylindrical shell structures of stepwise variable thickness. For a given model, the case with k=0, corresponding to a uniform thickness cylinder with the reference thickness of the top thinnest strake, can be examined to check if geometric nonlinearity has a significant effect. If not, it can safely stated that geometric nonlinearity can be ignored for this model with any changing pattern of wall thickness distribution which may be assessed using the method proposed in this thesis.

7.7.3 The relationship of the nonlinear buckling strength under wind pressure and uniform external pressure

The relationship between the buckling pressure ratio $\phi = p_{cr} / p_{cr,D}$ and the case factor k for cylinders under either uniform external pressure or wind loading is shown in Fig. 7-27. The critical buckling pressures p_{cr} are evaluated using ABAQUS. The boundary case factors k at which the buckle height changes can be determined according to the smeared wall method presented earlier in this chapter.

It can be seen that the dimensionless buckling pressure ratios ϕ for wind loading and for uniform external pressure have similar changes with changing wall thickness distributions. When whole buckling occurs, the dimensionless buckling pressure ratio has a steady increase with the increase of k due to the increasing restraint of the lower strakes (Fig. 7-28).

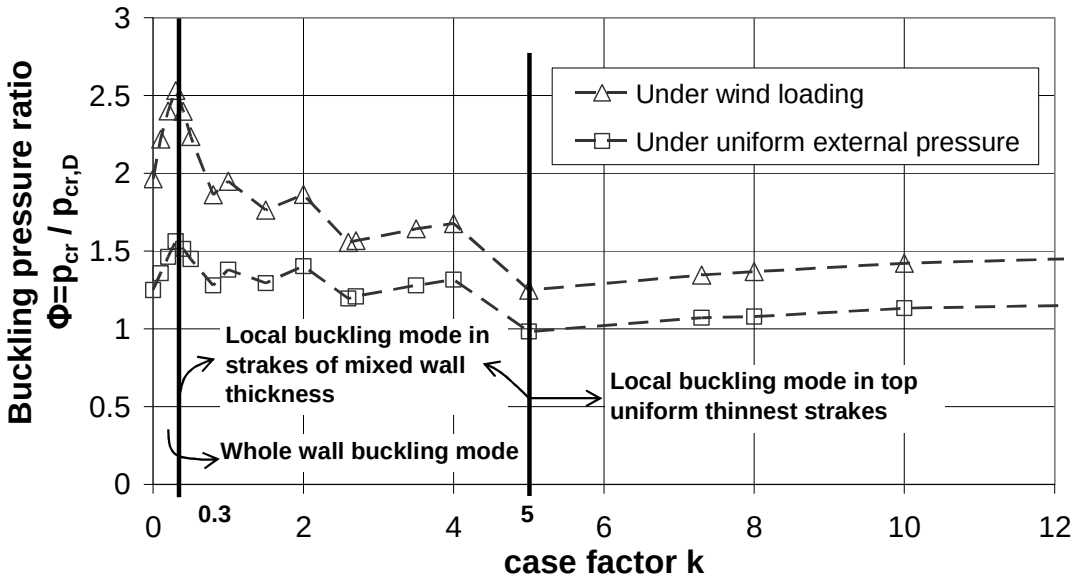

Figure 7-27: Linear critical buckling pressure for cylinders under uniform external pressure and wind loading with changing case factor *k* (Model 1)

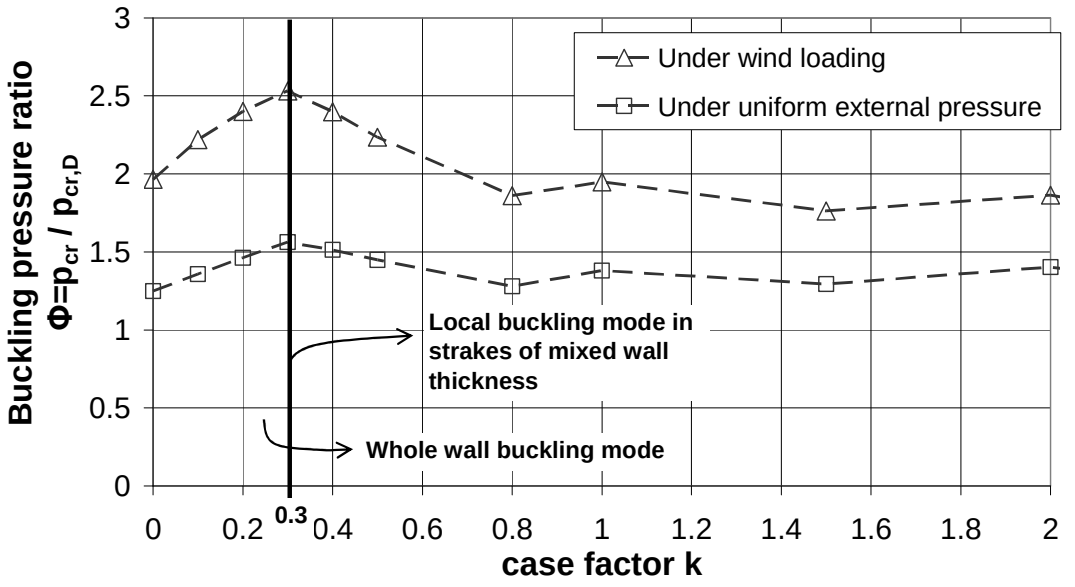

Figure 7-28: Detail of Fig. 7-27 for small values of *k*

When a local buckling mode with the buckle in strakes of mixed thickness occurs, the curves both have several waves as the value of *k* increases. These are caused by the steady change of the strake number involved in the buckle. When *k* is large enough, local buckling in the top thinnest strakes occurs, and the dimensionless buckling pressure shows a steadily slight change with increasing *k* due to the

increasing flexural stiffness of the strake below the buckle. The two load cases have closely matched changes throughout the full range of wall thickness distributions.

The relationship between the wind buckling pressure ratio $q_{cr,w} / q_{cr,u}$ and the length parameter Ω for cylinders of both uniform thickness and stepwise wall thickness is shown in Fig. 7-29. The critical buckling pressure for cylinders under wind loading is indicated as $q_{cr,w}$, which is the critical stagnation pressure. The critical buckling pressure for cylinders under uniform external pressure is indicated as $q_{cr,u}$.

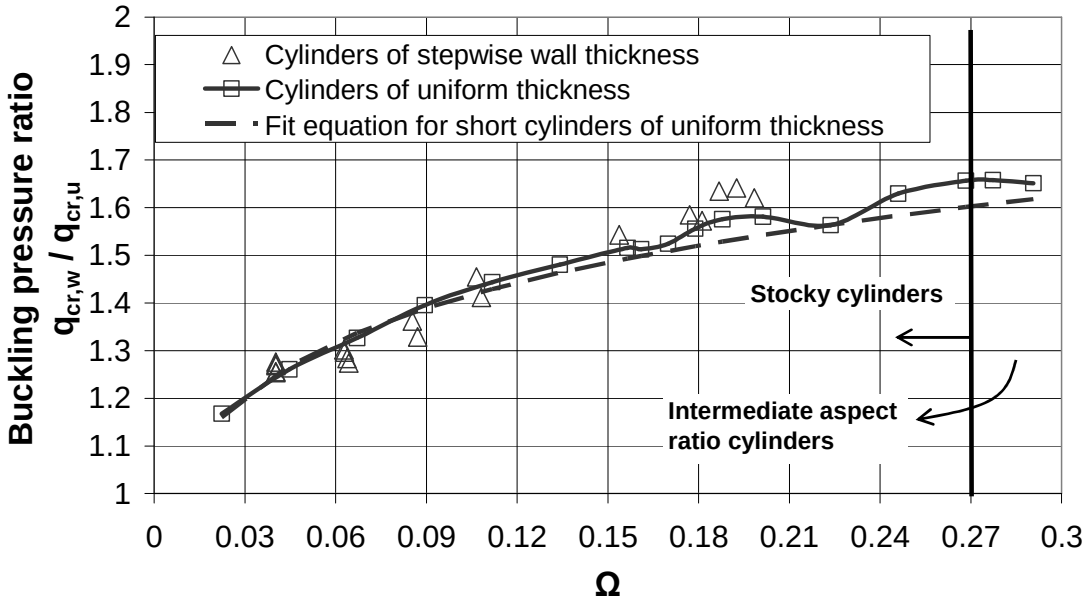

Figure 7-29: Relationship between the buckling pressure ratio $q_{cr,w} / q_{cr,u}$ and the length parameter Ω for cylinders of either uniform thickness or stepwise wall thickness

For stepped wall cylinders under wind loading, with changing values of *k*, different patterns of wall thickness distribution may produce the same buckle height. The value of Ω is affected by both the buckle height and the equivalent thickness, so Fig. 7-29 includes both effects with a single curve. Several close values of Ω may be caused at the same buckle height, as can be seen in Fig. 7-29 when Ω is close to 0.04, 0.06 or 0.18.

The value of $q_{cr,w}/q_{cr,u}$ for stepped wall cylinders could be either slightly larger or slightly smaller than the corresponding value for uniform thickness cylinders, depending on the specific values of k and Ω. Equation 7.33 (also used in Chapter 6), which shows the relationship between the linear elastic buckling pressure ratio $q_{cr,w}/q_{cr,u}$ and the length parameter Ω for stocky cylinders of uniform thickness, is indicated as the dashed line in Fig. 7-29. It can be seen this equation can also be used to represent the curves for stepped wall cylinders with good precision.

$$q_{cr,w}/q_{cr,u} = 1.90\Omega^{0.13} \tag{7.33}$$

It should be noted that Eq. 7.33 is only for stocky cylinders with the circumferential buckling mode. The slenderness limits for a stocky cylinder of uniform thickness under wind loading are (Chapter 6):

$$0 < \Omega \le 0.27 \tag{7.34}$$

For Model 1, Eq. 7-33 can be used safely for all patterns of wall thickness distribution. For a given cylinder with a different wall thickness distribution under wind loading, the influence of geometric nonlinearity should be checked first. The critical buckling pressure can be obtained using the following steps:

The critical buckling pressure in uniform external pressure is calculated first using the weighted smeared wall method. If the equivalent cylinder is stocky according to the definition of Eq. 7-34, then Eq. 7.33 can be used directly to calculate the critical buckling pressure for a cylinder of stepped wall thickness under wind loading. If the equivalent cylinder is of intermediate aspect ratio, the relationship between the nonlinear buckling pressures for the two loading conditions (Chapter 6) should be considered. However, this situation seems to be rather rare in typical designs of stepped wall cylinders. It should be noted that this two step process is also used in EN 1993-1-6(2007) and ECCS EDR5 (2008), and that the recommendations in these documents are also based on linear bifurcation analyses.

7.8 Conclusion

The buckling behaviour of cylinders of stepwise variable wall thickness under uniform external pressure and under wind loading has been studied in this chapter. The buckling pressure assessment in DIN 18800 (1990) and EN 1993-1-6 (2007) is rather awkward for the practical design of silos and tanks. This chapter has proposed a new weighted smeared wall method which is based on an idea proposed by Trahair et al. (1983) for non-uniform shells. It has produced a new design method that can give accurate results for a wide range of shell structures and is much easier to use than that in DIN 18800 (1990), EN 1993-1-6 (2007) or ECCS EDR5 (2008). The main conclusions are:

1. The weighted smeared wall method can accurately determine both the critical buckling mode and the buckling pressure.
2. Three categories of buckling mode have been identified: whole wall buckling, mixed thickness buckling, and top thinnest zone buckling. Which one is critical depends on the specific wall thickness distribution.
3. A new design method has been presented and verified over a huge number of designs. It gives accurate results for a very wide range of shell walls and is much easier to use than that of Greiner (1981). The direct predictions can be enhanced by minor modifications that account for adjacent restraint effects.
4. For stepped wall cylinders under wind loading with the circumferential buckling mode, the relationship of the critical buckling pressure ratio for stocky cylinders of uniform thickness under uniform external pressure and wind loading is still applicable. The weighted smeared wall method can be used to evaluate the critical buckling pressure.

Chapter 8 Minimum bending stiffness of the ring stiffener at the top edge of the cylinder under wind loading

8.1 Overview

Thin-walled tanks and silos are in danger of buckling under wind loading when they are empty or only partially filled. Chapters 6 analyzed the buckling behaviour of thin cylinders under wind loading. Chapter 7 analyzed the buckling behaviour of cylinders of stepwise wall thickness under uniform external pressure. Cylinders of either uniform thickness or stepped variable thickness were all discussed. At the top edge of the shell, a ring stiffener with enough bending stiffness was adopted to keep the circularity of the top edge, so that the ring was not involved in the buckling modes in either linear bifurcation analysis or geometrically nonlinear analysis. However, if the ring stiffener is not stiff enough, the ring may be involved in the buckling mode, and the buckling mode of the shell wall may also change as the bending stiffness of the ring stiffener changes.

In practical design, ring stiffeners should be designed against local buckling in the ring stiffener, and the ring stiffener should also restrain the top of the cylinder to be circular when shell wall buckling occurs. Furthermore, the buckling mode and buckling strength of the cylinder should have no significant change with a further increase in the bending stiffness of the ring stiffener. This chapter presents a study that explores the minimum bending stiffness of the ring stiffener required to achieve the above objectives. This is an important aspect of design of ring stiffeners.

Theoretical analysis of the buckling of ring stiffened cylinders under asymmetric wind loading is quite complex and difficult. For cylindrical shells with simple supports under a local path load similar to wind loading, Ansourian (2004) derived theoretical results by applying Flügge's equations (1973) in coupled form and using Galerkin's method. A membrane pre-buckling state was assumed in his solution. If the pre-buckling bending effect is considered (LA analysis), the problem becomes more complex. However, due to the asymmetry of the wind loading, pre-buckling

bending effects are usually large and the effect of the true pre-buckling stress distribution should thus be considered.

For stiffened cylindrical shells, Singer (2004) described the “smeared-stiffener theory” for the buckling analysis of stiffened shells. It is a satisfying method for closely stiffened shells that fail by general instability. The effect of a ring stiffener can be considered by an increase of the effective cross-sectional area of the shell. The equations for the forces and moments, considering the effect of the ring stiffener, can be found in Singer’s paper (2004). For a shell with wider stiffener spacing, only part of the shell can be “smeared” due to the stiffener. This method mostly employs “classical” linear theory, which assumes a membrane pre-buckling condition. The linear smeared-stiffener concept was developed at Technion (Burns, 1966) and employs the linear Donnell stability equations (Donnell, 1933). However, when local buckling occurs, it is outside the scope of this smeared-stiffener theory.

This chapter considers cylindrical shells with a single ring stiffener at the top edge of the shell, which corresponds to practical tanks and silos under wind loading. Considering the complexity and difficulty of theoretical analysis in practical use, this chapter uses only numerical investigations to explore the effect of the ring stiffener on the buckling behaviour of cylindrical shells under wind loading. An appropriate empirical design rule is recommended for practical application.

8.2 Rules in publications and standards

In current publications and standards, the rules of the minimum stiffness requirement of the top ring on a cylinder have mostly been derived from linear buckling theory for cylinders under uniform external pressure. The limiting dimensionless stiffness γ_R^*, derived by Resinger and Greiner (1982), Greiner (1987) may be usefully used to characterise the limiting value of the second moment of area $I_{r,\min}$ of the ring stiffener:

$$\gamma_R^* = \frac{12 I_{r,\min}\left(1-\nu^2\right)}{\ell t^3} \tag{8.1}$$

where ℓ is length of the cylindrical shell involved in the critical buckling mode, t is the thickness of the shell wall, and ν is Poisson's ratio. An analogous investigation was performed by Blackler (1986), resulting in a formula for the limiting value $I^*_{r,\min}$:

$$I^*_{r,\min} = 0.077 t^3 \ell n_r^{0.45} \tag{8.2}$$

where n_r is the number of the equidistant rings. This equation results in a slightly different limiting value of ring stiffness $I^*_{r,\min}$ from Eq. 8.1.

Design rules for the stability of ring-stiffened cylinders are given in ECCS Recommendation No. 56 (1988) and in the German Recommendations DASt-Richtlinie 017 (1992), where the effect of imperfections is accounted for by a second-order analysis of the pre-deformed ring stiffener (Greiner, 2004).

Blackler (1986) obtained another formula (Eq. 8.3) for the minimum stiffness requirement for a cylinder of constant thickness under uniform external pressure, based on classical eigenvalue analysis. He also recommended this formula for cylinders under wind loading.

$$I^*_{r,\min} = 0.048 \ell t^3 \tag{8.3}$$

For cylinders under wind loading, the API 650 (2007) Standard provides a design formula to specify the required section modulus of the ring for in-plane bending as:

$$Z_{\min} = 0.058 \times 10^6 D^2 L \tag{8.4}$$

Greiner (2004) referenced Blackler's (1986) equation, but proposed to increase the practical minimum ring stiffness for cylinders under wind loading to a value of about 5-10 times Blackler's proposal (Eq. 8.3) as

$$I^*_{r,\min} = 0.48 \ell t^3 \tag{8.5}$$

Schmidt (1998) proposed that the top stiffener for cylinders under wind loading, for a classical buckling design according to his strategy, should have a second moment of area of at least:

$$I^*_{r,\min} = 0.5\ell t^3 \tag{8.6}$$

In ECCS EDR5 (2008), the following rules are adopted:

The flexural rigidity EI_z of a ring at the top edge of the cylinder about its vertical axis (circumferential bending) should exceed the larger of:

$$EI_{z,\min} = k_1 E\ell t^3 \tag{8.7}$$

and

$$EI_{z,\min} = 0.08 C_w E r t^3 \sqrt{r/t} \tag{8.8}$$

Where $k_1 = 0.1$ is recommended, C_w is the wind pressure distribution coefficient given in Chapter 5.3.2.5.

The bending stiffness of the ring stiffeners should be sufficiently large to limit the ovalisation of the ring stiffened cross-sections under the wind action to 2%.

To achieve the required bending stiffness, the minimum second moment of area of the cross section of the ring stiffener $I_{\min,i}$ should be calculated as:

$$I_{\min,i} = \frac{r^3 \ell_{\inf,st,i} q_{\cos 2\theta}}{0.18E} \tag{8.9}$$

in which

$$q_{\cos 2\theta} = \eta q_{\cos\theta}$$

$$q_{\cos\theta} = \frac{2}{\pi} c_f q_p$$

$$\eta = 1.00 + \frac{12.5}{\ell} + 0.16\sqrt{\frac{\ell}{r}} \le 5$$

in which L and r are expressed in meters, $\ell_{\inf,st,i}$ is the influence length of the ring, which is adopted according to the following equation in EN 1993-1-6(2007).

$$\ell_{\inf,st,i} = 0.49 r\sqrt{r/t} \le 0.375L$$

The above recommendations present a wind range of values for the minimum ring size. The API 650 (2007) rule relates to bending strength rather than stiffness, so does not strictly address the buckling condition. The very wide range of values obtained from Blackler (1986), Schmidt (1998), Greiner (1987, 2004) and ECCS EDR5 (2008) indicates that a thorough study of the required minimum stiffness to restrain the buckling of the shell is urgently needed.

8.3 Method and objective in this Chapter

The above equations (Eqs 8.3 to 8.8) directly relate the minimum bending stiffness of the ring stiffener to the radius, length and thickness of the cylindrical shell walls. They are quite convenient to use in practical design. However, they are obtained based on the principle that the ring stiffener should be stiff enough to prevent a local ring buckling mode or an overall buckling mode including the ring. These rules are intended to guarantee that the ring is not involved in the buckling, but they do not discuss the permitted deformation of the ring stiffener under the buckling pressure. Under the buckling pressure, the ring may have a significant radial displacement even if it is not involved in the buckling mode. For the most part, these rules are based on classical buckling eigenvalue analyses and their derivation did not consider the effect of geometric nonlinearity, which is known to have a significant effect on the buckling behaviour of intermediate aspect ratio cylinders under wind loading (Chapter 6).

The rule for high aspect ratio cylinder (chimneys) in ECCS EDR5 (2008) is based on the research of Schneider et al. (2002). It gives a requirement for the minimum bending stiffness of the ring to limit the ovalisation of the ring stiffened cross-section. But it is complex to use and some parameters are difficult to determine.

In this chapter, the minimum bending stiffness of the ring was related to the length and thickness of the cylindrical shell. The bending stiffness of the ring was required to satisfy the following two requirements: First, it should prevent the local ring buckling mode (Ansourian, 1992; Schmidt et al., 1998). In another aspect, the stiffness should be so high that the ring does not take part in the global shell wall buckling mode. However, it is found that there is no limiting stiffness at which the

ring does not take part in the buckling at all under wind loading. As a result, very stiff rings lead to buckling pressures that asymptotically approach the value for an ideally rigid ring. To find a practically useful stiffness for this ring, it is therefore best to accept a defined shortfall from the buckling pressure associated with a rigid ring. This strategy is adopted in this study.

The initial numerical results show that when the bending stiffness of the ring stiffener is large, the critical buckling pressure of the shell can still be considerably increased with a further increase of the ring stiffness. An increase in the size of the ring raises an economic problem, but it can increase the buckling resistance of the shell greatly. It may be easier and more economical to increase the buckling resistance of the shell by changing the size of the ring than by changing the thickness of the shell.

This chapter focuses on the study of an appropriate ring stiffener size. It is expected to provide a more economical and reasonable rule for the design of ring stiffeners.

8.4 Minimum bending stiffness coefficient $k_{\min}$ for a ring stiffener under wind loading

The minimum bending stiffness coefficient $k_{\min}$ is expressed here as:

$$k_{\min} = \frac{I_{r,\min}}{\ell t^3} \tag{8.10}$$

in which $I_{r,\min}$ is the minimum second moment of area of the cross-section of the ring stiffener. In Blackler's (1986) analysis, Eq. 8.3 gives $k_{\min} = 0.048$. In Greiner's (2004) proposal, Eq. 8.5 gives $k_{\min} = 0.48$. In Schmidt's recommendation, Eq. 8.6 gives $k_{\min} = 0.5$. In EN 1993-4-1(2007), Eq. 8.7 gives $k_{\min} = 0.1$.

According to the two proposed requirements, the required values of $k_{\min}$ that the ring stiffener is required to achieve are explored next. Both linear bifurcation analysis and geometrically nonlinear analysis were conducted using finite element

software ABAQUS. The shell was made of an elastic isotropic material with Young's modulus $E = 2.0\times10^5 MPa$ and Poisson's ratio $\nu = 0.3$.

8.4.1 Linear bifurcation analysis (LBA)

8.4.1.1 Linear bifurcation analysis for cylinders with $r/t = 500$: introduction

Linear bifurcation analysis for cylinders with $r/t = 500$ under wind loading using different sizes of top ring stiffness was performed next.

The relationship between the linear critical stagnation buckling pressure and the bending stiffness coefficient k of the ring stiffener for cylinder with $L/r = 0.5$ is shown in Fig. 8-1. From Fig. 8-1, it may be observed that when k is small, a small increase of k can increase the critical pressure greatly. That is because in this stage, the buckling mode can be effectively restrained by increasing the stiffness coefficient k. Larger values of k can reduce the deformation of the ring stiffener considerably. However, when k is large, the critical load increases only slightly with a further increase of k. That is natural because at this stage, larger values of k do not cause much change to the buckling mode or the deformation of the ring stiffener and thus have only a slight beneficial effect on the buckling strength.

It can be seen from Fig. 8-1 that the buckling pressure increases steadily with continuous increase of k even at very large values of k, so only a very stiff ring may bring the pressure to within 10% of the asymptotic value and it may not be economic to try to achieve pressure too close to the rigid stiffener value.

Based on the numerical results from ABAQUS (Fig. 8-1), a function in terms of Eq. 8.11 can be found to fit the numerical results very precisely:

$$q = q_0 / \left(1 + \frac{a}{k^n}\right) \tag{8.11}$$

where q_0 is the asymptotic critical buckling pressure when k is infinitely large, q is the critical pressure corresponding to a defined value of k, and a is a constant to be found. An excellent fit for $r/t = 500$ and $L/r = 0.5$ is:

$$q = 0.107 / \left(1 + \frac{0.058}{k^{0.36}}\right) \tag{8.12}$$

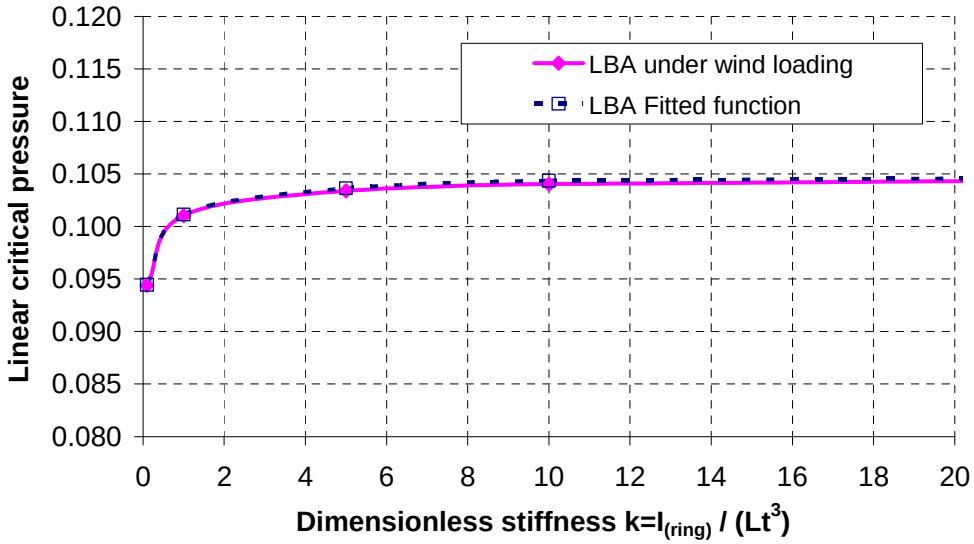

Figure 8-1: Linear critical pressure with changing bending stiffness of the ring stiffener $(r/t = 500, L/r = 0.5)$

The dotted line in Fig. 8-1 shows that Eq. 8.12 fits the numerical results very precisely. The asymptotic value of the critical pressure may be deduced as $q_0 = 0.107 N/mm^2$ and is taken as the reference value in choosing a value for $k_{\min}$. If the ring stiffener is required to provide enough stiffness to achieve a critical buckling pressure q that is only 2% below the asymptotic value q_0, then the minimum value of k is $k_{\min} = 18.2$. If the requirement is related to 5%, then $k_{\min} = 1.31$. If it is further related to 10%, then $k_{\min} = 0.16$. In this way, $k_{\min}$ may be determined according to the critical buckling pressure that is required to be achieved relative to the asymptotic pressure q_0.

The above description gives an insight into a possible method of obtaining a minimum stiffness requirement that has a more rigorous basis than previous attempt to address this problem.

8.4.1.2 Linear bifurcation analysis for cylinders with $r/t = 500$: changing aspect ratios

For cylinders with different values of L/r, the values of $k_{\min}$ can be determined based on the same method.

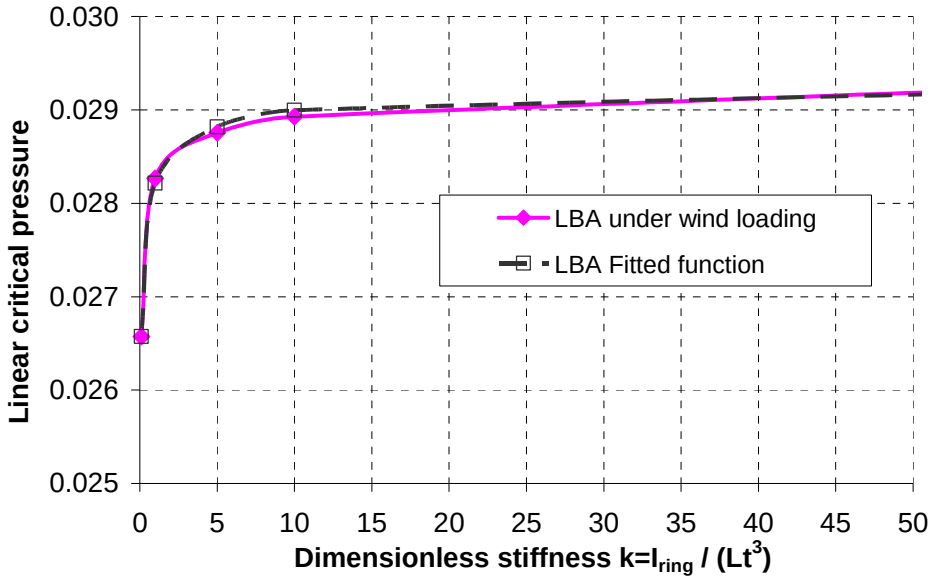

Figure 8-2: Linear critical pressure with changing bending stiffness of the ring stiffener ($r/t = 500, L/r = 2$)

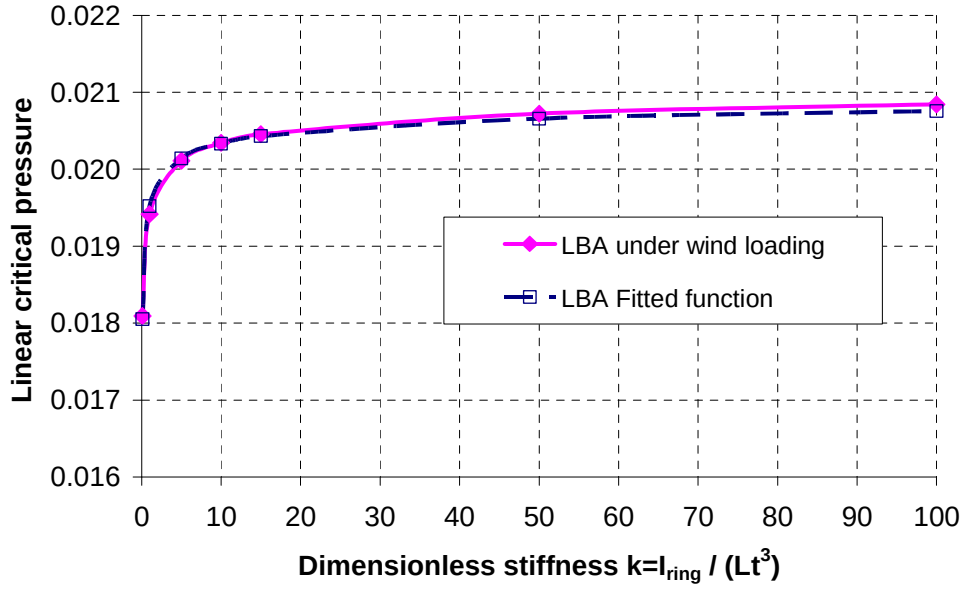

Figure 8-3: Linear critical pressure with changing bending stiffness of the ring stiffener ($r/t = 500, L/r = 3$)

The relationship between the linear critical buckling pressure and the bending stiffness coefficient of the ring stiffener for cylinders with $L/r = 2$ and $L/r = 3$ are shown in Figs 8-2 and 8-3. Based on the numerical results, equations in the form of Eq. 8.11 can be fitted to represent the results accurately. The required values of $k_{\min}$ may then be determined according to the fitted equations and the corresponding asymptotic pressure.

The linear buckling modes of cylinders with $L/r = 0.5$ with different sizes of top ring stiffener are shown in Fig. 8-4(a). When $k = 0.1$, the ring stiffener is partly involved in the overall global circumferential buckling mode and the stiffened cross-section has a noticeable deformation in the stagnation zone. The top cross-section cannot be kept circular because the bending stiffness of the ring stiffener is too low. With increasing values of k, the pattern of the buckling mode is unchanged, but the ring stiffener provides more bending stiffness to restrain the deformation of the shell. The stiffened boundary provides more restraint to prevent buckling and thus increases the buckling strength.

If the critical buckling pressure is required to be within 5% of the asymptotic value, the minimum ring bending stiffness coefficient for cylinders with different values of L/r is shown in Fig. 8-5. The corresponding values, if the requirements are related to 2% and 10% respectively, are also shown in Fig. 8-5.

When $L/r = 0.5$, which corresponds to a stocky cylinder (defined in Chapter 6), as Fig. 8-4(a) shows, the buckling mode is the circumferential buckling mode with changing values of k. The buckle extends over the whole length of the shell. The boundary conditions affect both the buckling mode and the buckling pressure a lot for short cylinders under uniform external pressure. So the critical buckling pressure is affected strongly by any change in k and approaches its asymptotic value at a larger value of k. The minimum ring stiffness coefficient, determined as a percentage reduction below the asymptotic pressure, is thus larger.

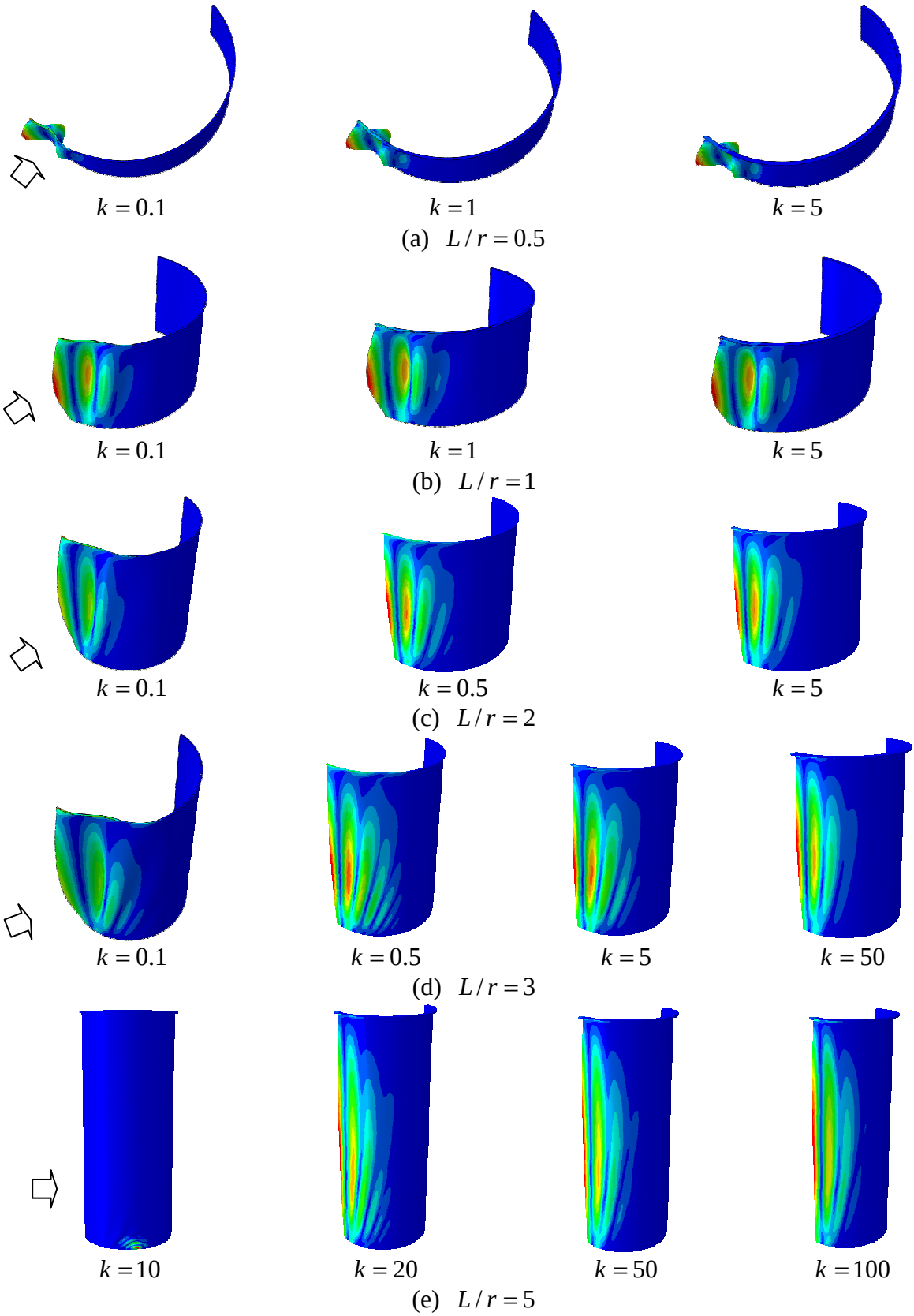

Figure 8-4: Linear buckling modes for stocky cylinders under wind loading with different ring stiffener ($r/t = 500$)

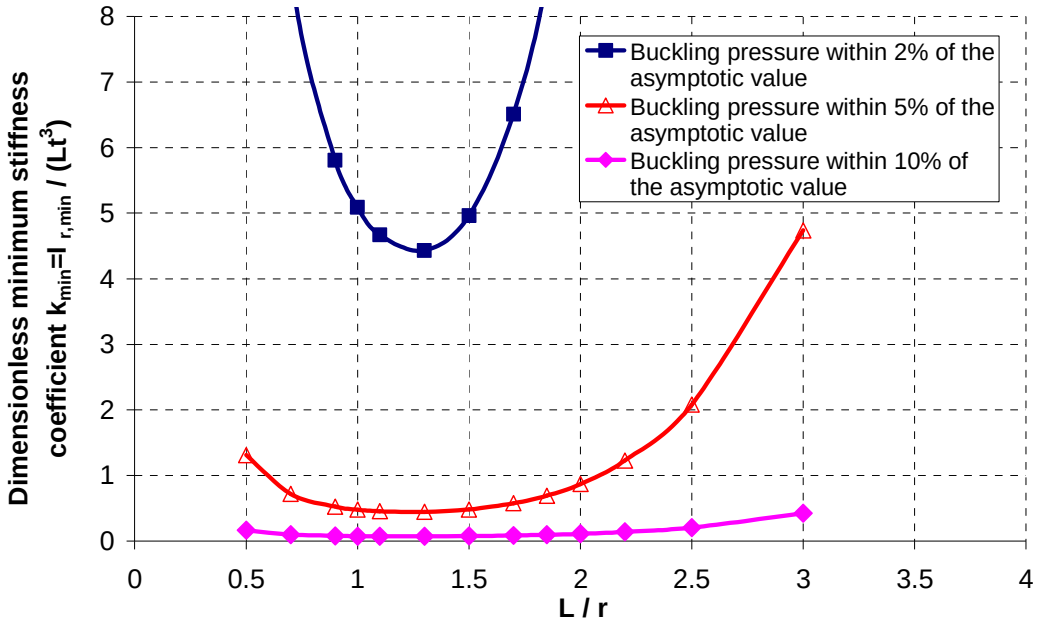

Figure 8-5: Minimum bending stiffness coefficient for cylinders with different L/r if the buckling pressure within 5% of the asymptotic value ($r/t=500$)

When $L/r=1$, which corresponds to a medium-length cylinder, as Fig. 8-4(b) shows, the circumferential buckling mode is the dominant mode for any value of k. When k is small ($k=0.1$), the ring stiffener is significant involved in the global buckling mode and has an obvious deformation. Then with increases in the value of k, the deformation of the ring stiffener is effectively prevented and the buckling strength rises. As described in Chapter 5 for cylinders under uniform external pressure, the effect of the boundary conditions on the buckling behaviour of intermediate aspect ratio cylinders is less significant than for stocky cylinders. So a smaller value of $k_{\min}$ or $L/r=1$ than for $L/r=0.5$ can achieve the required buckling pressure relative to the asymptotic pressure.

When $L/r=2$ and $L/r=3$, as Fig. 8-4(c) and (d) shows, when k is small ($k=0.1$), local buckling of the ring stiffener occurs. When $k=0.5$, although local buckling of the ring stiffener is prevented, the buckling mode is not the circumferential buckling mode, but the shear wall buckling mode with some fold-like buckles up the windward meridian as described in Chapter 6. With a further increase of k, the buckling mode changes to the global circumferential buckling mode. The ring stiffener with a larger bending stiffness changes the membrane stress

distribution and thus the buckling mode. This change is more complex than those for shorter cylinders with $L/r \le 1.5$. That is why in Fig. 8-5, the value of $k_{\min}$ rises as L/r increases in the range $L/r > 1.5$.

When $L/r = 5$, the situation becomes more complex. The linear buckling modes with changing k are shown in Fig. 8-4(e). It can be seen that even when the value of k is quite large ($k = 10$), the linear buckling mode is a local meridional buckling mode at the bottom of the cylinder caused by the large meridional membrane stress at that area. The meridional membrane stress distribution around the circumference at the bottom edge was discussed in Chapter 6. When a really big ring is used ($k = 20$), the buckling mode changes to the mode which is close to circumferential buckling mode, but with some small fold-like buckles following the main buckle on the windward generator. When $k \ge 20$, the buckling mode becomes closer to the circumferential buckling mode and the buckling pressure has no obvious change.

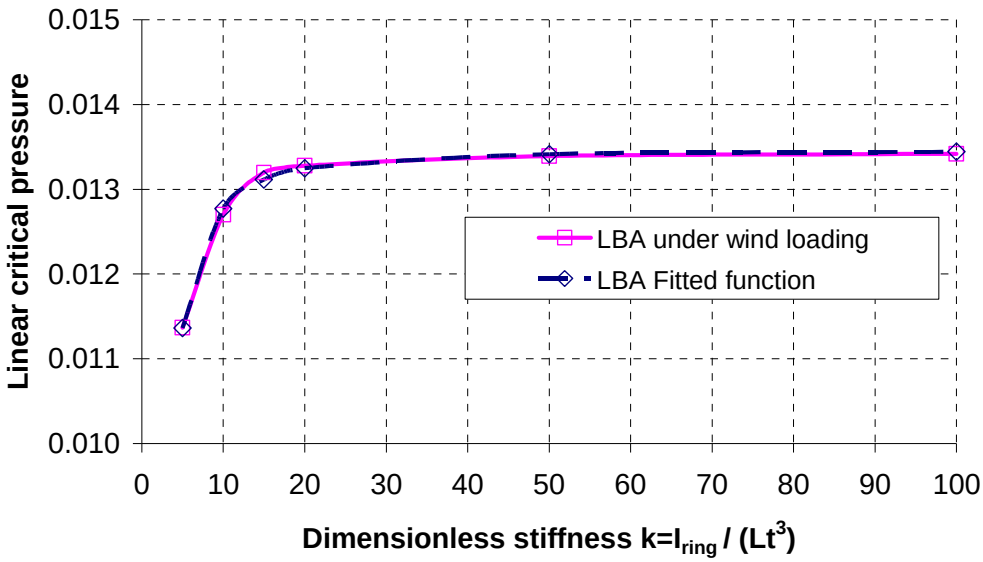

Figure 8-6: Linear critical buckling pressure with changing stiffness of the ring stiffener ($r/t = 500, L/r = 5$)

The relationship between the linear bifurcation critical stagnation pressure and the stiffness coefficient k of the ring stiffener for $L/r = 5$ is shown in Fig. 8-6. For these cylinders, once k is large enough and circumferential global buckling occurs (the second picture of Fig. 8-4e), the buckling pressure has no significant change

with further increase of k and larger values of k have little beneficial effect on the buckling strength. That is because longer cylinders are less influenced by the top boundary than shorter cylinders, but the required value of $k_{\min}$ to form the circumferential global buckling mode is much larger than for shorter cylinders.

When $L/r \geq 5$, the relationship between the linear bifurcation critical stagnation pressure and the stiffness coefficient k of the ring stiffener for $L/r = 6$ and $L/r = 7$ are shown in Figs 8-7 and 8-8. If the ring stiffener is stiff enough, the buckling strength is unaffected by a further increase in k. The formulation in terms of Eq. 8-11 is no longer suitable to fit the numerical results for these cylinders. The minimum values of k using the buckling pressure criterion are not explored further here, because the effect of geometric nonlinearity should be considered for these cylinders. From Figs 8-6 to 8-8, it was found that $k_{\min} = 15$ is a suitable value to adopt for cylinders with $5 \leq L/r \leq 7$ for all three possible buckling pressure criteria (2%, 5% and 10%).

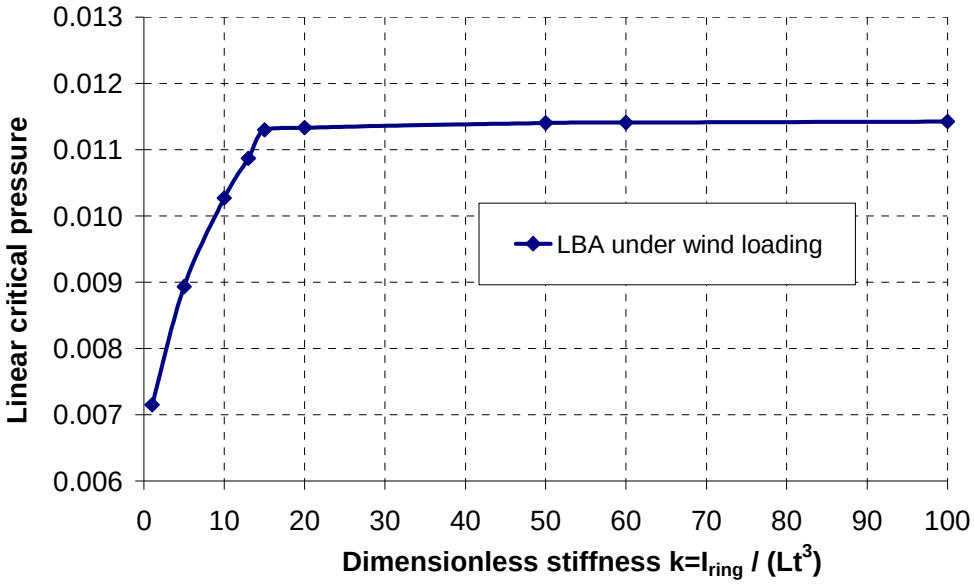

Figure 8-7: Linear critical pressure with changing bending stiffness of the ring stiffener ($r/t = 500, L/r = 6$)

For more slender cylinders, a local linear bifurcation buckling mode may occur at the bottom at the side even if the ring stiffener is rigid. The changes in the linear

buckling mode are more complex. However, for these cylinders, intermediate ring stiffeners are usually adopted in practice, which is outside the scope of this chapter.

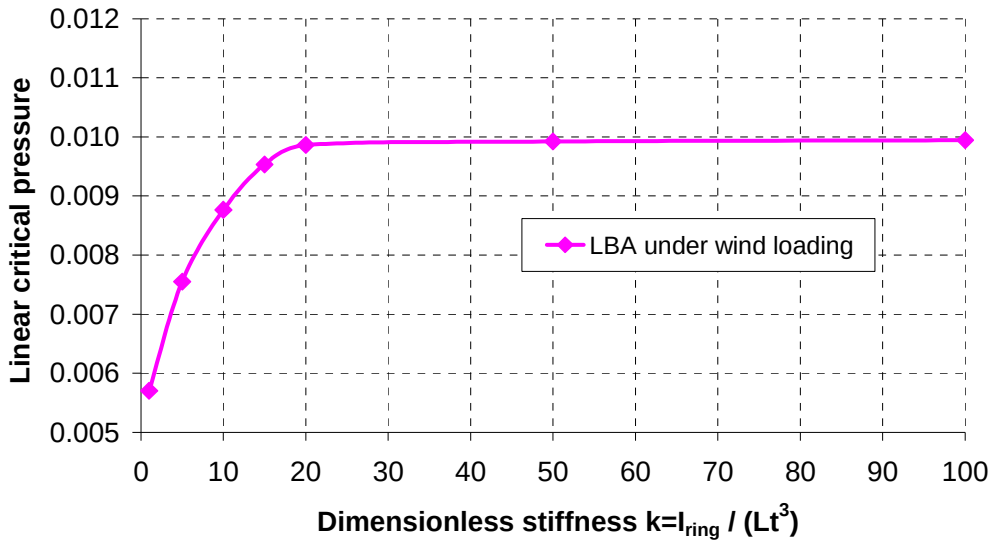

Figure 8-8: Linear critical pressure with changing bending stiffness of the ring stiffener ($r/t = 500, L/r = 7$)

8.4.1.3 Minimum bending stiffness coefficients for thin cylinders with different aspect ratios

Summarizing the results for cylinders with different values of r/t and L/r, and using different buckling pressure evaluation criteria, the minimum bending stiffness coefficients of the ring stiffener can now be determined.

If buckling pressure is required to be only within 10% of the asymptotic value q_0, the minimum bending stiffness coefficient for the ring stiffener for different values of r/t and L/r are shown in Fig. 8-9. The value of $k_{\min} = 0.048$ derived by Blackler (1986) can be used safely for short thin cylinders with $r/t \geq 1000$ in the range $0.5 \leq L/r < 3$. If $r/t = 2000$, a larger range of L/r can be covered by this value of $k_{\min}$. But if the cylinder is quite short ($L/r < 0.5$) or the cylinder is thicker ($r/t \leq 500$), a larger value of $k_{\min}$ is needed.

By contrast, $k_{\min} = 0.48$ derived by Schmidt (1998) and Greiner (2004) is suitable for a wider range of cylinders. However, it still underestimates the required stiffness

of the ring stiffener for comparatively thick and long cylinders, as Fig. 8-9 shows. Here the 10% criterion is adopted to evaluate the required buckling pressure. The buckling strength can be increased significantly by using stiffer rings.

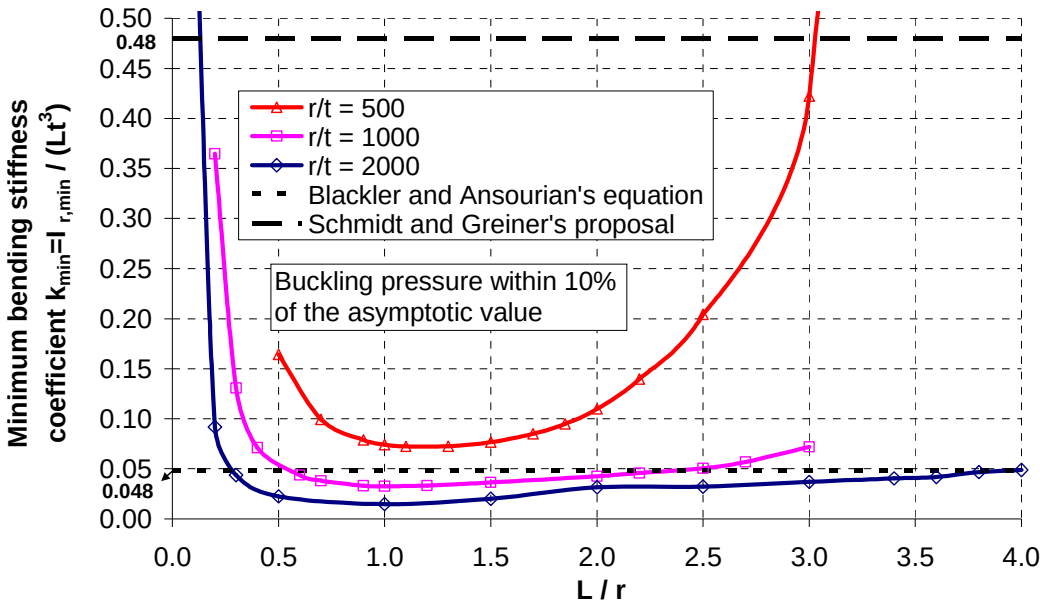

Figure 8-9: Minimum bending stiffness coefficient if the buckling pressure is within 10% of the asymptotic value q_0

For quite short cylinders, the required minimum bending stiffness coefficient $k_{\min}$ can be quite large (Fig. 8-9). As explained before, the buckling mode and buckling pressure are influenced more significantly by boundary conditions for shorter cylinders. The ring is more easily deformed under the larger critical buckling pressure for short cylinder. The value of the buckling pressure rises rapidly in shorter cylinders. The relationship between the dimensionless asymptotic pressure p_{asy} / p_{ref} and the length to radius ratio is shown in Fig. 8-10. The reference pressure p_{ref} is expressed as:

$$p_{ref} = E(r/L)(t/r)^{2.56} \tag{8.13}$$

A steady increase in the bending stiffness of the ring stiffener may significantly increase the buckling pressure for short cylinders, and the asymptotic pressure is thus reached at a higher value of k.

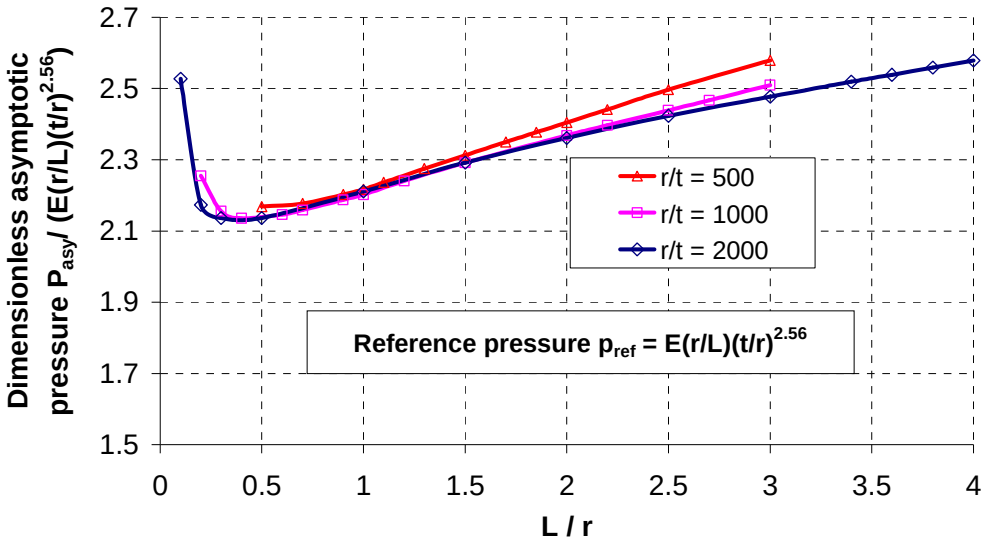

Figure 8-10: The asymptotic pressure with changing length to radius ratio *L / r*

When L/r lies in the intermediate range, the required value of $k_{\min}$ is comparatively stable (Fig. 8-9). The stable range is larger for thinner shells. In this range, the buckling mode is the global circumferential buckling mode. The buckling mode and buckling pressure are both influenced less by changes in L/r.

However, for longer cylinders, the linear buckling mode is affected a lot by the top boundary condition. If the ring is not stiff enough, the buckling mode is the shear buckling mode with several fold-like buckles around the circumference (Fig. 8-4d). Then as the bending stiffness of the ring stiffener is increased, the buckling mode and buckling pressure both change. The above phenomena lead to the asymptotic pressure being reached at a finite but large value of k, so the value of $k_{\min}$ that is needed to achieve the required buckling pressure is large.

If the required buckling pressure is required to be within 5% of the asymptotic value q_0, the minimum bending stiffness coefficient for the ring stiffener $k_{\min}$ for different values of r/t and L/r are shown in Fig. 8-11. The detail of Fig. 8-11 in the range $k_{\min} \le 1$ is shown in Fig. 8-12. It can be seen that $k_{\min} = 0.048$ from Blackler's (1986) equation is now not sufficient to satisfy the stiffness requirement for any geometry. The value $k = 0.48$ from Schmidt (1998) and Greiner's (2004)

proposal is still adequate for some thin shells in a limited range, but for shorter or longer shells, it is not adequate to satisfy the 5% stiffness criterion.

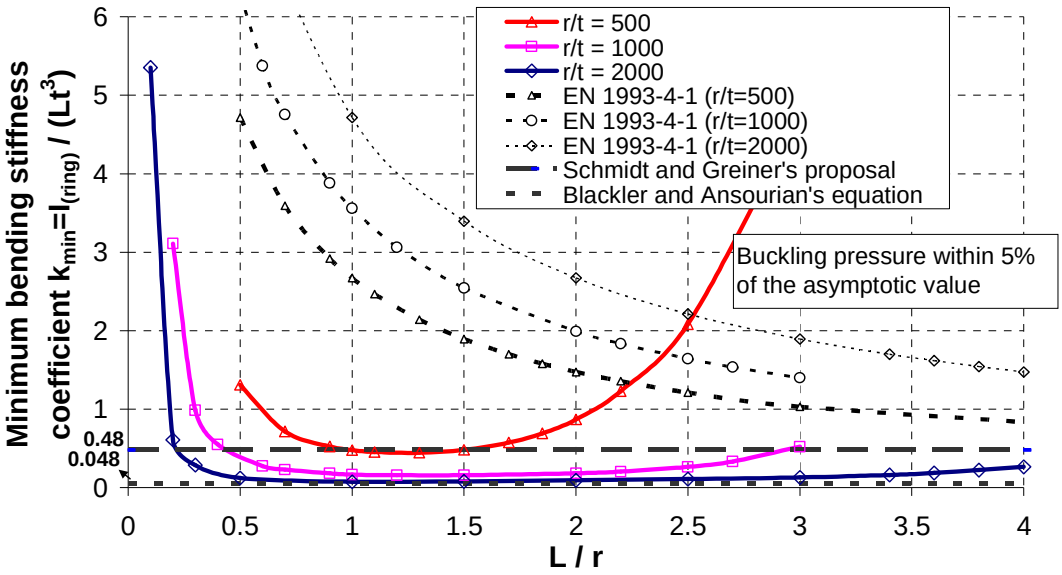

Figure 8-11: Minimum bending stiffness coefficient if the buckling pressure is within 5% of the asymptotic value q_0

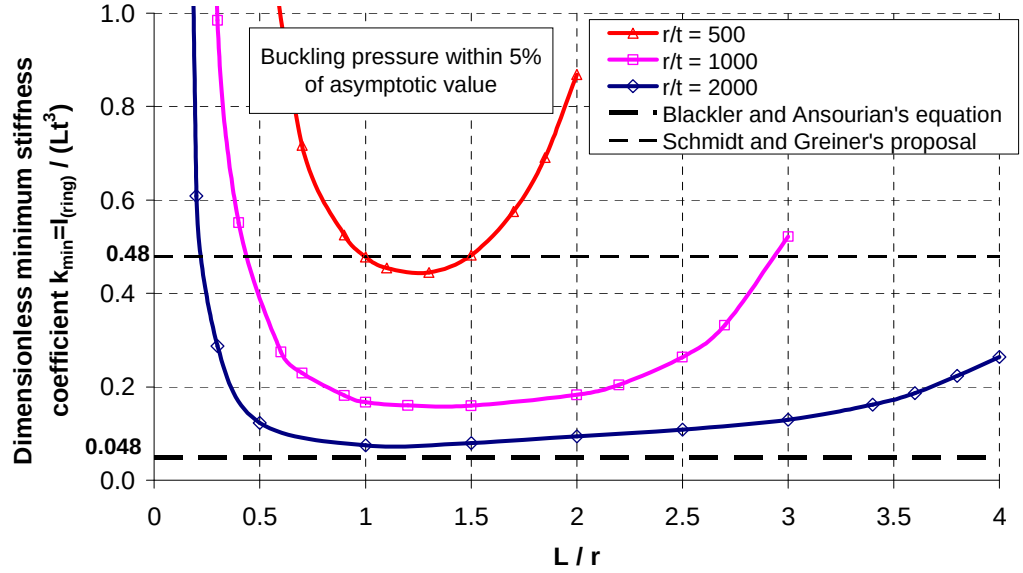

Figure 8-12: Minimum bending stiffness coefficient if the buckling pressure is within 5% of the asymptotic value q_0

The minimum bending stiffness coefficients according to Eqs 8.7 and 8.8 in the European standard on silos EN 1993-4-1 (2007) are also shown in Fig. 8-11. For short cylinders, they satisfy the stiffness requirement of the ring stiffener. However, the values of $k_{\min}$ in EN 1993-4-1 (2007) decrease steadily with increasing L/r, which does not meet the needs of longer cylinders. So for long cylinders, the rule in EN 1993-4-1 (2007) is unsafe. Furthermore, the required value of $k_{\min}$ for thicker cylinders in EN 1993-4-1 (2007) is smaller than that for thinner cylinders, which is also not consistent with these numerical investigations.

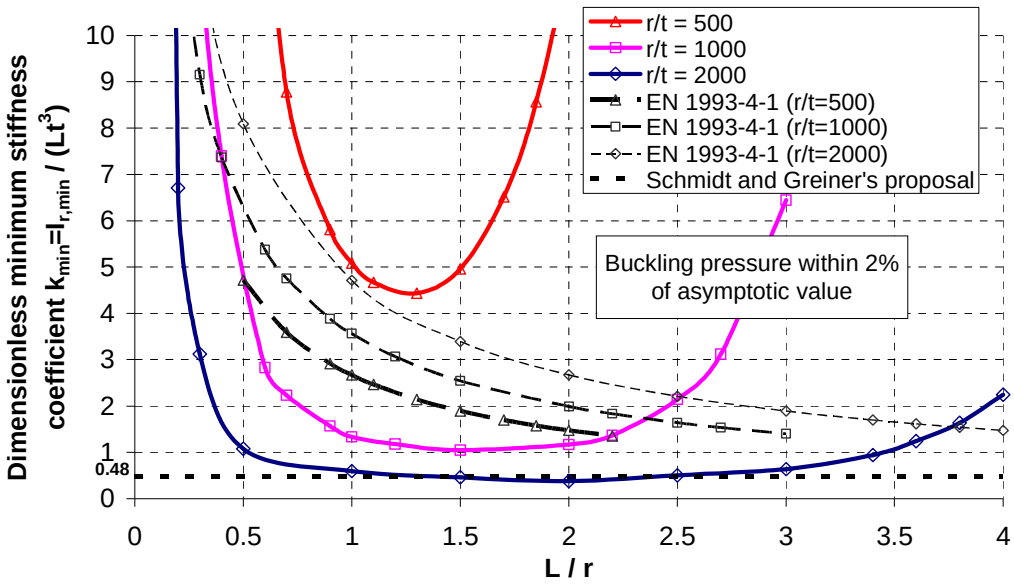

Figure 8-13: Minimum stiffness coefficient if the error of the buckling pressure is within 2% of the asymptotic value

If the required buckling pressure is required to be within 2% of the asymptotic value q_0, the minimum bending stiffness coefficients of the ring stiffener $k_{\min}$ for different values of r/t and L/r rise further and are shown in Fig. 8-13. It can be seen that $k_{\min} = 0.48$ from Schmidt and Greiner's proposal satisfies the stiffness requirement only for very thin cylinders with $r/t = 2000$ over a limited range of L/r. The rules in EN 1993-4-1 (2007) are suitable only for some thin short cylinders.

8.4.1.4 Conclusion

Linear bifurcation analysis was conducted on cylinders with different values of r/t and L/r under wind pressure. The effect of the bending stiffness of the ring stiffener on the buckling pressure was explored. The minimum bending stiffness coefficient of the ring stiffener $k_{\min}$ was determined, depending on how close the critical buckling pressure is required to be to the asymptotic pressure q_0. The results indicate that it is difficult to give a single general rule for all cylinders with different geometries.

Based on Figs 8-11 to 8-13, it is recommended that the chosen value of $k_{\min}$ should lead to buckling pressures that lie within 2% to 5% of the asymptotic pressure. The value of $k_{\min}$ is controlled by different geometric parameters of the shell. For cylinders with $r/t > 1000$ in the range $0.5 \le L/r \le 2$, $k_{\min} = 0.48$ maybe recommended. For cylinders with $500 \le r/t \le 1000$ in the range $0.5 \le L/r < 2$, $k_{\min} = 1$ is recommended. For all cylinders with $L/r < 0.5$, Eqs 8.7 and 8.8 in EN 1993-4-1 (2007) could be adopted. For longer cylinders outside above range, the significant influence of geometric nonlinearity on the buckling strength should be considered. The effect of geometric nonlinearity is discussed next.

8.4.2 Geometrically nonlinear analysis (GNA)

As described in Chapter 6, unlike cylinders under uniform external pressure, geometric nonlinearity plays an important role in affecting the buckling behaviour of cylinders under wind pressure. If effective boundary conditions are adopted, geometric nonlinearity only influences the buckling behaviour of intermediate aspect ratios cylinders as discussed in Chapter 6. However, if the bending stiffness of the ring stiffener is not enough, this influence becomes more complex. How geometric nonlinearity affects the nonlinear buckling behaviour of cylinders under wind pressure as the bending stiffness of the ring stiffener changes is discussed next.

The relationship between the linear and nonlinear critical buckling pressures and the bending stiffness coefficient of the ring stiffener for cylinders with $L/r = 3$ is

shown in Fig. 8-14. The nonlinear buckling modes with changing ring stiffness coefficient k are shown in Fig. 8-15.

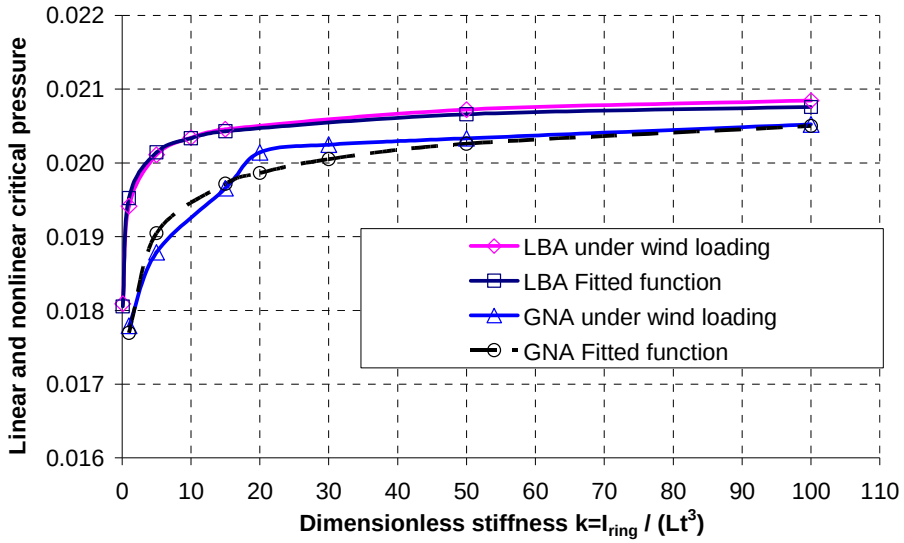

Figure 8-14: Linear and nonlinear critical buckling pressures with changing ring stiffener bending stiffness ($r/t = 500, L/r = 3$)

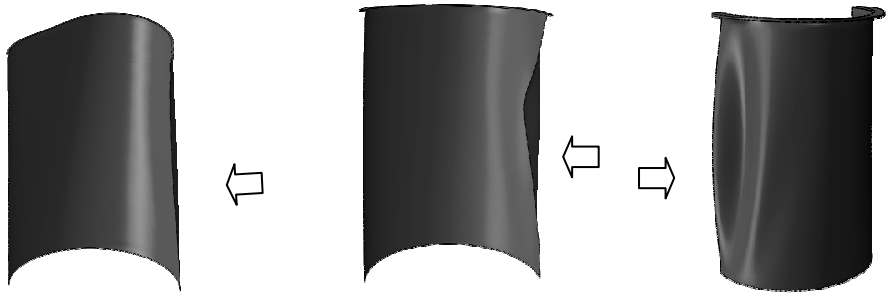

(a) $k = 0.1$ (b) $k = 5$ (c) $k \geq 20$

Figure 8-15: Nonlinear buckling modes with changing stiffness coefficient of the ring stiffener ($r/t = 500, L/r = 3$)

It was found that when k is small ($k = 0.1$), both the linear buckling mode (Fig. 8-4d) and the nonlinear buckling mode (Fig. 8-15a) are local ring buckling modes. The nonlinear critical pressure is 30% smaller than the linear critical pressure. This effect is caused by the pre-buckling ovalization of the ring stiffened cross-section. This situation should be avoided when designing cylindrical shell structures.

With increasing values of k, the linear buckling mode changes to the global buckling mode of the shell wall and the linear critical pressure increases smoothly

and continuously. However, when geometric nonlinearity is included, the buckling behaviour is more complex. The nonlinear buckling mode first changes to a local buckling mode with a long meridional buckle in the upper half of the shell when k has a fairly large value (Fig. 8-15b when $k = 5$), while the corresponding linear buckling mode is the circumferential global buckling mode (Fig. 8-4d). In this situation, geometric nonlinearity has a significant influence, causing a considerable reduction in the buckling pressure (Fig. 8-14).

When $k \geq 20$, the nonlinear buckling mode becomes the circumferential buckling mode of the cylindrical wall, which is similar to the linear buckling mode. The nonlinear critical pressure reaches a stable value and has no significant change with further increase of k. In this range, the ring stiffener can provide an effective restraint to limit the pre-buckling deformations, and the value of the nonlinear critical pressure is close to the linear critical pressure. This is because the linear and nonlinear buckling modes are then similar. Geometric nonlinearity causes a small reduction in the asymptotic buckling pressure, as shown in Fig. 8-14.

The results indicate that the nonlinear buckling behaviour of cylinders under wind pressure is more complex than the linear buckling behaviour when the stiffness of the ring stiffener changes. Different nonlinear buckling modes may occur as the bending stiffness of the ring stiffener is changed. The GNA curve in Fig. 8-14 thus displays a more complicated form as k changes. It is difficult to find a single asymptotic function that can be fitted to the entire curve. However, it was found that when $k \geq 20$, a larger value of k has little beneficial effect to improve the buckling pressure, so $k = 20$ might be chosen as the minimum stiffness coefficient that satisfies the required buckling pressure criterion for all three values of the proximity (2%, 5% and 10%).

The relationship between the linear and the nonlinear critical buckling pressures and the bending stiffness coefficient of the ring stiffener for cylinders with $r/t = 500$ and $L/r = 5$ is shown in Fig. 8-16, which shows a similar characteristic to that for $L/r = 3$. When $k = 5$, the local buckling mode in the upper half of the shell occurs, and the buckling pressure has a rapid increase with a small increase in

k. When k is large enough, the circumferential buckling mode occurs and the buckling pressure reaches a plateau and has no significant change with further increase of k. The value $k = 28$ might be chosen as the minimum stiffness coefficient that satisfies all three possible buckling pressure criteria (2%, 5% and 10%).

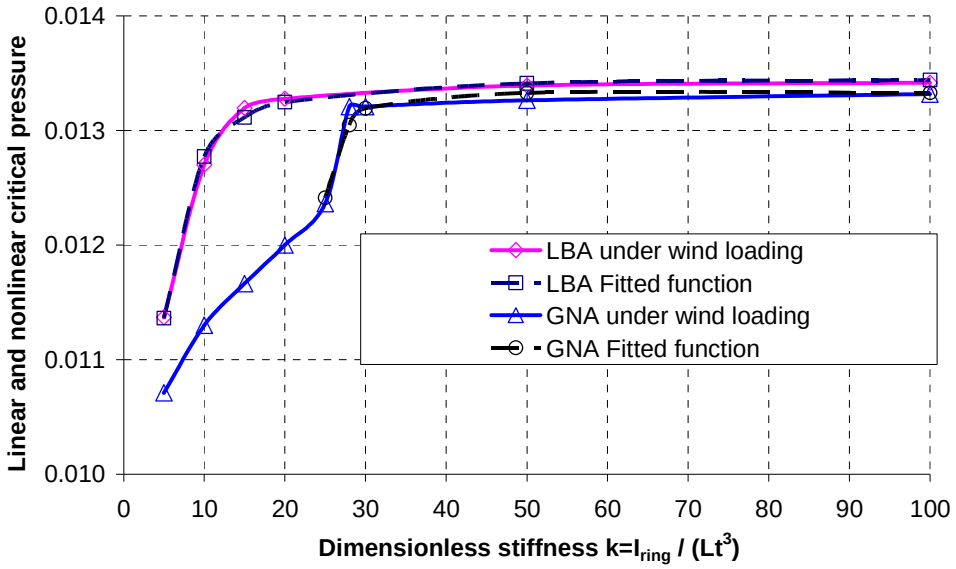

Figure 8-16: Linear and nonlinear critical buckling pressures with changing bending stiffness of the ring stiffener ($r/t = 500, L/r = 5$)

For cylinders with $r/t = 500$ and $L/r = 7$, the situation is different again. The relationship between both the linear and the nonlinear critical buckling pressures and the bending stiffness coefficient k is shown in Fig. 8-17. As the GNA results in Chapter 6 showed, for medium-length cylinders, the nonlinear buckling mode is the local buckling mode in the upper half of the shell even if the ring stiffener is quite stiff. Due to this nonlinear buckling characteristic, the GNA curve in Fig. 8-17 increases smoothly with an increasing value of k. An equation in the form of Eq. 8.11 can again be found to fit the numerical results and the previous buckling pressure criterion can be applied to find minimum stiffness coefficient. However, the resulting value of $k_{\min}$ may be very large (>20), which is not practical.

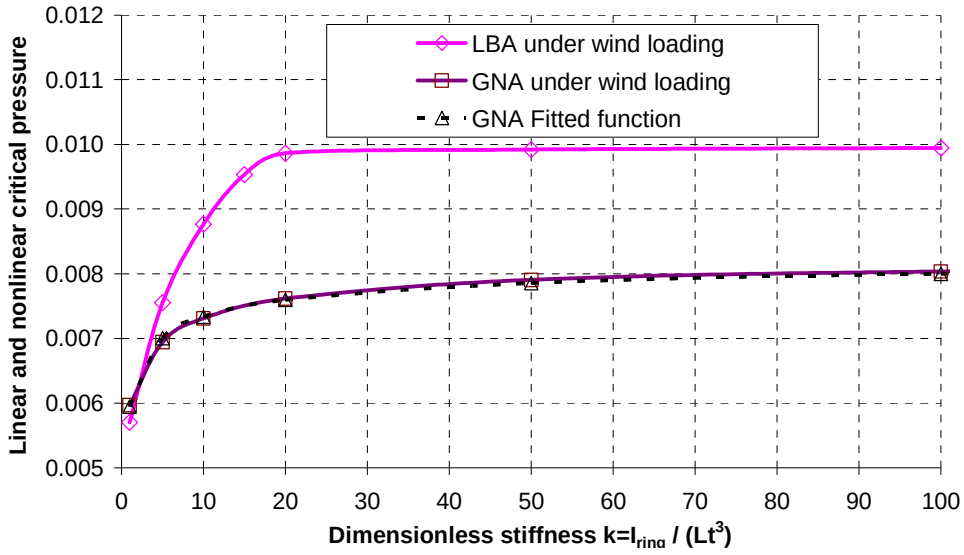

Figure 8-17: Linear and nonlinear critical buckling pressures with changing bending stiffness of the ring stiffener ($r/t=500, L/r=7$)

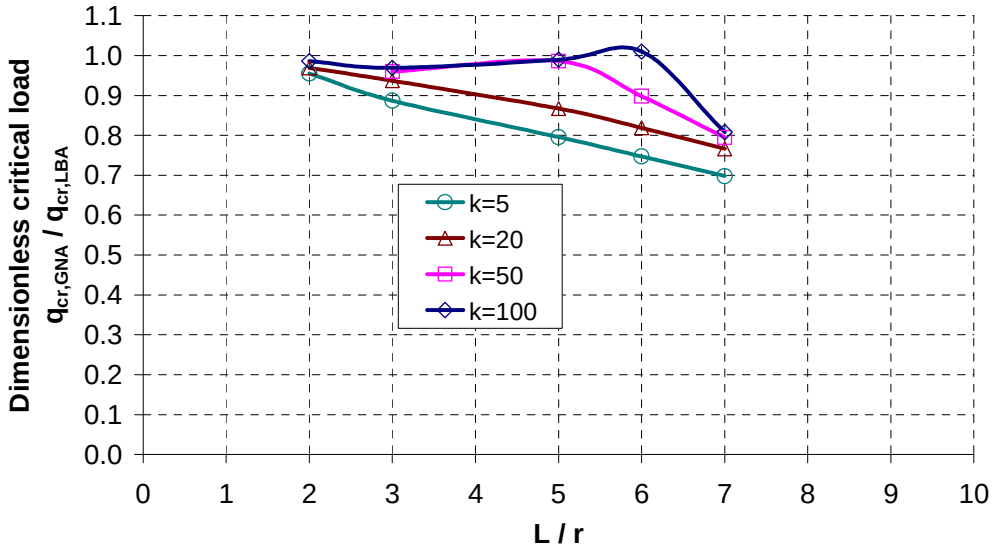

Figure 8-18: The relationship between the dimensionless critical load $q_{cr,GNA}/q_{cr,LBA}$ and L/r using different ring stiffener ($L/r=500$)

The relationship between the dimensionless critical load $q_{cr,GNA}/q_{cr,LBA}$ and L/r for different values of the stiffness coefficient k is shown in Fig. 8-18. Table 8-1 shows the linear and nonlinear buckling modes for cylinders under wind loading with different stiffness coefficient k. It can be seen that for cylinders with different values of L/r and k, the relationship between the linear and the nonlinear buckling

behaviour is different, which arises from the complex buckling behaviour of cylinders under asymmetric wind pressure.

Table 8-1: Linear and nonlinear buckling modes for cylinders under wind pressure with different ring stiffness coefficient k ($r/t = 500$)

L/r	Stiffness coefficient k	Linear buckling modes	Nonlinear Buckling modes
2	5	CBM	CBM
	20	CBM	CBM
	50	CBM	CBM
	100	CBM	CBM
3	5	SBM	LBMU
	20	CBM	CBM
	50	CBM	CBM
	100	CBM	CBM
5	5	LBMB	LBMU
	20	SBM	LBMU
	50	CBM	CBM
	100	CBM	CBM
6	5	LBMB	LBMU
	20	SBM	LBMU
	50	CBM	LBMU
	100	CBM	CBM
7	1	LBMB	LBMU
	5	LBMB	LBMU
	20	SBM	LBMU
	50	CBM	LBMU
	100	CBM	LBMU

CBM-Circumferential buckling mode;
SBM-Shear buckling mode;
LBMB-Local buckling mode at the bottom of leeward meridian;
LBMU-Local buckling mode at the upper half of the shell.

For cylinders in the range $L/r > 2$, geometric nonlinearity clearly influences the buckling behaviour significantly, depending on the bending stiffness of the ring stiffener. To reduce the effect of geometric nonlinearity on the buckling strength, a very large ring bending stiffness is required, but it is not practical to adopt ring stiffeners with disproportionate geometries. So a balance is needed between the geometry of the ring stiffener and the buckling pressure to be achieved with this ring stiffener. Examining the results of Figs 8-14 to 8-18, a balanced recommendation might be that $k_{\min} = 20$ as a single approximate value for these geometries.

8.5 Conclusion

Most shell buckling strength predictions and design rules assume single boundary conditions. The boundary condition at the top of a cylindrical silo or tank can only be kept circular by using a stiff ring. The minimum stiffness of the ring to achieve the assumed boundary condition has been studied.

Due to the complexity of the buckling behaviour, it is not easy to give a simple conclusion for this problem. LBA and GNA analyses were conducted separately. A new criterion was proposed to produce rings that allow the buckling pressure to approach the ideal value. The following rules were proposed on the basis of the results:

For cylinders with $r/t > 1000$ and $0.5 \le L/r \le 2$, $k_{\min} = 0.48$ is recommended. For cylinders with $500 \le r/t \le 1000$ and $0.5 \le L/r \le 2$, $k_{\min} = 1$ is recommended. For all cylinders with $L/r < 0.5$, Eqs 8.7 and 8.8 in EN 1993-4-1 (2007) could be adopted. For cylinders with $r/t \ge 500$ and $L/r > 2$, a large value $k_{\min} = 20$ is recommended due to the significant influence of geometric nonlinearity.

Chapter 9 Summary and Conclusions

9.1 Summary

Cylindrical shell structures are widely used in many fields. The strength of a shell structure is often controlled by buckling failure. The loading conditions for these shells are quite varied depending on the function of the shell. This thesis presented the buckling analysis of cylindrical shell structures under several different loading conditions.

Different shell buckling problems were investigated to give a comprehensive understanding of the shell buckling phenomenon. The historical and current developments for shell buckling research were generalized. The imperfection-sensitivity study of thin cylindrical shells, the elastic-plastic behaviour of thicker shells and the contents of shell buckling in EN 1993-1-6 (2007) were all reviewed.

Though the buckling of cylinders under axial compression is one of the most popular topics in shell buckling analysis, it is not the main theme in this thesis. For the axial compression buckling problem, current research and developments were discussed and outlined briefly. The buckling analyses of an imperfect elastic cylindrical shell with an imperfection in terms of either the perfect shell buckling eigenmode or a weld Type A depression were conducted using the finite element software ABAQUS. The results show the high sensitivity of the elastic buckling strength of a thin-walled cylindrical shell to initial imperfections, which corresponds to the well known conclusions in many publications and books. The results also indicate the effectiveness and accuracy of ABAQUS in performing nonlinear shell buckling analysis.

Due to the complexity and expense of the detailed careful experiments needed in this filed and the complexity of the theoretical algebraic analysis, most results in this thesis are based on numerical results derived from the powerful nonlinear finite element software ABAQUS. However, both engineers and researchers should understand the mechanical behaviour of the structure well for every buckling

problem, so the important aspects of the finite element analysis, such as the mesh, the elements, the boundary conditions and the analysis method are well understood and correctly applied to obtain accurate and reliable results for engineering design.

This thesis presented a series of related studies, including cylindrical shells under global bending, uniform external pressure and wind loading. These dealt with topics which overlap but which are commonly seen as distinct.

The final target was the behaviour of stepped-wall cylinders under wind loading, but this complex problem involves many separate aspects, each of which is worthy of a careful separate study.

Unsymmetrical loads lead to global bending, so a major study of elastic imperfect elastic-plastic cylinders with a wide range of thicknesses was thoroughly explored. Wind pressure produces external pressure conditions, so an extended study of externally pressurised cylinders of different lengths and thicknesses with different boundary conditions was undertaken. The effect of stepped walls on the buckling behaviour of cylinders under uniform external pressure was then extensively explored. Finally, both uniform and stepped wall cylinders under wind loading were related to the other studies. To complete the group, the requirements for an eaves ring stiffener under wind loading were extensively investigated.

All of these studies considered linear and nonlinear behaviour and imperfection sensitivity where appropriate. All these investigations involved comprehensive parametric studies that explore the full complexity of the behaviour and all led to new design recommendations suitable for inclusion in the European Standard EN 1993-1-6 (2007) on shell structures and in the European Recommendations of the ECCS.

9.2 Conclusions

9.2.1 Cylindrical shells under global bending

9.2.1.1 Buckling behavior of elastic cylindrical shells

Global bending is one of the common loading conditions in structural applications, such as chimneys, wind generation towers, tubular piles and tall silos. The nonlinear stability analysis of cylindrical shells under global bending with different aspect ratios was performed in Chapter 3. The buckling behaviour has the following characteristics:

- For short cylinders (except extremely short cylinders), local bifurcation buckling at the middle most compressed side of the shell occurs. There is little ovalization and the critical bending moment from GNA is close to the elastic critical reference moment M_{cr}. For extremely short cylinders, local snap-through buckling near the boundaries occurs due to the restraint of the boundary conditions, the critical bending moment may be several times larger than the elastic critical moment M_{cr}.

- For medium-length cylinders, a combination of ovalization instability and bifurcation instability occurs. The influence of ovalization of the cross-section should be emphasized because it may lead to a considerable reduction to the elastic critical moment. Longer cylinders display more obvious ovalization in the pre-buckling stage, leading to more significant reductions in the critical moment.

- For long cylinders, bifurcation buckling appears just before the snap-through buckling point and the two points are almost indistinguishable. The critical bending moment is approximately equal to the Brazier moment, when full ovalization of the cross-section develops.

- Geometric imperfections cause a considerable strength reduction for long elastic cylinders under global bending. Bifurcation buckling occurs at a reduced critical moment, leading to an alleviation of the ovalization of the

cross-section. The imperfection sensitivity study for medium-length cylinders with no obvious ovalization of the cross-section was investigated in Chapter 4.

It should be noted that for thick and short cylinders, plasticity might be involved in the buckling behaviour due to the high local bending stress concentration, which was discussed in Chapter 4.

9.2.1.2 Buckling behavior of medium-length cylindrical shells in the elastic-plastic range

For medium-length cylinders under global bending, plasticity may influence the failure behaviour. Either elastic-plastic buckling or yield failure may occur, depending on the specific geometry. Geometrically and materially nonlinear analyses were performed on thin cylindrical shells of moderate length under either pure global bending or combined axial compression and global bending in Chapter 4. Rotter and Teng's (1989) axi-symmetric Type A weld imperfection was adopted throughout this study. The following conclusions were obtained:

- The results of an imperfection-sensitivity study of cylindrical shells of moderate length under global bending in the elastic-plastic range indicate that elastic bifurcation buckling occurs in thin cylinders and plastic yield occurs in thick cylinders. For cylinders of moderate radius to thickness ratio, elastic-plastic bifurcation buckling occurs. The generalised capacity curves of EN 1993-1-6 (2007) were exploited to describe these different buckling behaviours. The capacity curves describe the relationship between the buckling strength and the relative slenderness. The buckling parameters: such as the elastic imperfection sensitivity factor α, plastic range factor β and interaction exponent η, were extracted with precision and are able to describe the capacity curves accurately.

- Two different material hardening models were studied to investigate the influence of material hardening on the buckling behaviour. By comparing the results for the three different material models, it can be concluded that

for very thin cylinders with $r/t \geq 500$, elastic bifurcation buckling occurs and plasticity has no influence on the buckling strength. For thicker cylinders with failure dominated by the plastic yield or elastic-plastic buckling, plasticity affects the buckling strength depending on the specific value of r/t. Strain hardening may increase the collapse moment for thick shells depending on how the strain hardening material behaviour is defined in the stress-strain curve. For cylinders with $r/t > 200$, the influence of any strain hardening on the collapse load is very small, irrespective of the hardening model.

- For cylindrical shells under combined global bending and axial compression in the elastic-plastic range, two different buckling modes may occur: "snap-through" or bifurcation buckling. Which one occurs depends on the specific geometry and loading condition. Interaction curves for axial compression and global bending were derived. The best fit interaction expressions derived from this study can be used to describe the interaction curves with much accuracy.

9.2.2 Cylindrical shells under uniform external pressure

Uniform cylindrical shells under uniform external pressure have been well studied by many researchers. The critical buckling stresses for short, medium-length and long cylinders are well defined in EN 1993-1-6 (2007). However, the external pressure buckling factor $C_{\theta s}$ for short cylinders takes no account of the meridional rotational restraint at boundaries. The results of Chapter 5 indicate that restraint of meridional end rotation increases the buckling strength, so new expressions of $C_{\theta s}$ that consider the meridional end rotation with the assumption of membrane pre-buckling stress were obtained for different boundary conditions.

In another aspect, the classical solutions are based on the assumption of a membrane pre-buckling stress state which is satisfactory for medium-long and long cylinders but not accurate for short cylinders. This assumption requires no restraint at the boundaries against displacements normal to the shell surface in the pre-buckling

stage, which is not practical for short cylinders. The results indicate that pre-buckling bending deformations have a significant influence on the buckling strength for very short cylinders, while for cylinders with $\omega > 5$, this effect is negligible.

9.2.3 Cylindrical shells of uniform thickness under wind pressure

The buckling behaviour of cylindrical shells under asymmetric wind pressure is quite complex. Cylinders with different aspect ratios may display totally different buckling behaviours. For cylinders under uniform external pressure, geometric nonlinearity has little effect on the buckling behaviour due to the small pre-buckling deformation, while the pre-buckling deformations may be large for cylinders under wind pressure and thence influence the buckling behaviour significantly. The linear buckling mode and the nonlinear buckling mode may be quite different. Linear bifurcation analysis (LBA) and geometrically nonlinear analysis (GNA) were performed in Chapter 6 to investigate the buckling behaviour of shells with different geometries comprehensively. The influence of material nonlinearity and imperfection sensitivity was also explored. The analyses focused on practical geometries used for silos and tanks. The results are summarized as follows:

- The results of LBA indicated that for stocky cylinders, the linear buckling modes are the circumferential buckling mode which is similar to cylinders under uniform external pressure. For intermediate long cylinders, it changes to a global buckling mode with a main buckle on the windward meridian caused by the combination of circumferential compressive stress and axial compressive stress, and then this global shear buckling mode changes to a local buckling mode at the bottom of the shell as the shell becomes more slender.

- For short cylinders with $\Omega = (L/r)(t/r)^{1/2} \leq 0.4$, the linear bifurcation critical buckling pressures of cylinders under uniform external pressure and wind pressure can be expressed in terms of the dimensionless length parameter Ω as $q_{w,LBA}/q_{u,LBA} = 1.90\Omega^{0.13}$. By using this equation and the general buckling resistance equations for cylinders under uniform external

pressure in EN 1993-1-6 (2007), the critical buckling pressure for cylinders under wind loading can be calculated accurately and directly.

- For short cylinders, geometric nonlinearity has little effect on the buckling mode and buckling strength. However, for intermediate long cylinders, geometric nonlinearity may play a significant role in affecting the buckling behaviour. Ovalization of the cross-section leads to a reduction in the buckling resistance under axial compressive stresses causing either snap-through buckling or local meridional short wavelength bifurcation buckles. The nonlinear critical buckling pressure can also be related to the general buckling resistance equations for cylinders under uniform external pressure in EN 1993-1-6 (2007).

- Material plasticity only affects the buckling behaviour of thick cylinders. For thin cylinders with $r/t \geq 500$, it has no effect on the buckling mode and buckling strength at all.

- Imperfection sensitivity is a complex problem for cylinders under wind loading, because the nonlinear buckling mode is very variable for cylinders of different aspect ratios. The failure mode may change greatly with a change in the geometric parameters. The imperfection sensitivity depends on the failure mode. For stocky cylinders, the nonlinear buckling mode is the circumferential compressive buckling mode, which is similar to the linear buckling mode, so the shell responds most sensitively to both the eigenmode imperfection and the nonlinear buckling mode imperfection. For intermediate aspect ratio cylinders, the nonlinear buckling mode is different from the linear buckling mode, so these cylinders respond most sensitively to the imperfections in the form of the nonlinear buckling mode. However, it is difficult to find an imperfection form that is both practical and detrimental.

9.2.4 Cylindrical shells of stepwise varying thickness under external pressure

For cylindrical shells of stepwise varying thickness under either uniform external pressure or asymptotic pressure, the method in DIN 18800 (1990) and EN 1993-1-6 (2007) is rather awkward for the practical design of silos and tanks. In Chapter 7, a new "weighted smeared wall method", which is based on an idea proposed by Trahair et al. (1983) for stepped wall cylinders under external pressure, was introduced. It has produced a new design method that can give accurate results for a wide range of shell structures and is much easier to use than that in DIN 18800 (1990), EN 1993-1-6 (2007) or ECCS EDR5 (2008). The following conclusions were obtained:

- The weighted smeared wall method can accurately determine both the critical buckling mode and the buckling pressure.

- Three categories of buckling mode have been identified: whole wall buckling, mixed thickness buckling, and top thinnest zone buckling. Which one is critical depends on the specific wall thickness distribution.

- A new design method has been presented and verified over a huge number of designs. It gives accurate results for a very wide range of shell walls and is much easier to use than that of Greiner (1981). The direct predictions can be enhanced by minor modifications that account for adjacent restraint effects.

- For stepped wall cylinders under wind loading leading to the circumferential buckling mode, the relationship of the critical buckling pressure for stocky cylinders of uniform thickness under uniform external pressure and wind loading is still applicable. The weighted smeared wall method can be used to evaluate the critical buckling pressure.

9.2.5 Requirement of the minimum bending stiffness of the ring stiffener for cylindrical shells under wind pressure

A ring stiffener is usually used at the tope edge eaves junction of tanks and silos to provide the top boundary. In practical design, the stiffness of this ring stiffener should be designed against local buckling in the ring stiffener, and the ring stiffener also needs to keep the circularity of the top edge when global shell wall buckling occurs. The requirement of the minimum bending stiffness of the ring stiffener for cylindrical shells under wind pressure was investigated in Chapter 8. Cylindrical shells with different aspect ratios were studied. The influence of the bending stiffness of the ring stiffener on the buckling behaviour of each cylinder was investigated. Both linear bifurcation analysis (LBA) and geometrically nonlinear analysis (GNA) were performed and presented separately. A new criterion is recommended to determine the minimum stiffness that should be used in design as follows:

- For cylinders with $r/t > 1000$ and $0.5 \le L/r \le 2$, $I^*_{r,\min} = 0.48\ell t^3$ is recommended. For cylinders with $500 \le r/t \le 1000$ and $0.5 \le L/r \le 2$, $I^*_{r,\min} = \ell t^3$ is recommended. For all cylinders with $L/r < 0.5$, the rule in EN 1993-4-1 (2007) could be adopted.

- For cylinders with $r/t \ge 500$ and $L/r > 2$, a large value $I^*_{r,\min} = 20\ell t^3$ is recommended due to the significant influence of geometric nonlinearity.

9.3 Future research

This thesis has presented a comprehensive study of the buckling behaviour of cylindrical shells under different loading conditions. Many practical problems were explored. Different buckling behaviours were investigated. Due to the complex mechanical behaviour of shell structures, many shell buckling problems are usually difficult to understand completely, and some questions need to be answered apart from those discussed in this thesis.

For cylindrical shells under global bending, the full plastic moment defined according to small displacement theory was adopted as the plastic reference

resistance throughout the study. However, due to the complex bending and stretching behaviour of the shell in bending, this definition seems to cause some unexpected problems which are represented in the capacity curves as described in Chapter 4. So a better definition of the plastic reference resistance should be found to improve the capacity curves.

Buckling analysis for cylindrical shells under wind pressure is a complex problem. Many aspects of the buckling behaviour are still not understood completely yet. For cylinders under symmetric loading conditions, such as uniform axial compression and uniform external pressure, EN 1993-1-6 (2007) has clear definitions of the buckling stress as well as the buckling parameters. These definitions are based on extensive researches and well understood. By contrast, for cylindrical shells under wind loading, the information in EN 1993-1-6 (2007) is inadequate. There are many aspects that are not even mentioned in either EN 1993-1-6 (2007) or ECCS EDR5 (2008). Based on the study in Chapter 6, the following aspects need to be explored or improved in future research:

- For high aspect ratio cylinders where the geometric parameters are beyond the range of Chapter 6, the linear buckling behaviour and the nonlinear buckling behaviour need to be studied. The buckling behaviour of slender cylinders has been shown to be different from stocky and intermediate aspect ratio cylinders (Schneider, 2001).

- Imperfection sensitivity plays an important role in shell buckling analysis. However, due to the complexity of the buckling behaviour of cylinders under wind pressure, it is difficult to find an appropriate imperfection form for common use. Cylinders with different geometries may display different buckling behaviour and thus respond most sensitively to different imperfection forms. So it is not simple to define a practical and worst imperfection form for a cylinder under wind loading.

- To study the imperfection-sensitivity of cylindrical shells under dynamic loads such as periodic load or earthquake loads in the elastic-plastic range.

As to the cylindrical shells of stepwise varying wall thickness under either uniform external pressure or wind loading, the weighted smeared wall method was introduced to predict the buckling mode and the buckling strength. However, there are also some problems in this method. The weighted smeared wall method is based on the assumption that the boundaries of the buckle are simply-supported, the shape of the buckle is in the form of a half sine wave vertically, and the restraining effect of the strakes below the buckle is neglected. This assumption results in the calculated results that always have slight difference from the accurate results. Though accurate prediction has been achieved by empirical equations, a good approach considering the influence of the restraint below the buckle may be found to improve the weighted smeared wall method.

References

1. Abdelmoula, R. and Leger, A. (2008) “Singular perturbation analysis of the buckling of circular cylindrical shells.” European Journal of Mechanics A/Solids,27 (2008), pp706-729.

2. ACI 313-91 (1991) “Standard Practice for Design and Construction of Concrete Silos and Stacking Tubes for Storing Granular Materials”, ACI 313-91, with Commentary (ACI 313R-91) American Concrete Institute, Detroit, 27pp.

3. Adam Jan Sadowski (2010) “Modelling of failures in thin-walled metal silos under eccentric discharge” Phd thesis, Institute of Infrastructure and Environment, University of Edinburgh, Edinburgh.

4. Almroth, B.O. (1963) “Postbuckling Behavior of Axially Compressed Circular Cylinders”, AIAA Journal, March 1963, Vol. 1, No. 3, pp. 630-633

5. Almroth, B.O. (1966) “Influence of Edge Conditions on the Stability of Axially Compressed Cylindrical Shells”, Journal of the American Institute of Aeronautics and Astronautics, Vol. 4, No. 1, pp 134-140.

6. Almroth, B.O. (1966) “Influences of Imperfections and Edge Restraints on the Buckling of Cylindrical Shells under Axial Compression”. CR-432, NASA.

7. Amazigo, J.C. (1969) “Buckling under Axial Compression of Long Cylindrical Shells with Random Axisymmetric Imperfections”, Quart. Appl. Math., Vol. 26, pp 537-566.

8. Ansourian, P. (2004) “Cylindrical shells under non-uniform external pressure”, in Buckling of Thin Metal Shells, eds J.G. Teng & J.M. Rotter, Spon, London, pp 175-197.

9. ANSI (1982) “Minimum design loads for building s and other structures, ANSI A58.1”, American National Standards Institutte, New York, NY.

10. API STD 650 Welded Tanks for Oil Storage, American Petroleum Institute, 2007.

11. AS3774-1996 (1996) “Loads on Bulk Solids Containers”, Australian Standard, Standards Association of Australia, Sydney, October.

12. Axelrad, E.L. (1962) “Flexure and instability of thin-walled pressurized tubes”, Izvestiya Akademii Nauk SSSR, Otdelenie Tekhnicheskikh Nauk, Mekhanika i Mashinostroenie 1, 98–114, in Russian.

13. Axelrad, E.L. (1965) “Refinement of buckling-load analysis for tube flexure by way of considering precritical deformation”, Izvestiya Akademii Nauk SSSR, Otdelenie Tekhnicheskikh Nauk, Mekhanika i Mashinostroenie 4, 133–139, in Russian.

14. Axelrad, E.L. and Emmerling, F.A. (1984) “Collapse load of elastic tubes under bending”, Isr. J. Technol. 22, 89–94.

15. Bardi F.C., Yun, H.D. and Kyriakides S. (2003) “On the axisymmetric progressive crushing of circular tubes under axial compression”, International Journal of Solids and Structures, 40 (2003), 3137–3155.

16. Batdorf, S.B. (1947) A simplified method of elastic stability analysis for thin cylindrical shells. NACA TN No.1341.

17. Bathe, K.L. and Wilson, E.L. (1976) “Numerical Methods in Finite Element Analysis”, Prentice Hall, Inc. Englewood Cliffs, New Jersey.

18. Batterman, S.C. (1965) “Plastic buckling of axially compressed cylindrical shells”, AIAA Journal, 3 (1965), 316–325.

19. Blachut, J. (1998) “Some Recent Developments in Strength and Buckling of Pressure Vessel Components”, Progress in Structural Engineering and Materials, Vol. 1, No. 4, July, pp 418-427.

20. Blackler, M.J. (1986) “Stability of Silos and Tanks under Internal and External Pressure”, PhD Thesis, School of Civil and Mining Engineering, University of Sydney, Australia.

21. Brazier, L.G. (1927) “On the flexure of thin cylindrical shells and other ‘thin’ sections”, Proc. Roy. Soc. London Series A, 116, 104-114.

22. Brush, D.O. (1968) “Imperfection sensitivity of stringer stiffened cylinders”, AIAA Journal 6(12), 2445-2447.

23. Brush, D.O. and Almroth, B.O. (1975) “Buckling of Bars, Plates and Shells”, McGraw-Hill, New York.

24. BSI (1972) “Code of basic data for the design of buildings, Ch.5, Part 2, Wind Loads”, BSI CP3, British Standards Institution, London.

25. Budiansky, B. and Sanders, J.L. (1963) “On the 'Best' First Order Linear Shell Theory”, Progress in Applied Mechanics, The Prager Anniversary Volume, Macmillan, New York, pp 129-140.

26. Burns, A.B. (1966) “Structural optimization on axially compressed cylinders, considering ring-stiffener eccentricity effects”, Journal of Spacecraft and Rockets 3(8), 1263-1268.

27. Bushnell, D. (1985) “Computerized buckling analysis of shells”, Martinus Nijhoff Publishes, Dordrecht.

28. Cai, M.J. (2003) “Buckling of cylindrical shells under non-uniform loads”, PhD Thesis, Institute for Infrastructure and Environment, University of Edinburgh.

29. Calladine, C.R. (1983) Theory of Shell Structures, Cambridge University Press, Cambridge.

30. Chen, L., Doerich, C. and Rotter, J.M. (2008) “A Study of Cylindrical Shells under Global Bending in the Elastic-Plastic Range”, Steel Construction—Design and Research, 1 (2008), 59-65.

31. Chen, Y.N. and Kempner, J. (1976) “Buckling of oval cylindrical shells under compression and asymmetric bending”, AIAA Journal 14, 1235–1240.

32. Cheung, N.J. and Melbourne, W.H. (1983) “Turbulence effects on some aerodynamic parameters of a circular cylinder at supercritical Reynolds numbers”, Jouranl of Wind Engineering and Industrial Aerodynamics, Vol. 14, pp 399-410.

33. Clough, R.W. (1960) “The Finite Element Method in Plane Stress Analysis”, Proceeding of 2nd ASCE Conference on Electronic Computation, Pittsburg, PA, September, 1960.

34. Cohen, G.A. (1971) “Computer Analysis of Imperfection Sensitivity of Ring-Stiffened Orthotropic Shells of Revolution”, Journal of the American Institute of Aeronautics and Astronautics, Vol. 9, pp 1032-1039.

35. Combescure, A. (1986) “Static and dynamic buckling of large thin shells”, Nuclear Engineering and Design, Vol. 92, pp 339-354.

36. Cook N.J. and Redfearn, D. (1980). “Full-scale wind pressure measurements on cylindrical silos: a preliminary report”, Department of the Environment Note No. N103/80, Building Research Establishment, September.

37. Corona, E. and Kyriakides, S. (1988) “On the collapse of inelastic tubes under combined bending and pressure”, International Journal of Solids and Structures 24, 505–535.

38. Crisfield, M.A. (1983) “An Arc-Length Method including Line Searches and Accelerations”, Int. J. Numerical Methods in Engg, Vol. 19, pp 1269-1289.

39. DASt-Ri 017 (1992) DASt–Guideline No. 017 – Beulsicherheitsnachweise für Schalen, spezielle Fälle (Buckling Design of Shells, Special Cases). Köln: Stahlbau-Verlag.

40. Davenport, A.G., (1967) “Gust Loading factors”, Journal of the structural Division, ASCE, Vol.93, No. ST3.

41. Davenport, A.G. and Surry, D. (1975) “The Pressures on low rise structures in turbulent wind”, The Structural and Environmental Effect of Wind on Buildings and Structures, Lecture No. 16, Monash University, May.

42. Derler, P. (1993) “Zum Tragverhalten zylindrischer Behälter unter Windlast”; Doctoral Thesis, Technical University of Graz, Institute for Steel, Timber and Shell Structures, Graz, Austria.

43. DIN 1055 (1987) “Design Loads for Buildings: Loads in Silo Bins”, DIN 1055 Part 6, Deutsches Institut für Normung, Berlin, May.

44. DIN18800 (1990) Steel Structures: Stability, Buckling of Shells. Berlin, November 1990, Deutsches Institut fuer Normung.

45. Ding, X.L. (1992) “Precise Engineering Surveying - Application to the Measurement of Large Scale Steel Silos”, PhD Thesis, University of Sydney, Australia, July 1992.

46. Ding, X.L., Coleman, R.D. and Rotter, J.M. (1996) “Surface profiling system for measurement of engineering structures”, Journal of Surveying Engineering, ASCE, Vol. 122, No. 1, Feb. 1996, pp 3-13.

47. Doerich, C. (2007) “Strength and Stability of locally supported cylinders.” Phd thesis, Institute of Infrastructure and Environment, University of Edinburgh, Edinburgh.

48. Dow, M.B. and Peterson, J.P. (1960) “Bending and Compression Tests of Pressurised Ring-stiffened Cylinders”, NASA TN D-360, 1960.

49. Donnell, L.H. (1933) “Stability of Thin-Walled Tubes under Torsion”, NACA Report No. 479.

50. Donnell, L.H. (1976) “Beams, Plates and Shells”, McGraw Hill, New York.

51. Donnell, L.H. and Wan, C.C. (1950) “Effect of imperfections on buckling of thin cylinders and columns under axial compression”, Journal of Applied Mechanics, ASME, 17(1), 73-83.

52. Ebner, H. (1952) “Theoretical and experimental investigations on buckling of cylindrical tanks subjected to reduced pressure”, (in German), Stahlbau, Vol. 21, pp 153-159.

53. ECCS (1988) European Recommendations for Steel Construction: Buckling of Shells, 4th edition, European Convention for Constructional Steelwork, Brussels, 131 pp.

54. ECCS EDR5 (2008) European Recommendations for Steel Construction: Buckling of Shells, 5th edition, Edited by J.M. Rotter and H. Schmidt, European Convention for Constructional Steelwork, Brussels.

55. Elchalakani, M., Zhao, X.L. and Grzebieta, R.(2002) “Bending tests to determine slenderness limits for cold-formed circular hollow sections”, Journal of Constructional Steel Research **58**, 1407–1430.

56. EN 1991-1-4 (2005) Eurocode 1: Actions on structures, Part 1-4: General actions — Wind actions, CEN, Brussels.

57. EN 1991-4 (2006) Eurocode 1: Basis of Design and Actions on Structures, Part 4 - Silos and Tanks, Eurocode 1 Part 4, CEN, Brussels.

58. EN 1993-1-6 (2007) Eurocode 3: Design of steel structures, Part 1.6: Strength and stability of shell structures. CEN, Brussels.

59. EN 1993-4-1 (2007) Eurocode 3: Design of steel structures, Part 4.1: Silos, Eurocode 3 Part 4.1, CEN, Brussels.

60. EN 1993-4-2 (2007) Eurocode 3: Design of steel structures, Part 4.2: Tanks, Eurocode 3 Part 4.2, CEN, Brussels.

61. ESDU (1980) “Mean forces, pressures and flow field velocities for circular cylindrical structures: finite length cylinders in uniform and shear flow”, Data Item ESDU 81017.

62. Esslinger, M. and Geier, B. (1972) “Gerechnete Nachbeulasten als untere Grenze der experimentellen axialen Beulasten von Kresiszylindern”, Der Stahlbau, Vol. 41, No. 12, pp 353-360.

63. Fabian, O. (1977) “Collapse of cylindrical, elastic tubes under combined bending, pressure and axial loads”, International Journal of Solids and Structures 13, 1257–1270.

64. Fakhim, Y.G., Showkati, H. and Abedi, K. (2009) “Experimental study on the buckling and post-buckling behaviour of thin-walled cylindrical shells with varying thickness under hydrostatic pressure”, Proceedings of the International Association for Shell and Spatial Structures (IASS) Symposium 2009, Valencia, Spain.

65. Farell, C. (1981) “Flow around fixed circular cylinders: fluctuating loads”, Journal of Engineering Mechanics Division, ASCE, Vol. 107, No. EM3, Proc.Paper 16330, pp 565-588.

66. Fischer, G. (1962) “Uber die berechnung der kritischen axiallasten gelenkig gelagerter kreiszylinderschalen mit hilfe des mehrstellenverfahrens”, Zeitschrift für Angewandte Mathematik und Mechanik, Vol. 42.

67. Fischer, G. (1963) “Ueber den einfluss der gelenkigen lagerungauf die stabilitat dunnwandiger kreiszylinderschalen unter axiallast und innendruck”, Zeitschrift für Flugwissenschaften, 11, 111-119.

68. Flügge, W. (1932) “Die Stabilität der Kreiszylinderschale”, Ing.-Arch., Vol. 3, No 5, pp 463-506.

69. Flügge, W. (1973) “Stresses in shells”, 2nd ed, New York/Heidelberg/Berlin: Springer.

70. Fung, Y.C. and Sechler, E.E. (1957) “Buckling of Thin-Walled Circular Cylinders under Axial Compression and Internal Pressure”, Jnl Aeronaut. Sci., Vol. 24, No. 5, pp 351-356.

71. Gettel, M. and Schneider, W. (2007): Buckling strength verification of cantilevered cylindrical shells subjected to transverse load using Eurocode 3. Journal of Constructional Steel Research, (in press, doi:10.1016/j.jcsr.2007.01.003)

72. Goto. Y., Zhang, C.J. and Kawanishi, N. (1999) “Transition of Plastic Buckling Modes in Cylindrical Shells”, Proceedings of The Second International Conference on Advances in Steel Structures, 15–17 December 1999, Hong Kong, China, 1999, Pages 705-712.

73. Greiner, R. (1980) “Ingenieurmäßige Berechnung dünnwandiger Kreiszylinderschale”, Heft 1-1980, Inst. f. Stahlbau, Holzbau u. Flächentragwerke, TU Graz, 1980.

74. Greiner, R. (1981) “Zum Beulnachweis von Zylinderschalen unter Winddruck bei abgestuftem Wanddickenverlauf”; Stahlbau, Vol. 50, pp. 176-179.

75. Greiner, R. (1981) “Buckling of cylindrical shells with stepped wall thickness under wind pressure”, (in German), Der Stahlbau, 50, No. 6, pp. 176-179.

76. Greiner, R. (1983) “Analysis and construction of cylindrical steel cylinders under non-symmetric loading (in German), Proc. Wissenscbaft und praxis, Vol. 31, FHS Biberach/Riss.

77. Greiner, R. (1983) “Structural Problems of Silos and Tanks”, (in German), Austrian Conference of Constructional Steelwork, 1983.

78. Greiner, R and Derler, P (1995) “Effect of imperfections on wind-loaded cylindrical shells”, Thin-Walled Structures, 23(1995), 271-281.

79. Greiner, R. (1998) “Cylindrical shells: wind pressure”, in Silos-Fundamentals of theory, behaviour and design, edited by C.J. Brown & J. Nielsen, E & FN Spon, London, pp 378-414.

80. Greiner, R. (2004) “Cylindrical shells under uniform external pressure”, in Buckling of Thin Metal Shells, eds J.G. Teng & J.M. Rotter, Spon, London, pp 154-174.

81. Greiner, R. and Guggenberger, W. (2004) “Tall cylindrical shells under wind pressure”, in Buckling of Thin Metal Shells, eds J.G. Teng & J.M. Rotter, Spon, London, pp 198-206.

82. Greiner, R., Guggenberger, W. and Schneider, W. (2008) “Cylindrical shells and Wind loading”, Chapter 12 in Stability of Steel Shells: European Design Recommendations: Fifth Edition, eds J.M. Rotter and H. Schmidt, Publication P125, European Convention for Constructional Steelwork, Brussels.

83. Greiner, R. and Rotter, J.M. (2008) “Cylindrical shells of stepwise variable wall thickness”, Chapter 11 in Stability of Steel Shells: European Design Recommendations: Fifth Edition, eds J.M. Rotter and H. Schmidt, Publication P125, European Convention for Constructional Steelwork, Brussels.

84. Grognec, P.L. and Le van, A. (2008) “Elastoplastic bifurcation and collapse of axially loaded cylindrical shells.” International Journal of Solids and Structures, 45 (2008), 64-86.

85. Harris, L.A., Suer, H.S., Skene, W.T. and Benjamin, R.J. (1957) “The Stability of Thin-Walled Unstiffened Circular Cylinders under Axial Compression including the Effects of Internal Pressure”, Jnl Aeronat. Sci., Vol. 24, No. 8, pp 587-596.

86. Hibbitt, Karlsson and Sorensen (2003) “ABAQUS User’s Manual” Ver 6.2, Hibbit, Karlsson and Sorensen Inc., Pawtucket, Rhode Island, USA.

87. HKS (2006) ABAQUS Version 6.6 Standard user’s guide and theoretical manual, Hibbit, Karlsson and Sorensen Inc., Pawtucket, Rhode Island, USA.

88. Ho, B.P.C. and Cheng, S. (1963) “Some problems in stability of heterogeneous aeolotropic cylindrical shells under combined loading”, AIAA J., 1(1963), 1603-1607.

89. Hoff, N.J. (1966) “The perplexing behaviour of thin cylindrical shells in axial compression.” Israel Journal of Technology, Vol. 4, No.1, 1-28.

90. Holmes, J.D., Kwok, K.C.S. and MacDonald, P.A. (1985) Unpublished data on extenrnal pressure coefficients for bins, silos and tanks of circular cross-section.

91. Holmes, J.D., MacDonald, P.A. and Kwok, K.C.S. (1987) "Wind Loads on Storage Bins and Silos of Circular Cross-Section", Proc. First National Structural Engineering Conference, Instn of Engineers, Australia, Melbourne, August, Vol. 1, pp 7-11.

92. Holst, J.M.F.G., Rotter, J.M. and Calladine, C.R. (2000) "Imperfections and buckling in cylindrical shells with consistent residual stresses", Journal of Constructional Steel Research, Vol. 54, pp 265-282.

93. Houliara, S. and Karamanous, S.A. (2006) "Buckling and post-buckling of long pressurized elastic thin-walled tubes under in-plane bending", International Journal of Non-Linear Mechanics, (2006) 491-511.

94. Hughes, T.J.R. (1987) "The finite element method", PRENTICE-HALL, INC., Englewood Cliffs, New Jersey.

95. Hunt J.C.R. and Fernholtz, H. (1975) "Wind Tunnel Simulation of the Atmospheric Boundary Layer", Journal of Fluid Dynamics, Vol.70.

96. Hutchinson, J.W. (1965) "Axial Buckling of Pressurised Imperfect Cylindrical Shells", AIAA Jnl, Vol. 3, No. 8, 1965, pp 1461-1466.

97. Hutchinson, J.W. and Koiter, W.T. (1970) "Postbuckling Theory", Appl. Mech. Reviews, Vol.23, No. 12, Dec. 1970, pp 1353-1366.

98. Hutchinson, J.W., Tennyson, R.C. and Muggeridge, D.B. (1971) "Effect of a Local Axisymmetric Imperfection on the Buckling Behaviour of a Circular Cylindrical Shell under Axial Compression", AIAA Jnl, Vol. 9, No. 1, Jan., pp 48-53.

99. Jaca, R.C., Godoy, L.A., Flores, F.G. and Croll J.G.A. (2007) "A reduced stiffness approach for the buckling of open cylindrical tanks under wind loads", Thin-Walled Structures, 45(2007) 727-736.

100. Jullien, J-F. and Limam, A. (2002) "Buckling of thin pressurised cylindrical shells under bending load", Proc., International Conference on Advances in Steel Structures, ICASS'02, Vol. 2, Hong Kong, December 2002, pp. 675-682.

101. Karamanos, S.A. and Tassoulas, J.L. (1991) "Stability of inelastic tubes under external pressure and bending", Journal of Engineering Mechanics, ASCE 117 (12), 2845–2861.

102. Karamanos, Spyros A. (2002) "Bending instabilities of elastic tubes", International Journal of Soilds and Structures, 39 (2002), 2059-2085.

103. Kareem, A. (1985) "Wind Tunnel Modelling", Design of steel bins for the storage of bulk solids, edited by J.M. Rotter, 1985, Sydney, 40-48.

104. Karman, T. von and Tsien, H.S. (1941) "The buckling of thin cylindrical shells under axial compression", Journal of Aerospace Sciences, 8, 303-312.

105. Koiter, W.T. (1945) “On the Stability of Elastic Equilibrium”, (in Dutch) PhD Thesis, Delft University, (see also Translation AFFDL-TR-70-25 Wright Patterson Air Force Base, 1970).

106. Koiter, W.T. (1963) “The Effect of Axisymmetric Imperfections on the Buckling of Cylindrical Shells under Axial Compression”, Koninklike Nederlandische Akademie van Wetenshappen, Proc. Ser. B66, pp 265-279.

107. Kyriakides, S., Shaw, P.K. (1982) “Response and stability of elastoplastic circular pipes under combined bending and external pressure”, International Journal of Solids and Structures 18 (11), 957–973.

108. Kwok, K.C.S. (1985) “Wind loads on circular storage bins.” Design of steel bins for the storage of bulk solids, edited by J.M. Rotter, 1985, Sydney, 49-54.

109. Lee, L.H.N. (1962) “Inelastic buckling of initially imperfect cylindrical shells subject to axial compression”, Journal of Aeronautical Sciences, 29 (1962), 87–95.

110. Libai, A. and Bert, C.W. (1994) “A mixed variational principle and its application to the nonlinear bending problem of orthotropic tubes—II. Application to nonlinear bending of circular cylindrical tubes”, Int. J. Solids Struct. 31, 1019–1033.

111. Li, H.Y. (1994) “Analysis of steel silo structures on discrete supports.” Phd thesis, Department of Civil Engineering & Building Science, University of Edinburgh, Edinburgh.

112. Li, L.Y. and Kettle, R. (2002) “Nonlinear bending response and buckling of ring-stiffened cylindrical shells under pure bending.” International Journal of Solids and Structures, 39(2002), 765-781.

113. Limam, A., Lee, L.-H, Corona, E. and Kyriakides, S. (2010) “Inelastic wrinkling and collapse of tubes under combined bending and internal pressure”, International journal of Mechanics Sciences, 52 (2010), 637-647.

114. Limam, A. et al. (2011) “Effect of multiple localized geometric imperfections on stability of thin axisymmetric cylindrical shells under axial compression”, International journal of solids and structures, 48 (2011), 1034-1043.

115. Lorenz, R. (1908) “Buckling of a Cylindrical Shell under Axial Compression” (in German) Zeitschrift des Vereines Deutscher Ingenieure, Vol. 52, 1908, p 1766.

116. MacDonald, P.A. (1987) “Wind Loads on Circular Cross-Section Bins, Silos and Tanks”, M. Eng. Sci. Thesis, Univ. Sydney.

117. MacDonald, P.A., Kwok, K.C.S. and Holmes, J.D. (1988) “Wind Loads on Circular Storage Bins, Silos and Tanks: I. Point Pressure Measurements on Isolated Structures”, Journal of Wind Engineering and Industrial Aerodynamics, Vol. 31, pp 165-188.

118. MacDonald, P.A., Holmes, J.D. and Kwok, K.C.S. (1990) “Wind Loads on Circular Storage Bins, Silos and Tanks: II. Effect of Grouping”, Journal of Wind Engineering and Industrial Aerodynamics, Vol. 34, pp 77-95.

119. Macdonald, P.A., Holmes, J.D. and Kwok, K.C.S. (1990) “Wind loads on circular storage bins, silos and tanks. III. Fluctuating and peak pressure distributions”, Journal of Wind Engineering and Industrial Aerodynamics. Vol. 34, no. 3, pp. 319-337.

120. Martin, H.C. and Carey, G. F., (1975) Introduction to Finite Element Analysis- Theory and Applications, Tata McGraw-Hill Publishing Company Ltd., New Delhi.

121. Mathon, L., Limam, A. (2006) “Experimental collapse of thin cylindrical shells submitted to internal pressure and pure bending”, Thin-Walled Structures, 44 (2006), 39-50.

122. Mehta, K.C. (1979) “Wind Load Standards and Codes”, Proceedings, Fifth International Conference on Wind Engineering, J.E. Cermak, Pergamon Press, pp. 1305-1318.

123. Mehta, K.C. (1984) “Wind Load Provisions of ANSI A58.1-1982”, Journal of Structural Engineering, ASCE, Vol.110, No.4, Proc.Paper No. 18758, pp 769-784.

124. Mehta, K.C. (1985) “Wind Loads”, Design of Steel Bins for the Storage of Bulk Solids, edited by Rotter, J.M, Sydney.

125. Moody, L. F. (1944), “Friction factors for pipe flow”, Transactions of the ASME 66 (8): 671–68.

126. Munson, B.R., Young, D.F. and Okllshl, T.H (1998) Fundamentals of Fluid Mechanics, 3rd edn, John Wiley & Sons, Inc, New York.

127. Nash, W.A. (1954) “Buckling of cylindrical shells subject to hydrostatic pressure”, J. Aeron. Sci., 21 (1954), 354-355.

128. NRCC (1980) “Live loads due to wind, subsection 4.1.8, National Building Code of Canada, NRCC No.17303”, National Research Council of Canada, Ottawa.

129. Pircher, M., Berry, P.A., Ding, X.L. and Bridge, R.Q. (2001) “The shape of circumferential weld-induced imperfections in silos and tanks”, Thin-Walled Structures, Vol. 39, pp 999-1014.

130. Pircher, M (2004) “Medium-length thin-walled cylinder under wind loading-case study”, Journal of Structural Engineering, Vol. 130, No. 12, December 1, 2004, 2062-2069.

131. Pircher, M (2004) “The influence of a weld-induced axi-symmetric imperfection on the buckling of a medium-length silo under wind loading”, International Journal of Solids and Structures, 41(2004), 5595-5610.

132. Portela, G. and Godoy, L.A., etc. (2005) “Wind pressures and buckling of cylindrical shell tanks with a conical roof”, Journal of Constructional Steel Research, 61(2005), 786-807.

133. Portela, G. and Godoy, L.A., etc. (2005) “Wind pressures and buckling of cylindrical shell tanks with a doom roof”, Journal of Constructional Steel Research, 61(2005), 808-824.

134. R.Abdelmoula and A.Leger (2008) “Singular perturbation analysis of the buckling of circular cylindrical shells.” European Journal of Mechanics A/Solids,27 (2008), pp706-729.

135. Ramm, E. (1981) “Strategies for Tracing Nonlinear Response Near Limit Points”, in Nonlinear Finite Element Analysis in Structural Mechanics, (Eds. W. Wunderlich, E. Stein and K.J. Bathe), Springer-Verlag, New York, pp 68-89.

136. Reddy, B.D. and Calladine, C.R. (1978) “Classical buckling of a thin-walled tube subjected to bending moment and internal pressure”, International Journal of Mechanical Sciences, 20, 641-50.

137. Reinhold, T. (1982) “Wind Tunnel Modelling for Civil Engineering Application.” Cambridge University Press.

138. Reissner, E. (1959) “On finite bending of pressurized tubes”, Journal of Applied Mechanics, ASME 26, 386–392.

139. Reissner, E. (1961) “On finite pure bending of cylindrical tubes”, Osterr. Ingenieur Archives 15, 165–172.

140. Resinger, F. and Greiner, R. (1974) “Zum Beulverhalten von Kreiszylinderschalen mit abgestufter Wanddicke unter Manteldruck”, Stahlbau, Vol. 43, pp. 182-187.

141. Resinger, F. and Greiner, R. (1976) “Praktische Beulberechnung oberirdischer zylindrischer Tankbauwerke für Unterdruck”, Stahlbau, Vol. 45, pp. 10-15.

142. Resinger, F. and Greiner, R. (1981) “Circular Cylindrical Shells under Wind Pressure: Application of the Calculations to Above-Ground Tanks”, Der Stahlbau, Vol. 50, Heft 3, 1981, pp 65-72.

143. Resinger, F. and Greiner, R. (1982) “Buckling of Wind-Loaded Cylindrical Shells - Application to Unstiffened and Ring-Stiffened Tanks”. Buckling of Shells, E. Ramm, ed., Springer-Verlag, Berlin, 1982, pp 305-332.

144. Riks, E. (1979) “An Incremental Approach to the Solution of Snapping and Buckling Problems”, International Journal of Solids and Structures, Vol. 15, pp 529-551.

145. Rish, R.F., (1936) “Collapse of cylindrical elastic shells under wind loading”. The Engineer, 216, pp.669-672.

146. Rotter, J.M. (1985) “Stability Problems in Cylindrical Bins under Axial Compression”, Proceedings, Joint US/Australian Workshop on the Loading,

Analysis and Stability of Thin Shell Bins, Tanks and Silos, University of Sydney, March 1985, pp 106-117.

147. Rotter, J.M. (1986) “Recent Advances in the Structural Design of Steel Bins and Silos”, Pacific Steel Structures Conference, Auckland, Aug. 1986, Vol. 4, pp 177-194.

148. Rotter, J.M. (1987a) “Membrane Theory of Shells for Bins and Silos”, in Design of Steel Bins for the Storage of Bulk Solids, edited by J.M. Rotter, University of Sydney, March 1985, pp 58-70.

149. Rotter, J.M. (1987b) “Bending Theory of Shells for Bins and Silos”, Transactions of Mechanical Engineering, Institution of Engineers, Australia, Vol. ME12 No.3 September, pp 147-159.

150. Rotter J.M. (1990) “Local inelastic collapse of pressurised thin cylindrical steel shells under axial compression.” Jrnl. Struct. Eng., ASCE, 116(7), 1955-1970.

151. Rotter, J.M. (1996) “Elastic plastic buckling and collapse in internally pressurised axially compressed silo cylinders with measured axisymmetric imperfections: interactions between imperfections, residual stresses and collapse”, Proc. International Workshop on Imperfections in Metal Silos: Measurement, Characterisation and Strength Analysis, CA-Silo, Lyon, France, 19 April, pp 119-140.

152. Rotter, J.M. (1997a) “Design standards and calculations for imperfect pressurised axially compressed cylinders.” Proc., Int. Conf. on Carrying Cap. Shell Structures, Brno, 354-360.

153. Rotter, J.M. (1997b) “Pressurised axially compressed cylinders”, Proc. Int. Conf. on Carrying Capacity of Steel Shell Structures, Brno, 1-3 October 1997, pp 354-360.

154. Rotter, J.M. (1998) “Shell Structures: The New European Standard and Current Research Needs”, Thin-Walled Structures, 31(1-3), 3-23.

155. Rotter, J.M. (1999) “Proposal for generalisation of the elastic-plastic buckling interaction rule for Eurocode 3 Part 1.6”, submission to CEN TC250/SC3/PT4 and ECCS TWG8.4 Buckling of Shells, March, 8pp.

156. Rotter J.M. (2000) “Background Document for the Guide to the Economic Design of Circular Metal Silos.” Research Report R0-021, The University of Edinburgh, School of Civil and Environmental Engineering.

157. Rotter, J.M. (2001a) Guide for the economic design of circular metal silos, Spon Press, London, pp133-134.

158. Rotter, J.M. (2001b) “Wind pressure distributions on squat silos and tanks”, Research Report R01-02, Institute for Infrastructure and Environment, Univ. of Edinburgh.

159. Rotter, J.M. (2002) “Shell Buckling and Collapse Analysis for Structural Design: The New Framework of the European Standard.” New Approaches to

Structural Mechanics, Shells & Biological Structs. Eds H.R. Drew & S. Pellegrino, Kluwer Academic, London, 355-378.

160. Rotter J.M. (2004). "Buckling of cylindrical shells under axial compression", Chapters 2 in Buckling of Thin Metal Shells, Eds J.G. Teng & J.M. Rotter, Spon, London, pp 1-87.

161. Rotter, J.M. (2005a) "The philosophy of shell buckling design according to EN 1993-1-6", Proc., 5th International Conference on Computation of Shell and Spatial Structures, June 1-4, 2005 Salzburg, Austria.

162. Rotter, J.M. (2005b) "The Practical Design of Shell Structures Exploiting Different Methods of Analysis" in Shell Structures: Theory and Applications, Eds Pietraszkiewicz, W. and Szymczak, C., Taylor and Francis, London, 71-86.

163. Rotter, J.M. (2005c) "Stability and plasticity in structural analysis: a new conceptual framework", Invited keynote paper, Proc., Fourth International Conference on Advances in Steel Structures, ICASS'05, Shanghai, July 2005, pp. 1815-1826.

164. Rotter, J.M. (2006) "Elephant's foot buckling in pressurised cylindrical shells", Stahlbau, Vol 75, Heft 9, Special Edition in honour of Profs Schmidt, Greiner and Wunderlich, Sept 2006, pp 742-747.

165. Rotter, J.M. (2007) "A Framework for Exploiting Different Computational Assessments in Structural Design." 6th International Conference on Steel and Aluminium Structures." 2007, Oxford, 26-39.

166. Rotter, J.M. (2008a) "Rules for the plastic limit state and plastic reference load assessment", Chapter 7 in Stability of Steel Shells: European Design Recommendations: Fifth Edition, eds J.M. Rotter and H. Schmidt, Publication P125, European Convention for Constructional Steelwork, Brussels.

167. Rotter, J.M. (2008b) "The elastic-plastic imperfection sensitivity of axially compressed cylinders with weld depressions." 5th European Conference on Steel and Composite Stuctures, Graz, Austria, September 2008.

168. Rotter J.M., Coleman R., Ding X.L. & Teng J.G. (1992) "The measurement of imperfections in cylindrical silos for buckling strength assessment." Proc. of the 4th Int. Conf. on Bulk Materials Storage, Handling and Transportation, IEAustralia, Wollongong, 473-479.

169. Rotter, J.M. and Jumikis, P.T. (1988) "Nonlinear Strain-Displacement Relations for Thin Axisymmetric Shells", Research Report R563, School of Civil and Mining Engineering, University of Sydney, Feb. 1988.

170. Rotter, J.M. and Teng, J.G (1989) "Elastic Stability of Cylindrical Shells with Weld Depressions", Journal of Structural Engineering, American Society of Civil Engineers, Vol 115, No. 5, May 1989, pp 1244-1263.

171. Rotter, J.M. and Zhang, Q. (1990) "Elastic Buckling of Imperfect Cylinders containing Granular Solids", Journal of Structural Engineering, ASCE, Vol. 116, No. 8, August 1990, pp 2253-2271.

172. SAA, (1983) “Australian Standard 1170, SAA Loading Code Part 2-Wind Forces”, Standards Association of Australia, North Sydney, NSW, Australia.

173. Sabransky, I.J. (1984) “Wind pressure distribution on cylindrical grain storage silos”, Master of Engineering Science Thesis, Department of Civil E ngineering, Monash University, February.

174. Sanders, J.L., “Nonlinear Theories for Thin Shells”, Quarterly Journal of Applied Mathematics, Vol 21, 1963, pp 21-36.

175. Schmidt, H, Binder, B., Lange, H. (1998) “Postbuckling strength design of open thin-walled cylindrical tanks under wind load”, Thin-walled structures, 31, pp 203-220.

176. Schmidt, H. and Greiner, R. (1998) “Erläuterungen zu DIN 18800 Teil 4” (“Elucidations of DIN 18800-4”). in Beuth-Kommentar Stahlbauten, 3rd edition, eds J. Lindner, J. Scheer & H. Schmidt, Beuth and Ernst & Sohn, Berlin, pp. 333-417.

177. Schmidt, H. and Rotter, J.M. (2008) “Rules for the buckling limit state assessment using global numerical analysis”, Chapter 8 in Stability of Steel Shells: European Design Recommendations: Fifth Edition, eds J.M. Rotter and H. Schmidt, Publication P125, European Convention for Constructional Steelwork, Brussels.

178. Schmidt, H. and Rotter, J.M. (2008) “Cylindrical shells of constant wall thickness under general loading”, Chapter 10 in Stability of Steel Shells: European Design Recommendations: Fifth Edition, eds J.M. Rotter and H. Schmidt, Publication P125, European Convention for Constructional Steelwork, Brussels.

179. Schmidt, H. and Winterstetter, T.A. (2001) “Substitute geometrical imperfections for the numerical buckling assessment of cylindrical shells under combined loading”, Proc., European Mechanics Conference: Euromech 424, Rolduc-Kerkrade, Germany, 3-5 Sept 2001, pp 82-84.

180. Schneider, W., Thiele, R. and Bohm, S. (1997) “Carrying capacity of slender wind-loaded cylindrical shells”, Proc., Int. Conf. on Carrying Capacity of Steel Shell Structures, Brno, 1-3 October 1997, pp 171-177.

181. Schneider, W. and Thiele, R. (1998) “Eine unerwartete Versagensform bei schlanken windbelasteten Kreiszylinderschalen”. Stahlbau 67 (1998), 870-875.

182. Schneider, W. and Thiele, R. (1998) “Tragfähigkeit schlanker windbelasteter Kreiszylinderschalen”, Stahlbau 67 (1998), 434-441.

183. Schneider, W., Höhn, K., Timmel, I. and Thiele, R. (2001) “Quasi-collapse-affine imperfections at slender wind-loaded cylindrical steel shells”, Second European Conference on Computational Mechanics, Cracow, Poland, June, Vol. 2, pp 1000-1001.

184. Schneider, W., Brede, A. and Thiele, R. (2002) “Bemessung der Ringsteifen stählerner Kamine” (Design of the ring stiffeners of steel chimneys), Stahlbau Vol. 71, pp. 670-677 (in German).

185. Schneider, W., Timmel, I. and Höhn, K. (2005) “The Conception of Quasi-Collapse-Affine Imperfections - A new Approach to Unfavourable Imperfections of Thin-Walled Shell Structures.” Thin-Walled Structures Vol. 43/8, pp. 1202-1224.

186. Schneider, W. and Brede, A. (2005) “Consistent equivalent geometric imperfections for the numerical buckling strength verification of cylindrical shells under uniform external pressure.” Thin-Walled Structures Vol. 43/2, 175-188.

187. Schneider, W. and Gettel, M. (2007) “Numerical Buckling Strength Verification of Cylindrical Steel Shell Structures Subject to Combined Loading.” Int. J. of Structural Stability and Dynamics, Vol.7, No.2, 295-311.

188. Scrutton, C. and Rogers, E.W.E. (1971) “Steady and Unsteady Wind Loading on Buildings and Structures”, Phi. Trans. Royal Soc., A269, PP353-383.

189. Seide, P. and Weingarten, V.I. (1961) “On the Buckling of Circular Cylindrical Shells Under Pure Bending”, Journal of Applied Mechanics, 28 (1), 112-116.

190. Singer, J. (1982) “The Status of Buckling Investigations of Shells”, Buckling of Shells, Ed. E. Ramm, Springer-Verlag.

191. Singer, J. (1983) “Vibration and buckling of imperfect stiffened shells-recent developments, in Collapse: The Buckling of Structures in theory and Practice”, (eds J.M.T. Thompson and G.W. Hunt), Cambridge University Press, Cambridge, 443-479.

192. Singer, J. (2004) “Stiffened cylindrical shells”, in Buckling of Thin Metal Shells, eds J.G. Teng & J.M. Rotter, Spon, London, pp 286-343.

193. Sobel, L.H. (1964) “Effects of boundary conditions on the stability of cylinders subject to lateral and axial pressure”, AIAA J., 2(1964) 1437-1440.

194. Song, C.Y., Teng, J.G. and Rotter, J.M. (2004) “Imperfection sensitivity of thin elastic cylindrical shells subject to partial axial compression”, International Journal of Solids and Structures, Vol. 41, July, pp 7155-7180.

195. Southwell, R.V. (1913) “On the collapse of tubes by external pressure” Phil. Mag. Vol 25 (1913), pp 687-698, Vol. 26 (1913), p502 and Vol. 29 (1915), p67.

196. Southwell, R.V. (1914) “On the General Theory of Elastic Stability”, Phil. Trans. Royal Soc., Vol. 213, 1914, pp. 187-244.

197. Stephens, W., Starnes Jr., J.H. and Almroth, B.O. (1975) “Collapse of long cylindrical shells under combined bending and pressure loads”, AIAA J. 13, 20–25.

198. Suer, H.S., Harris, L.A., Skene, W.T. and Benjamin, R.J. (1958) “The bending stability of thin-walled unstiffened circular cylinder including the effects of internal pressure”, J Aeronaut Sci, 25(5), 281–287.

199. Surry, D. and Stathopoulos, T. (1977) “An Experimental Approach to the Economical Measurement of Spatially Averaged Wind Loads.” Journal of Industrial Aerodynamics, Vol. 2.

200. Tang, S.C., Chu, C.C. and Yeung, K.S. (1984) “Collapse of long, noncircular, cylindrical shells under pure bending”, Computers and structures, Vol. 21, No. 6, pp 1345-1353.

201. Tatiana Vodenitcharova and Peter Ansourian (1996) “Buckling of circular cylindrical shells subjected to uniform laternal pressure.” Engineering Structures, Vol. 18, No. 8, pp.604-614, 1996.

202. Tatting, B.F., Gurdal, Z. and Vasiliev, V.V. (1995) “Nonlinear shell theory solution for the bending response of orthotropic finite length cylinders including the Brazier effect”, Proceedings of the 36th Structures, Structural Dynamics and Materials Conference, New Orleans, LA, pp. 966–976.

203. Teng, J.G. and Rotter, J.M. (1989) “Elastic-Plastic Large Deflection Analysis of Axisymmetric Shells”, Computers and Structures, Vol. 31, No. 2, pp 211-235, 1989.

204. Teng, J.G. and Rotter, J.M. (1989) “Non-Symmetric Buckling of Plate-End Pressure Vessels”, Journal of Pressure Vessel Technology, American Society of Mechanical Engineers, Vol. 111, No. 3, August, 1989, pp 304-311.

205. Teng, J.G. and Rotter, J.M. (1992) “Buckling of pressurized axisymmetrically imperfect cylinders under axial loads.” Journal of Engineering Mechanics, Vol. 118, No.2, 1992, 229-247.

206. Teng, J.G. (1996) “Buckling of thin shells: recent advances and trends”, Applied Mechanics Reviews, Vol. 49, No. 4 April, pp 263-274.

207. Teng, J.G. (2000) “Intersections in Steel Shell Structures”, Progress in Structural Engineering and Materials, Vol. 2, No. 4, July, pp 459-471.

208. Teng, J.G. and Rotter, J.M. (2004) “Buckling of thin shells: an overview”, Chapter 1 of the book Buckling of Thin Metal Shells, eds J.G. Teng & J.M. Rotter, Spon, London, pp 1-41.

209. Teng, J.G., Lin, X., Rotter, J.M. and Ding, X.L. (2005) “Analysis of geometric imperfections in full-scale welded steel silos”, Engineering Structures, Vol. 27, No 6, May 2005, 938-950.

210. Timoshenko, S.P. and Gere, J.M. (1961) “Theory of Elastic Stability”, 2nd edn, McGraw-Hill, New York.

211. Trahair, N.S., Abel, A., Ansourian, P., Irvine, H.M., Rotte, J.M. (1983) Structural Desigh of Steel Bins for Bulk Solids, Australian Institute of Steel Construction, Sydney.

212. Tvergaard, V., “Buckling Behaviour of Plate and Shell Structures”, Proc., 14th Int. Cong. Theor. Appl. Mech., Delft, 1976, pp 232-247.

213. Tvergaard, V. (1983a) “On the transition from a diamond mode to an axisymmetric mode of collapse in cylindrical shells.” International Journal of Solids and Structures, 19 (10), 845–856.

214. Tvergaard, V. (1983b) “Plastic buckling of axially compressed circular cylindrical shells.” Thin-Walled Structures, 1 (2), 139–163.

215. Vickery, B.J. and Ansourian, P. (1974) “An investigation of the failure due to wind action of a group of six silos at Boggabri, NSW”, Investigation Report S152, School of Civil Engineering, University of Sydney, Sydney.

216. Vodenitcharova, T.M. and Ansourian, P. (1996) “Buckling of circular cylindrical shells subjected to uniform lateral pressure.” Engineering Structures, Vol. 18, No. 8, pp.604-614, 1996.

217. Vodenitcharova, T.M. and Ansourian P. (1998) “Hydrostatic, wind and non-uniform lateral pressure solutions for containment vessels”, Thin-Walled Structures 31 (1998) 221-236.

218. Wempner, G.A. (1971) “Discrete Approximations Related to Nonlinear Theories of Solids”, International Journal of Solids and Structures, Vol. 7, pp 1581-1599.

219. Weingarten, V.I., Morgan, E.J. and Seide, P. (1965) “Elastic Stability of Thin-Walled Cylindrical and Conical Shells under Combined Internal Pressure and Axial Compression”, AIAA Jnl, Vol. 3, No. 6, June, pp 1118-1125.

220. Yamaki, N. (1984) “Elastic Stability of Circular Cylindrical Shells”, North Holland, Elsevier Applied Science Publishers, Amsterdam, 1984.

221. Zienkiewicz, O.C. (1971) “The Finite Element Method in Engineering Science”, McGraw-Hill, London.

Appendix - ABAQUS Input Program for cylindrical shells of stepped wall cylinders under uniform external pressure

The following input programme shows an example of LBA analysis for Model 1 (as can be seen in Chapter 7) under uniform external pressure with case factor *k=1*. For cylinders under global bending and wind pressure, the input files are generated by ABAQUS CAE and are so large that are impossible to be shown here, but the author is happy to communicate with anyone who is interested in them.

```
**********************
*HEADING
Elastic stepped wall thickness cylinders under uniform external pressure
(L / r=8.1, r / t(min)=2000, case factor k=1)
********
*NODE,SYSTEM=C
 1,2001.425,0,0
 401,2001.425,180,0
4011,2001.425,0,1800
4411,2001.425,180,1800

4412,2001.2625,0,1800
4812,2001.2625,180,1800
8422,2001.2625,0,3600
8822,2001.2625,180,3600

8823,2001.1,0,3600
9223,2001.1,180,3600
12833,2001.1,0,5400
13233,2001.1,180,5400

13234,2000.9375,0,5400
```

13634,2000.9375,180,5400
21254,2000.9375,0,7200
21654,2000.9375,180,7200

21655,2000.775,0,7200
22055,2000.775,180,7200
29675,2000.775,0,9000
30075,2000.775,180,9000

30076,2000.625,0,9000
30476,2000.625,180,9000
38096,2000.625,0,10800
38496,2000.625,180,10800

38497,2000.5625,0,10800
38897,2000.5625,180,10800
42507,2000.5625,0,12600
42907,2000.5625,180,12600

42908,2000.5,0,12600
43308,2000.5,180,12600
46918,2000.5,0,14400
47318,2000.5,180,14400

47319,2000.5,0,14400
47719,2000.5,180,14400
51329,2000.5,0,16187.19566
51729,2000.5,180,16187.19566

51730,2000.5,0,16200
52130,2000.5,180,16200

100001,2001,0,16187.19566

100401,2001,180,16187.19566

100402,2064.52172,0,16187.19566

100802,2064.52172,180,16187.19566

100803,2001,0,16200

101203,2001,180,16200

101204,2064.52172,0,16200

101604,2064.52172,180,16200

***

** GENERATE POINTS WHERE THE PLATE THICKNESS CHANGES

*NGEN,LINE=C,NSET=BOTTOM,SYSTEM=C

 1,401,1, ,0.,0.,0.,0,0,1.0

*NGEN,LINE=C,NSET=top,SYSTEM=C

 51730,52130,1, ,0.,0.,16200.,0,0,1.0

*NGEN,LINE=C,NSET=MID1,SYSTEM=C

 4011,4411,1, ,0.,0.,1800.,0,0,1.0

*NGEN,LINE=C,NSET=MID2,SYSTEM=C

 4412,4812,1, ,0.,0.,1800.,0,0,1.0

*NGEN,LINE=C,NSET=MID3,SYSTEM=C

 8422,8822,1, ,0.,0.,3600.,0,0,1.0

*NGEN,LINE=C,NSET=MID4,SYSTEM=C

 8823,9223,1, ,0.,0.,3600.,0,0,1.0

*NGEN,LINE=C,NSET=MID5,SYSTEM=C

 12833,13233,1, ,0.,0.,5400.,0,0,1.0

*NGEN,LINE=C,NSET=MID6,SYSTEM=C

 13234,13634,1, ,0.,0.,5400.,0,0,1.0

*NGEN,LINE=C,NSET=MID7,SYSTEM=C

 21254,21654,1, ,0.,0.,7200.,0,0,1.0

*NGEN,LINE=C,NSET=MID8,SYSTEM=C

 21655,22055,1, ,0.,0.,7200.,0,0,1.0

*NGEN,LINE=C,NSET=MID9,SYSTEM=C

 29675,30075,1, ,0.,0.,9000.,0,0,1.0

```
*NGEN,LINE=C,NSET=MID10,SYSTEM=C
 30076,30476,1, ,0.,0.,9000.,0,0,1.0
*NGEN,LINE=C,NSET=MID11,SYSTEM=C
 38096,38496,1, ,0.,0.,10800.,0,0,1.0
*NGEN,LINE=C,NSET=MID12,SYSTEM=C
 38497,38897,1, ,0.,0.,10800.,0,0,1.0
*NGEN,LINE=C,NSET=MID13,SYSTEM=C
 42507,42907,1, ,0.,0.,12600.,0,0,1.0
*NGEN,LINE=C,NSET=MID14,SYSTEM=C
 42908,43308,1, ,0.,0.,12600.,0,0,1.0
*NGEN,LINE=C,NSET=MID15,SYSTEM=C
 46918,47318,1, ,0.,0.,14400.,0,0,1.0
*NGEN,LINE=C,NSET=MID16,SYSTEM=C
 47319,47719,1, ,0.,0.,14400.,0,0,1.0
*NGEN,LINE=C,NSET=MID17,SYSTEM=C
 51329,51729,1, ,0.,0.,16187.19566,0,0,1.0
**********************************************
** GENERATE  POINTS WHERE THE PLATE THICKNESS CHANGES
*NGEN,NSET=r1,SYSTEM=C
 1,4011,401
*NGEN,NSET=r2,SYSTEM=C
 4412,8422,401
*NGEN,NSET=r3,SYSTEM=C
 8823,12833,401
*NGEN,NSET=r4,SYSTEM=C
 13234,21254,401
*NGEN,NSET=r5,SYSTEM=C
 21655,29675,401
*NGEN,NSET=r6,SYSTEM=C
 30076,38096,401
*NGEN,NSET=r7,SYSTEM=C
 38497,42507,401
```

```
*NGEN,NSET=r8,SYSTEM=C
 42908,46918,401
*NGEN,NSET=r9,SYSTEM=C
 47319,51329,401
*NGEN,LINE=C,NSET=ring1,SYSTEM=C
100001,100401,1, ,0.,0,16187.19566,0.,0,1.0
*NGEN,LINE=C,NSET=ring2,SYSTEM=C
100402,100802,1, ,0.,0,16187.19566,0.,0,1.0
*NGEN,LINE=C,NSET=ring3,SYSTEM=C
100803,101203,1, ,0.,0,16200,0.,0,1.0
*NGEN,LINE=C,NSET=ring4,SYSTEM=C
101204,101604,1, ,0.,0,16200,0.,0,1.0
*nset,nset=bnd1,GENERATE
1,51730,401
*NGEN,NSET=L1,SYSTEM=C
 401,4411,401
*NGEN,NSET=L2,SYSTEM=C
 4812,8822,401
*NGEN,NSET=L3,SYSTEM=C
 9223,13233,401
*NGEN,NSET=L4,SYSTEM=C
 13634,21654,401
*NGEN,NSET=L5,SYSTEM=C
 22055,30075,401
*NGEN,NSET=L6,SYSTEM=C
 30476,38496,401
*NGEN,NSET=L7,SYSTEM=C
 38897,42907,401
*NGEN,NSET=L8,SYSTEM=C
 43308,47318,401
*NGEN,NSET=L9,SYSTEM=C
 47719,51729,401
```

```
*nset,nset=bnd2,GENERATE
401,52130,401
*NSET,NSET=BRING1,GENERATE
100001,101204,401
*NSET,NSET=BRING2,GENERATE
100401,101604,401
******
*Nfill,NSET=REST1
bottom,MID1,10,401
*Nfill,NSET=REST2
MID2,MID3,10,401
*Nfill,NSET=REST3
MID4,MID5,10,401
*Nfill,NSET=REST4
MID6,MID7,20,401
*Nfill,NSET=REST5
MID8,MID9,20,401
*Nfill,NSET=REST6
MID10,MID11,20,401
*Nfill,NSET=REST7
MID12,MID13,10,401
*Nfill,NSET=REST8
MID14,MID15,10,401
*Nfill,NSET=REST9
MID16,MID17,10,401
*NSET,NSET=ALL
BND1,BND2,BOTTOM,TOP,REST1,REST2,REST3,REST4,REST5,REST6,REST
7,REST8,REST9
******
*ELEMENT,TYPE=S4
 1, 1,402,403,2
*ELGEN,ELSET=EBOTTOM
```

1, 400,1,1, 10,401,400
*ELEMENT,TYPE=S4
4001, 4412,4813,4814,4413
*ELGEN,ELSET=Et1
4001, 400,1,1, 10,401,400
*ELEMENT,TYPE=S4
8001, 8823,9224,9225,8824
*ELGEN,ELSET=Et2
8001, 400,1,1, 10,401,400
*ELEMENT,TYPE=S4
12001, 13234,13635,13636,13235
*ELGEN,ELSET=Et3
12001, 400,1,1, 20,401,400
*ELEMENT,TYPE=S4
20001, 21655,22056,22057,21656
*ELGEN,ELSET=Et4
20001, 400,1,1, 20,401,400
*ELEMENT,TYPE=S4
28001, 30076,30477,30478,30077
*ELGEN,ELSET=Et5
28001, 400,1,1, 20,401,400
*ELEMENT,TYPE=S4
36001, 38497,38898,38899,38498
*ELGEN,ELSET=Et6
36001, 400,1,1, 10,401,400
*ELEMENT,TYPE=S4
40001, 42908,43309,43310,42909
*ELGEN,ELSET=Et7
40001, 400,1,1, 10,401,400
*ELEMENT,TYPE=S4
44001, 47319,47720,47721,47320
*ELGEN,ELSET=Et8

```
 44001, 400,1,1, 10,401,400
*ELEMENT,TYPE=S4
48001, 51329,51730,51731,51330
*ELGEN,ELSET=Etop
 48001, 400,1,1, 1,401,400
*ELEMENT,TYPE=C3D8
 300000, 100001,100402,100403,100002,100803,101204,101205,100804
*ELGEN,ELSET=Ering
 300000, 400,1,1,
**
*SHELL SECTION,ELSET=Ebottom,MATERIAL=MAT
 2.85,13
*SHELL SECTION,ELSET=Et1,MATERIAL=MAT
 2.525,13
*SHELL SECTION,ELSET=Et2,MATERIAL=MAT
 2.2,13
*SHELL SECTION,ELSET=Et3,MATERIAL=MAT
 1.875,13
*SHELL SECTION,ELSET=Et4,MATERIAL=MAT
1.55,13
*SHELL SECTION,ELSET=Et5,MATERIAL=MAT
 1.25,13
*SHELL SECTION,ELSET=Et6,MATERIAL=MAT
 1.125,13
*SHELL SECTION,ELSET=Et7,MATERIAL=MAT
 1.0,13
*SHELL SECTION,ELSET=Et8,MATERIAL=MAT
 1.0,13
*SHELL SECTION,ELSET=EtOP,MATERIAL=MAT
 1.0,13
*SOLID SECTION,MATERIAL=MATRING,ELSET=RING
*MATERIAL,NAME=MAT
```

```
*ELASTIC
 2.0E5,0.3
*MATERIAL,NAME=MATring
*ELASTIC
 2.0E5,0.3
*DENSITY
   7.85e-006
*ElSET, elset=EALL1, generate
1,48000, 1
*Surface, type=ELEMENT, name=EALLS
EALL1, SNEG
*ElSET, elset=TOPSUR1, generate
48001,48400,1
*ElSET, elset=ring, generate
300000,300399, 1
*Surface, type=ELEMENT, name=RINGSUR
RING, S6
*Surface, type=ELEMENT, name=LRING
RING, S4
*Surface, type=ELEMENT, name=TOPOUT
TOPSUR1, SNEG
*TIE,NAME=TIE1
RINGSUR,TOPOUT
**
*MPC
beam,mid2,mid1
beam,mid4,mid3
beam,mid6,mid5
beam,mid8,mid7
beam,mid10,mid9
beam,mid12,mid11
beam,mid14,mid13
```

```
beam,mid16,mid15
**
**
*BOUNDARY
BND1,2
BND1,4
BND1,6
BND2,2
BND2,4
BND2,6
BRING1,2
BRING1,4
BRING1,6
BRING2,2
BRING2,4
BRING2,6
*Transform,nset=bottom,type=c
0,0,0,0,0,1
*BOUNDARY
bottom,1,3
bottom,4
bottom,6
*RESTART,WRITE
***
*STEP
*Buckle
4,,12,2000
*DSLOAD
EALLS,P,1
LRING,P,1
*RESTART,WRITE
*OUTPUT,FIELD,FREQUENCY=1
```

```
*ELEMENT OUTPUT
S,E,PE,PEEQ,PEMAG
*NODE OUTPUT
U,RF
*OUTPUT,HISTORY,FREQUENCY=1
*EL FILE, FREQUENCY=1
S,E,
*NODE PRINT,MODE=1,LAST MODE=6
U,
*NODE FILE,MODE=1,LAST MODE=6
U
*MODAL FILE
*END STEP
```